Geochemical mapping of the extrusive sequence of the Troodos Ophiolite, Cyprus: an investigation into the relationship between lava compositions and proximity to a paleo-subduction zone and a paleo-transform fault

Charles Alexander Wake

Submitted in partial fulfilment of the requirement for the degree of Ph.D.

Cardiff University

September 2005

ProQuest LLC
789 East Eisenhower Parkway
P.O. Box 1346
Ann Arbor, MI 48106-1346

Abstract

Analysis of 240 samples for a wide suite of major and trace elements enable geochemical maps of the extrusive series of the Troodos Massif using ArcView 3.2 (a Geographic Information Systems application). Proxies for mantle source depletion, degree of partial melting, lithospheric component, subduction-derived input and fractional crystallisation form the basis of the maps.

No substantial difference in mantle source depletion or subduction-derived component was detected between the three stratigraphically-defined lava units (Basal Group, Lower Pillow Lavas and Upper Pillow Lavas). Variation between the lava units is a function of the degree of partial melting of the mantle source and the degree of fractional crystallisation of the resulting magma, both of which are generally highest in the Basal Group and lowest in the Upper Pillow Lavas.

Proximity to the paleo-transform fault has three effects on lava composition prior to component addition. Lavas within 10 km of the fault become increasingly primitive. The mantle source becomes strongly depleted on approximately the same scale. The lithospheric (OIB-like) component is also greatest close to the fault.

The subduction-derived component is greatest in the north west of the Troodos Massif, in crust generated at the Solea Graben, the oldest of the grabens within the Troodos Massif. The younger Mitsero and Larnaca Grabens have progressively lower subduction-derived components. Taking into account rotation of the Troodos Massif since its formation, the areas of strongest subduction enrichment originally lay to the north. Therefore, the paleo-subduction zone where the Paleotethys ocean floor was being subducted beneath the Troodos supra-subduction spreading centre probably lay to the north of Cyprus, with a southerly dip.

Index of contents

Chapter 1 – The Troodos Ophiolite – an introduction 7

- 1.1 – The Troodos Massif 7
- 1.2 – Structure of the Troodos Massif 12
- 1.3 – The lava groups 19
- 1.4 – Geochemical fingerprinting of the Troodos Massif, an evolution of ideas 22
- 1.5 – Aims and Objectives of the Thesis 58

Chapter 2 – Sampling, laboratory preparation, analysis and data handling 60

2.1 - Sampling and analysis 60

- 2.1a) - Choosing sampling areas 60
- 2.1b) – Field sampling methods 61
- 2.1c) – Trimming and grinding 62
- 2.1d) – Loss on Ignition and ICP-OES preparation 63
- 2.1e) – Inductively coupled plasma mass spectrometry (ICP-MS) 65
- 2.1f) – Blanks, contamination, standards and spikes 66
- 2.1g) – Data quality and arithmetic procedure 68

2.2 – Interpretation Techniques 73

- 2.2a) - Geographic Information Systems (G.I.S.) 73
- 2.2b) - Compiling data 73
- 2.2c) – G.I.S. Maps 74

2.3 - Graphical methods and data presentation

- 2.3a) – Trendline Construction 78
- 2.3b) – Graphs – other information 78

Chapter 3 – Discussion of results and presentation of data 79

3.1 - Mapping source depletion, partial melting and oxygen fugacity within the Troodos Massif using the Myashiro (TiO_2 – FeO/MgO) projection and FeO - MgO relationships. 79

- 3.1a) - Effects of f_{O2} on Fe, Mg and Ti content in basalts 79
- 3.1b) - History of f_{O2} research within the Troodos Massif and its analogues 80
- 3.1c) - Troodos regions FeO* v MgO 82
- 3.1d) - Interpretations of geochemical regions of the lavas of the Troodos Massif by comparison to experimental QFM and QFM+3 trends of Juster et al. (1989) and a marginal basin analogue (Lau Basin) 87
- 3.1e) - Troodos regions TiO_2 v FeO* / MgO 90
- 3.1f) - Comparison of TiO_2 v FeO*/MgO trends from the Troodos Massif with trends from analogue regions 94
- 3.1g) - Regional variation across the Troodos Massif and its analogues 98

3.2 - Geochemical mapping using Titanium and Vanadium content to investigate variations in source depletion and enrichment. 102

- 3.2a) – Theory 102
- 3.2b) - Troodos lava Ti-V contents 104
- 3.2c) - Fractionation within the Troodos Massif and comparison with analogues 113

3.3 - Measuring mantle source depletion, partial melting and fractional crystallisation using Cr and Y 117

- 3.3a) – Theory 117
- 3.3b) - Chromium and yttrium properties of the Troodos Massif 119
- 3.3c) - Troodos Lava Cr – Y profiles by region 123
- 3.3d) - Depletion, partial melting and analogues 128

3.4) - Measuring subduction input using Th-Nb and Th-Ta covariations 132

- 3.4a) - Nb, Ta, Yb and their behaviour in subduction-related magmas and lavas 132
- 3.2b) - Th/Nb variations within the Troodos Massif. 135
- 3.4c) - Comparison of Troodos lavas Th/Nb properties with analogue regions 150

3.5) - Determining source depletion and subduction enrichment using rare earth element profiling 154

- 3.5a) – Theory 154
- 3.5b) - REE profiles of Troodos lava types 157
- 3.5c) - REE profiles from selected regions of the Troodos Massif 160
- 3.5d) - REE variation across the Troodos Massif and comparison with analogue regions 168

3.6) - Determining mantle, lithospheric and subduction-derived source components from extended incompatible element profiles (Spider diagrams) 177

- 3.6a) – Theory 177
- 3.6b) - Variations in extended incompatible element profiles across the Troodos Massif 178
- 3.6c) - Variations in source depletion, low-degree partial melt addition and subduction-derived input 185
- 3.6d) - Comparison with analogue regions to the Troodos Massif (Lau Basin and the Garrett Transform in the East Pacific Rise) 188

Chapter 4 - Implications for Petrogenesis and Tectonic setting of the Troodos Massif 191

4.1 - Summary of results 191

- 4.1a) - Distribution of depleted mantle 191
- 4.1b) - Distribution of the subduction-derived component 195
- 4.1c) - Distribution of fractionated lavas 198
- 4.1d) - Distribution of enriched lithosphere (or OIB) component 199
- 4.1e) - Source and component variations between the Basal Group, Lower Pillow Lavas and the Upper Pillow Lavas 202

4.2 - Implications for petrogenesis 204

- 4.2a) - Comparison with models provided by analogue regions 204
- 4.2b) - Comparison of previous Troodos Massif models 208
- 4.2c) - Relationship between the Troodos Massif, the paleo-subduction zone, the Neotethys basin and the Paleotethys Ocean. 211

Chapter 5 – Conclusions **215**

- 5.1 - Data collection and geochemical mapping 215
- 5.2 - Implications for the relationship between the stratigraphic lava groups 216
- 5.3 - Implications for graben development 216
- 5.4 - Implications for the effect of a transform fault on lava composition 217
- 5.5 - Implications for the tectonic setting of the Troodos Massif within the Eastern Mediterranean 217

Appendix 1) Data tables **218**

Appendix 2) Bibliography **240**

Acknowledgements

I would like to acknowledge the help of and thank the following:

My parents for making this all possible and supporting me through thick and thin.

Chris Johnson for being my best mate and having confidence in me even when things have been tough.

Professor Julian Pearce for the expert guidance provided throughout the four years that this thesis has taken and putting up with me for this time.

Dr Chris MacLeod for firing my enthusiasm for the Troodos Ophiolite in the first place. Get well soon.

Dr Iain McDonald and **Eveline de Vos** for your support and patience with my laboratory work.

Dr Rex Taylor (Southampton Oceanography Centre) for allowing me to use your samples.

The Cypriot Geological Survey for allowing me to work on the island.

All my Cardiff University colleagues and friends who have helped me through this time.

This one's for you. I couldn't have done this on my own

1) The Troodos Ophiolite – An Introduction

1.1) The Troodos Massif

The Troodos ophiolite is a relatively undeformed, allochthonous complex with a complete Penrose stratigraphy as defined at the 1st GSA Conference on Ophiolites. The first detailed attempt to map it was by Wilson (1959), Bagnall (1960), Bear (1960) and Gass (1960). It is thought to be a preserved section of Mesozoic Tethyan crust (Moores and Vine, 1971). Zircons from two plagiogranites in the plutonic section of the Troodos ophiolite yield U-Pb dates between 90.3 $\pm$ 0.7 and 92.4 $\pm$ 0.7 Ma (Mukasa and Ludden, 1987). These dates agree with Campanian biostratigraphic ages obtained by Blome and Irwin (1985) from radiolaria in umbers directly overlying the uppermost lavas. Magnetic work carried out in the eastern Mediterranean shows the presence of north-south trending lineations in the oceanic crust in the Cyprus area (Gass, 1968).

The Troodos Massif is recognised as one of the world's best known and most studied ophiolite complexes. Outcropping over an area of about 120 x 50 km, all stratigraphic layers of a typical ocean crust and upper mantle sequence are exposed. The ophiolite sequence is exposed in the form of a breached elongate dome, with the lowest structural units exposed near the centre, and the uppermost units at the rim. The completeness of the ophiolite led the participants of the Penrose Conference (1972) to use the Troodos Massif as the template for the 'typical' ophiolite sequence, also known as the 'Penrose Stratigraphy'. The idealised Penrose stratigraphy is shown in Fig. 1.1-1.

The main units of the Troodos Massif are: Mantle sequence; Plutonic Complex, comprising mainly gabbros with cumulates in the lower section and plagiogranites near the upper boundary; Sheeted Dyke Complex consisting of dolerite dykes and the lava sequence. The lava sequence was subdivided into three groups; the Basal Group, the Lower Pillow Lavas and the Upper Pillow Lavas (Wilson, 1959).

Fig. 1.1-1 Idealised Penrose Stratigraphy, redrawn after Gass (1979)

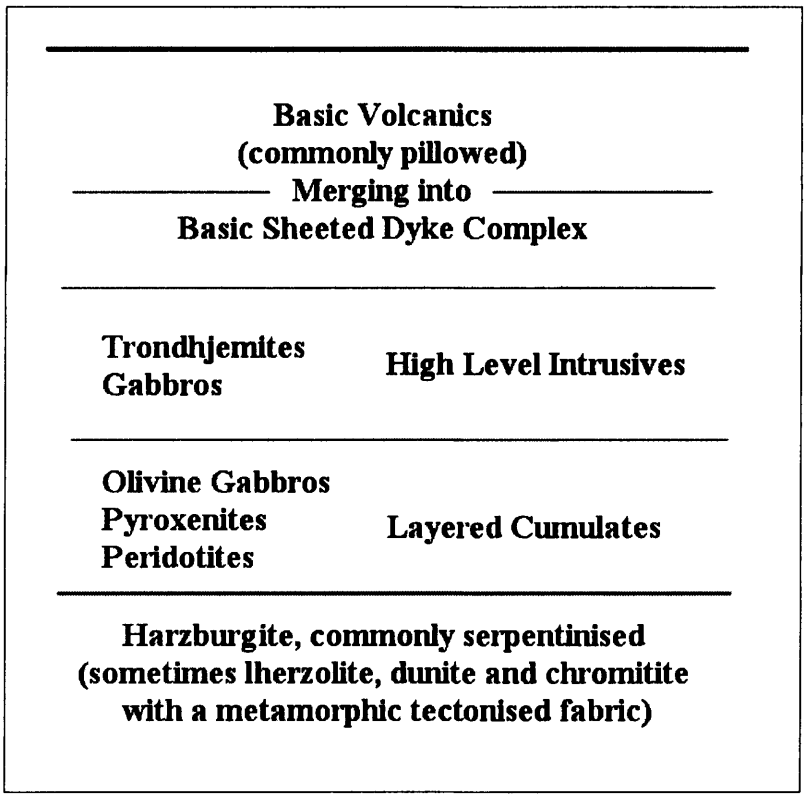

The mantle portion of the Troodos Massif comprises mainly depleted, and partially serpentinised, tectonised harzburgites containing sporadic dunite and chromite deposits. Chromite and serpentinite in the form of asbestos are found in historically commercially viable quantities. A large negative gravity anomaly beneath Mt Olympus may represent a serpentinite diapir that may also be responsible for the Uplift of the ophiolite (Gass and Masson-Smith, 1963).

The majority of the plutonic complex is a 1.5 km thick (average) layer of gabbros. At its base, there is a thin layer of mainly clinopyroxenite cumulate, before the material grades upward into coarse gabbro. Within the gabbro, especially near the base, there are also noritic and wehrlitic bodies. Benn and Laurent (1987) interpreted the plutonic sequence of the Troodos Massif as composed of several structurally distinct suites resulting from multiple magma supply events. Ultramafic peridotite to pyroxenite cumulates in the lower levels of the plutonic complex may represent the floor of magma chambers initially filled with picritic magmas (Thy, 1990). The gabbros are

fresh and display mostly primary mineral assemblages, with actinolite generally replacing pyroxenes only along grain margins, indicating insufficient fluids at depth to promote metamorphic reactions (Hebert and Laurent, 1990). Towards the upper boundary of the gabbros, dykes of zircon-bearing plagiogranite can be found. At the roof of the complex, plagiogranite bodies (diorite to granophyre) are found as sills, dykes, and screens within the gabbros. The top of the plutonic complex grades into the Sheeted Dyke Complex.

The majority of the exposed ophiolite comprises the Sheeted Dyke Complex (SDC). The majority of the dykes within the SDC have an approximately north-south trend. In the south east of the ophiolite, just to the north of a prominent valley (visible on Fig. 1.1-2 as the east-west trending line of lavas cutting the southern portion of the SDC) these dykes trend more north east-south west and curve asymptotically into the valley. Near the village of Mandria, about 5 km south of the summit of Mount Olympus, the strike of the dykes changes from asymptotically curved to straight and approximately north-south. The sheeted dyke complex is generally about 2 km thick, although the thickness is somewhat variable. Such variability caused the failure of the CY4 borehole to reach the Moho, as the SDC proved particularly thick around the village of Palaichori where CY4 was sited.

Diabase dykes, ranging from basalt to rhyolite, represent magma in transit from crustal reservoirs to the ocean floor. The dykes, fine-grained and only sparsely phyric, are extensively altered to greenschist-facies. The relatively high-temperature oceanic metamorphism (i.e. greenschist facies), contrasting with very low temperature alteration of the pillow-lava series and relatively fresh condition of the plutonic complex, is ascribed to a combination of heat from the plutons and diminished flow of circulating marine waters from above (Baragar et al. 1990). Igneous textures and clinopyroxene relicts are commonly preserved in the lower part of the section. Up to 1-km-wide epidosite zones formed at the base, directly above high-level plutons, a product of hydrothermal reactions at temperatures of 350°–400°C (Richardson et al. 1987). Dykes at the lower boundary both cut, and are cut by, gabbros and plagiogranites of the plutonic complex and pass upward to the volcanic assemblage through a mixed zone with lava screens some tens of meters to 2.3 km thick ("Basal Group"). The zone composed entirely of dykes is about 750 m thick.

A broken ring of lavas surrounding the SDC forms the outer rim of the Troodos Massif. The lava sequence varies between 0.5 and 1.5 km thick (Wilson, 1959), (Rautenschlein et al., 1985). The lava pile is composed of mainly basaltic to andesitic pillow lavas interspersed with sheet flows and dykes.

In the north of the Troodos Massif, the lava outcrop stretches from Kokkina in the west to Margi in the east, and is generally 3 – 6 km across. The easternmost 10km of the exposed ophiolite, from Margi to Stavrovouni (at the south eastern corner of the Troodos Massif), is composed entirely of lavas, the majority of which belong to the Upper Pillow Lava unit (UPL). 10 km to the east of the main outcrop of the Troodos Massif lies the Troulli Inlier, also composed mainly of UPL. Lavas are exposed in a narrow, broken band along the southern margin of the ophiolite, from Lefkara (in the south eastern portion of the lava outcrop) to Limni at the far western edge of the lava outcrop. Tectonic activity has broken up the southern Troodos lava sequence considerably. The lava sequence in this section is no greater than 4km wide in the Limni area. 10 km to the west of Limni lies the Akamas area. The Akamas area is detached from the main portion of the ophiolite by faulting and is composed of a broken sequence of SDC and lavas. The overall layout of the Troodos Massif is shown in Fig. 1.1-2.

A number of metal sulphide bodies are located within the lava sequence, typically, but not always at the upper boundary of the Lower Pillow Lava sequence. These copper-rich massive sulphide deposits are relicts of hydrothermal vent systems, which are associated with black smoker vents at modern ocean ridges. These massive sulphide deposits have been commercially viable. Metal-rich hydrothermal deposits are also responsible for the intermittent umber deposits that overlie the Upper Pillow Lavas. The umbers and Upper Pillow Lavas are in turn overlain by radiolarian cherts.

Fig. 1.1-2 Location and geological map of the Troodos ophiolite based on the Geological map of Cyprus (Geological Survey of Cyprus, 1995)

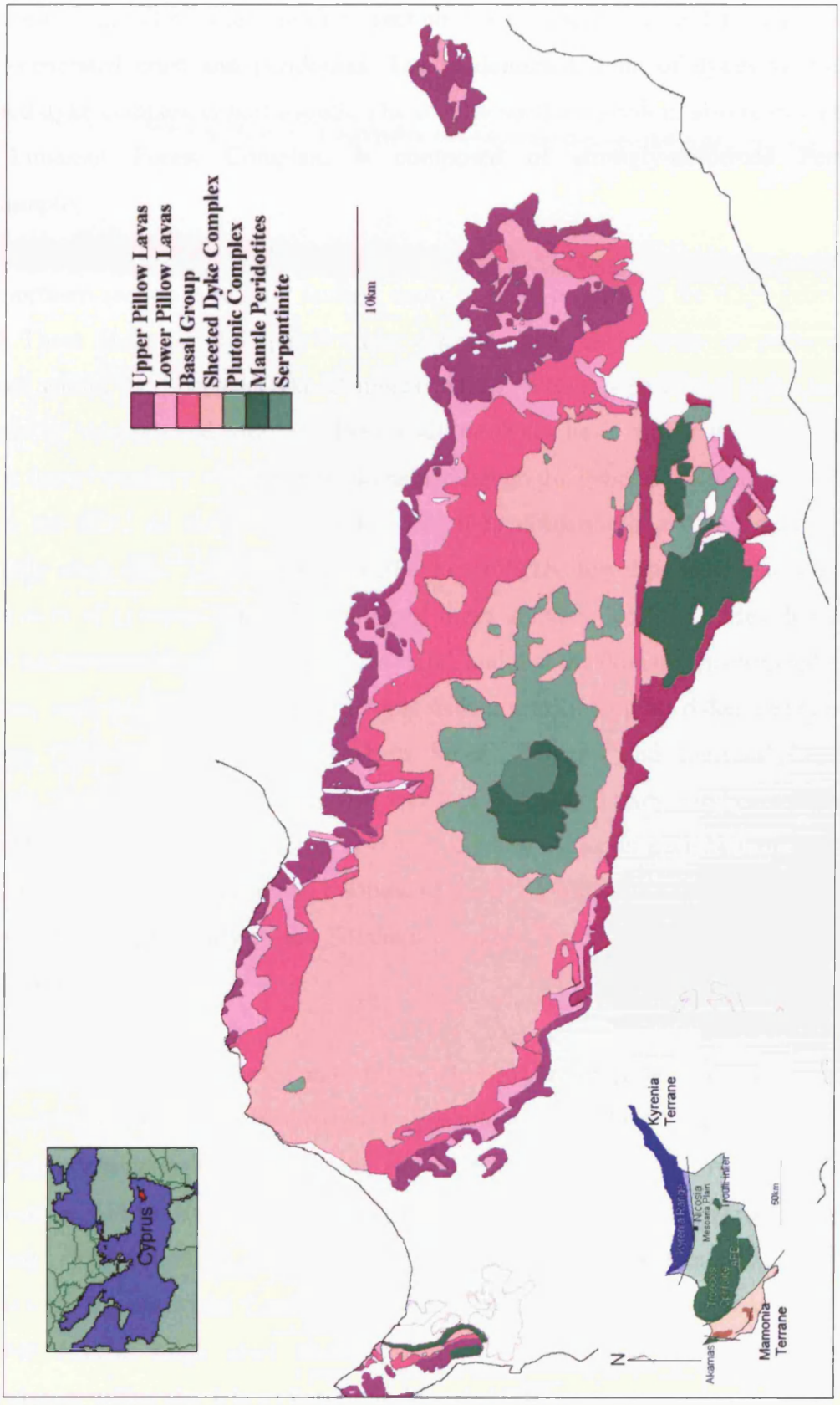

1.2) Structure of the Troodos Ophiolite

The Troodos Massif is composed of two main sections that are separated by a fossil transform fault. The larger, northern section is composed of complete sequence of ridge-generated crust and peridotites. The predominant trend of dykes within the sheeted dyke complex is north-south. The smaller southern section, also referred to as the Limassol Forest Complex, is composed of strongly-deformed Penrose stratigraphy.

The northern section is heavily faulted, many of them original to the ridge-generated crust. These faults cut the ophiolite into discrete units. These units are particularly evident within the Sheeted Dyke Complex (SDC). Within a particular unit, (termed domain by Verosub and Moores, (1981)), all the dykes have similar trends and dips, with a sharp boundary with the next domain although the general orientation of dykes within the SDC of the main Troodos Massif is north-south and the dykes have generally steep dips. Tectonically rotated dykes with shallow dips may also be found in the axes of grabens. Further mapping of these domains led to the idea that there was a ductile transition at the base of the SDC, and that the domains determined three grabens, each trending north to northwest with inwardly-dipping dykes (Varga and Moores, 1985). They named these grabens 'Solea', 'Mitsero' and 'Larnaca'. Fig. 1.2-1 shows the boundaries of the grabens and their calculated axes. Graben axes were calculated from the relationships of inwardly-dipping dykes on each side of the axis. Also shown are dyke orientations throughout the SDC, indicating the change in dyke orientation with proximity to the Southern Troodos Transform Fault (STTF) to the east of Mandria.

The eastern flanks of the Solea and Mitsero Grabens are considerably narrower than their western flanks. Also, the cross-cutting relationships of faults and dykes indicate that graben formation was progressing eastwards, truncating older structures (Varga and Moores, 1985). He termed this 'ridge-jumping'. The distance covered by ridge-jumping is approximately 8km between the Solea and Mitsero Grabens and 11km between the Mitsero and Larnaca Grabens. The Larnaca graben is complex and involved several ridge crest re-orientations, resulting in complex cross-cutting relationships within the dykes (Varga and Moores, 1985).

Fig. 1.2-1 Simplified map of dyke domains within the Sheeted Dyke Complex of the Troodos Massif. This shows the relative position of the three major graben structures (Solea, Mitsero and Larnaca) as well as their margins and axes. Section A-B shows location of Fig. 1.2-2 (Allerton and Vine, 1991).

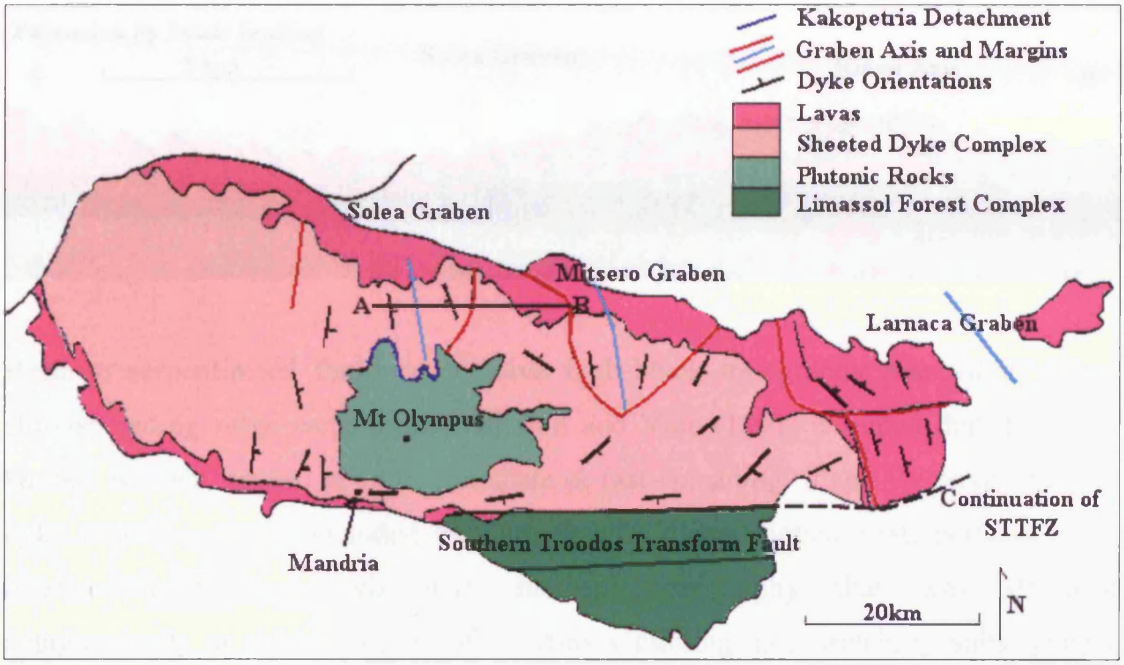

Within the axis of the Solea Graben, some of the tectonic blocks have been back-tilted by up to 90°. Wherever dykes and lavas could be measured at the same outcrop, they are perpendicular to each other. This is proof that the dykes were originally vertical. However, sediments overlying the ridge-generated crust do not show graben-type faulting, proving that the grabens are an ophiolite structure, not a later tectonic structure. Magnetic anomalies were used to determine exactly how much the blocks had been rotated, in order to re-assemble the structure. The recent Karyotis Valley runs down the centre of the graben due north of Mount Olympus. In places, the SDC is exposed in the riverbed of the valley, yet the surrounding hills composed of gabbro. The 10° northward tilt imparted to all of the northern ophiolite by the uplift of Mount Olympus provides a full three-dimensional view of the graben.

On the western side of the graben, the dykes dip steeply several kilometres from the graben axis, the dips becoming less towards the axis. On the eastern side, the dips are fairly steep, with occasional blocks of shallow-dipping dykes (Allerton and Vine,

1987) as shown in Fig 1.2-2. The unusual thinness of the plutonics beneath the Solea Graben may be a result of post-magmatic tectonic extension (Varga, 1991).

Fig. 1.2-2 Solea Graben cross section (Allerton and Vine, 1987)

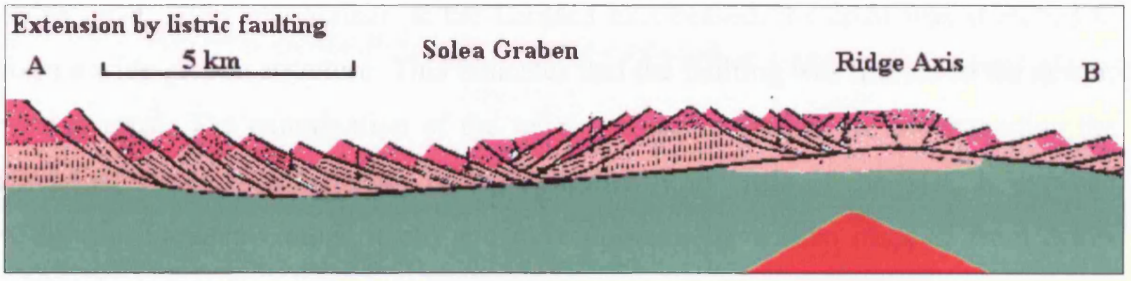

Because serpentinised faults or massive fault-block topography associated with a slow-spreading ridge were found, Allerton and Vine (1991) assumed that the Solea Graben was not formed at an intermediate or fast-spreading ridge. By reconstructing dyke domains, they concluded that the Solea Graben formed first, perhaps at an intermediate-spreading axis with subdued topography that was stretched amagmatically at the end of its life. Off-axis faulting and stretching subsequently produced the Mitsero Graben to the east. Formation of this graben was not accompanied by magmatism.

Some blocks within the Solea Graben may have been re-tilted during the migration of tectonic activity eastwards. As the spreading direction changed, the Solea axis became amagmatic, stretching on a listric detachment along the brittle-ductile transition line (Kakopetria detachment), which formed the Solea Graben. Later dykes are recorded cutting the Kakopetria detachment (Malpas, 1991). These late-stage dykes have mineralogies similar to those observed within the UPL, which overlies the extensively tilted Lower Pillow and Basal lava sequence. This would indicate that, in this area at least, the UPL post-date major tectonic activity.

There are two main sets of faults within the Solea Graben: low angle detachment faulting at the base of the SDC, composed of a number of short fault segments and steeper ramps and steps; and graben-defining faults (Hurst et al., 1994). The fracture

zone around the detachment may be up to 100m thick, extending 30m into the SDC. However, in other places, gabbro only 1m from the fault is undisturbed.

The Larnaca Graben is a kinked structure, containing a minor leaky transform (Varga and Moores, 1985) located around Kornos, which cuts into the eastern side of the Solea crust. After magmatism at the Larnaca axis ceased, the crust was stretched to form a wide graben structure. This indicates that the faulting was limited to the newer, weaker crust. The examination of the relict grabens is the key to understanding the spreading structure and history of the ophiolite. Very little of the SDC is exposed within the Larnaca Graben itself, and dyke domains have been mapped from dykes within the lavas.

The Arakapas Fault Belt (AFB) and Limassol Forest Complex (LFC)

The Limassol Forest Complex is separated from the main portion of the Troodos Massif by a paleo-transform fault, originally termed the Arakapas Fault Belt (AFB) or Southern Troodos Transform Fault Zone (STTFZ) (MacLeod, 1990). Much of the area commonly mapped as the LFC comprises transform fault material, spread over 5 – 10 km. The exposure of the fault zone is wider in the Western LFC (WLFC) than the Eastern LFC (ELFC) (Fig 1.2-3). The present Arakapas Valley mimics the original AFB topography at reduced relief, the valley floor containing volcaniclastic sediments and lava flows (Simonian and Gass, 1978). Within the transform fault zone, blocks of serpentinite and gabbro are exposed. The serpentinites have probably been intruded diapirically as also been proposed for some modern transforms (Bonatti, 1976).

The Arakapas Fault Belt is a major strike-slip fault zone, trending east-west in the southern portion of the Troodos ophiolite. It is an ocean-floor feature, overlain by undeformed pelagic sediments and orientated perpendicular to the general strike of the SDC. It has been recognised as the foremost example of a fossil transform fault within an ophiolite. The slip direction is thought to be dextral (MacLeod and Murton, 1993).

To the south of the Arakapas Fault Belt (AFB) lies about 50 km^2 of oceanic crust (MacLeod and Murton, 1993) which also displays the 'standard' ophiolite

stratigraphy defined by the Penrose Conference on Ophiolites in 1972. This region is also referred to as the 'Anti-Troodos' plate (Fig. 1.2-3), formed from the southwards (current orientation) continuation of the spreading ridge axis. The Limassol Forest Complex was mapped in detail in two parts: the eastern side formed the basis of the PhD thesis of MacLeod (1988), and the western part formed the basis of the PhD thesis of Murton (1986). These workers continued studies by Gass et al. (1975).

The mapping by MacLeod et al. (1990) just to the north of the Arakapas Fault Belt (AFB) reveals a sudden change in the strike of the dykes in the Sheeted Dyke Complex around the village of Mandria. Mandria lies in line with the Solea Graben (Varga and Moores, 1985), and the dykes change from AFB-parallel to AFB-perpendicular at this location. MacLeod (1990) interpreted this as the result of the changeover from transform-rotated dykes (Allerton and Vine, 1987) to non-rotated dykes that formed on the inactive fracture zone side of the ridge-transform intersection. In this area, there are also wedge-shaped dykes with their wider ends nearer the AFB. The fact that they cut the SDC means that they are later and may represent in-fill between rotated blocks. Paleo-magnetic studies by MacLeod (1990) also showed that the entirety of the Troodos Massif has been rotated 90° anticlockwise since its formation. This rotation has implications for the interpretation of geochemical patterns.

Fig. 1.2-3 Map of dyke domains and inferred locations of the Southern Troodos Transform Fault, and an Extensional Relay Zone in the Western Limassol Forest Complex. (MacLeod, 1990)

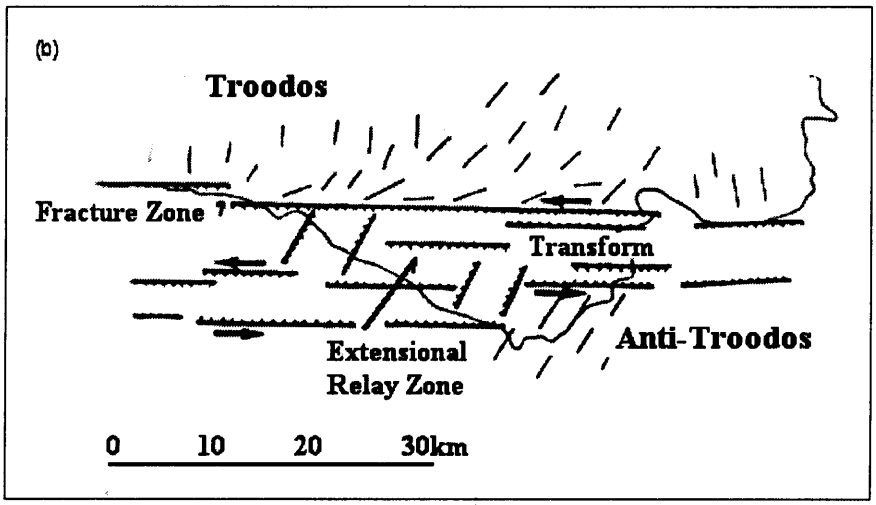

The width of the transform Fault in the ELFC is estimated at about 5km (MacLeod, 1990), somewhat less than estimated by Murton in the WLFC. An analogy for the STTFZ could be the Tamayo Transform (MacDonald et al., 1979), a complex transform that has extensional relay zones resulting from the instability of single zone in a fast or medium slip transform (Fox and Gallo, 1984). The presence of an extensional relay zone allows for magmatism and exhumation of mantle peridotites within the transform environment.

Unusual boninite lavas found in the transform zone were fed from dyke swarms associated with ultrabasic plutons intruded into the transform while it was still mobile. The transform sequence gabbros typically have a hydrous mineralogy, including minerals such as various green amphiboles (Murton, 1986). Within the western Limassol Forest Complex and the Akapnou Forest there are a number of shear zones, between 20 and 500m wide and traceable over several km, that contain mainly serpentinised mantle and gabbros. Evidence of brittle deformation exists as well as ductile serpentinised shear zones which, on closer inspection, show evidence of sinistral shear (Murton and Gass, 1986).

The coexistence of brittle and ductile shear together with evidence for unconformities within the lava sequence led MacLeod and Murton (1993) to infer that the Western Limassol Forest Complex (WLFC) mantle sequence underwent progressive exhumation. The dip of some of the lavas from increases over a short distance. Tilting of the seabed during magmatic activity has resulted in slight angular unconformities in some places. This is therefore evidence for concurrent magmatism and tectonism. Clasts of mantle rocks within sediments are evidence for exposure of harzburgites on the seafloor.

Early mapping of the Eastern Limassol Forest Complex (ELFC) by Pantazis (1967) did not record such a strong east-west tectonic fabric as found in the WLFC. Detailed re-mapping has shown that the structure of this portion of the ELFC is comprised of a series of blocks of 4km thick axis-generated crust which is highly tilted and separated by low angle detachment faults (MacLeod, 1988).

Stratigraphic reconstructions from the main part of the Troodos Massif indicate that the axis sequence is approximately 5.5km thick (Wilson, 1959). However,

reconstructions from the Kapilio area of the WLFC indicate that the axis sequence is only about 3.6 km thick. The WLFC is comprised mainly of serpentinised harzburgites surrounded and overlain by axis lithologies. It contains a strong E-W tectonic fabric with brittle deformation commonplace. A number of serpentinised shear zones and basic intrusions also cut the ultrabasic core. The harzburgite is regarded as the residual mantle from axis melting (Moores and Vine, 1971, Gass and Smewing, 1973). The latest dykes cutting the complex are picritic and may be associated with wehrlitic intrusions. They trend at approximately 050°. The lavas in the Kapilio and Akrounda (Fig. 1.2c-4) areas are divided into two units, a lower aphyric unit, much like LPL and an upper unit of olivine-phyric basalts and limburgites (glassy orthopyroxene-bearing high MgO and low TiO_2 basalts) intermixed with volcaniclastic sediment.

The northern part of ELFC in the Akapnou area contains some mantle rocks, consisting of harzburgites and dunites cut by E-W trending serpentinite mélange zones. There is also evidence for transform magmatism similar to that from WLFC in the form of a few mafic dykes, which are presumably feeders to boninite lavas. To the south of the AFB lies the Anti-Troodos Plate (ATP), on which there are exposed pillow lavas and SDC. The lavas of the ATP are geochemically variable, with some lavas that are similar to those from the northern portion of the Troodos Massif, and others that are boninitic. Boninitic lavas are generally found in proximity to the AFB, but they have also been recorded from Kalavasos, Monagroulli and Parekklisha (Fig. 1.2-4) (Cameron, 1985; MacLeod, 1988). Fig 1.2-4 shows locations of all sites named in this section.

Fig. 1.2-4 Map of locations discussed in this chapter

1.3) The lava groups

Upper pillow lavas (UPL)

The UPL are a relatively uniform accumulation of basalt flows that are largely free from intrusive material (Wilson, 1959). The main rock types within the UPL are pillowed basalt, olivine basalt and picrite. The UPL are dominantly olivine-bearing augite basalts with picritic and limburgitic units. Generally, they are heavily altered by seafloor weathering processes.

Taylor (1987) noted that, in the Margi area, the UPL were extruded in several cyclical units, with a picritic base, grading upward into aphyric basalt and topped with glassy, olivine-phyric basalts. Within this area, there are ultrabasic lavas in addition to the more widespread basalts. Because of their titanium content they have also been termed 'Low Titanium Series' LTS lavas (Bednarz and Schmincke, 1994). The composition of the olivines is such that they are unlikely to have come from crystal settling from basaltic magma, but more likely to have crystallised from a homogeneous melt. Cumulus olivine crystals within UPL reduce the concentration of most elements except Ni and Mg by dilution; Cr is also increased by the presence of Cr spinel. Proposed origins for UPL include an off-axis seamount (Gass and Smewing, 1973) and off-axis fissures (Schouten and Keleman, 2002). In the Margi area, which lies mainly within the UPL, small ultrabasic lava flows have been recognised and sampled (Gass, 1960). These authors described the UPL as reddish grey rocks with phenocrysts of olivine and clinopyroxene.

An unconformity has also been noted in places between the lower and upper lavas (Gass, 1968; Gass and Smewing, 1963). The unconformity separates the silica under-saturated UPL from the silica-oversaturated basalts of the LPL which also display extensive silica metasomatism. There is also a break in the metamorphic grade of the units, the LPL belonging to upper zeolite and greenschist facies and to lower zeolite facies, this implies that alteration took place mainly before the extrusion of the UPL, during a hiatus in volcanic activity. Coarse picritic sills are common except in the upper 100m of the UPL.

Lower Pillow Lavas (LPL)

The LPL may contain up to 50% intrusive material and have a complicated contact with the UPL that is gradational in places and unconformable in others. Pillows may have glassy rims and are vesicular (Wilson, 1959). They are mainly aphyric, consisting mainly of altered augite and plagioclase and glass. Alteration is typically of the lower greenschist facies, with silica, and celadonite smectite, epidote and chlorite commonplace. The LPL are formed of massive sheet flows and pillowed flows and breccias (Taylor and Nesbitt, 1988) and have a tholeiitic composition.

The Akaki canyon in the north east of the Troodos Massif is considered to be the type section for the LPL. The Akaki section is comprised of twelve distinct units (Rautenschlein et al., 1985), having formed from successive extrusive events. As part of the Cyprus Crustal Study Project, several boreholes were sunk through the lava sequence in the Akaki and Agrokipia areas. At the CY2A borehole, the LPL mostly consists of massive sheet flows rather than pillow lava (Erzinger et al., 1992). Multiple flow units were recognised within the CY1 and CY1A boreholes (Malpas, 1991) The total thickness of the lava pile in the Akaki canyon is about 1600m with part of the section repeated by faulting (Schmincke et al., 1983). Compositionally, they have higher titanium and other incompatible element contents than the UPL or the Basal Group indicating that they are more fractionated (Robinson, 1983, Taylor and Nesbitt, 1988, Sobolev et al., 1993).

The absence of a cross-cutting relationship between the LPL and BG led Wilson (1959) to conclude that the two groups represent a single volcanic episode. However, he was able to distinguish them on the basis of intrusive content, defining BG as having over 50% intrusive material and LPL containing less than 50% intrusive material.

Basal Group (BG)

The 'Basal Group' was a term coined by Wilson (1959) to describe the lowest portion of the lava pile. The Basal Group is composed of altered dykes separated by screens of altered (up to greenschist facies) pillow lava, rarely over 50 feet wide. Dykes are

still discernible as their chilled margins weather less rapidly than coarser dyke interiors. Glassy pillow rims have been recorded within the lavas of the Basal Group in the Yialias area by Portnyagin et al. (1997).

Bear (1960) decided that the BG were a downward continuation of the LPL based on mineralogy. However, olivine phyric basalts and picrites were discovered near Lithrodonda (Desmet, 1976), indicating that, at least in places, the composition of the lavas varies with depth. Similar primitive BG lavas were later found in the Yialias canyon (Taylor, 1986).

The use of differing methods and study areas used by various authors has caused significant inconsistencies in mapping the boundaries between the lava units. Earlier workers, such as Wilson (1959) and Bear (1960) used field evidence, such as mineralogy (especially olivine content and metamorphic grade) and proportion of intrusive material. Robinson et al. (1983) used ratios of major elements to determine variations in depletion and fraction in glasses from the UPL and LPL in the Akaki area. Later workers such as Schmincke et al. (1991) and Sobolev (1993) have focused more closely on element contents and ratios working in the Margi and Lithrodonda areas. They, however, obtained very different results than Cameron (1985) and Flower and Levine (1987) who concentrated on lavas from the Limassol Forest Complex and south western Troodos. This variation in opinion indicates that there is no 'right' or 'wrong' way to classify the lavas.

1.4) Geochemical fingerprinting of the Troodos Massif, an evolution of ideas.

Gass, 1968

Gass and Masson-Smith (1963) postulated that the Troodos Massif formed in an oceanic environment. Gass (1968) tested this hypothesis by analysing 33 samples from the Troodos lava sequence for major elements. The results were highly variable as a result of "hydration, saussuritization, uralitization and chloritization". Generally the data most resembled tholeiitic basalts. Compared to Hawaiian basalts (OIB), they were lower in TiO_2 and Fe_2O_3 and higher in alkali elements (K_2O, Na_2O). Compared to abyssal basalts (MORB), they were lower in TiO_2, Al_2O_3, CaO and Na_2O, but higher in K_2O. Gass (op. cit.) concluded that that the Troodos Massif most likely formed as a volcanic pile that evolved on the Tethys mid-ocean ridge.

Moores and Vine, 1971

Moores and Vine (1971) found that major element analyses of Upper Pillow Lavas (UPL), Lower Pillow Lavas (LPL) and Basal Group (BG) / upper sheeted dyke complex (SDC) are chemically similar to known oceanic tholeiites. UPL specimens had low SiO_2 and variable alkali content, showing some calc-alkaline affinities. LPL were characterised by high and variable SiO_2 and low K_2O, with an alkali content which is less variable than that of the UPL (Fig. 1.4-1). On this diagram, LPL plots mainly within the tholeiite field and the UPL within the alkali field. This would imply that the lavas had different sources. Comparison of the K_2O content between UPL, LPL and the SDC showed that LPL and SDC were compositionally similar, but that the UPL formed a distinct group (Fig. 1.4-2). Distribution of K_2O abundances, when plotted on a histogram, show that the majority of LPL and SDC samples have K_2O content between 0.1 and 0.9 wt% and the peak value around 0.25%. The spread of K_2O contents from the UPL samples was far wider, with highly variable K_2O contents. However, Moores and Vine (op. cit.) did note that metabasalts from Australia revealed the possibility that the high and variable alkali content could have been due to alteration.

Fig. 1.4-1. Alkali - silica plot for the upper pillow lavas (UPL) and lower pillow lavas (LPL) of the Troodos Massif from Moores and Vine, (1971). The dividing line between Alkali and Tholeiite based on Hawaiian basalts (McDonald and Katsura 1964) Total alkali content = $Na_2O + K_2O$

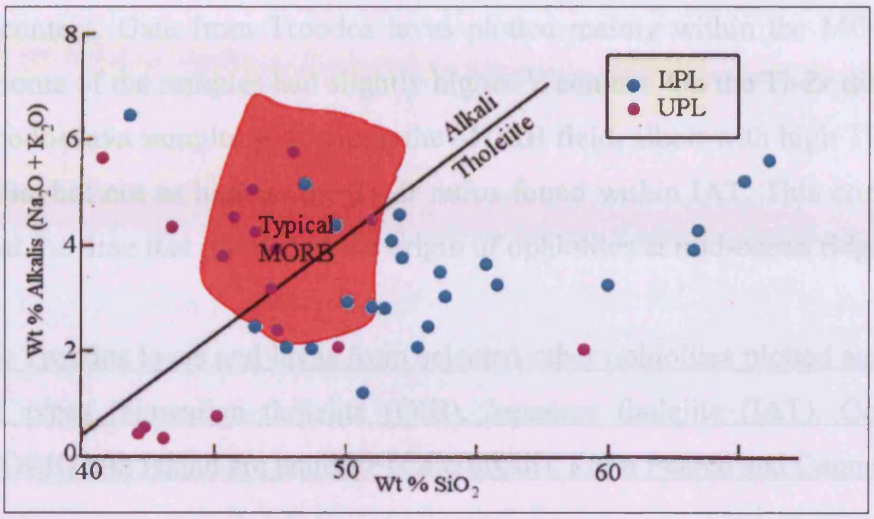

Fig. 1.4-2. Histogram of K_2O contents between lava groups of Upper Pillow Lavas (UPL), Lower Pillow Lavas (LPL) and Basal Group (BG) / upper sheeted dyke complex (SDC) from Moores and Vine, (1971)

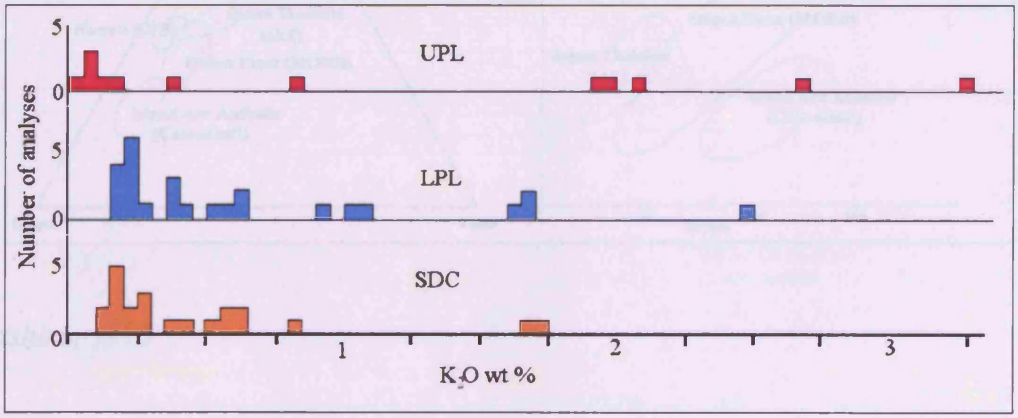

Pearce and Cann, 1971

Using a Ti-Zr graph and a Ti-Zr-Y plot (Fig. 1.4-3), Pearce and Cann (1971) attempted to classify four ophiolites by plotting them against known lava types. The lava types used were ocean-floor basalt (equivalent to MORB), Japanese tholeiite

(type of IAT), Hawaiian tholeiite (example of OIB) and island arc andesite. Samples from Troodos (and most other ophiolites) plotted mainly within the ocean-floor basalt field, with a couple of outliers within the Japan tholeiite field (Fig. 1.4-3). On the Ti-Zr-Y diagram, the calc-alkali, MORBs and the IAT lavas all have approximately equal Y content with Zr content increasing from IAT to calc-alkaline. OIBs have lower Y content. Data from Troodos lavas plotted mainly within the MORB field, although some of the samples had slightly higher Y content. On the Ti-Zr diagram, all of the Troodos lava samples plot within the MORB field, albeit with high Ti-Zr ratios for MORBs, but not as high as the Ti-Zr ratios found within IAT. This corroborated evidence at the time that pointed to the origin of ophiolites at mid-ocean ridges.

Fig. 1.4-3. Troodos lavas and lavas from selected other ophiolites plotted against lava 'standard' types (Hawaiian tholeiite (OIB), Japanese tholeiite (IAT), Ocean-floor basalt (MORB) and Island arc andesite (Calc-alkali). From Pearce and Cann (1971)

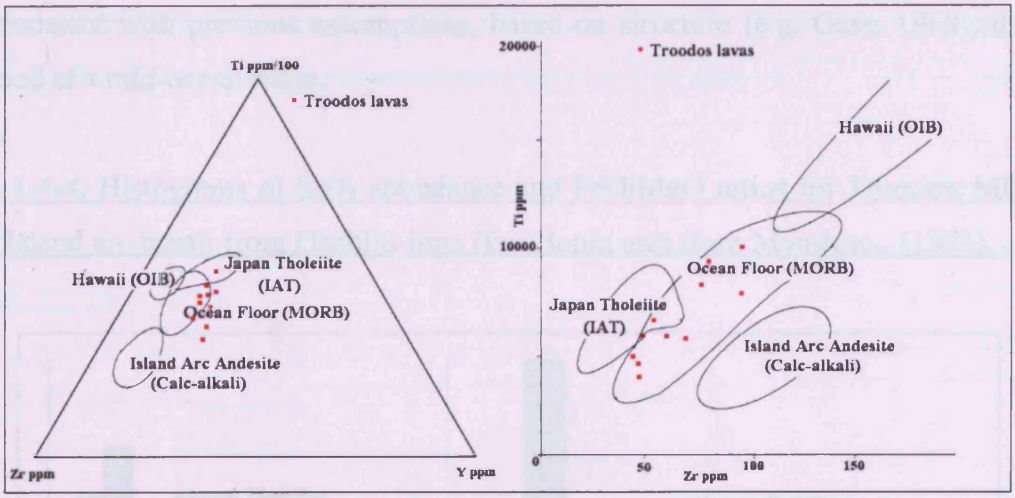

Myashiro, 1973

Myashiro (1973) determined that, using major elements, about one third of the samples analysed from the Troodos lava sequence displayed affinities to calc-alkaline volcanics. He claimed that the geochemistry was consistent with the idea that Troodos formed as a basaltic volcano in an island arc. He used frequency histograms of element abundance and ratios to compare Troodos with MORB and with lavas from Hachijo-jima, an island arc volcano in the Izu-Bonin arc south of Japan. Troodos

lavas most resembled Hachijo-jima in terms of dispersion of SiO_2 values and FeO/MgO ratios (Fig. 1.4-4). Frequency histograms of SiO_2 content of MORBs show a narrow range of compositions, typically with 75% of values between 47 and 52% SiO_2. Histograms of SiO_2 content of lavas from Hachijo-jima show a wide dispersion, with lavas between 47 and 70% SiO_2. Histograms of the SiO_2 content of lavas from the Troodos Massif also show a wide range of compositions, with lavas between 47 and 75% SiO_2, which is similar to lavas from Hachijo-jima.

Histograms of FeO/MgO ratios of MORBs also show a narrow range of compositions, with FeO/MgO ratios between 0.5 and 2. Histograms of FeO/MgO ratios of lavas from Hachijo-jima show a wide range of ratios between 1.5 and 5.5. Histograms of FeO/MgO ratios of lavas from the Troodos Massif also show a wide range of compositions, with ratios between 0.5 and 7. There is a peak in the Troodos between 1 and 2.5. This would indicate that the Troodos lavas have some properties intermediate between MORB and IAT. However, the idea that Troodos formed at an island arc was inconsistent with previous assumptions, based on structure (e.g. Gass, 1968), that it formed at a mid-ocean ridge.

Fig. 1.4-4. Histograms of SiO_2 abundance and FeO/MgO ratios for Troodos, MORB and Island arc basalt from Hachijo-jima (Izu-Bonin arc) from Myashiro, (1973).

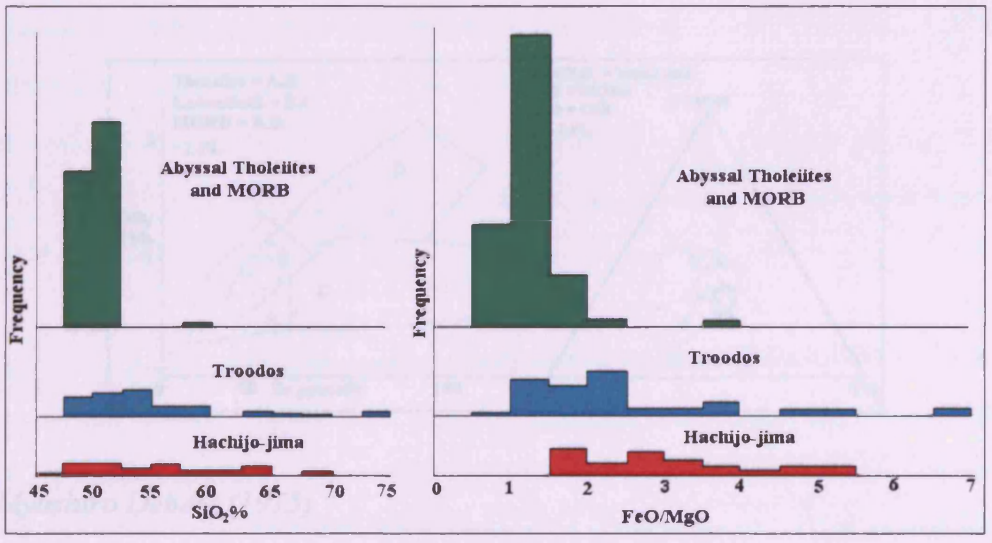

Pearce and Cann, 1973

Pearce and Cann (1973) attempted to expand their geochemical database and their basalt discrimination methods using Ti, Zr, and Y (Pearce and Cann, 1971) by including Sr and Nb. They tested these discrimination methods on ophiolite basalts, including the Troodos Massif. Sr is mobile during weathering, so the Ti-Zr-Sr plot can only be used for fresh material. On a Ti v Zr diagram, including the addition of extra data, Troodos LPL plots mainly within MORB and IAT fields (which overlap considerably). Plotting the data on a Ti-Zr-Y triangle produces a similar result (Fig. 1.4-5). The clarity of the diagram was improved by using Y ppm *3 instead of Y ppm in Pearce and Cann (1971). Although this does not help much in determining whether the basalts had an island arc or mid-ocean ridge origin, it does rule out a calc-alkaline origin, contradicting the Myashiro (1973) assertions. Pearce and Cann (1973) also proposed the use of Nb as an alkalinity indicator for altered rocks because Na/K values are affected by alteration. A Y/Nb ratio of over 8 indicates tholeiitic characteristics. Troodos samples all had Y/Nb > 8, demonstrating that the samples with alkaline major-element characteristics were, in fact, altered.

Fig. 1.4-5. Ti-Zr and Ti-Zr-Y diagrams for Troodos Lower Pillow Lavas (LPL) showing that island arc or MORB lava origins were both possible (from Pearce and Cann, 1973)

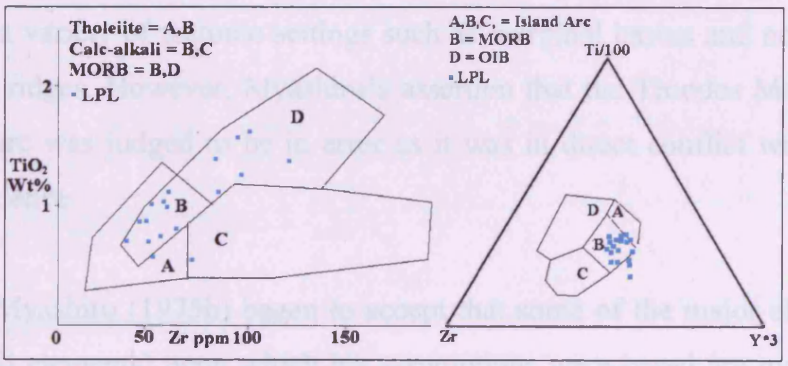

The Myashiro Debate (1975)

The apparent inability to reconcile the differences between the 'island arc' hypothesis of Myashiro (1973) and the 'ocean ridge' hypothesis of other workers, such as Pearce

and Gass concerning the origin of the Troodos Massif caused a lively debate, played out on the pages of *Earth and Planetary Science Letters* in 1975.

Hynes (1975) criticised Myashiro's work on the basis that the heavily-altered rocks of the LPL and SDC cannot validly be compared with fresh material, either from the ocean floor or an island arc. From mineralogical data alone, it was not possible to distinguish between a mid-ocean ridge or island arc origin for the Troodos Massif. However, by comparison with other ophiolites (such as those in Greece; Hynes et al., 1972), structural evidence supports a mid-ocean ridge origin. Therefore he argued that bulk chemical analyses of altered rocks can have little weight in the argument.

In defence, Myashiro (1975a) claimed that the samples used were not heavily metasomatised, and also that these rocks were genuinely andesitic or dacitic. In addition he stated that volcanic rocks with FeO/MgO ratios between 2 and 4 were common in island arcs, whereas ocean floor basalts have FeO/MgO ratios between 0.7 and 2. As a result, he claimed that, because about one half of the Troodos samples had FeO/MgO ratios between 2 and 4, this was ample evidence against mid-ocean ridge formation. The lack of discrimination between island arc lava and MORB on the Pearce and Cann (1973) diagram (Fig 1.4-5) using immobile trace elements failed to disprove Myashiro's (1973) theory because of the overlap between these fields.

Later Moores (1975) accepted that Myashiro was correct to speculate that ophiolites may form in a variety of tectonic settings such as marginal basins and not be limited to mid-ocean ridges. However, Myashiro's assertion that the Troodos Massif formed in an island arc was judged to be in error as it was in direct conflict with field and structural evidence.

In response, Myashiro (1975b) began to accept that some of the major elements (for example alkali elements) upon which his assumptions were based are mobile during seafloor weathering. He also acknowledged that also some of the structural similarities between Troodos and mid-ocean ridge crust point to a ridge origin for the ophiolite. He did however reject much of the geochemical arguments put forward, including that of extensive silica metasomatism, claiming that such high levels were not possible at ocean ridges.

Pearce, 1975

Pearce (1975) added new data for UPL to the Ti v Zr and Ti-Zr-Y diagrams of Pearce and Cann (1973). These data had much lower concentrations of incompatible elements than LPL (Fig. 1.4-6). On the Pearce and Cann (1973) diagram, the UPL plot within the IAT field.

In addition to the work done on immobile, incompatible elements, Pearce (1975) studied the immobile compatible element, chromium. Plotting Cr against Ti, MORB and IAT can easily be distinguished (Fig. 1.4-7) This discrimination diagram demonstrates that all Troodos lavas analysed at that time, both UPL and LPL, fell within the IAT sector. Plotting Ti against Cr also distinguished well between LPL and UPL as the UPL had much lower Ti-Cr ratios than the LPL. By using this method to assign provenance to the lava groups, Pearce (op. cit.) showed that some of the high silica samples actually belong to low-silica lava types and therefore that the anomalous silica content was a result of secondary alteration.

Fig. 1.4-6. Ti-Zr and Ti-Zr-Y diagrams for Troodos of upper pillow lavas (UPL) and lower pillow lavas (LPL) showing lower overall incompatible element abundances of the UPL compared to LPL and the location of UPL data within the island arc field. From Pearce (1975)

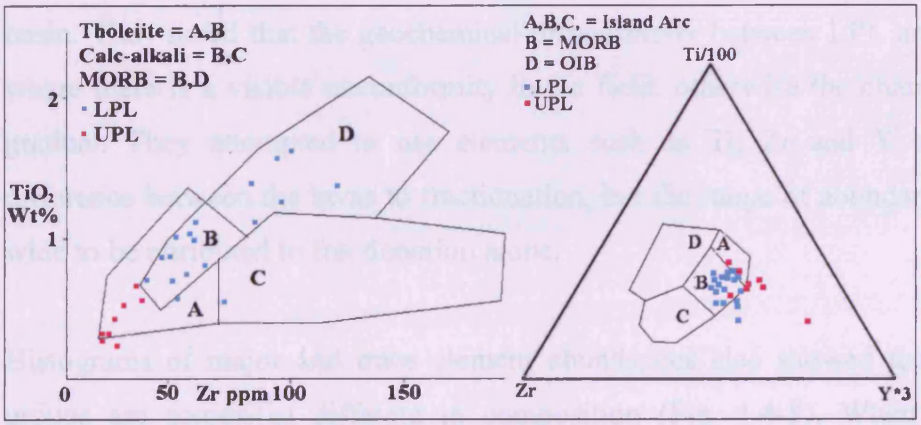

Fig. 1.4-7. Ti-Cr diagram for Troodos lavas from Pearce showing that although both Upper and Lower Pillow Lavas plot within the IAT field, the two lava types have differing compositions (Pearce, 1975).

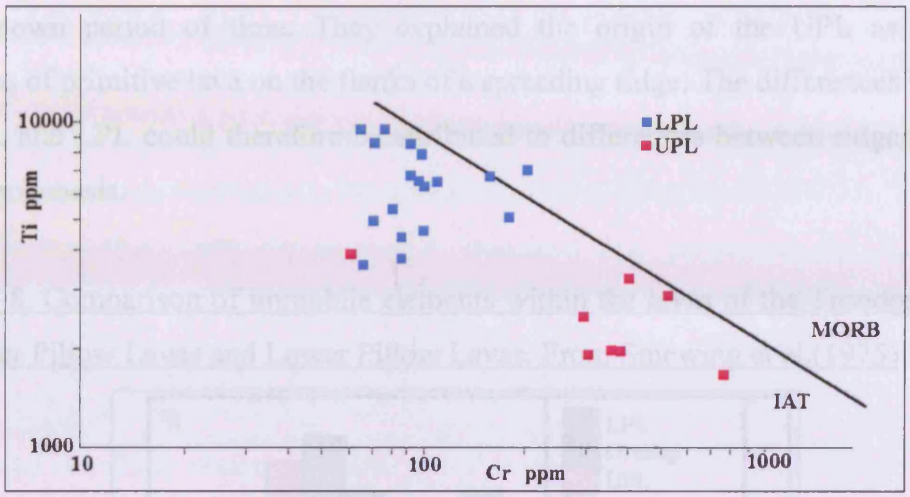

Smewing et al. (1975)

Smewing et al. (1975) also used element abundance histograms to demonstrate that Troodos rocks differ significantly from MORB and are more similar to island arc rocks. Building on the work of Myashiro (1973), and acknowledging the altered nature of the rocks, Smewing et al. (1975) used a range of immobile elements instead. They used Ti, Zr, Hf, Sc, Yb and Y, and Ce and Sr were also reported. They further proposed that the Troodos Massif formed at a slow-spreading ridge in a marginal basin. They noted that the geochemical discontinuity between LPL and UPL is stark where there is a visible unconformity in the field, otherwise the changeover is more gradual. They attempted to use elements such as Ti, Zr and Y to attribute the difference between the lavas to fractionation, but the range of abundances proved too wide to be attributed to fractionation alone.

Histograms of major and trace element abundances also showed that the two lava groups are somewhat different in composition (Fig. 1.4-8). When normalised to MORB, elements such as Ti, Zr, Hf, Yb and Y were generally more abundant in the LPL than in the UPL, although there was some overlap. However, the majority of, even LPL, samples were depleted relative to MORB. Some of the LPL samples had

Zr and Y (and Sr if the values are to be trusted) had sample/MORB ratios greater than 1, but the peak values were between 0.4 and 0.7. Only Cr, a compatible element, was scarce in the LPL, but enriched in the UPL, having sample/MORB ratios greater than 1.5. They therefore proposed that there were two distinct melt sources, separated by an unknown period of time. They explained the origin of the UPL as off-axis eruptions of primitive lava on the flanks of a spreading ridge. The differences between the UPL and LPL could therefore be attributed to differences between ridge and off-axis petrogenesis.

Fig. 1.4-8. Comparison of immobile elements within the lavas of the Troodos Massif for Upper Pillow Lavas and Lower Pillow Lavas. From Smewing et al.(1975)

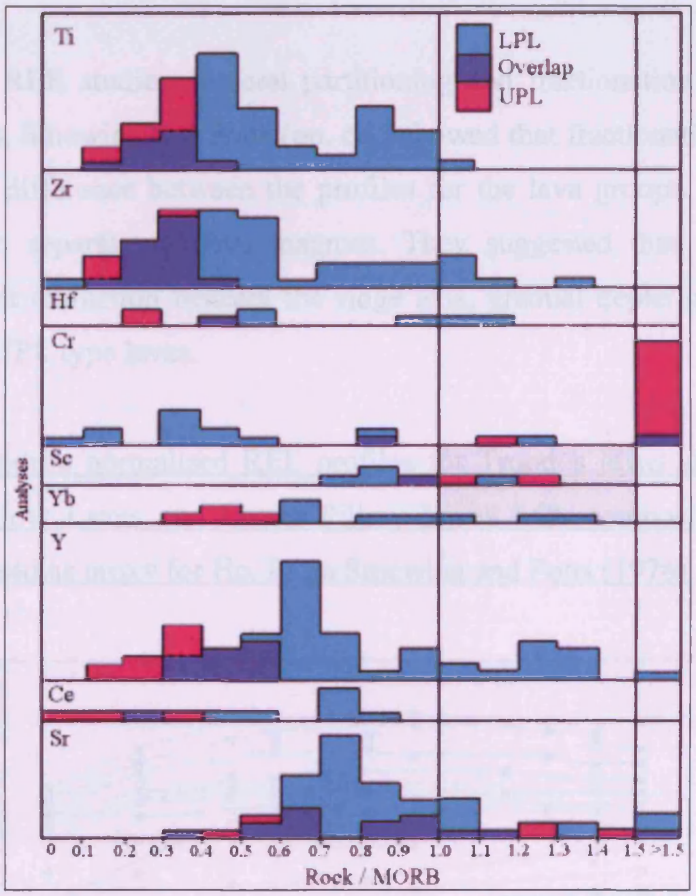

Smewing and Potts, 1976

Smewing and Potts (1976) analysed twelve basalts from the Troodos Massif. Of these, half were from the UPL and half from the LPL. Only three were fresh, the rest were

altered to zeolite facies. No appreciable difference was noted between the fresh and altered samples, demonstrating that REE profiles are not susceptible to alteration under zeolite facies metamorphism.

When plotted as chondrite normalised patterns, olivine-phyric (UPL) samples were found to have variably lower REE concentrations. Sometimes up to an order of magnitude less, and a greater degree of LREE depletion than the LPL samples (Fig 1.4-9). LPL samples were said to resemble bulk ocean-floor basalt profiles (Smewing and Potts, op. cit.). They also plotted a 'threshold line' separating samples where Sm/Lu was greater than 1 and all profiles were parallel (mainly LPL) from samples where Sm/Lu was less than 1 and profiles converged.

Continuing the REE studies, mineral partitioning and fractionation experiments of Schilling (1971), Smewing and Potts (op. cit.) showed that fractionation alone cannot account for the difference between the profiles for the lava groups. Therefore there must have been separate parental magmas. They suggested that, by incremental melting and melt extraction beneath the ridge axis, gradual depletion of the source would produce UPL type lavas.

Fig. 1.4-9. Chondrite normalised REE profiles for Troodos lavas showing samples from Upper Pillow Lavas and Lower Pillow Lavas with compositional threshold marked and Y used as proxy for Ho. From Smewing and Potts (1976).

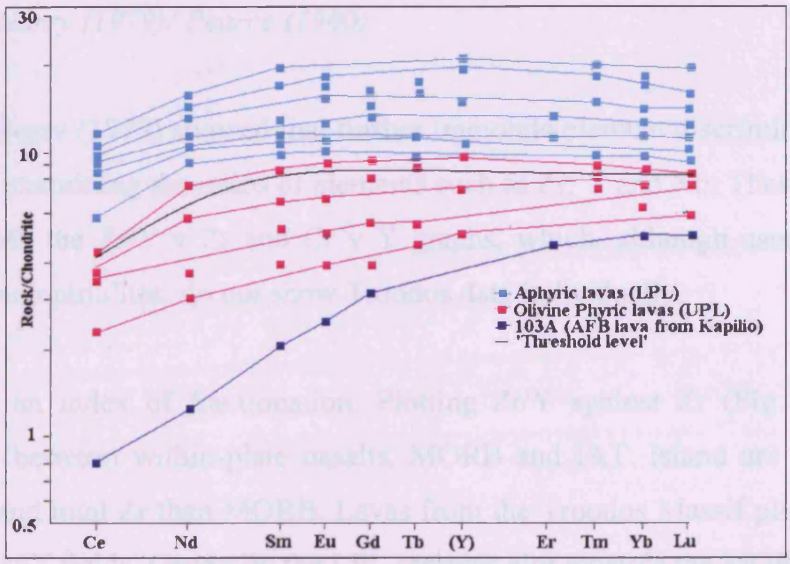

Kay and Senechal (1976)

Kay and Senechal (1976) also focussed on REE concentrations in Troodos lavas. They found that the REE profiles were similar in most of the samples analysed, with the exception of one sample described as komatiite-like with extreme LREE depletion. All the others showed an island arc-like profile (Fig. 1.4-10). They also found that REE were not mobile during submarine weathering. Then they were able to demonstrate from Eu anomalies that some of the silica rich lavas were silicified basalts, not andesites or dacites.

Fig. 1.4-10. REE profiles for Troodos lower pillow lavas compared with MORB and IAT from Kay and Senechal (1976).

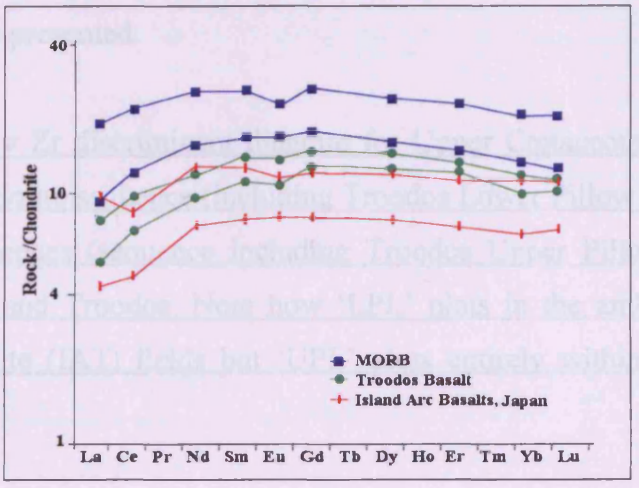

Pearce and Norry (1979)/ Pearce (1980)

Pearce and Norry (1979) showed that further immobile element discrimination can be achieved by examining the ratios of elements such as Zr, Y and Nb. These two papers introduce both the Zr/Y v Zr and Cr v Y graphs, which, although used for eastern Mediterranean ophiolites, do not show Troodos data individually.

Zr provides an index of fractionation. Plotting Zr/Y against Zr (Fig. 1.4-11) can discriminate between within-plate basalts, MORB and IAT. Island arc basalts have lower Zr/Y and total Zr than MORB. Lavas from the Troodos Massif plot in both the MORB and IAT fields. Generally the LPL samples plot towards the MORB end of the

sample array, and the UPL plotted within the IAT array. As on most discrimination diagrams, there is some overlap between the two lava types. The Zr/Nb ratio is insensitive to variations in partial melting so can be used to examine melt sources and fractionation trends.

Plotting Cr against Y (Fig. 1.4-12) allows the comparison of an incompatible element with a compatible one that is also an index of fractionation. This is a derivation of the Ti-Cr diagram from Pearce (1975) but is not affected by magnetite crystallisation. Troodos lavas plot almost exclusively in the IAT field, with Cr contents of the UPL around 200 ppm and between 70 and 100 ppm for the LPL. This shows that the LPL are somewhat more fractionated than the UPL. Y contents are also higher in the LPL than UPL, again a result of the difference in degree of fractionation. Pearce (1980) also plotted Cr against Ce/Sr for discrimination purposes similar to Cr –Y, but no Troodos data were presented.

Fig. 1.4-11. Zr/Y v Zr discriminant diagram for Upper Cretaceous ophiolite basalts showing main ophiolite sequence (including Troodos Lower Pillow Lavas (LPL)) and Upper Lava Sequences (sequence including Troodos Upper Pillow Lavas (UPL)). Data from Oman and Troodos. Note how 'LPL' plots in the ambiguous MORB – Island Arc Tholeiite (IAT) fields but 'UPL' plots entirely within IAT field. From Pearce, (1980).

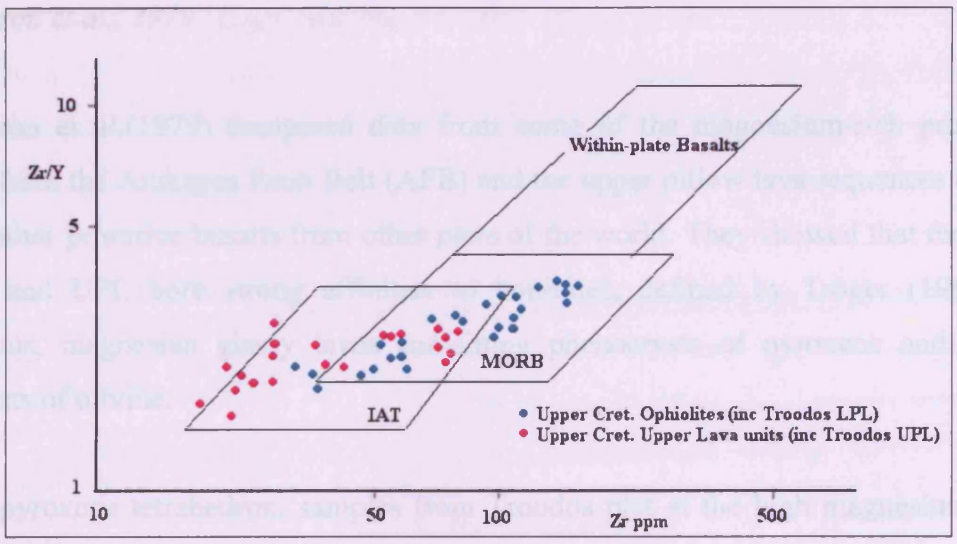

Fig. 1.4-12. Cr v Y discriminant diagram for lavas from the Troodos Massif. This shows that the Troodos lavas, both Upper Pillow Lavas and Lower Pillow Lavas lie within the island arc field. There is no overlap between island arc and MORB on this diagram. From Pearce, (1979).

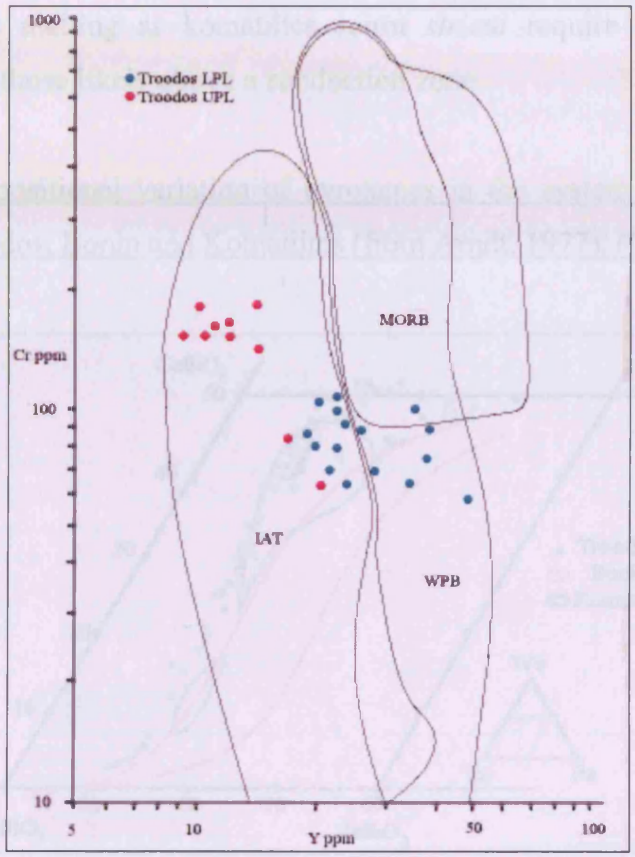

Cameron et al., 1979

Cameron et al.(1979) compared data from some of the magnesium-rich primitive lavas from the Arakapas Fault Belt (AFB) and the upper pillow lava sequences (UPL) with other primitive basalts from other parts of the world. They showed that the AFB lavas and UPL bore strong affinities to boninites, defined by Tröger (1969) as siliceous, magnesian glassy lavas containing phenocrysts of pyroxene and lower amounts of olivine.

On a pyroxene tetrahedron, samples from Troodos plot at the high magnesium end, following a trend similar to samples from Bonin Island but richer in magnesium (Fig. 1.4-13). These trends reflect thermal history as well as source composition. The

Troodos lavas, have a lower $FeSiO_3$ component and so a higher source temperature than lavas from Bonin Island. Lavas from the AFB had previously been described as basaltic komatiites but have significantly lower titanium that is more similar to boninites. Their Ti-Zr ratio is however approximately chondritic at about 100. Cameron et al. (1979) proposed that this type of lava could only have formed as the result of hydrous melting as komatiites *sensu stricto* require far higher mantle temperatures than those likely above a subduction zone.

Fig. 1.4-13. Compositional variation of pyroxenes in the system $MgSiO_3$- $FeSiO_3$-$CaSiO_3$ from Troodos, Bonin and Komatiites (from Arndt, 1977). (Cameron, 1979)

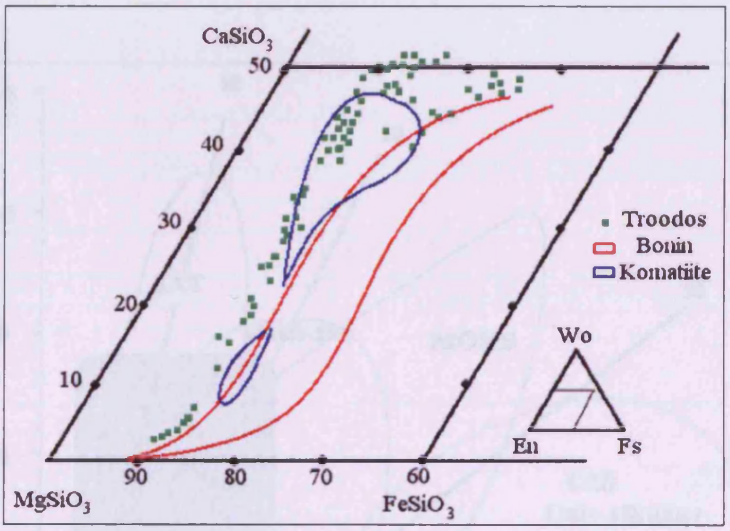

Shervais, 1982

Shervais (1982) extended the use of incompatible immobile elements for basalt discrimination to cover vanadium. Early analyses using XRF was not as accurate for vanadium as it was for titanium or zirconium, and also the vanadium value is cut drastically in the lavas when there has been iron oxide precipitation in the magma chamber. It also has multiple partition coefficients due to its multiple valences. Study of a large number of samples from MORB, IAT, OIB, back-arc basin basalts and boninites led Shervais (op. cit.) to be able to assign generally mutually exclusive fields for these lava types, therefore allowing the use of Ti v V as a discriminant function.

On Troodos, the lower pillow lavas (LPL) have a higher dispersion and average value of Ti and V than the upper pillow lavas (UPL), which have a narrow range almost within the boninite field (Fig. 1.4-14). In general the LPL have a higher Ti-V ratio than the UPL and some of the Ti-rich samples plot within the back-arc or MORB fields. This plot thus agreed at the time with growing consensus that the Troodos formed in a supra-subduction environment, while also adding to the argument for the presence of boninites within the UPL.

Fig. 1.4- 14. Ti-V variation fields of Shervais (1982) for lower pillow lavas (LPL) and upper pillow lavas (UPL) from the Troodos Ophiolite compared with generic lava-type fields.

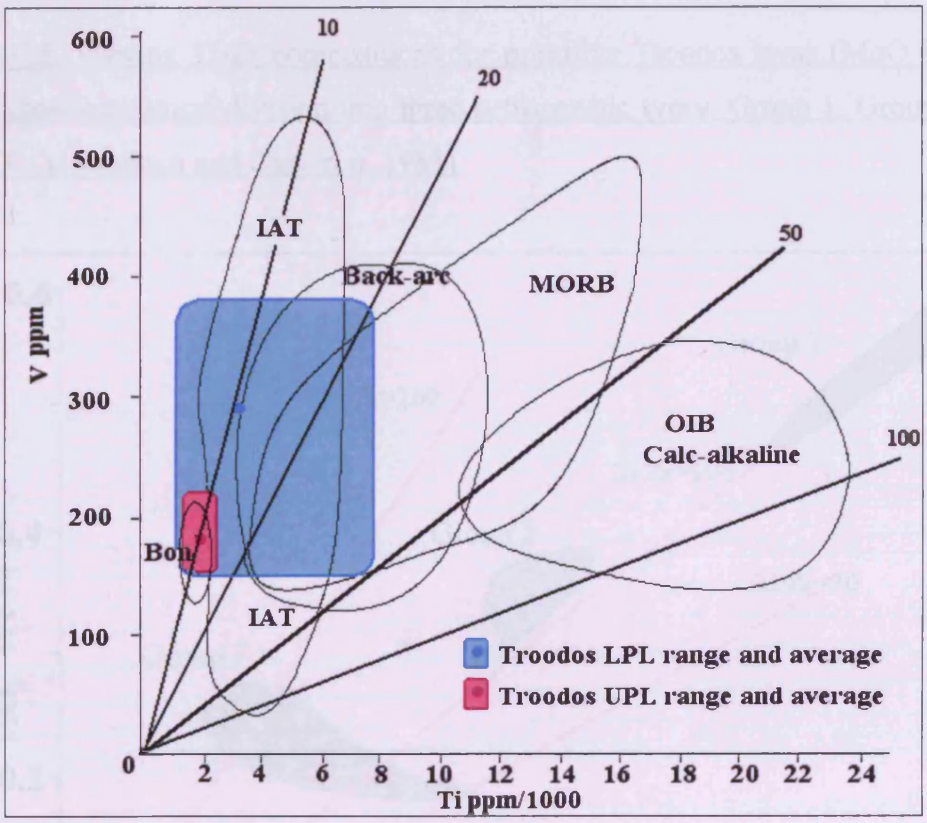

McCulloch and Cameron, 1983

Analysis of a number of samples taken from the Upper Pillow Lavas (UPL), primarily for the purposes of examining Nd and Sr isotope ratios, allowed McCulloch and Cameron (1983) to confirm the supra-subduction zone origin to the Troodos lavas. In addition, they found the UPL to comprise three distinct lava types on the basis of Ti-

Zr values and ratios. 'Group 1' lavas were identified from the Margi area, with the highest overall Ti and Zr values and a chondritic Ti-Zr ratio. 'Group 2' lavas were identified from most of the periphery of the ophiolite and some of the AFB. They have lower overall Ti-Zr values but a chondritic Ti-Zr ratio. 'Group 3' lavas were identified from the western end of the AFB and the western LFC, and have overall Ti and Zr contents and a high Ti-Zr ratio (Fig. 1.4-15).

Rare earth profiles showed that Group 1 lavas had similar profiles to LPL, but more depleted. Group 2 lavas were also generally depleted with a small amount of LREE addition. Group 3 lavas showed a typical boninitic U-shaped REE profile with extensive LREE enrichment. They were also more varied in composition than the other groups (Fig. 1.4-16).

Fig. 1.4-15. Varying Ti-Zr compositions for primitive Troodos lavas (MgO 8% and above) showing natural division into three petrogenetic types, Group 1, Group 2 and Group 3. (McCulloch and Cameron, 1983)

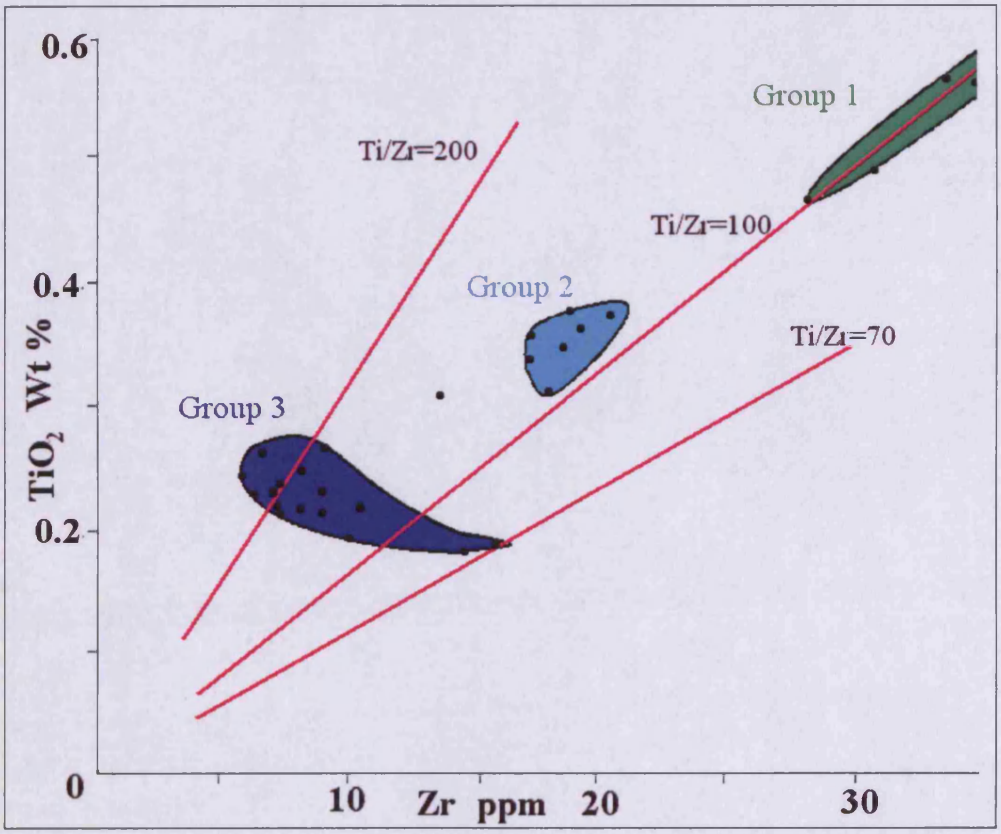

Fig. 1.4-16. Varying Rare Earth Element profiles chondrite normalised to Taylor and Gorton (1977) compositions for primitive Troodos lavas (MgO 8% and above) showing natural division into three petrogenetic types, Group 1, Group 2 and Group 3. (McCulloch and Cameron, 1983)

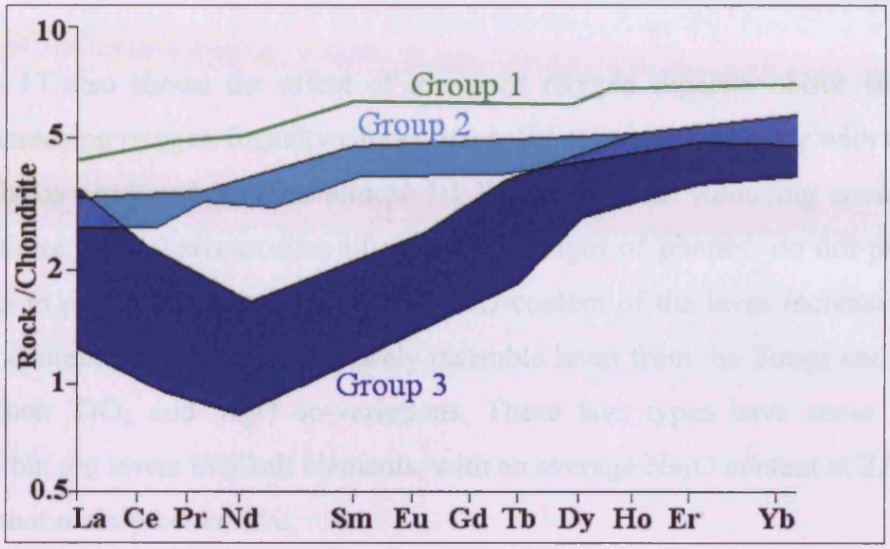

Robinson et al. (1983)

Although the lavas of the Troodos Massif had been analysed for their major element content since the 1960's, the 'Myashiro debate' showed that alteration left the mobile major elements unreliable for geochemical fingerprinting. Robinson et al. (1983) attempted to solve this problem by using fresh glass from the rims of pillows. Mobile element ratios from fresh glass would be original. Glasses were taken from Akaki, Kambia and Kalavasos.

Robinson et al. (1983) used major elements to show that Troodos lavas are not typical of MORB, but are higher in silica and lower in Ti and Fe oxides. They are also higher in Mg than normal IAT for given silica content and higher in Fe than IAT for a given Mg content. The glasses form two series: a low Mg series that corresponds to LPL (Troodos Rhyodacites, pale blue, Fig. 1.4-17), and a high Mg series with a roughly constant Fe oxide content that corresponds to the UPL (Troodos Basalts, pink, Fig. 1.4- 17).

In conjunction with structural evaluation undertaken with Schmincke et al. (1983), Robinson et al. (1983) found that there was a geochemical discontinuity in the lower part of the lava pile, roughly corresponding with the Basal Group – Lower Pillow Lava boundary. They interpreted this as the change from initial arc spreading to more mature spreading.

Fig. 1.4- 17 also shows the effect of increased oxygen fugacity above subduction zones. Increasing oxygen fugacity causes magnetite to precipitate early with the result that the lavas produced have an almost 1:1 Fe to Mg ratio. Reducing environments such as those with characteristics of mid-ocean ridges or plumes, do not permit the magnetite to precipitate out easily, so the FeO content of the lavas increases rapidly with Mg content. The UPL most closely resemble lavas from the Tonga and Mariana arcs in their TiO_2 and MgO co-variations. These lava types have some boninitic affinities but are lower in alkali elements, with an average Na_2O content at 2.5% and a K_2O content mainly below 1%.

Fig. 1.4-17. Variation of MgO and FeO within Troodos glasses. Supra-subduction zone lavas such as Troodos and Cascades Range (NW USA) show low Fe-Mg ratios while intraplate and ridge lavas such as Skaergaard (Greenland) and Galapagos Rift (MORB) show increased iron content (Robinson, 1983)

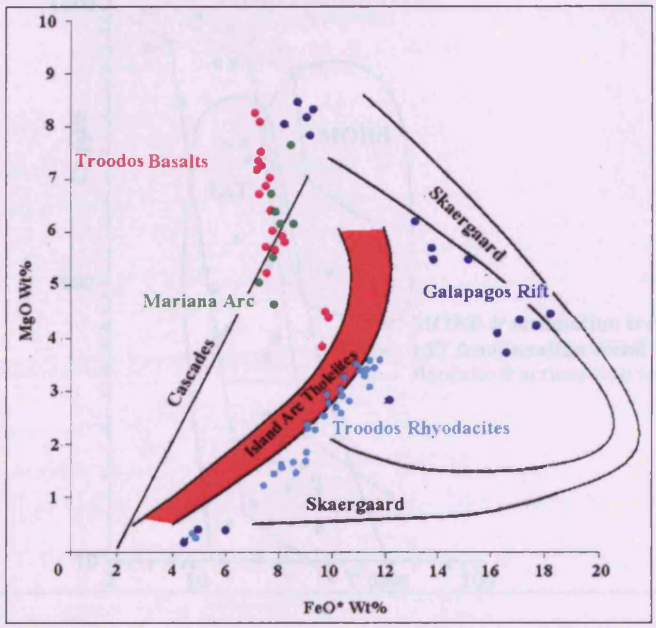

Pearce et al. (1984)

Pearce et al. (1984) expanded on previous work (Wood et al., 1979 and Pearce, 1982) to evaluate data from the Troodos Massif. Plotting Cr and Y data from Pearce (unpublished), he confirmed that the Troodos lavas mainly fell within Island Arc Tholeiite compositional range. He further showed that the main Troodos axis sequence lavas, which has tholeiitic affinities, probably resulted from a 20-30% partial melt of non-depleted mantle. These rocks were variably fractionated, with contents of Cr varying between 200 ppm (unfractionated) and less than 5 ppm (extensively fractionated). Some of the Troodos samples also plotted along a boninite fractionation trend, calculated to have formed from a partial melt of an already depleted mantle residue (Fig. 1.4-18).

Fig. 1.4-18. Cr-Y diagram of Troodos lavas (Data from Pearce (unpublished), showing basalt compositions (green dots) relative to calculated melting / fractionation trends and island arc tholeiite (IAT) and MORB ranges.

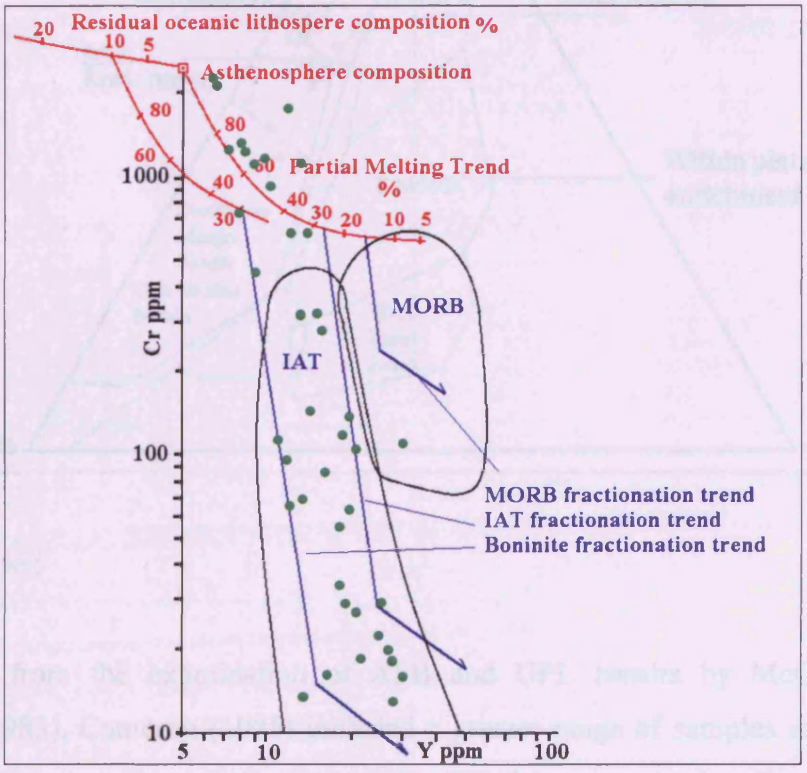

Pearce (1984) added data points for Troodos lavas and petrogenetic trends for within-plate depletion or enrichment and supra-subduction enrichment on the Ta-Th-Hf diagram of Wood et al. (1979), Wood (1980) (Fig. 1.4-19). This diagram supported the Cr-Y diagram that some Troodos basalts were of IAT origin and some of boninitic origin. Thus Troodos type ophiolites may be attributed to a supra-subduction zone environment. However, in view of the lack of evidence of arc volcanism, may be pre-arc in origin rather than syn-arc.

Fig. 1.4-19. Th Hf Ta plot for MORB, Island Arc Tholeiite (IAT) and Ocean Island Basalt (OIB) showing relative discrimination fields. From Wood et al., (1979) (Black lines), modification by Wood et al. (1979) shown in blue. Data and trend lines from Pearce (1984).

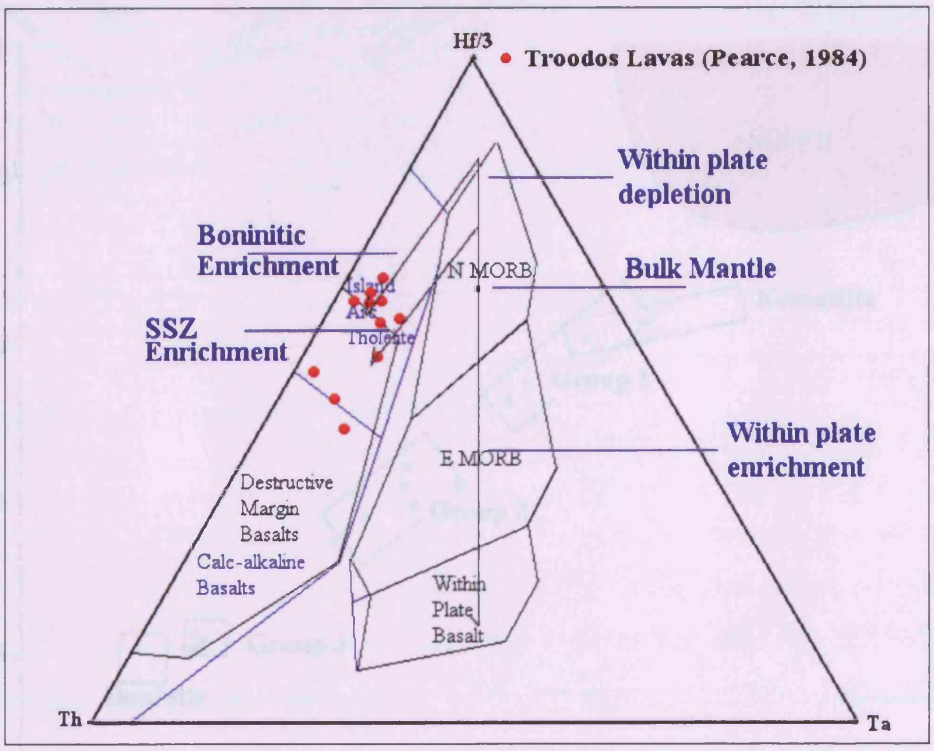

Cameron, 1985

Continuing from the examination of AFB and UPL basalts by McCulloch and Cameron (1983), Cameron (1985) included a greater range of samples and elements analysed. The same three lava groups are picked out by plotting Ti v Zr as per McCulloch and Cameron (1983) and by plotting Ti/V against Ti/Sc. On this plot, (Fig

1.4-21) the V/Sc ratio is constant at about 6, with the groups picked out by their differing Ti content. This plot also shows some similar lava types (possible proxies) such as komatiites and boninites. Profiling of rare earth element contents picks out the difference between LPL, Groups 1 and 2 UPL and Group 3 UPL. The profiles of the LPL and Group 1 UPL are similar, just with lower overall abundances within the UPL, Group 3 UPL shows extreme LREE depletion, with some of the profiles showing secondary LREE enrichment (Fig 1.4-22). All of these plots show that UPL types are related by incremental depletion of the source material, with a secondary input to Group 3 from subduction-related fluids.

Fig. 1.4-21. Variation of Ti/V and Ti/Sc in primitive Troodos lavas compared to other similar rock types including Komatiite and Boninite. (Cameron, 1985)

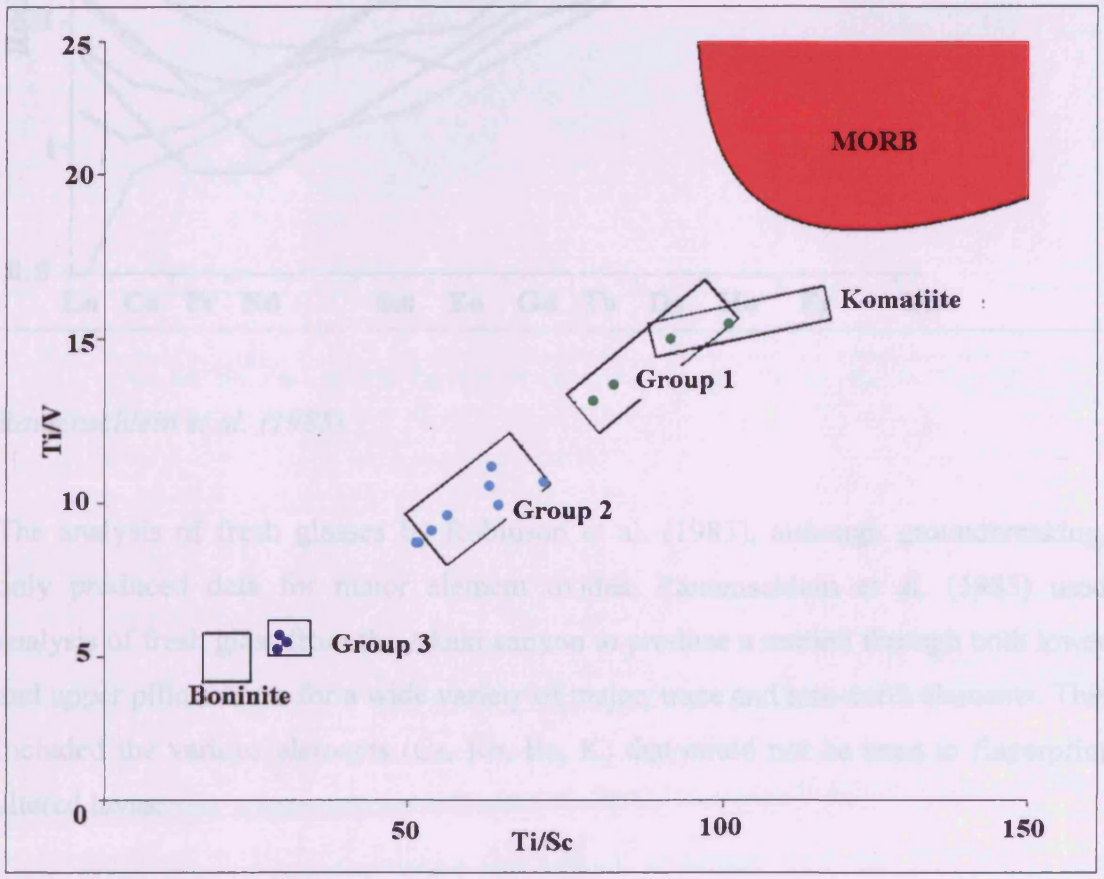

Fig. 1.4-22. Variation of REE profile and content within primitive lavas of the Troodos Massif. Sample X103 (Kay and Senechal, 1976) original analysis as thinner blue trace, re-analysis shows U-shaped profile. Colour scheme as Fig. 1.4-21 (Cameron, 1985)

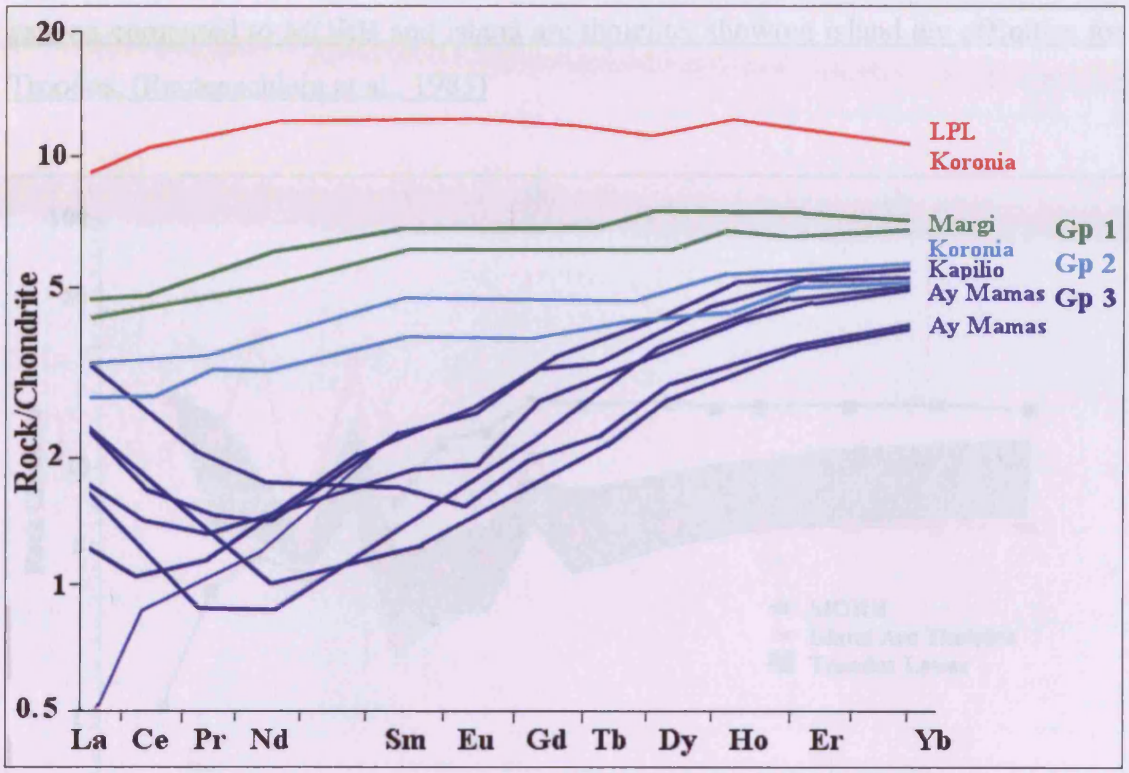

Rautenschlein et al. (1985)

The analysis of fresh glasses by Robinson et al. (1983), although groundbreaking, only produced data for major element oxides. Rautenschlein et al. (1985) used analysis of fresh glass from the Akaki canyon to produce a section through both lower and upper pillow lavas for a wide variety of major, trace and rare-earth elements. This included the various elements (Cs, Rb, Ba, K) that could not be used to fingerprint altered lavas.

Analysis of the glasses showed that the volatile content was consistently high compared to MORB and the high values of Sc and Co showed that the samples were relatively unfractionated. Extended incompatible element plots show positive La and Th, or negative Nb anomalies, typical of arc environments. Significantly, Cs, Rb, Ba

and K were all enriched. Most HFS elements are depleted relative to MORB with the general trend of incompatible elements shadowing the trend for normal island arc tholeiite (Fig. 1.4-23)

Fig. 1.4-23 Extended incompatible element spider diagram for glasses form the Akaki canyon compared to MORB and island arc tholeiite, showing island arc affinities for Troodos. (Rautenschlein et al., 1985)

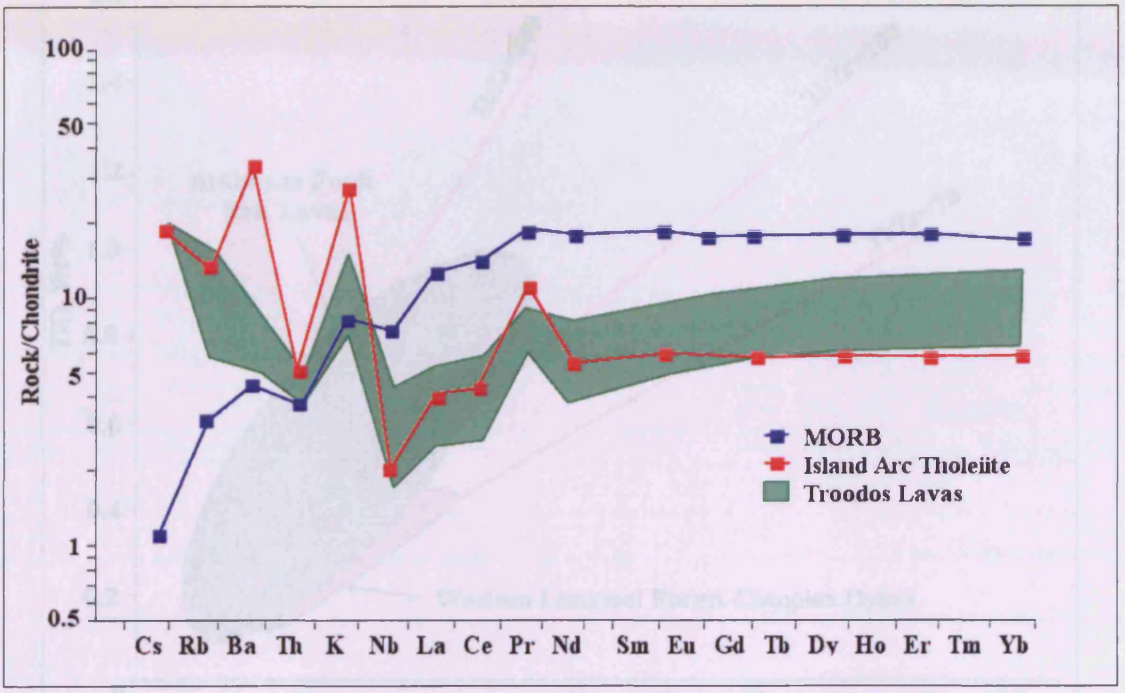

Murton, 1986

Murton (1986) found that there was a progressive stratigraphic change in lava composition in the western Limassol Forest Complex (WLFC) with lavas nearest the AFB and highest stratigraphically having the most depleted source, yet showing the most secondary enrichment. Rocks that belong to Group 3 of the McCulloch and Cameron classification were defined as 'Active Transform Sequence'; having been erupted into the transform zone while it was under tension. These rocks are highly depleted in incompatible elements, with a high Ti/Zr ratio of about 200. As other lava groups have Ti/Zr ratios of about 100 (chondritic), these lavas probably have a

different source (Fig. 1.4-24). The second group plotted, the WLFC dykes, have a much lower Ti/Zr ratio of about 70 – 100, which would imply that they are similar to the Group 2 lavas of McCulloch and Cameron (1983)

Fig. 1.4-24. Comparison of Ti-Zr contents from lavas of the Arakapas Fault Belt Lavas and Western Limassol Forest Complex (Murton 1986)

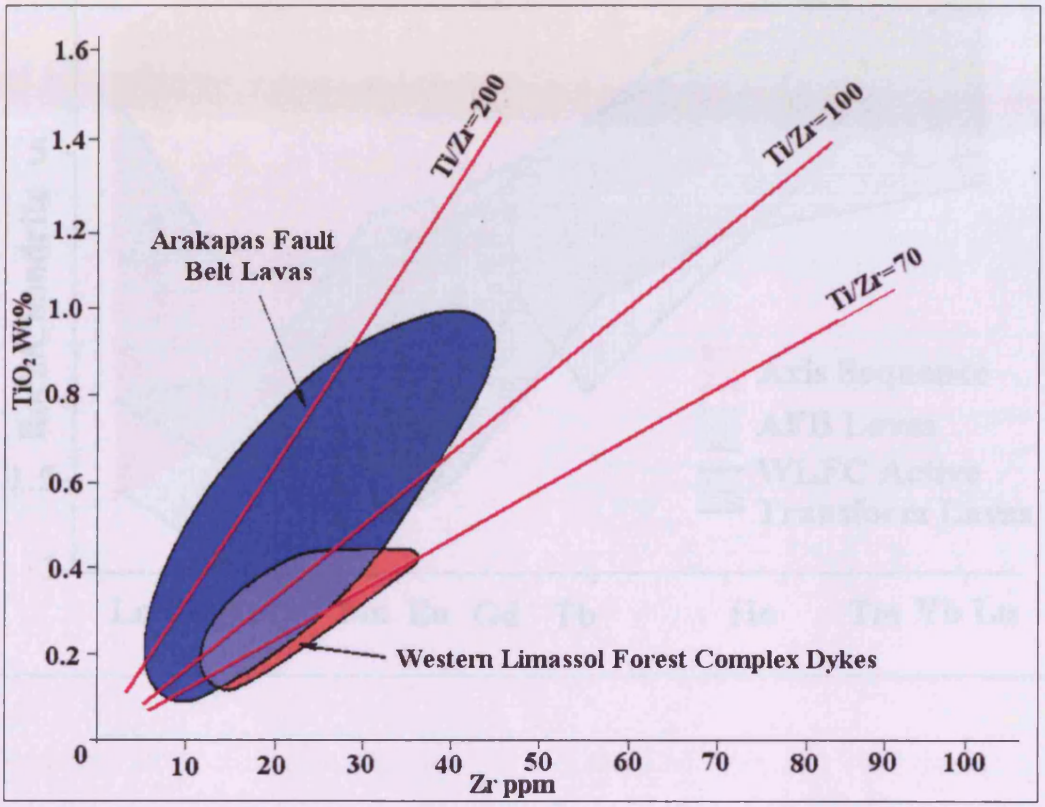

Profiles across the Troodos Massif show increasing LREE depletion towards the transform zone, although only Group 3 lavas show U-shaped profiles. Murton (1986) attributed this to the melting of a previously depleted peridotite source (one which had already been partially melted to produce 'MORB') modified by the addition of LREE rich subduction related fluids (Fig. 1.4-25).

Fig. 1.4-25. Comparison of Rare-earth element profiles from lavas of the Active Transform Series and Western Limassol Forest Complex (WLFC) showing increased LREE enrichment in the WLFC lavas compared to AFB lavas (Murton 1986)

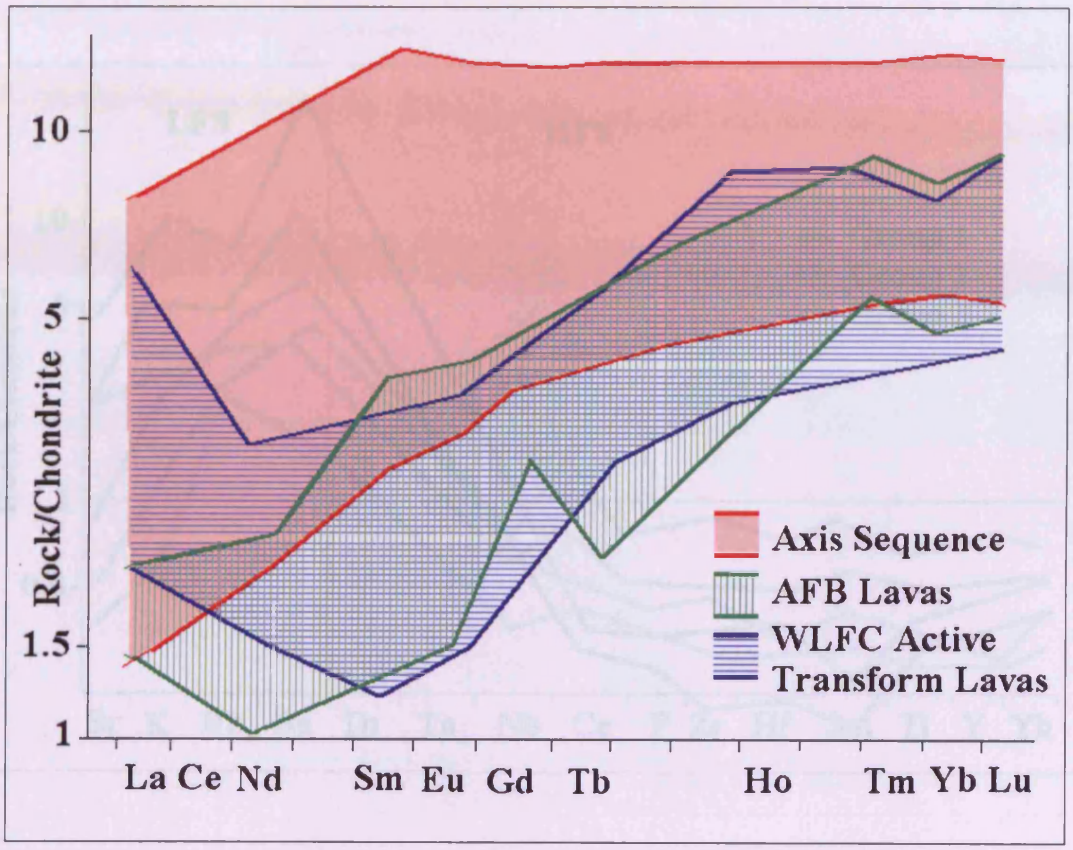

Flower and Levine, 1987

Flower and Levine (1987) followed up work of Cameron (1985) and Murton (1986) on the variably depleted lavas of the western Limassol Forest Complex and Arakapas Fault Belt. They found the same three lava groups as Cameron (1985). Groups 1 and 2 were described as variably depleted arc tholeiite and Group 3 as high calcium boninite. The theories explaining the LFS enrichment include contamination of the supra-subduction zone mantle wedge with ocean island basalt derivatives or slab-derived melt. Group 3 lavas were also most enriched in elements such as Ta, Th and Ba, but most depleted in HFS elements such as P, Zr and Hf. (Fig. 1.4-26)

Fig. 1.4-26. Chondrite normalised comparison of low and high field strength element (including selected rare earth) contents within primitive lavas of the Troodos Massif. These profiles show increasing LFS enrichment and HFS depletion towards the Group 3 lavas. (Flower and Levine, 1987)

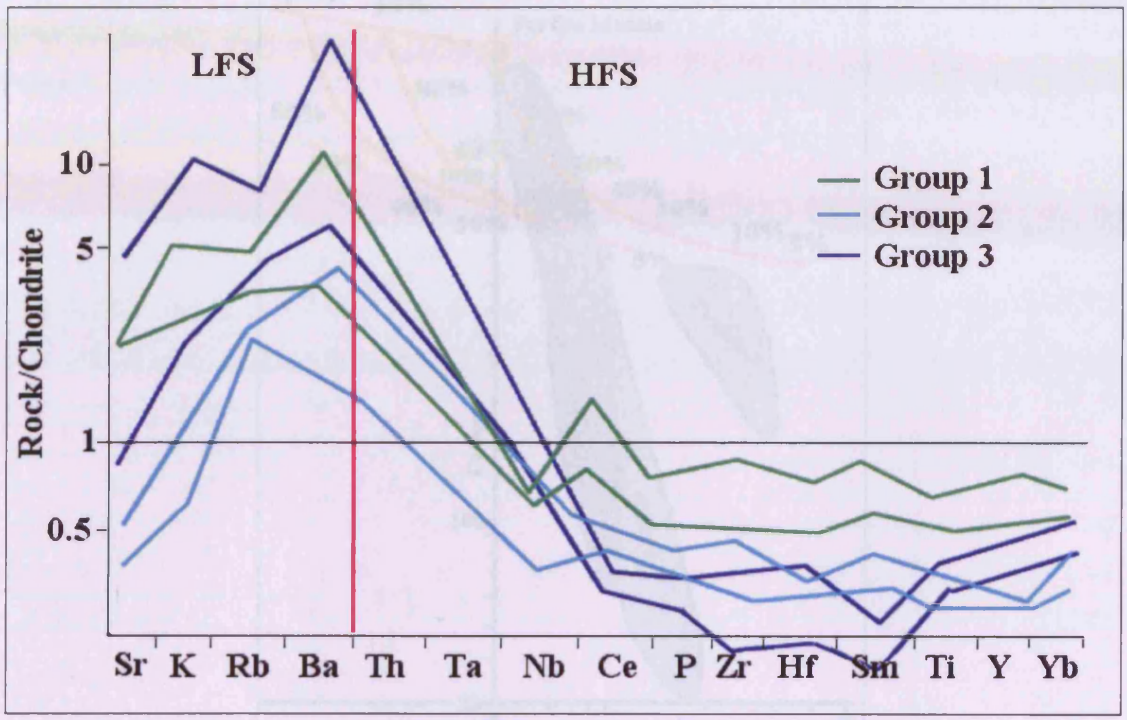

Calculation of fractionation trends based on the Cr-Y diagram of Pearce (1982) suggests that Group 1 UPL can result either from a 30% partial melt of non-depleted mantle or from a 5% partial melt of 10% depleted mantle or conditions somewhere between the two. Both of these scenarios are plausible but the general depleted nature of the UPL in general favours the latter. Both Groups 2 and 3, on a Cr-Y diagram, would require an unlikely 80% partial melt of fresh peridotite or a more reasonable 10% melt of 20% depleted mantle source (Fig. 1.4-27). It is also important to note that the UPL in general and the Group 3 lavas in particular, are volumetrically small compared to the lower pillow lavas and sheeted dyke complex.

Fig. 1.4-27. Cr - Y diagram based on Pearce (1982) showing partial melting curves for variably depleted mantle source and primitive lavas of the Troodos Massif. (Flower and Levine, 1987)

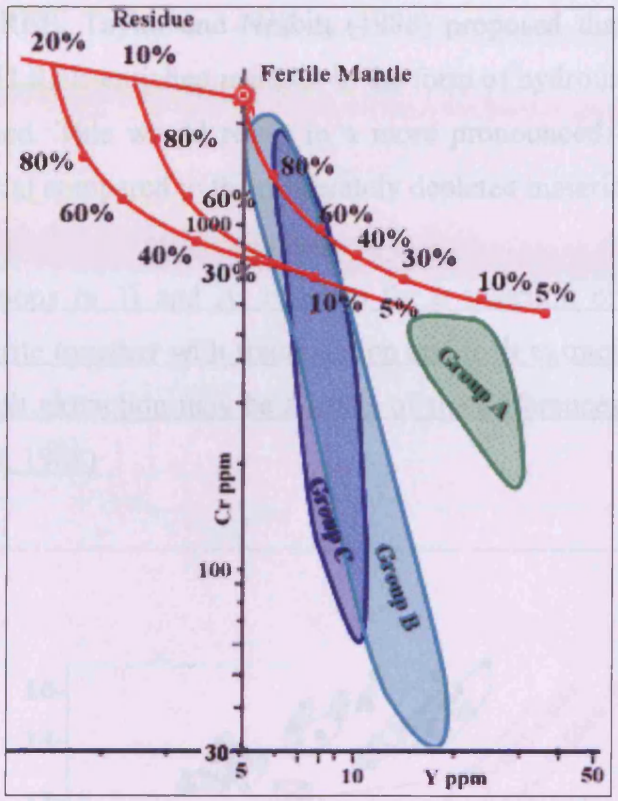

Taylor and Nesbitt, 1988

Various methods were used by Taylor and Nesbitt, (1988) to determine the extent of supra-subduction enrichment within the Troodos ophiolite. The lavas have undergone enrichment of low field-strength and light rare-earth elements. One of the methods was to use a depletion index, in this case, Al_2O_3/TiO_2 for a selection of Margi lavas. Fig. 1.4-28 shows how the relative fractionation and melt extraction vectors affect overall Ti and Al content. Within a single unit that is undergoing fractionation, the overall Ti/Al ratio remains constant. The differences between the units may thus be at least partially explained by progressive melt extraction from the mantle.

On the basis of major elements, Taylor and Nesbitt (1988) suggested that Group 2 UPL is related to Group 1 UPL by a higher degree of melting of a variably depleted source. This does not however explain the variation in REE profile or Nd isotope ratio. The samples with the highest LREE enrichment are also the ones most depleted in Ti and middle REE. Taylor and Nesbitt (1988) proposed that the addition of a constant amount of LREE-enriched material in the form of hydrous silicate melt to the magma was required. This would result in a more pronounced enrichment for the ultradepleted material compared to the moderately depleted material.

Fig. 1.4-28. Variations in Ti and Al contents for a selection of Margi UPL, both glassy lava and picrite together with fractionation and melt extraction trends showing that progressive melt extraction may be a cause of the differences between the lavas (Taylor and Nesbitt, 1988)

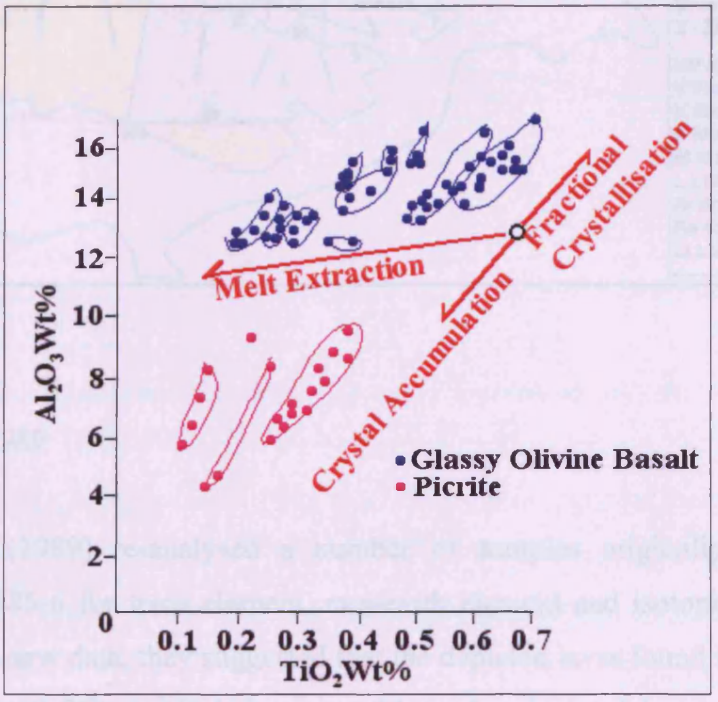

From examination of REE profiles and Zr/P data, Taylor and Nesbitt (1988) demonstrated that the UPL series of most of the ophiolite is subduction-enriched. However, UPL from the section of the northern outcrop between Margi and Koronia (within the Ayios Epiphianos and Kambia Grabens) is less subduction-enriched than the rest of the ophiolite. This depletion is not symmetrical about any of the grabens, leading Taylor and Nesbitt (1988), to infer, based on evidence of eastward structural

younging (Varga and Moores, 1985), that there was a reduction in subduction input with time. They presented their results in map form – a precursor to this study (Fig. 1.4-29).

Fig. 1.4-29. Distribution of subduction enriched Upper Pillow lavas of the Troodos Massif based on rare-earth profiles and Zr/P values. (Taylor and Nesbitt, 1988)

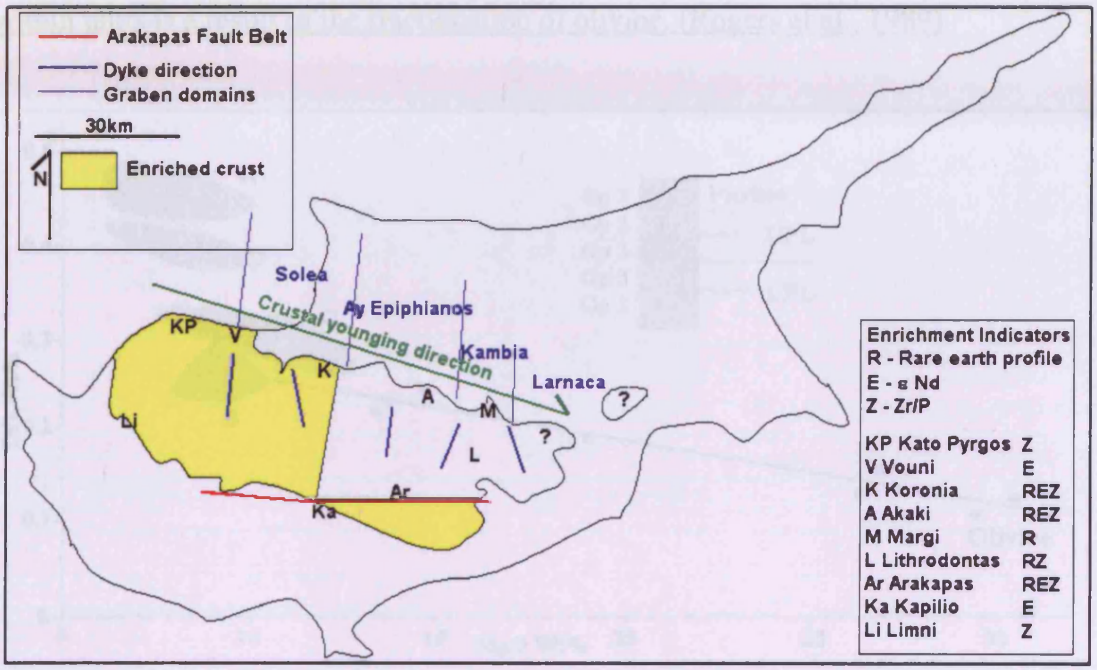

Rogers et al., 1989

Rogers et al. (1989) re-analysed a number of samples originally collected by MacLeod in 1985-6 for trace element, rare-earth element and isotopic contents. On the basis of the new data, they suggested that the depleted lavas found in the Limassol Forest Complex (LFC) resulted from remelting of a depleted harzburgite, residual after the extraction of the Troodos axis sequence that had then been subsequently enriched by LILE enriched subduction-derived fluids and mafic melt.

Previously, authors such as Taylor (1987) and Flower and Levine (1987) had proposed that the lava sequence became progressively more primitive upwards. However, stratigraphically controlled data, when plotted on a TiO_2 v MgO diagram

(Fig. 1.4-30), shows that the variably depleted and primitive lavas are sandwiched together in the LFC. Therefore multiple magma sources must have existed at one time. Because of the effects of alteration on MgO content, only fresh samples, with low volatile contents were used.

Fig. 1.4-30. TiO_2 V MgO diagram showing sandwiched layers of Group 2 and 3 upper pillow lava types in the Kalavasos area of the Limassol Forest Complex. Variation within units is a result of the fractionation of olivine. (Rogers et al., 1989)

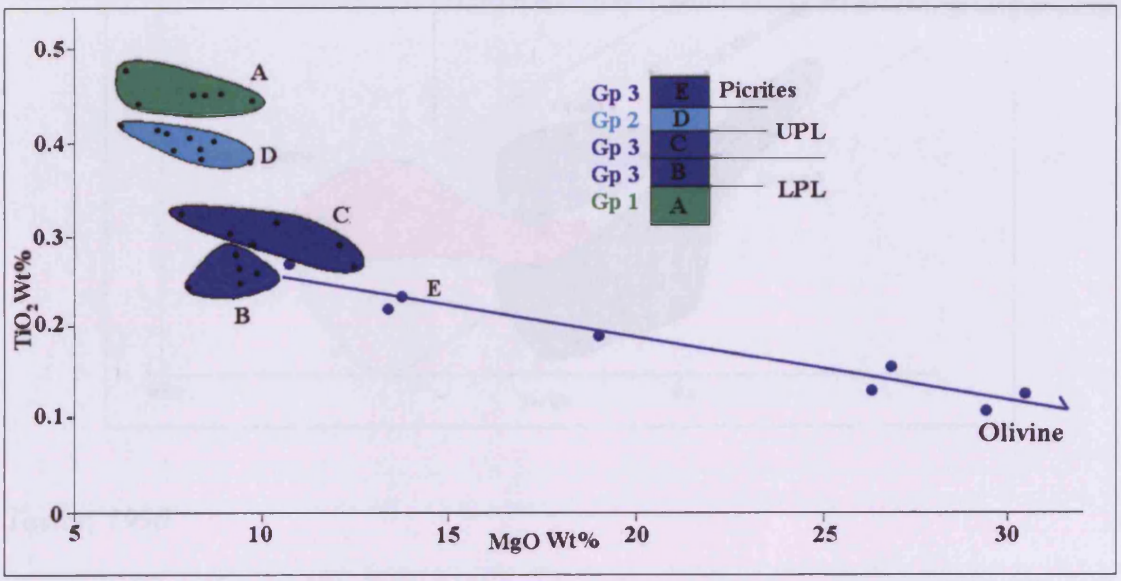

Examination of elements such as REE, Th and Ta gives an indication of subduction enrichment. Plotted onto a diagram indicating subduction zone enrichment (Ce/Yb v Ta/Yb: Fig. 1.4-31), samples from the Akaki LPL show slight subduction enrichment relative to the MORB array, which is what could be expected from supra-subduction zone lavas. The Group 2 lavas show more LREE enrichment than the Akaki lavas, but also more tantalum enrichment, so lying a little further along the MORB array, possibly the result of enrichment by low-degree mantle melts. Group 3 lavas are more variable; some have very low Ce/Yb, showing that these lavas are extremely LREE depleted (like the original analysis of 103A; Smewing and Potts, 1976) but others are substantially enriched in Ce and Ta, lying on the MORB array towards intraplate basalt. This shows that the Group 3 lavas were variably enriched by heterogeneous mantle melts.

Fig. 1.4-31. Ce/Yb v Ta/Yb diagram showing variations in subduction input and in intraplate input for Groups 2 and 3 Upper Pillow Lavas and for Lower Pillow Lavas from Akaki Canyon (Rautenschlein et al., 1985). Group 3 lavas appear below the MORB trend because of the enrichment of tantalum coupled with depletion in cerium. (Rogers et al., 1989)

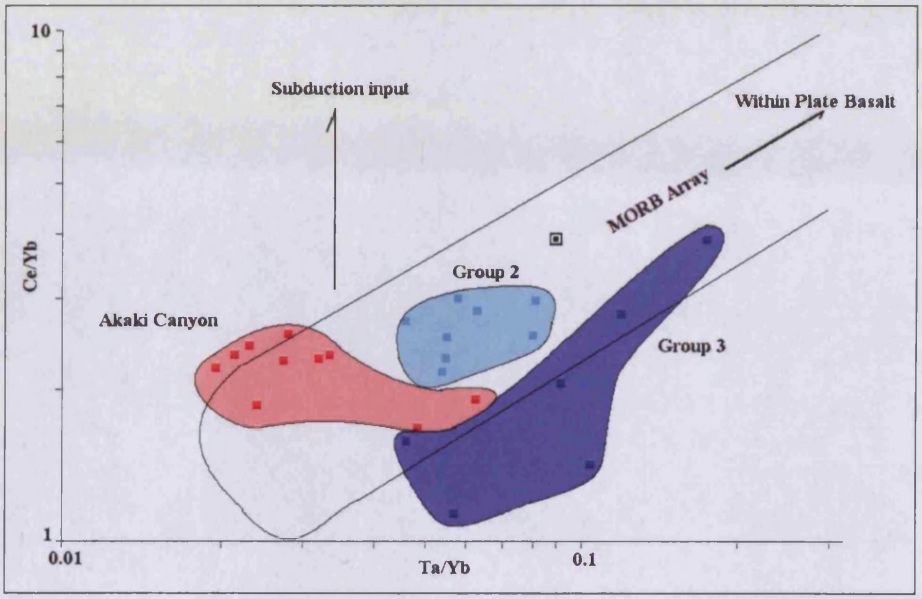

Taylor, 1990

Following up the spatial enrichment variations discussed in Taylor and Nisbet (1988), Taylor (1990) examined geochemical stratigraphic sections through the northern Troodos lavas. These sections were at Margi, Aloupos, and Koronia. In the Margi area, the UPK is formed by a cyclical series, in which each cycle includes increasingly primitive picritic lava. The UPL lies unconformably on the LPL, this unconformity occurring only in Larnaca Graben lavas. Plotting Ti v Ni (Fig. 1.4-32) shows the differences between the units. Further to the west at Aloupos, there is no unconformity between the lava groups, but the geochemistry of the lava types is inconsistent. Although the two primitive units are comparable, the more evolved units are not co-genetic on the basis of their IS values (IS values are a method of comparing the ratio of compatible to incompatible elements in melt that negates the effect of fractionation). This raises the possibility that multiple magma chambers near the surface fed these lavas. Further to the west at Koronia, the UPL are more subduction-

enriched than at Margi (Taylor and Nesbitt, 1988). These lavas have variable but lower Ti/Zr ratios than lavas at Margi. These lavas also have LREE enrichment. Koronia LPL are not enriched.

The variations discussed within the Larnaca Graben lavas could have resulted from incremental partial melting of a single homogeneous source. Alternatively they could have resulted from melting of a heterogeneous source, the first melts from the enriched parts of the mantle, with melting progressing to more depleted mantle rocks with time. The evidence from Aloupos supports a heterogeneous source theory.

Fig. 1.4-32. Ti v Ni diagram showing increasing depletion of these incompatible elements in Margi picrite units 1 through 4 (Taylor, 1990)

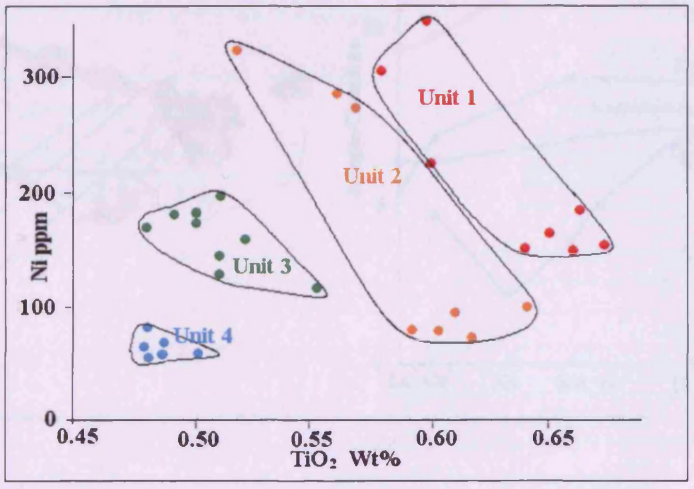

Thy and Xenophontos, 1991

Thy and Xenophontos (1991) analysed fresh glasses from locations in the north of Troodos, from both Upper Pillow Lava (UPL) and Lower Pillow Lavas (LPL). Samples from Kambia and Kythreotis were interpreted as basaltic andesites from the UPL and samples from Pedeous and Plesterika as andesites and dacites from the LPL.

They found that the dacite and andesite glasses have very similar REE profiles and therefore can be related by fractionation (Fig. 1.4-33). These profiles are similar to profiles obtained from Troodos LPL. The basaltic andesite glasses are profoundly

different. The Kythreotis sample (KY) is LREE-depleted and roughly parallels the LPL profile, corresponding to the Group 1 lava of McCulloch and Cameron (1983). The Kambia sample (KA) shows an almost flat REE profile, showing slight LREE enrichment, indicating that this is a Group 2 lava. This contradicts evidence from Taylor (1987) that UPL in the Kambia area is a Group 1 type.

Fig. 1.4-33. Rare Earth Element profiles for samples analysed, showing variations in depletion and secondary enrichment between lava types including AFB lava from Flower and Levine (1987) (Thy and Xenophontos, 1991)

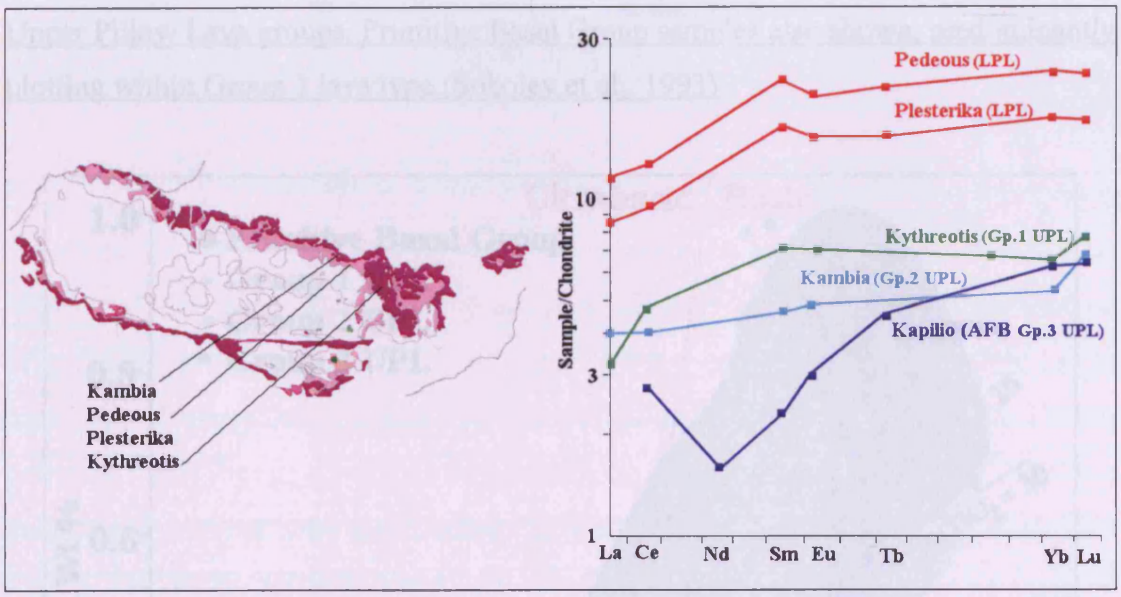

Sobolev et al., 1993

Sobolev et al. (1993) analysed a selection of primitive basalts from the eastern portion of the Troodos Massif. By collating and expanding the dataset for this particular rock type, they were able to expand on and better model the subdivisions within the Upper Pillow Lavas (UPL) first noted by McCulloch and Cameron (1983). In addition to samples of UPL, some samples of primitive Basal Group (BG) lava were taken.

Restricting their work to immobile incompatible elements, they plotted all available data for TiO_2 and Al_2O_3. On a TiO_2 - Al_2O_3 plot, Groups 1,2 and 3 lavas separate well, the boundaries approximating to Ti/Al ratio of 30 between Groups 1 and 2, and a ratio

of 40 between Groups 2 and 3 (Fig. 1.4-34). Basal group samples plot dominantly within the Group 1 field. Group 1 UPL could also be split into two parts: 1A, with a Ti/Al ratio of less than 25; and 1B with a Ti/Al ratio of 25-30 and with a slightly more depleted incompatible element profile than type 1A lavas. On the incompatible element plot (Fig. 1.4-35), BG lavas plot mainly within the Group 1 field, but are less enriched in LIL elements than the other lavas. Within the UPL groups, there is an increasing depletion in HFS elements from Groups 1 through 3. Tantalum is, however, enriched in Group 3 lavas compared to Groups 1 and 2.

Fig. 1.4-34. TiO_2 v Al_2O_3 diagram showing different ratios of Ti:Al for the different Upper Pillow Lava groups. Primitive Basal Group samples also shown, predominantly plotting within Group 1 lava type (Sobolev et al., 1993)

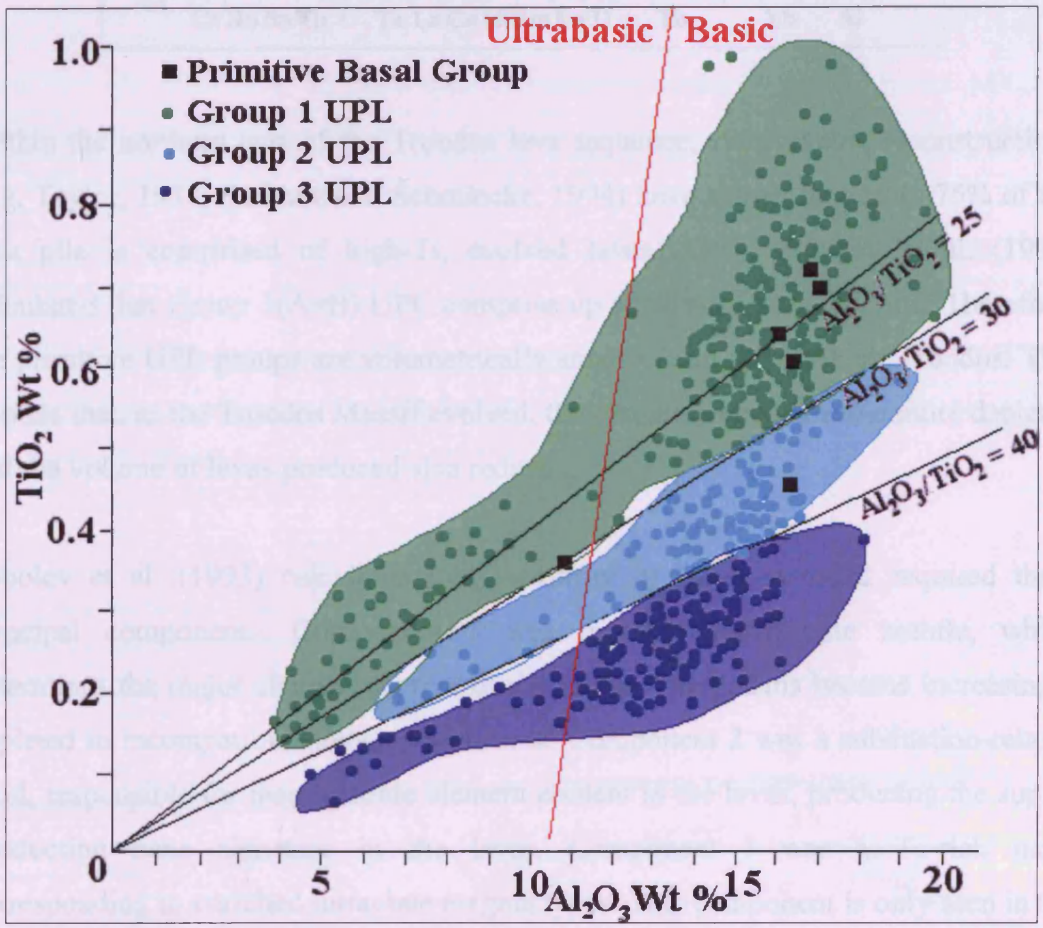

Fig. 1.4-35. Incompatible element diagram for Upper Pillow Lava groups (UPL-1, 2 and 3), Lower Pillow Lavas (LPL) from Rautenschlein et al., (1985) and Basal Group average (BG). (Sobolev et al., 1993)

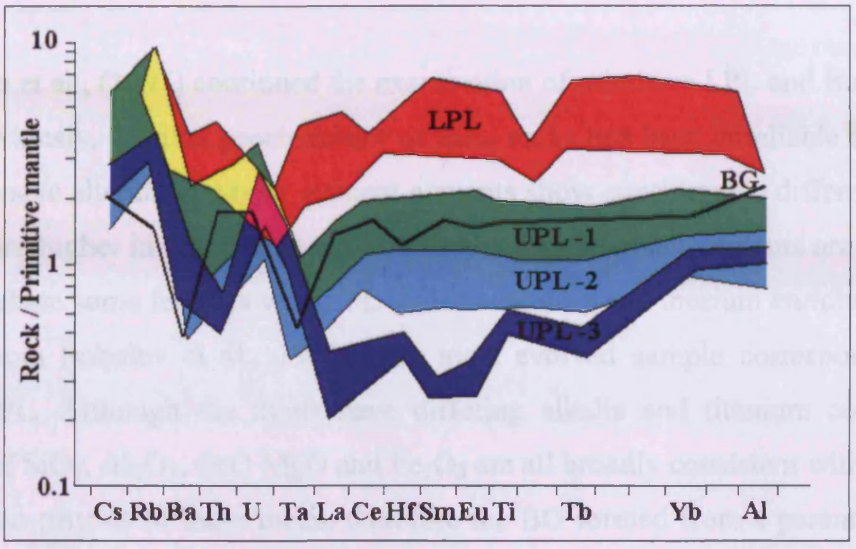

Within the northern part of the Troodos lava sequence, stratigraphic reconstructions (e.g. Taylor, 1987, Bednarz and Schmincke, 1994) have shown that 50 to 75% of the lava pile is comprised of high-Ti, evolved lavas (LPL). Sobolev et al. (1993) calculated that Group 1(A+B) UPL comprise up to 80% of the UPL pile. Therefore, the primitive UPL groups are volumetrically small within the northern Troodos. This implies that, as the Troodos Massif evolved, the magma source became more depleted and the volume of lavas produced also reduced.

Sobolev et al. (1993) calculated that the array of lavas recorded required three principal components. Component 1 was lherzolite-harzburgite mantle, which determines the major element content of the primary melt. This became increasingly depleted in incompatible elements with time. Component 2 was a subduction-related fluid, responsible for incompatible element content in the lavas, producing the supra-subduction zone signature in the lavas. Component 3 was a Ta-rich melt, corresponding to enriched intraplate magma types. This component is only seen in the highly depleted Group 3 UPL and may have arisen from low degrees of melting of primitive mantle. This work effectively quantifies the 'three-group' models of McCulloch and Cameron (1983) etc. Group 1 is composed primarily of 'Component

1' source material. Groups 2 and 3 are composed of 'Component 1' source (variably depleted) with the addition of 'Components 2' and '3' respectively.

Portnyagin et al., 1997

Portnyagin et al., (1997) continued the examination of primitive LPL and Basal Group lavas. Previously, detailed geochemistry of these rocks had been unreliable because of their pervasive alteration. Major element contents show considerable differences with UPL but are higher in Mg (Fig. 1.4-36), whereas trace element contents are similar to UPL, but share some features with LPL such as caesium and thorium enrichment (Fig. 1.4- 35 from Sobolev et al., 1993). The most evolved sample corresponded with normal LPL. Although the melts have differing alkalis and titanium content, the amounts of SiO_2, Al_2O_3, CaO MgO and Fe_2O_3 are all broadly consistent with the LPL, implying co-genesis of these melts, therefore the BG formed from a parental melt to the LPL. The variability in trace and incompatible elements would be an effect of variations in the amount of subduction input (Component 2 of Sobolev et al., 1993).

Fig. 1.4-36. FeO, CaO, TiO_2, SiO_2 v MgO for primitive Basal Group lavas. These data plot along the same trends as the LPL, but are more primitive with higher MgO and CaO. (Portnyagin et al., 1997) Red = Lower Pillow Lava compositions, yellow = Upper Pillow Lava glass compositions and green = bulk Upper Pillow Lavas compositions. The black trend and points represents the Basal Group.

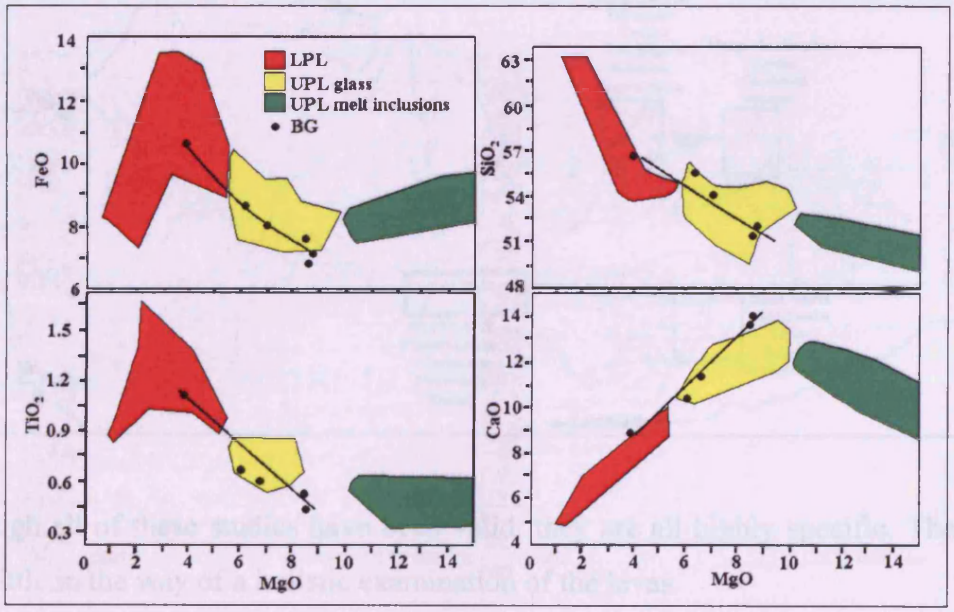

1.5 – Aims and objectives of thesis

1.5a) – Limitations of previous work

The almost continuous period of detailed research on lavas from the Troodos Massif ends with Portnyagin et al. (1997). There has been no Cyprus-specific lava-based work published since then. The use and expansion of geochemical fingerprinting methods in tandem with improved analytical technology has merely moved to other locations. Three of these other locations; the Lau Basin, the Mariana Basin and the South Sandwich Arc/East Scotia Ridge system are analogous in some way to the Troodos Massif. The relationship will be discussed in Chapter 4.

Work so far on the lavas of the Troodos Massif is fragmented and inconsistent. Analytical techniques have changed over the period of previous study, resulting in datasets obtained using INAA, XRF and even 'wet-chemistry' methods. Fig. 1.5-1 illustrates the fragmentary nature of locations sampled before this work.

Fig. 1.5a-1 Areas of the Troodos Massif lava sequence sampled for geochemical analysis. Locations coloured by authors.

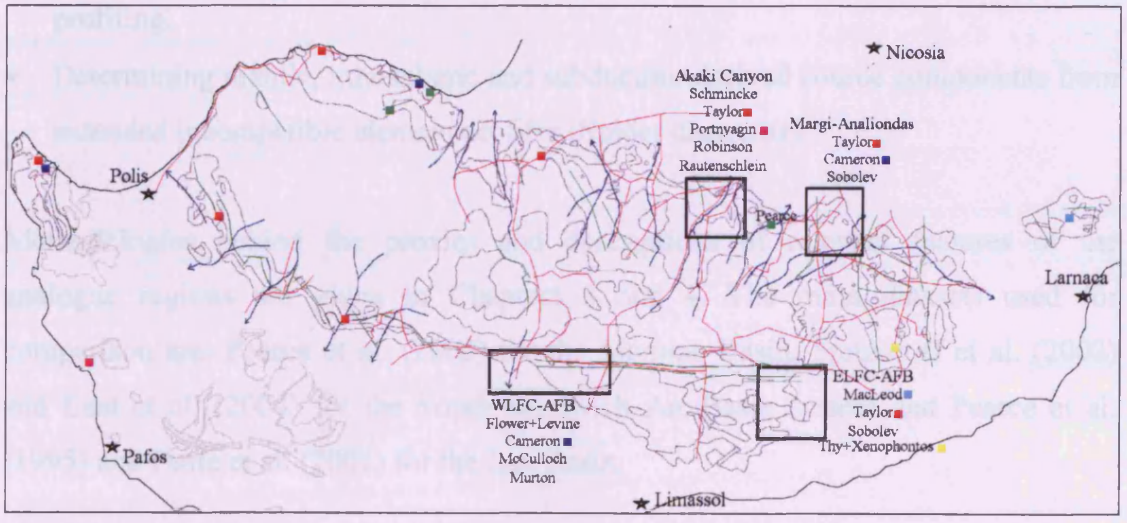

Although all of these studies have been valid, they are all highly specific. There has been little in the way of a holistic examination of the lavas.

1.5b) Aims of the thesis

The main aims of the thesis are:

- Create a high quality geochemical database with modern analytical equipment.
- Extend geochemical coverage to the entirety of the lavas section of the Troodos Massif.
- Apply Geographic Information System software in conjunction with more traditional graphical methods to present results spatially.

In addition this work will evaluate the database in terms of proxies of geochemical processes. The proxies used are:

- Mapping source depletion, partial melting and oxygen fugacity within the Troodos Massif using the Myashiro (TiO_2 – FeO/MgO) projection and FeO - MgO relationships.
- Geochemical mapping using Titanium and Vanadium content to investigate variations in source depletion and enrichment.
- Measuring mantle source depletion, partial melting and fractional crystallisation using Cr and Y.
- Measuring subduction input using Th-Nb and Th-Ta covariations.
- Determining source depletion and subduction enrichment using rare earth element profiling.
- Determining mantle, lithospheric and subduction-derived source components from extended incompatible element profiles (Spider diagrams).

Methodologies behind the proxies and descriptions of relevant features of the analogue regions are given in Chapters 3 and 4. The main datasets used for comparison are: Pearce et al. (2005) for the Mariana Basin, Fretzdorff et al. (2002) and Leat et al. (2004) for the South Sandwich Arc/Basin system and Pearce et al. (1995) and Peate et al. (2001) for the Lau Basin.

2) Sampling, laboratory preparation, analysis and data handling

2.1) Sampling and analysis

2.1a) Choosing sampling areas

The choice of sampling area is dictated by both the aims of the thesis and the extent of previous work. In order to investigate properly the spatial and temporal geochemical variation, both with relation to distance from a paleo-subduction zone and distance from a paleo-transform fault, an even spread of samples was ideally required in terms of stratigraphic group and geographic location. The literature survey highlighted sampling gaps in both geographical and stratigraphic terms. To ensure consistency with previous work, a few samples were also taken from areas that had already been sampled by others. Fig. 2.1a-1 shows the extent of previous sampling. On this basis, I focussed on the central part of the northern lava outcrop, the Larnaca Graben and the south western area, between Polis and the WLFC, collecting a total of 130 samples.

Analysis of these samples and re-analysis of a number of samples from Taylor (1986) and J.A. Pearce and C.J. MacLeod (pers. comm.) gave a dataset totalling 180 analyses. Detailed examination of this dataset indicated that a second sampling expedition was required to fill some gaps that turned out to be critical in the Larnaca Graben, north western Troodos and the Limassol Forest Complex. Some of these gaps were created when old XRF data was found to be unreliable and where reported data was missing critical elements e.g. full rare-earth element spectra and also Nb, Ta and Th. The eventual dataset totalled 240 analyses.

2.1b) Field sampling methods

The first field trip was undertaken in February 2002. Locally, sampling was limited by access, which meant a continuing absence of samples from remote areas, parts of the ophiolite in the Turkish sector and military enclaves. Sampling of fresh rock was preferred as it permits a greater suite of elements to be analysed, however altered rock

can still be analysed for immobile elements. Once sample areas had been identified, the field sampling techniques were as follows. First a suitable outcrop was located, i.e. one in which the rock was mineralogically representative of the location and as fresh as possible. Many of the new road cuttings dug for a recent program of road improvements provided suitable outcrops. The next step was to locate the site using GPS and record this as well as other relevant information such as rock type and sample number. Co-ordinates were taken using the UTM 1984 grid. After that, the samples were hammer-trimmed to remove the worst of the weathered material and reduce size and weight for transit. They were then bagged and labelled. 130 samples were taken and a total mass of about 60kg was shipped to Cardiff.

The second trip was undertaken in February 2005. Sampling locations in which 60 samples were collected from the north west of the Troodos Massif, the Larnaca Graben and the Limassol Forest Complex. Similar field practices were used as the first trip.

As noted above, 240 samples from the Troodos Massif were prepared and analysed by ICP-MS in Cardiff. Only samples from the first expedition were analysed by ICP-OES for major elements. Locations of all samples documented in this thesis are shown in Fig. 2.1b-1.

Fig 2.1b-1. Locations of samples analysed for this thesis.

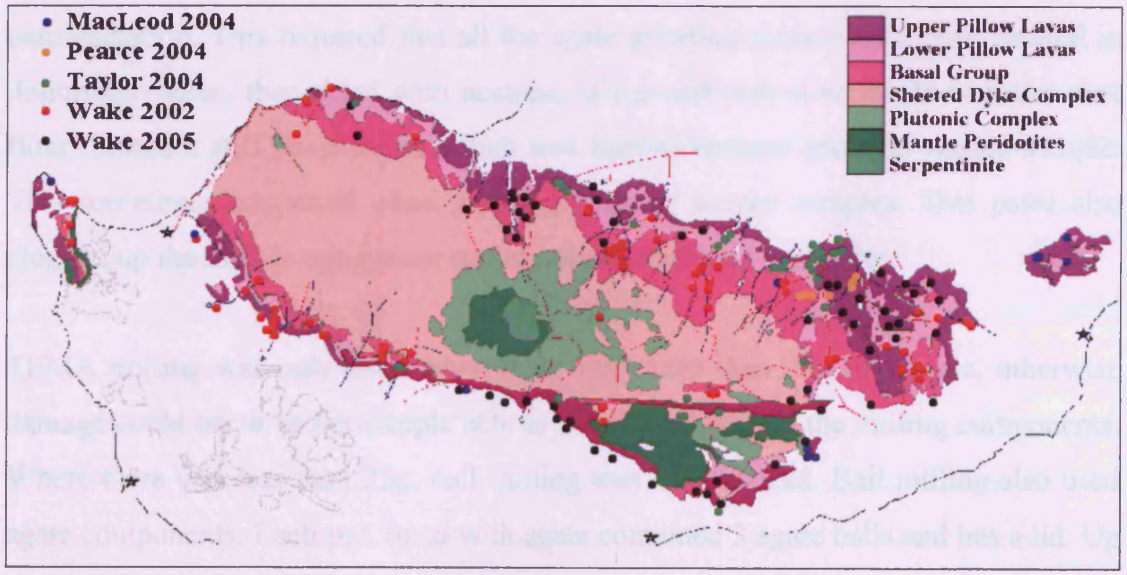

2.1c) Trimming and grinding

Rough rock specimens were first trimmed of their weathered margins. Tablets of rock produced by the trimming process (the off-cuts are kept as they may be useful for a comparison between weathered and fresh rock) were then ground into fine rock flour. Usually between 4 and 10 grams of powder was produced. Depending on the rock type involved, the first stage can vary. Hard samples were crushed into a gritty consistency in a jaw crusher. The jaws of the crusher used steel. To reduce the amount of cross-contamination between samples the crusher was cleaned between each run to remove rock debris. If the sample was heavily altered and soft, a pestle and mortar was used instead. Samples containing glass were treated differently: firstly glassy rims, such as pillow rinds were chipped off their substrate with a pair of pliers or similar implement and then glassy shards were then separated visually from rock fragments.

Depending on the quantity of rock to be ground, samples were processed in a TEMA mill or a rotary ball mill. The TEMA mill consists of an agate bowl with an agate ring about 2/3 the diameter and an agate cylinder 2/3 the internal diameter of the ring. Crushed rock is placed in the mill, which was then closed, and mechanically shaken for 2 minutes. Agate rather than tungsten carbide was used to prevent contamination of the sample from the mill as WC also contains tantalum. Agate, being SiO_2, will not contaminate samples. Although this was an efficient way to grind the sample, the mill needed to be thoroughly cleaned and dried before re-use in order to prevent cross-contamination. This required that all the agate grinding components were washed in de-ionised water, then dried with acetone. If the mill was used while wet, the rock flour formed a stiff paste inside which was hard to remove and also wasted sample. This sometimes happened when grinding hydrous altered samples. This paste also clogged up the mill, leaving some of the sample unground and gritty.

TEMA milling was only used when there was more than 25g of sample, otherwise damage could occur as the sample acts as a cushion between the milling components. Where there was less than 25g, ball milling was used instead. Ball milling also used agate components. Each pot, lined with agate contained 3 agate balls and has a lid. Up to 8 of these pots (which are numbered to prevent confusion) could be used at any

time. Once the mills are loaded, the machine centrifuges them at 300 rpm for 10 minutes. As with the TEMA mill, the equipment was thoroughly cleaned after use. Ground samples are then bagged and labelled. Where the sample volume was very small (under 10g), the samples were ground in a pestle and mortar.

2.1d) LOI + ICP-OES preparation

Loss on Ignition (LOI)

This is the first stage of analysis. Approximately 2g of sample were weighed out into clean porcelain crucibles and the mass recorded to an accuracy of 4 decimal places. These crucibles were fired for 1 hour at 900°C in a furnace to ensure they were dry. Samples are then placed in a furnace at 900°C for 2 hours. After removal, the samples were allowed to cool and are then re-weighed. LOI itself is calculated using the formula:

$$\text{LOI} = \frac{(\text{initial mass} - \text{baked mass})}{\text{initial mass}} \times 100$$

Fired samples were kept for analysis by ICP-OES.

Inductively Coupled Plasma – Optical emission spectroscopy (ICP-OES)

To prepare samples for ICP-OES analysis, 0.4 g of flux (analytical grade lithium metaborate) was added to 0.1+ 0.001g of powdered sample to reduce its melting temperature together with a potassium iodide wetting agent (KI). This combination of sample, flux and KI was mixed and put into a platinum crucible. Pt was used because it is relatively chemically inert and will not contaminate the sample or be altered during the experimental process. In addition, none of the samples prepared this way required Pt. The crucibles were then inserted into a 'Fluxy' machine where they were heated to melting temperature for about 3 minutes and melted. The fused samples were then emptied automatically into 50 ml 4% nitric acid for solution. They were then topped up (using a volumetric flask) to 100ml for storage and analysis. The 'Fluxy' can handle samples in groups of three. While one set was running, the next set was prepared in order to increase efficiency.

Analysis

For analysis, approximately 10ml of each dissolved sample were transferred into clean and pre-rinsed sample analysis bottles. The samples were then loaded into an autosampler. Prior to analysis, the machine was calibrated against a set of international and laboratory standards (section 2.1f) chosen to represent the range of expected compositions of the unknown samples.

A typical analysis run consisted of 20 to 60 samples. After calibration, the run was arranged as follows. The first sample was a procedural blank. This was followed by standards prepared in the same batch as the samples to be analysed. The remainder of the run consisted of the 'unknowns' with a standard inserted at intervals to monitor drift. I also re-made one or more unknowns for each run to monitor consistency between runs.

Analyses were reported in oxide weight percent for Si, Ti, Al, Fe, Mg, Mn, Ca, K, Na and P and in ppm for Ba, Co, Cr, Cu, Ni, Sc, Sr, V, Y and Zr.

2.1e) Inductively-Coupled Plasma - Mass spectrometry (ICP-MS)

The preparation for ICP-MS used non-fired samples. Preparation runs were usually done in batches of around 30. Each run of 30 typically consisted of 26 unknown samples, one procedural standard (JB1A), one repeated sample (CC2/029) and two procedural blanks.

To prepare each one, the method of Pearce et al. (1995) was used. In this each 0.1g sample was accurately weighed into a cleaned and labelled Savillex beaker (Savillex is a trade name for a small Teflon beaker with a screw-on lid). The mass of sample used was noted as this was needed to calculate analyte dilution factors during analysis. Once all 30 beakers had been prepared; they were transferred into a 'clean-lab' for acid digestion. The first acid step was to add 1ml concentrated nitric acid. This dissolved safely any carbonate in the samples. Any samples that fizzed excessively were noted, as this was a sign of high carbonate content which indicated

extensive alteration. After any reaction subsided, 4 ml HF was added and the beakers were then closed. The lidded samples were then heated on a hotplate at 125° for 24-48 hours. The excess HF was evaporated off after the digestion had completed; a process that also drove off silica. 1ml concentrated nitric acid was added to the samples that were then lidded and left on the hotplate for at least 2 hours but usually overnight. The samples in nitric acid were evaporated down and the process was repeated. Evaporation took about 2 hours. The samples were then spiked with 1 ml of a solution containing 2.5 ppm rhodium and rhenium. They were then diluted with distilled water to a volume of 50ml. They were now ready for storage and analysis. After use, the Savillex beakers underwent a cycle in a dishwasher before being washed with concentrated nitric acid and rinsed in de-ionised (DI) water.

Prior to analysis, the dissolved samples were diluted further in 2% nitric acid to 20% of their previous concentration and an overall dilution of 1:500 based on sample weight. Dilution factors (based on sample weight) were programmed into the computer to adjust the raw data for inconsistencies in the sample concentration. The machine set-up was very similar to that for ICP-OES, involving transferring to pre-rinsed sampling bottles, loading the autosampler and calibrating the machine against the set of standards that I had chosen. The analysis run for each sample was as follows. For a standard 4 'sweep' analysis, this took 6 minutes per sample. Each sweep took 30 seconds, with a 5-second delay between each. There was also a 2-minute acid wash and 90 second pre rinse between each sample. Every 7 samples a detergent (Triton-X) and acid blank was run followed by a drift monitor.

The elements reported were:
Fifteen trace elements as parts per million: Sc, V, Cr, Co, Ni, Cu, Zn, Ga, Rb, Sr, Y, Zr, Nb, Cs, Ba,
Fourteen Rare Earth Elements as parts per million: La, Ce, Pr, Nd, Sm, Eu, Gd, Tb, Dy, Ho, Er, Tm, Yb, and Lu
Five heavy elements as parts per million: Hf, Ta, Pb, Th, and U

2.1f) Blanks, contamination, standards and spikes

Blanks

Blanks are samples made in the same way as normal samples but without the rock powder. They were made with the same equipment and same chemicals as normal samples. A blank was usually run first during analysis, the blank value being deducted automatically from the sample totals. Subsequent blanks were placed at intervals through the run. If the blank values were high or variable, this increased the acceptable limits of detection, causing some of the lower analyses to have to be repeated or rejected. This could be a result of either poor calibration of the machine or contamination of the chemicals used.

Blanks for ICP-OES were made from 0.5g lithium tetraborate flux with the rest of the procedure as described in 2.1.4.

Blanks for ICP-MS contained no sample but beakers were left open to the air during sample weighing (to allow for airborne dust contamination), and then prepared in the same way as the other samples. Acid blanks were also used. These were merely a spiked sample of the acid used at the last stage of dilution.

Contamination

Many of the elements that were being analysed exist in the samples in ppm levels. Therefore they were sensitive to contamination. Within a sample suite, contamination between samples may not have a drastic effect but outside contamination can. Contact with enriched rock samples (such as granite) was thus avoided. Standard clean-laboratory procedures were used to minimise contamination risk.

Standards

Standards are rock specimens of known composition. They have been produced in bulk and have been analysed many times. They are mostly supplied by such agencies as national geological survey departments. A set of standards was chosen that was

similar in composition to the unknown samples. Several standards are usually run at the start of an analytical run in order to calibrate the machine. A calibration curve is produced by plotting the recorded values for each element in the standard against the recommended values. The official values are usually obtained from the relevant Geological Survey department. A calibration curve links counts obtained by the machine to concentrations of element recorded. Standards used for this study, for which the rock types are predominately boninitic, basaltic and basaltic andesitic are:

JB1a – Japanese Survey standard, Basalt from Kyushu Island
W2 - USGS rock standard, Augite dolerite from Virginia State
MRG1 – Canadian Survey standard, Gabbro.
X108 – Boninite from Bonin Island, (Pearce laboratory standard)
JA2 – Japanese survey standard, Andesite from Shikoku Island
BHVO1 – USGS rock standard, Basalt Hawaii Volcanic Observatory, 1919 Pahoehoe flow
ENDV – MORB from EPR (MORB inter-laboratory standard by Perfit)
BIR1 - USGS rock standard, Basalt, Icelandic coarse olivine tholeiite.

Spiking

Spiking is the addition of a controlled amount of particular elements to the analyte. Cardiff laboratory procedures use a spike that imparts a Rh and Re concentration equivalent to 25 ppm in the original sample. The computer controlling the analytical machinery automatically re-scales the recorded values to match the spike concentration to the expected level.

2.1g) Data quality and arithmetical procedures

Detection limits

Conceptually, the "limit of detection" is the smallest amount of a substance that an analytical method can reliably distinguish from zero. More formally, it is the minimum concentration or amount of a target analyte that produces a signal the tester

can distinguish, at a specified confidence level, from the signal produced by a blank. The limit of quantification is the minimum concentration or amount of an analyte that a method can measure with a specified degree of precision. The procedure for calculating the limit of detection is to collect and analyse a series of blank samples. The standard deviation of the results was then calculated. Multiplying the standard deviation by three produces a limit of detection at roughly the 99% confidence level. Multiplying the standard deviation by ten produces the quantification limit.

To convert from individual counts on the ICP-MS to ppm values, the 3 or 10 times standard deviation value is divided by the counts/ppm value. The counts/ppm value is obtained by dividing the mean counts value of a standard by its certified value. In this example, the USGS standard W2 was used.

Table 2.1g-1 overleaf shows mean counts obtained from the first blank of my analytical runs, together with the standard deviations and calculations necessary to produce detection and quantification limits in parts per million. Generally the quantification limits are very low. The high quantification limit for Ni is caused by the nickel cone used in the ICP-MS machine itself. Most other quantification limits are considerably lower (by 3 orders of magnitude) than the values found in my sample suite. Cr has a quantification limit of 0.5 ppm, and some highly fractionated samples had Cr contents of 1 or 2 ppm. Also the Cs concentration in most samples is about the same as the quantification limit hence a very high standard deviation of Cs values.

Table 2.1g-1 ICP-MS Detection limits

	Mean Counts	SD	%RSD	3 x SD	10 x SD	W2 certified value (ppm)	Counts / ppm	Detection limit (ppm)	Quantification limit (ppm)
Sc	2112.2	100.1	4.7	300.3	1001.0	36.0	11197.5	0.02682	0.08940
Ti	472.5	35.9	7.6	107.8	359.4	6360.0	620.5	0.17378	0.57926
V	1096.1	104.7	9.6	314.0	1046.8	260.0	11351.9	0.02766	0.09221
Cr	24432.9	297.9	1.4	893.6	2978.6	92.0	6066.1	0.16076	0.53586
Co	1294.1	41.5	3.2	124.5	415.1	43.0	14290.1	0.00871	0.02905
Ni	43242.9	274.1	1.3	822.3	2741.1	70.0	2868.5	0.54119	1.80398
Cu	10809.6	314.9	2.9	944.6	3148.6	110.0	3801.9	0.24845	0.82817
Zn	11675.6	152.4	1.3	457.2	1524.1	80.0	2616.9	0.17472	0.58240
Ga	184.0	10.5	5.7	31.4	104.6	17.0	8645.0	0.00363	0.01209
Rb	576.5	31.0	5.4	93.1	310.5	21.0	14229.0	0.00655	0.02182
Sr	3105.5	74.8	2.4	224.3	747.6	190.0	20513.9	0.01093	0.03644
Y	360.3	21.5	6.0	64.6	215.3	23.0	22405.0	0.00288	0.00961
Zr	1774.4	53.6	3.0	160.9	536.5	100.0	11186.2	0.01439	0.04796
Nb	857.4	69.2	8.1	207.7	692.3	7.9	19970.8	0.01040	0.03467
Cs	209.7	15.1	7.2	45.3	151.0	1.0	27934.3	0.00162	0.00541
Ba	2866.5	97.0	3.4	290.9	969.6	170.0	4093.1	0.07106	0.23688
La	362.0	13.0	3.6	38.9	129.6	10.0	39711.3	0.00098	0.00326
Ce	1870.9	36.8	2.0	110.4	368.0	23.0	37185.4	0.00297	0.00990
Pr	87.8	4.6	5.3	13.9	46.5	3.0	44051.4	0.00032	0.00105
Nd	73.0	7.3	10.1	22.0	73.5	13.0	8150.1	0.00271	0.00902
Sm	17.3	6.4	37.1	19.2	64.0	3.3	7153.6	0.00268	0.00894
Eu	11.0	3.7	33.2	11.0	36.5	1.0	30505.3	0.00036	0.00120
Gd	11.3	3.1	27.5	9.3	31.0	3.5	8894.8	0.00348	0.00104
Tb	17.0	2.9	17.3	8.8	29.4	0.6	53263.6	0.00017	0.00055
Dy	15.0	6.3	42.2	19.0	63.3	3.6	14791.0	0.00128	0.00428
Ho	14.0	3.5	24.7	10.4	34.6	0.8	58110.9	0.00018	0.00060
Er	8.8	1.0	10.9	2.9	9.6	2.5	17246.5	0.00017	0.00055
Tm	3.5	1.7	49.5	5.2	17.3	0.4	49801.8	0.00010	0.00035
Yb	7.5	1.9	25.5	5.7	19.2	2.1	12878.7	0.00045	0.00149
Lu	4.8	2.2	46.7	6.7	22.2	0.3	54729.3	0.00012	0.00041
Hf	51.1	6.3	12.2	18.8	62.5	2.6	15909.4	0.00118	0.00393
Ta	10.0	0.8	8.2	2.4	8.2	0.5	52021.1	0.00005	0.00016
Pb	7931.2	104.5	1.3	313.6	1045.3	9.3	22669.1	0.01383	0.04611
Th	89.4	4.1	4.6	12.3	40.9	2.4	46042.1	0.00027	0.00089
U	195.8	9.0	4.6	26.9	89.7	0.5	49512.6	0.00054	0.00181

Drift monitoring

Although, before a run commences, the machine is calibrated to a set of standards, the calibration may drift during the run. The only way to monitor this, as it does not always happen at a predictable rate, is to carry out multiple analyses of the same

sample throughout a run. Drift can also affect different elements to different extents. A drift monitor, usually a standard, was run every 7 unknowns. To account for drift of a particular element, the drift monitor value was divided by the initial value of the same sample to obtain a drift factor. Drift factors between drift monitors were corrected by interpolation. Drift correction was done manually after the run has finished.

Repeat analysis

In order to ensure consistency between the various analytical runs, one standard and one sample from my suite were analysed in each run. Consistency between runs for sample and standard was calculated by comparing the runs arithmetically and comparing the relative standard deviation of the figures. If the RSD was low the runs were consistent and the data can be trusted.

Table 2.1g-2 shows inter-run consistency for standard JB1a. Consistency between runs was measured using the relative standard deviation (RSD) of the runs. RSD is quoted as a percentage.

$$\text{RSD} = \frac{\text{Standard deviation}}{\text{Average}} \times 100\%$$

The values obtained for each run are shown, together with an average, standard deviation (SD) and relative standard deviation in %. Samples highlighted in yellow show a relative standard deviation greater than 20% and samples highlighted in grey show a relative standard deviation between 10% and 20%, indicating that there are inconsistencies between the runs for these elements. Nickel and zinc were the least consistent, though the inconsistency of nickel is to be expected because of its presence within the ICP-MS machinery: the analyte passes through a nickel cone before entering the plasma torch.

Fig 2.1g-3 shows inter-run consistency for the repeated sample, CC2/029, a Basal Group basalt from northern Troodos. Fig 2.1g-4 shows a comparison of RSD's of

both JB1a and CC2/029. Inter-run consistency for CC2/029 is lower because CC2/029 has lower contents of incompatible elements and the values are therefore closer to the detection limits. Cs content in CC2/029 is below the detection limit.

Table 2.1g-2 Inter-run consistency for standard JB1a

	Run	*Run*	*Run*	*Run 5*	*Run 6*	*Run*	*Run*	*Run*	*Run 7a*	*Run 7b*	*Ave.*	*SD*	*RSD %*
Sc	30	27	28	28	27	27	27	27	27	24	27	1	**5.09**
Ti	12059	12380	12820	12260	12470	13083	13083	13383	12930	11980	12645	480	**3.80**
V	200	182	186	181	199	215	207	203	197	182	195	12	**6.11**
Cr	435	437	438	483	420	429	446	462	408	369	433	31	**7.07**
Mn	1483	1395	1437	1449	1450	1427	1436	1453	1470	1350	1435	38	**2.66**
Ni	73	139	141	143	145	121	123	191	160	121	136	30	**22.43**
Cu	57	54	57	56	52	58	57	58	57	53	56	2	**3.65**
Zn	78	66	91	76	107	82	85	81	91	85	84	11	**13.13**
Ga	19	17	18	18	18	18	18	18	18	17	18	1	**2.80**
Rb	39	40	41	39	40	40	40	41	41	40	40	1	**2.03**
Sr	461	431	450	451	449	440	440	445	459	438	446	10	**2.14**
Y	23	23	24	24	23	24	24	24	25	23	24	0	**1.91**
Zr	143	145	151	143	143	149	150	149	150	140	146	4	**2.63**
Nb	24.02	26.84	27.38	28.39	26.81	28.71	28.84	28.88	29.78	27.76	27.74	1.62	**5.85**
Cs	1.15	1.16	1.34	1.15	1.19	1.19	1.21	1.22	1.30	1.22	1.21	0.06	**5.01**
Ba	496	498	516	497	503	520	535	531	561	527	518	21	**4.01**
La	39.94	37.95	38.35	38.82	38.67	40.09	39.56	40.43	41.99	39.52	39.53	1.18	**2.98**
Ce	69.72	64.94	65.57	66.74	65.66	69.64	68.58	69.96	71.50	67.24	67.96	2.24	**3.29**
Pr	7.52	7.06	7.10	7.41	7.31	6.97	6.93	7.07	7.12	6.68	7.12	0.25	**3.45**
Nd	27.09	25.70	25.89	26.92	26.46	28.09	27.94	28.51	28.77	26.95	27.23	1.06	**3.90**
Sm	5.09	4.92	4.99	5.16	5.09	5.25	5.24	5.36	5.40	5.06	5.15	0.16	**3.04**
Eu	1.57	1.47	1.49	1.52	1.52	1.53	1.52	1.57	1.66	1.56	1.54	0.05	**3.45**
Gd	5.00	4.69	4.77	4.80	4.79	4.78	4.73	4.83	5.14	4.83	4.84	0.13	**2.78**
Tb	0.73	0.71	0.72	0.72	0.71	0.71	0.71	0.71	0.75	0.70	0.72	0.01	**1.91**
Dy	4.01	3.96	3.96	4.06	4.02	4.08	4.07	4.11	4.28	3.98	4.05	0.10	**2.35**
Ho	0.80	0.78	0.80	0.76	0.76	0.80	0.79	0.81	0.83	0.78	0.79	0.02	**2.65**
Er	2.17	2.14	2.15	2.20	2.16	2.21	2.20	2.24	2.36	2.18	2.20	0.06	**2.89**
Tm	0.33	0.33	0.33	0.33	0.33	0.34	0.34	0.34	0.36	0.33	0.34	0.01	**2.48**
Yb	2.09	2.04	2.04	2.09	2.09	2.06	2.08	2.10	2.24	2.05	2.09	0.06	**2.68**
Lu	0.32	0.32	0.32	0.32	0.32	0.32	0.32	0.33	0.35	0.32	0.32	0.01	**2.58**
Hf	3.49	3.41	3.44	3.49	3.55	3.67	3.69	3.75	3.85	3.51	3.58	0.15	**4.08**
Ta	1.74	1.79	1.81	1.77	1.82	1.73	1.75	1.76	1.88	1.70	1.78	0.05	**2.90**
Pb		6.33	6.91	6.93	6.99	6.32	6.36	6.62	7.78	7.15	6.82	0.48	**6.99**
Th	8.26	8.38	8.53	8.39	8.57	8.61	8.63	8.76	9.30	8.89	8.63	0.30	**3.47**
U	1.65	1.66	1.64	1.48	1.61	1.63	1.64	1.65	1.76	1.67	1.64	0.07	**4.19**

Table 2.1g-3 Inter-run consistency for sample CC2/029

CC2/029	*Run 1-2*	*Run 3-4*	*Run 5*	*Run 6*	*Run RNT*	*Ave.*	*SD*	*RSD%*
Sc	34	31	32	32	30	32	2	**4.84**
Ti	7924	7836	8460	7548	7992	7952	331	**4.16**
V	379	392	424	376	392	393	19	**4.82**
Cr	11	10	12	7	10	10	2	**17.62**
Mn	1437	1402	1486	1486	1450	1452	36	**2.45**
Ni	37	39	48	38	35	41	5	**13.21**
Cu	44	46	47	49	45	46	2	**4.24**
Zn	33	26	29	39	21	30	7	**22.07**
Ga	17	15	16	16	16	16	0	**2.71**
Rb	8	8	8	8	8	8	0	**2.32**
Sr	101	88	87	97	93	7	**7.21**
Y	38	37	36	36	37	37	1	**2.53**
Zr	73	68	77	74	68	72	4	**5.18**
Nb	1.02	1.19	1.02	1.18	1.10	0.10	**8.64**
Cs	0.01	0.01	0.03	0.02	0.01	0.01	0.01	**53.89**
Ba	29	28	29	28	29	28	1	**1.90**
La	2.94	2.51	2.44	2.55	2.39	2.57	0.22	**8.46**
Ce	9.24	7.83	7.93	8.12	7.80	8.18	0.60	**7.35**
Pr	1.65	1.43	1.47	1.52	1.47	1.51	0.09	**5.68**
Nd	9.14	8.00	8.24	8.38	8.20	8.39	0.44	**5.23**
Sm	3.34	3.00	3.09	3.15	3.06	3.13	0.13	**4.21**
Eu	1.13	1.03	1.07	1.08	1.05	1.07	0.04	**3.77**
Gd	4.70	3.98	4.08	4.23	4.02	4.20	0.29	**6.99**
Tb	0.88	0.80	0.83	0.85	0.80	0.83	0.03	**3.73**
Dy	5.73	5.37	5.55	5.65	5.44	5.55	0.15	**2.66**
Ho	1.26	1.20	1.23	1.19	1.16	1.21	0.04	**3.37**
Er	3.67	3.46	3.58	3.65	3.51	3.58	0.09	**2.49**
Tm	0.58	0.56	0.58	0.58	0.57	0.58	0.01	**1.55**
Yb	3.70	3.52	3.65	3.75	3.60	3.64	0.09	**2.48**
Lu	0.57	0.56	0.58	0.60	0.57	0.58	0.01	**2.60**
Hf	2.20	2.13	2.21	2.32	2.22	2.22	0.07	**3.13**
Ta	0.09	0.09	0.09	0.09	0.09	0.09	0.00	**2.86**
Pb	0.16	0.20	0.10	0.08	0.14	0.13	0.05	**36.16**
Th	0.22	0.23	0.24	0.25	0.24	0.24	0.01	**5.64**
U	0.13	0.13	0.10	0.13	0.10	0.12	0.02	**13.63**

2.2) Interpretation techniques

2.2a) G.I.S.

G.I.S. is the abbreviation of the term "Geographic Information Systems". This is an umbrella term defining a number of hardware and software packages. G.I.S. work for this thesis was carried out on ArcView version 3.2 for MS Windows. G.I.S. allows maps and spatially indexed population data to be displayed together, for example allowing element concentrations to be mapped out accurately. Once data has been uploaded onto the system, it can be queried quickly.

2.2b) Compiling data

For this thesis, data were obtained from as many sources as possible, as described in Section 2.1. Within the context of geochemical mapping of the Troodos Massif, any published data that includes locations were considered valid. Some datasets were provided with co-ordinates. Others have been supplied with a location map, from which the co-ordinates could be worked out. Although this may be less accurate, one has to decide what resolution is required. Over the scale of the Troodos ophiolite (approximately 125 x 30km), location accuracy better than 100m or so is not necessary as 100m variations cause placement errors of about 0.1% across the ophiolite. This is smaller than the icon size on a G.I.S. map when showing the whole ophiolite, and therefore within acceptable plotting error margins.

ArcView accepts both map/image data and tabular data. Maps or aerial/satellite imagery need to be converted into "Tiff" files (*.tif). The corner co-ordinates of the map are registered by adding a 'world' file. This file specifies the co-ordinates of the top left corner (north west) of the map, as well as a conversion factor giving ArcView the ground distance covered by each pixel. This file is saved with the same name as the map, but with a *.tfw suffix.

Data tables need to be converted into comma-separated text. This is not the same as a *.csv file (another way MS Excel can store tabular data). It is easier to copy the

required table (or section) into MS notepad and save as *.txt. To modify these files, they have to be opened in notepad and manually modified, or a new file copied from a spreadsheet.

2.2c) G.I.S. Maps

There are two types of map used in the G.I.S. program. There are 'base' maps and output maps. Base maps are the original maps or aerial photographs. These may be outline maps, geological maps, street maps etc. The base maps used in this thesis are based on the 1995 Cyprus Geological Survey map. The images used are: colour scan of map, greyscale map, outline map and outline with main roads and rivers.

Output maps display 'population' data as points, either as unique values or as graduated symbols/colours. This may be either numerical, such as element abundances, one element normalised to another (ratios), or 'unique value' which refers to a label, such as rock type or an author of a paper. Colour schemes and point icons are user-customisable. Fig. 2.2c-1 illustrates some of the basic functions of ArcView.

Fig. 2.2c-1 Typical ArcView display window

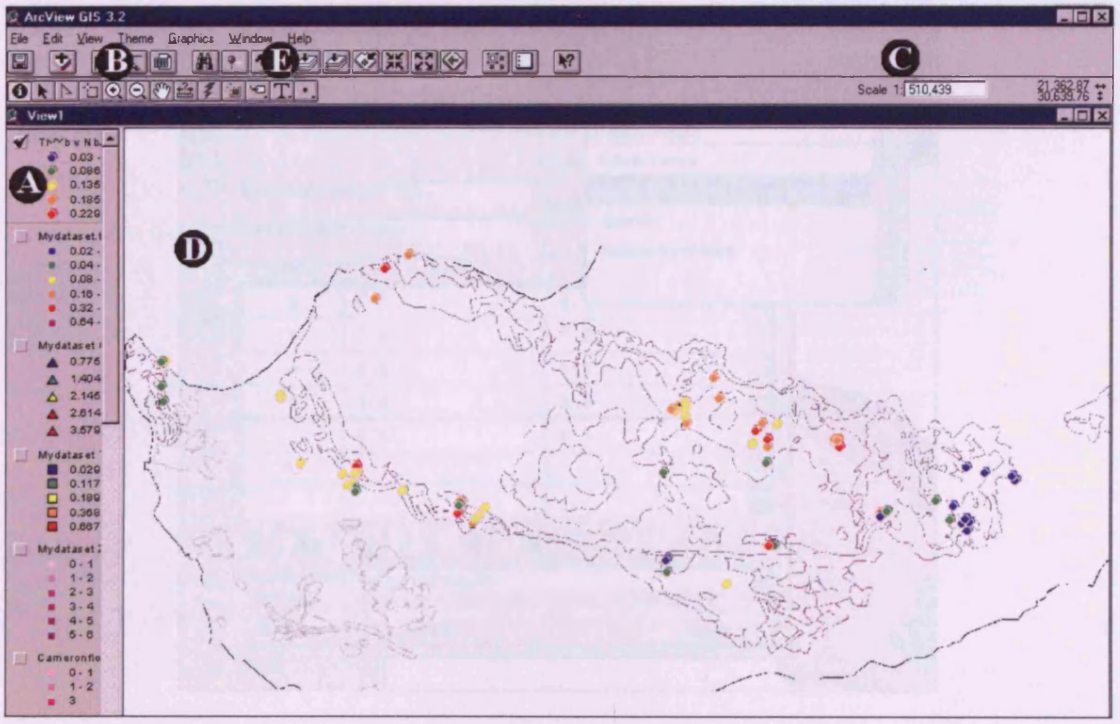

A) This toolbar serves two functions. It serves as a key for symbols and allows the available themes (datasets, either data or image) to be edited. Points are only displayed for themes which are checked in the box in the top left corner, and are overlayed in ascending order from bottom to top. There is no upper limit to how many themes can be displayed, though displaying more than one property per location can cause image clutter.

Double-clicking on a particular 'event theme' brings up a menu allowing the properties to be changed. One can vary which attributes of the source data table are used, for example by changing which element is displayed. It is also possible to adjust the point icon type and colour from this toolbar. The default is red monochromatic. However, variations on a rainbow scheme proved to be most clear. Fig. 2.2c-2 shows the window used to make theme adjustments. Contour breaks are set at 'natural breaks' by default, but can also be set to 'equal interval', 'quantile', 'standard deviation' or achieved manually by entering the contours in the table marked 'value'. The 'statistics' button brings up minimum, maximum, sum, mean and standard deviation of the selected data. Although the theme shown is a pre-calculated ratio (Th/Ta), ArcView can also perform this task using the 'normalise by' function.

Fig. 2.2c-2 Theme editor window

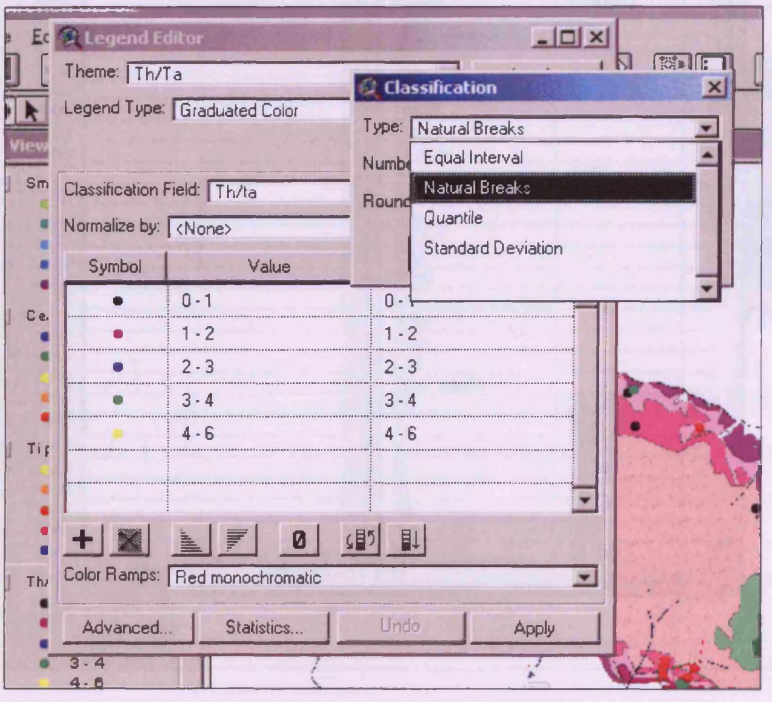

B) The 'View' and 'Theme' buttons allow the user to select which themes are in use at any one time.

C) This shows the scale the map is being displayed at, and allows the user to adjust display scale. This can also be done using zoom in/out tools.

D) This is the map display, comprising an overlay of base map and point/polygon data. Coloured points customisable from (A) display location and properties of data. The colour scheme used shows blue for low abundances and red for high abundances. Data shown in this window can be queried by clicking on the required data-point. This brings up a window (Fig. 2.2c-3) showing all data fields recorded for this point. Data may also be shown for close-lying points depending on the zoom level of the map.

Fig. 2.2c-3 Data query

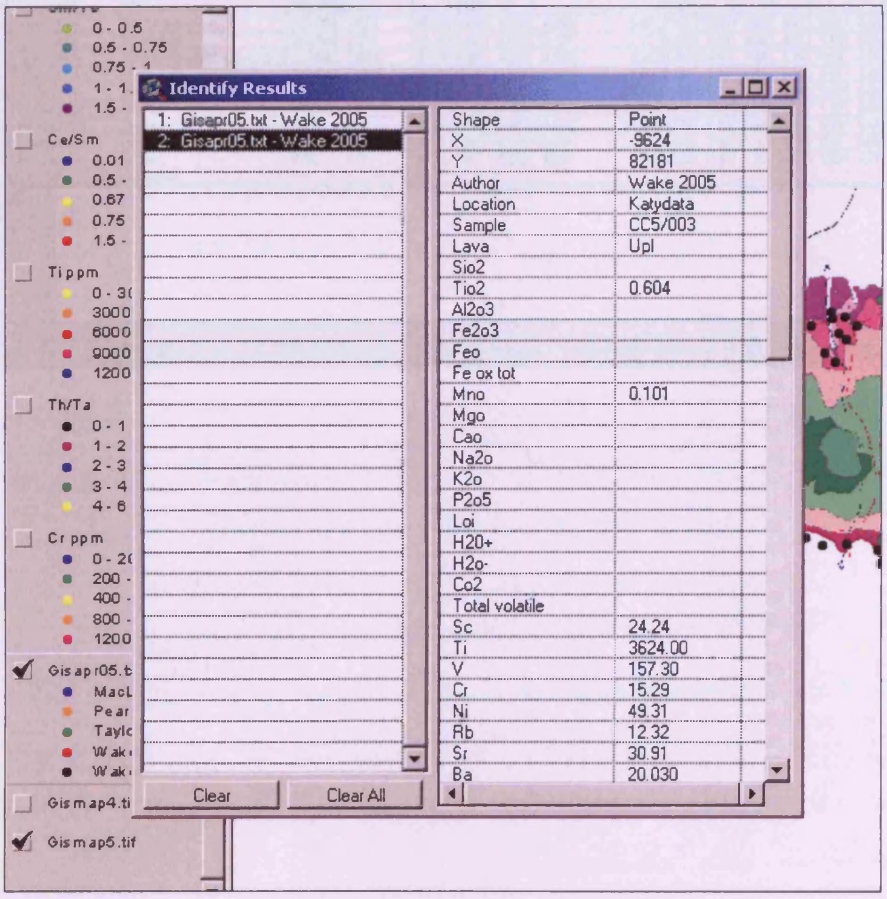

E) The 'window' function switches between any ArcView open windows. Typically these would be *.apr (the generic file) the map display and any data tables. If the data table windows are closed, the data disappears from the map display. Data in these tables cannot be edited from the ArcView window. Fig. 2.2c-4 shows a section of the source data table.

Fig. 2.2c-4 Source data table

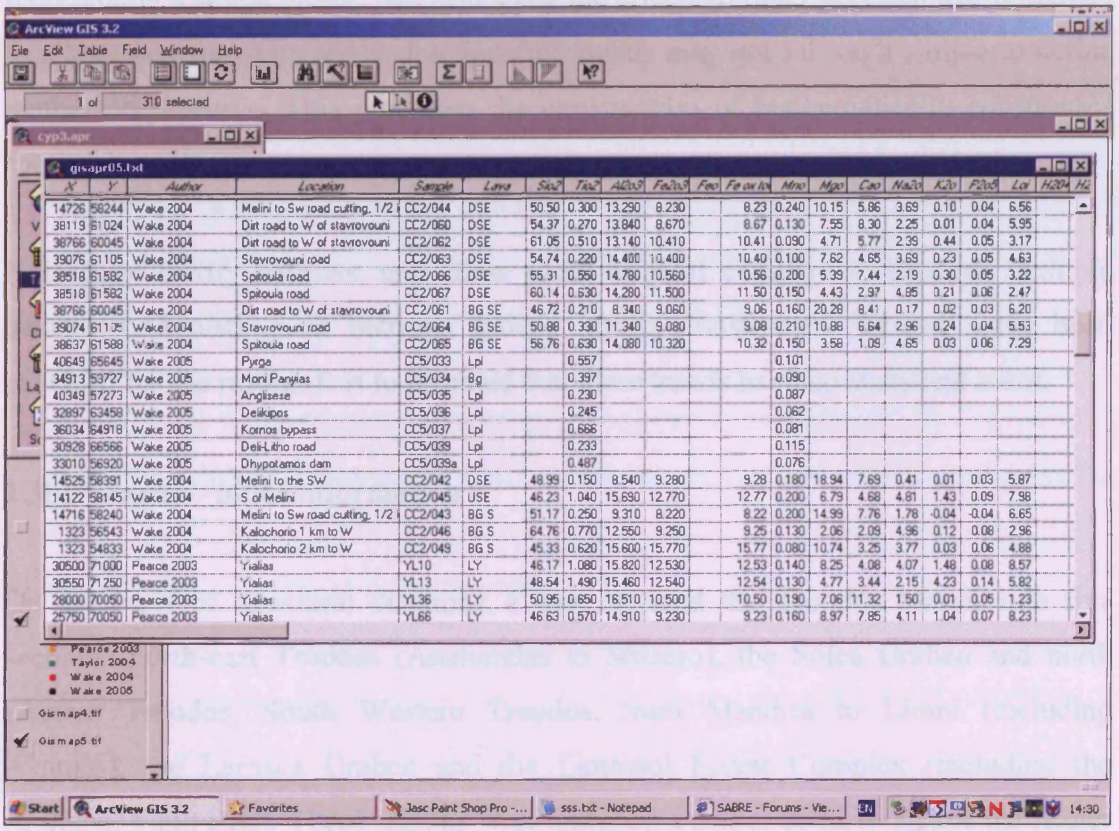

2.3) Graphical methods and data presentation

2.3a) Trendline construction

In order to display groups of data pertaining to particular proxies under scrutiny, bivariate plots will be used extensively. Typically they will present large datasets that are difficult to assess visually. In addition, each graph, although primarily representing a single proxy, will also show the effects of other geochemical processes to a lesser extent. As a result, fractionation trends may not fall on a simple to define mathematical curve. This precludes the construction of mathematically constructed 'best-fit' trends.

Instead, to clarify datasets, and allow some form of comparison between multiple datasets and distinguish between groups, trends constructed 'by-eye' have been provided for the reader. It is to be noted that these trends have no statistical merit.

2.3b) Graphs – other information

On the basis of structural divisions, I have divided the Troodos Massif into five sections: north-east Troodos (Analiondas to Mitsero), the Solea Graben and north western Troodos, South Western Troodos, from Mandria to Limni (including Akamas), the Larnaca Graben and the Limassol Forest Complex (including the Arakapas Fault Belt). These regions were assigned a colour code, to enable the reader to quickly identify the region in concern at a glance, as well as to allow comparison between lavas from different regions. The colour code is as follows: Green = North east Troodos, Yellow = North west Troodos and Solea Graben, Red = South West Troodos, Blue = Larnaca Graben and Purple = Limassol Forest Complex.

A number of outlying points exist on some of the plots. Extensive checking of data sources and if necessary, re-analysis reduced the probability that these points are errors. As the work was done on a regional basis, rather than localised, it is likely that these outliers may be the result of localised anomalies, that would be better determined on a higher-scale study and as such could form the basis of future research.

Chapter 3 – Discussion of results and presentation of data

3.1) Mapping source depletion, partial melting and oxygen fugacity within the Troodos Massif using the Myashiro (TiO_2 – FeO/MgO) projection and FeO - MgO relationships

3.1a) Effects of f_{O2} on Fe, Mg and Ti content in basalts

Oxygen fugacity (f_{O2}) is a measure of the chemical potential of oxygen in an igneous system. In magmas, higher oxygen fugacity causes oxides of some metals, including those of Fe and Ti, to precipitate early in the crystallisation sequence. Therefore, lavas formed within such environments are depleted in FeO and TiO_2 compared to lavas from reducing environments. The high f_{O2} values in lavas above subduction zones are largely related to addition of subduction-derived fluids to the melt. Pearce et al. (1995) found that, within the Lau Basin, the degree of subduction-derived enrichment is dependent on the distance of melt generation from the subduction zone. Lavas were sampled from spreading centres at various distances 'behind' (to the west of) the Tonga Arc, and their f_{O2} values estimated by comparing iron enrichment trends in the lavas with those in calibrated experiments.

When plotted against MgO, FeO* (FeO* = Total Fe or FeO + Fe_2O_3) in MORB type basalts have a considerable iron enrichment peak, but the more oxidising conditions within arcs produce a lower, straight profile in the range MgO = 0-7 wt%. At higher MgO contents, FeO* content stays at approximately 10% regardless of f_{O2}. FeO* and MgO are mobile during alteration, so a greater degree of scatter may be expected if the rocks are altered rather than fresh. Both FeO* and MgO usually increase in the rock during seafloor weathering processes.

When plotted against, FeO*/MgO in MORB-type basalts, TiO_2 increases considerably relative to FeO*/MgO (high TiO_2 /(FeO*/MgO) ratio at low values of FeO*/MgO). The oxygen fugacity of magma will affect the minerals crystallising from the magma and their crystallisation order. As noted earlier, at higher oxygen fugacities, elements such as iron and titanium precipitate in their oxide form within the magma chamber, removing these elements from the remaining melt. As the oxygen fugacity of the

magma increases, there is a small TiO_2 increase with increasing FeO*/MgO. For some of the most oxidising magma types, such as calc-alkaline magmas, TiO_2 contents remain constant or even decreases a FeO*/MgO rises.

3.1b) History of f_{O2} research within the Troodos Massif and its analogues

As reported in Section 1.3, Myashiro (1973) first noted the elevated oxygen fugacity of supra-subduction zone (SSZ) magmas with respect to MORBs based on plots of titanium against iron and magnesium. He also showed that the lavas from the Troodos Massif displayed trends very similar to the observed SSZ trend. The titanium content of SSZ lavas did not increase greatly or linearly with respect to FeO*/MgO. This was in contrast to the steep and linear increase noted for MORBs. Within the context of the Troodos Massif, the variation within the sample suite may be due either to variations in the f_{O2} of the subduction fluids, assuming a constant melt supply to the ridge, or to the combination of a constant amount of oxidising fluids with variable melt production.

Robinson et al. (1983) demonstrated that fresh glass from the Akaki Canyon (north-east Troodos) plotted close to the established island arc tholeiite (IAT) trend when FeO* (total iron oxide, FeO and Fe_2O_3) and MgO were plotted. Robinson et al. (1983) also showed the differences in Fe-Mg profile between MORB like magmas, those from the Skaergaard and Galapagos rift, and supra-subduction magmas including island arc tholeiites and lavas from calc-alkaline arcs such as the Cascades and Marianas.

The hypotheses of Myashiro (1973) and Pearce (1975), that the Troodos Massif had formed in a supra-subduction environment, has led to the search for current analogues, both structurally and geochemically, in order to prove or disprove the theory. Chosen analogues include parts of the Lau Basin, the Marianas Basin and the East Scotia Ridge. FeO*-MgO profiles for the Tonga Arc were first plotted against Troodos lavas by Myashiro (1973). More recently, Jenner et al. (1987) and Pearce et al. (1995) have provided extensive datasets for comparison. Pearce et al. (1995) first provided direct evidence of the relationship between oxygen fugacity of supra-subduction magmas and the distance from the subduction zone. This was achieved by

comparing the FeO* - MgO profiles of lavas from each region within the Lau-Tonga area with their respective distances from the subduction zone. These profiles were then compared with experimentally-derived FeO*-MgO profiles for varying oxygen fugacities quoted with respect to the quartz-fayalite-magnetite (QFM) buffer. The buffer takes into account that oxygen fugacity is pressure and temperature dependant.

Fig. 3.1b-1 shows experimental trends of Juster et al. (1989) and FeO* v MgO profiles of lavas from the Lau Basin (Pearce et al., 1995). There is a variation of three orders of magnitude in the f_{O2} of magmas generated at the Tonga Arc and the Central Lau Spreading Centre (MORB like). The Valu Fa Ridge lies about 60 km behind the Tonga Arc, with the Eastern Lau Spreading Centre (ELSC) lying 75 – 100km behind the arc and the Central Lau Spreading Centre (CLSC) lying at 175 – 200km behind the arc. The other analogue regions used with relation to TiO_2 v FeO*/MgO plotting are: the Mariana Basin which lies about 100km behind its arc and the East Scotia Ridge (ESR) which lies about 150 – 200km behind the South Sandwich Arc.

Fig. 3.1b-1. Comparison of Lau Basin Lavas (Pearce et al. 1995) with the quartz-fayalite-magnetite (QFM) mineral system at varying oxygen fugacities (Juster et al. (1989). (QFM = QFM profile at MORB f_{O2}, QFM+3 = QFM profile at f_{O2} three orders of magnitude greater than QFM.

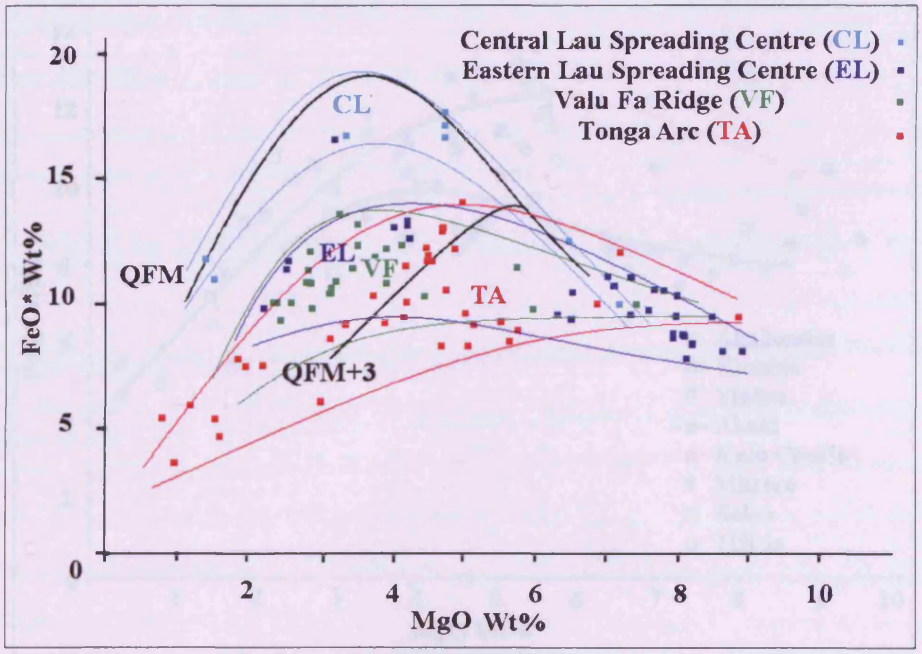

3.1c) Troodos regions FeO* v MgO

Northern Troodos

Fig.3.1c-1 is a FeO* v MgO plot showing regional trends for lavas from northern Troodos. There are two clear trend types. The majority of the lavas lie on a high-FeO* trend, with a maximum FeO* content of 12% at a MgO content of 6%. Lavas from Analiondas, Yialias, Kambia and Kalo Chorio lie on this trend (see Fig.3.1c-2 for locations). The other trend is lower in FeO* content, with its maximum of 10% at a MgO content of 5%. Lavas from Akaki and the Solea Graben axis lie on this trend. The scatter in each trend is not great enough to prevent the two trends being distinguished. This scatter is possibly a result of a combination of variable and variable oxygen fugacities and primary magma compositions. There are also a number of samples not shown on the diagram with MgO contents above 10%, belonging mainly to the Upper Pillow Lavas (UPL). Alteration of mobile elements, such as Na_2O and K_2O can affect overall FeO* and MgO analysis as concentrations are recalculated to 100%.

Fig.3.1c-1 FeO* - MgO plot showing data and trends for lavas from the North of Troodos, coloured by locality.

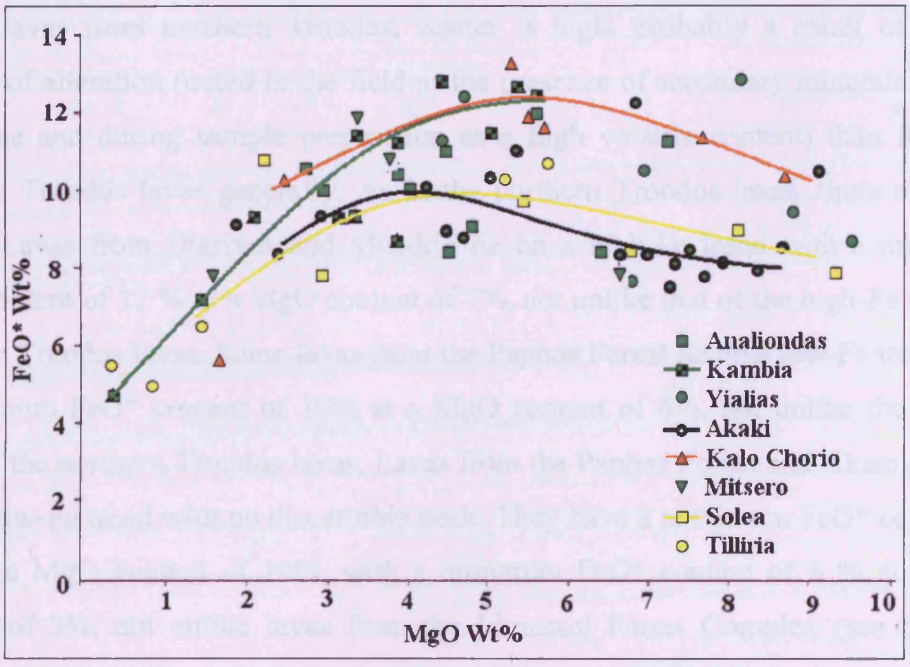

Fig.3.1c-2 Location map of localities and regions mentioned in relation to FeO* v MgO and TiO_2 v FeO*/MgO fingerprinting. These localities appear throughout Chapter 3

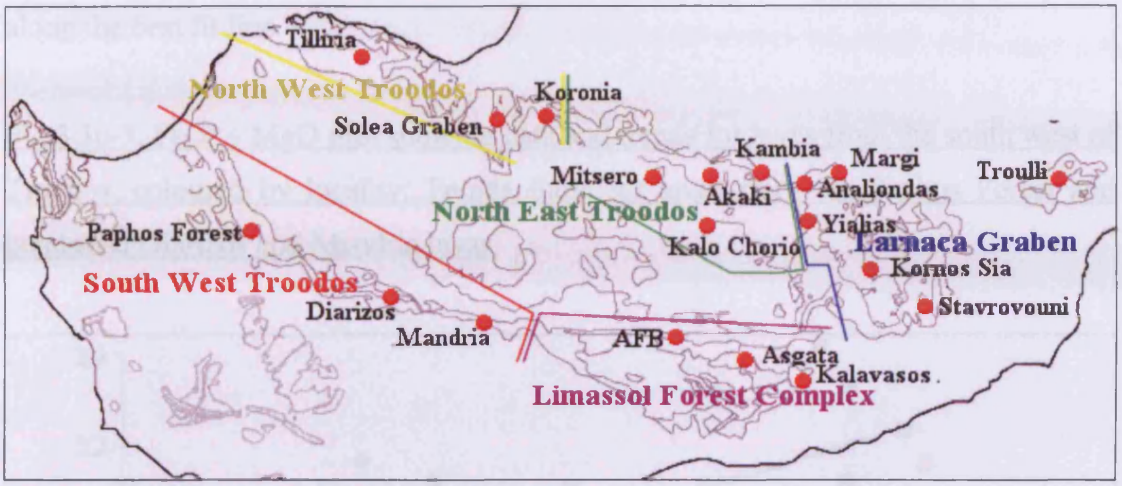

South West Troodos

Fig.3.1c-3 shows FeO* v MgO points and trends for lavas from the south west of the Troodos Massif. It shows that lavas from the south west of the Troodos Massif have approximately 8% FeO* at 10% MgO which is about the same as for both the northern Troodos lava trends which converge on this value.

Unlike lavas from northern Troodos, scatter is high, probably a result of greater degrees of alteration (noted in the field as the presence of secondary minerals such as carbonate and during sample preparation as a high volatile content) than found in northern Troodos lavas generally. As in the northern Troodos lavas, there are three trends. Lavas from Diarizos and Mandria lie on a high-Fe trend with a maximum FeO* content of 12 % at a MgO content of 7%, not unlike that of the high-Fe trend of northern Troodos lavas. Some lavas from the Paphos Forest lie on a low-Fe trend with a maximum FeO* content of 10% at a MgO content of 6%, not unlike the low-Fe trend of the northern Troodos lavas. Lavas from the Paphos Forest and Akamas lie on a very low-Fe trend with no discernible peak. They have a maximum FeO* content of 8 % at a MgO content of 10%, with a minimum FeO* content of 6 % at a MgO content of 3%, not unlike lavas from the Limassol Forest Complex (see the next section). MgO contents are however higher for particular FeO* contents than lavas

from northern Troodos, indicating that they are more primitive. Considering the aforementioned scatter, these trends are less reliable than those from the northern Troodos lavas. The low-Fe trend of lavas from Akamas and some from the Paphos Forest is tighter than the other trends observed (i.e. has a lower standard deviation along the best fit line.

Fig.3.1c-3. FeO* - MgO plot showing data and trends for lavas from the south west of Troodos, coloured by locality. Trends show for lavas from the Paphos Forest and combined Diarizos and Mandria lavas.

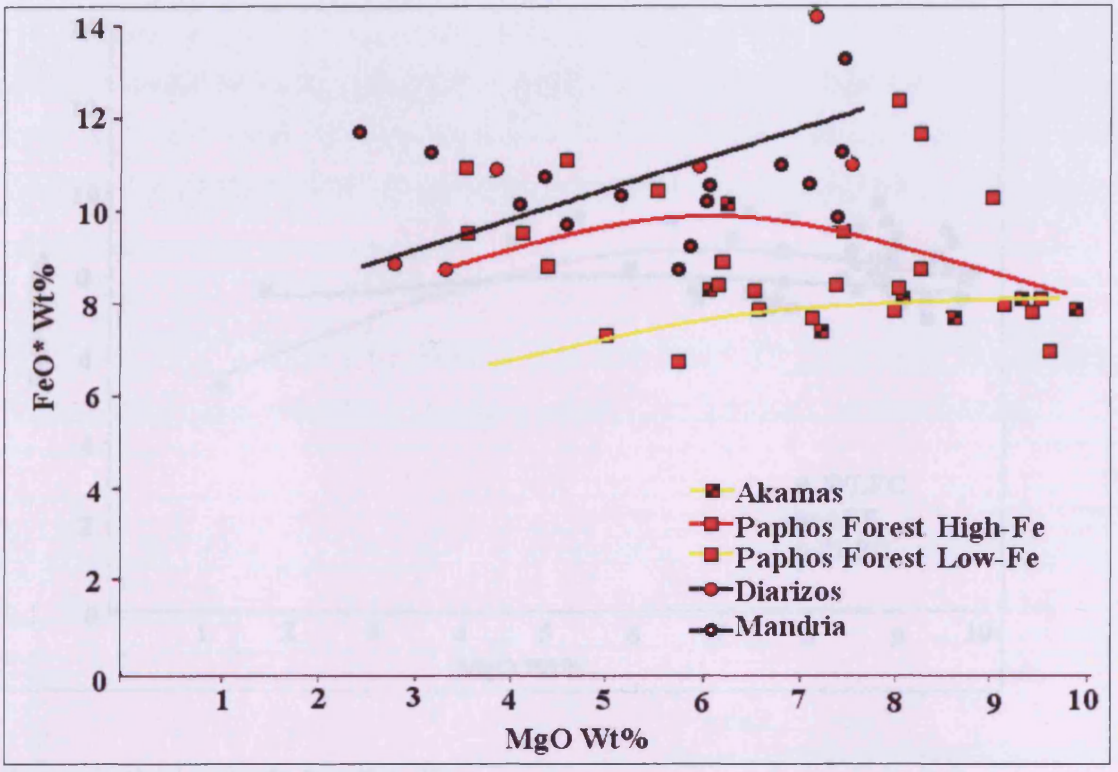

Limassol Forest Complex and Arakapas Fault Belt

Lavas from the Limassol Forest Complex (LFC) and Arakapas Fault Belt (AFB) generally have high MgO contents. Those few samples with MgO contents <10% vary from the Troodos 'normal' 8% FeO* at 10% MgO down to 5% FeO* at 1% MgO with very little evidence of a peak (Fig.3.1c-4). Lavas from both the LFC and AFB have similar trends, although lavas from the AFB all have a roughly constant FeO* content. The trend estimated for lavas from the Paphos Forest and Akamas is

somewhat similar, with generally low FeO* contents, somewhat lower those observed elsewhere around the Troodos Massif. Scatter resulting from alteration is slightly lower than that from the south west of Troodos, indicating that the latter are more reliable.

Fig.3.1c-4 FeO* - MgO plot showing data and trends for lavas from the south west of Troodos and Limassol Forest Complex, coloured by locality. WLFC = Western Limassol Forest Complex (LFC), SLFC = Southern LFC and AFB = Arakapas Fault Belt.

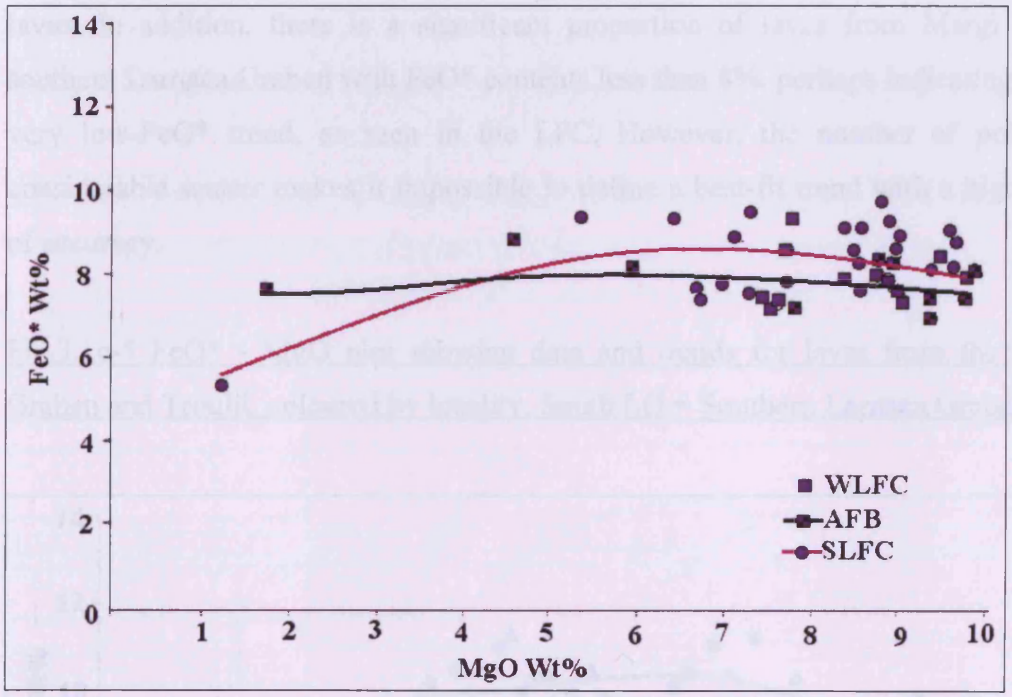

Larnaca Graben including Troulli

Many samples from the Larnaca Graben are considerably altered. Variable and sometimes high degrees of alteration (identified either in the field or during sample preparation) contributes to extensive geochemical variation in MgO and FeO*. In addition, most of the samples from the Larnaca Graben were taken from the Upper Pillow Lavas, which are mainly primitive and Mg-rich.

The relative absence of evolved rocks reduces the length (and therefore utility) of the trend lines. There were many samples containing over 10% MgO, but lavas with such

high MgO contents cannot be used for MgO v FeO* profiling as the FeO* content remains constant at about 9 or 10% for MgO >10%.

Fig.3.1c-5 shows FeO* and MgO contents of lavas from the Larnaca Graben and two best-fit trends. The trends have been constructed for lavas from the southern Larnaca Graben (anywhere south of Kornos) and for lavas from Margi in the far north west of the graben. Lavas from the southern Larnaca Graben have a peak FeO* content of just over 10% at a MgO content of 7%. Lavas from Margi increase from a FeO* content of 8% at a MgO content of 10%, to a FeO* content of 10% at a MgO content of 5%. This is similar to the profile obtained from lavas of the low-Fe northern Troodos lavas. In addition, there is a significant proportion of lavas from Margi and the southern Larnaca Graben with FeO* contents less than 8%, perhaps indicating another very low-FeO* trend, as seen in the LFC. However, the number of points and considerable scatter makes it impossible to define a best-fit trend with a high degree of accuracy.

Fig.3.1c-5 FeO* - MgO plot showing data and trends for lavas from the Larnaca Graben and Troulli, coloured by locality. South LG = Southern Larnaca Graben.

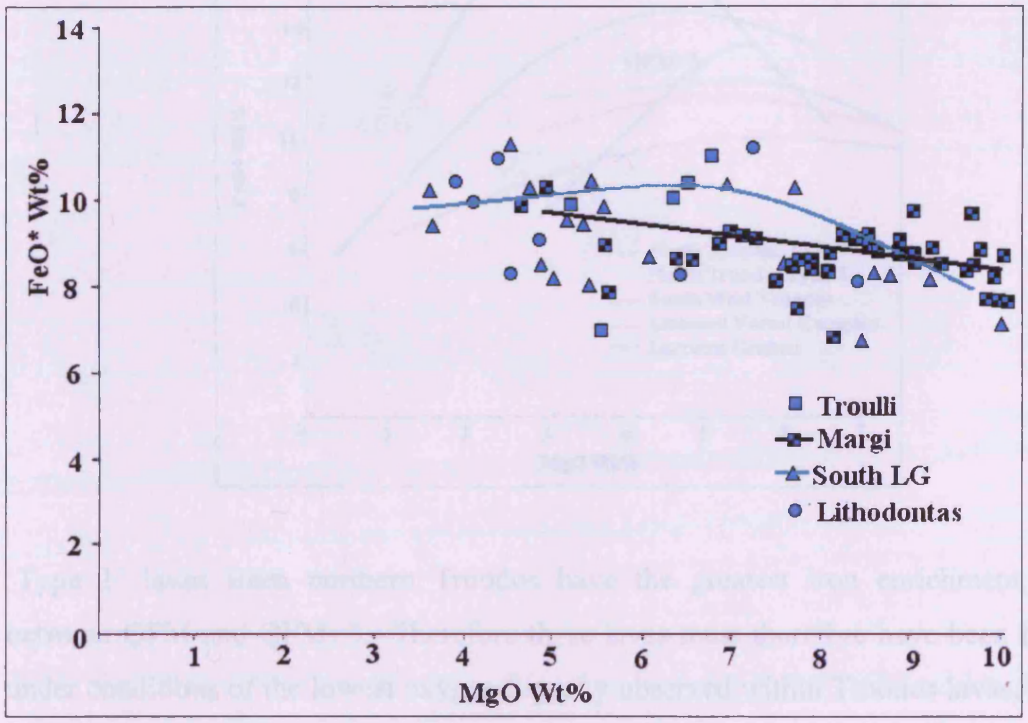

3.1d) Interpretations of geochemical regions of the lavas of the Troodos Massif by comparison to experimental QFM and QFM+3 trends of Juster et al. (1989) and a marginal basin analogue (Lau Basin)

Although the shape of fractionation curves obtained from the QFM buffer system and basaltic lavas are slightly different, as demonstrated by Fig 3.1b-1, which compared the QFM system to lavas from the Lau Basin, comparison with QFM is still applicable to lavas from the Troodos Massif. Fig.3.1d-1 shows FeO* v MgO trends for lavas overlain with QFM and QFM+3 trends from Juster et al. (1989). Lavas from northern Troodos are divided into two distinct types by FeO* content. These are termed Type 1 and Type 2. Trends representative of lavas for south west Troodos, the Larnaca Graben and the Limassol Forest Complex are also plotted.

Fig.3.1d-1 FeO* v MgO trends for low magnesium lavas from the Troodos Massif overlaid with experimental QFM and QFM+3 trends from Juster et al. (1989)

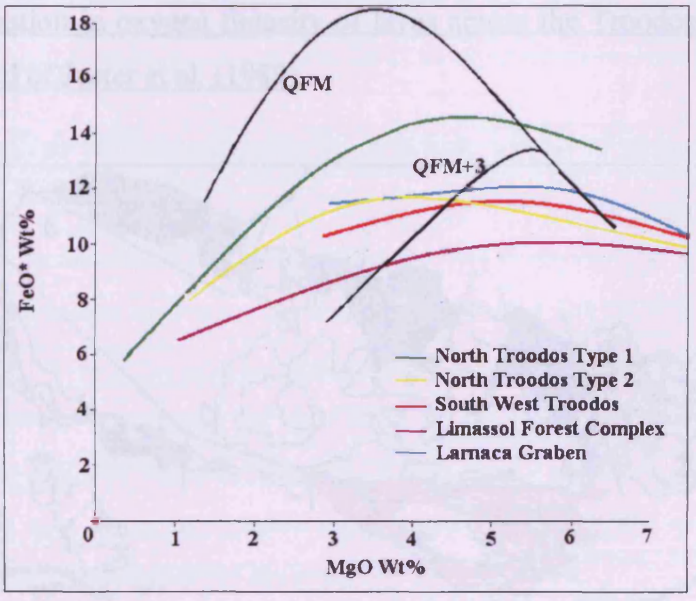

'Type 1' lavas from northern Troodos have the greatest iron enrichment, lying between QFM and QFM+3. Therefore these lavas must therefore have been formed under conditions of the lowest oxygen fugacity observed within Troodos lavas, and so probably have the lowest subduction input of lavas within the Troodos Massif. These

lavas approximate to QFM+1. 'Type 2' lavas from northern Troodos and lavas from southwestern Troodos and the Larnaca Graben all have similar trends with less iron enrichment. Therefore these lavas would have formed under conditions of greater oxygen fugacity. These lavas approximate to QFM+2. Lavas from the Limassol Forest Complex have the least iron enrichment and therefore would have formed under conditions of the greatest oxygen fugacity. The Limassol Forest Complex trend approximates to QFM+3.

Fig.3.1d-2 is a map of the Troodos Massif contoured by oxygen fugacity relative to QFM. Lavas equivalent to QFM+1 have oxygen fugacities one order of magnitude greater than lavas equivalent to QFM. Regions are coloured on the basis of the trend that samples fall on, rather than individual sample FeO* v MgO properties. This map clearly demonstrates the oxygen fugacity variations between the lavas. It highlights the lavas from the Solea Graben and Akaki in northern Troodos that have higher oxygen fugacities than the rest of northern Troodos and also the lower oxygen fugacity of lava from Diarizos in south western Troodos.

Fig.3.1d-2. Variation in oxygen fugacity of lavas across the Troodos Massif relative to the QFM trend of Juster et al. (1989)

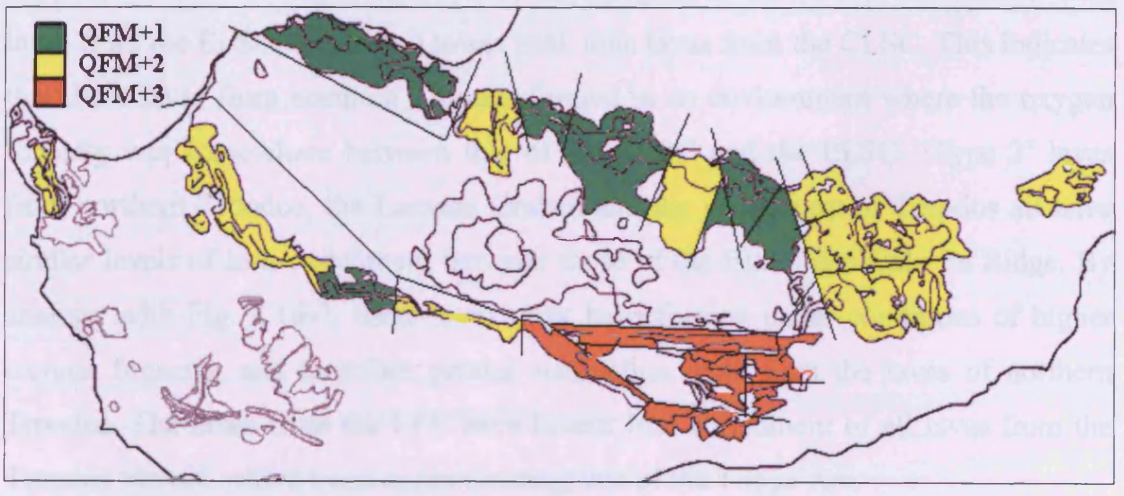

Fig.3.1d-3 depicts FeO* v MgO trends for lavas from the five aforementioned regions of the Troodos lava sequence. They are compared with the analogous regions of the

Lau Basin and Marianas Basin. The Lau Basin is subdivided into the Central and Eastern Lau Spreading Centres (C/ELSC), the Valu Fa ridge and the Tonga Arc.

Fig.3.1d-3 FeO* v MgO trends for low magnesium lavas from the Troodos Massif and the SSZ Lau Basin. (CLSC = Central Lau Spreading Centre, ELSC = Eastern Lau Spreading Centre)

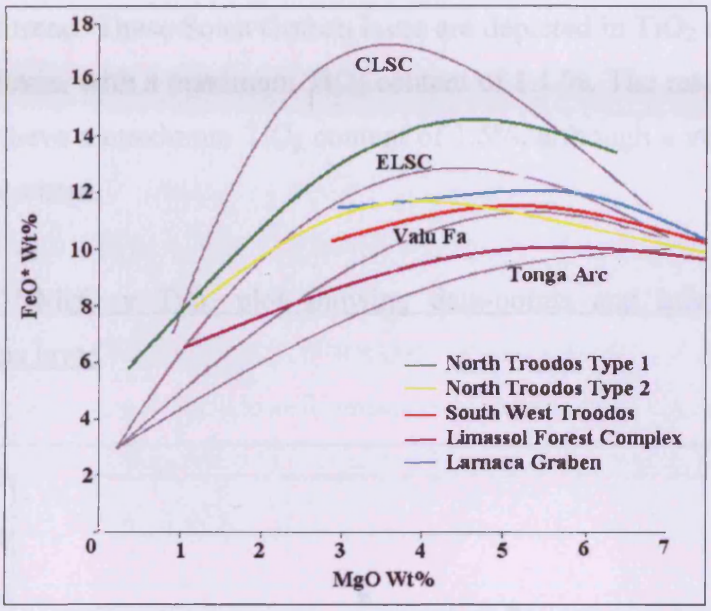

'Type 1' lavas from northern Troodos have higher levels of iron enrichment than lavas from the ELSC, but have a lower peak than lavas from the CLSC. This indicates that these lavas from northern Troodos formed in an environment where the oxygen fugacity was somewhere between that of the CLSC and the ELSC. 'Type 2' lavas from northern Troodos, the Larnaca Graben and the south west of Troodos all have similar levels of iron enrichment between those of the ELSC and Valu Fa Ridge. By analogy with Fig. 3.1d-1, these lavas must have formed under conditions of higher oxygen fugacity, and therefore greater subduction input than the lavas of northern Troodos. The lavas from the LFC have lowest iron enrichment of all lavas from the Troodos Massif, with a trend approximating that of the Tonga Arc.

3.1e) Troodos regions TiO_2 v FeO* / MgO

Northern Troodos

Lavas from the north of the Troodos Massif fall into two groups when TiO_2 v FeO* / MgO is plotted. Fig.3.1e-1 shows that the majority of the northern Troodos lavas follow a single trend, whereas lavas from the axis of the Solea Graben lie on a separate low-Ti trend. These Solea Graben lavas are depleted in TiO_2 compared to the other northern lavas, with a maximum TiO_2 content of 1.1 %. The rest of the northern lavas generally have a maximum TiO_2 content of 1.5%, although a very few samples have higher Ti content.

Fig.3.1e-1 FeO*/MgO v TiO_2 plot showing data-points and inferred trends for northern Troodos lavas

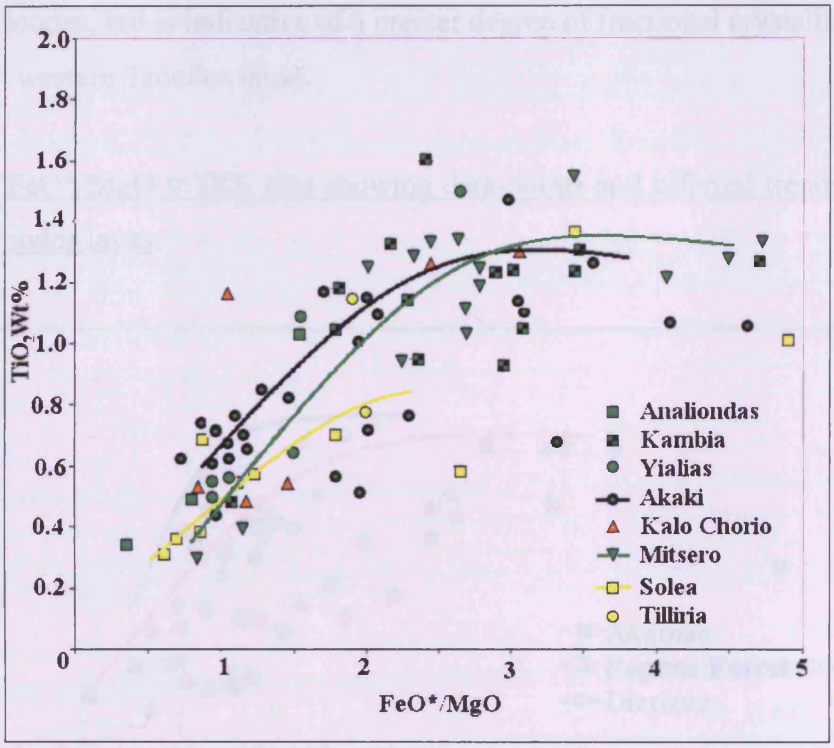

This similarity of the northern Troodos lavas indicates that prevailing conditions during the formation of these lavas (at the Solea Graben) were roughly constant in terms of source depletion, fractionation and oxygen fugacity. Only lavas that are in the axis of the Solea Graben, which were the last to have been erupted before the

magmatism ceased, have lower Ti contents. This may indicate that these last-batch lavas were sourced from depleted mantle. This would be expected if lavas were being extracted from a source that no longer was being replenished.

South West Troodos

Lavas from the south west of Troodos have trends quite unlike those of northern Troodos. The overall Ti content is far lower than the average with a maximum value of 1% TiO_2 (Fig.3.1e-2). Samples from the AFB, including Kapilio, have a small range of compositions with approximately 0.3 % TiO_2 and a FeO*/MgO ratio of about 1. The restricted range of titanium values displayed by these lavas is evidence for lack of fractionation. In addition, the very low titanium contents of the most primitive lavas are indicative of extremely depleted mantle source. Samples with higher TiO_2 content (up to 1%), indicating higher degrees of fractionation, are found in the Diarizos and Mandria areas. This is still considerably lower than contents observed in northern Troodos, but is indicative of a greater degree of fractional crystallisation than other south western Troodos lavas.

Fig.3.1e-2 FeO*/MgO v TiO_2 plot showing data-points and inferred trends for south western Troodos lavas

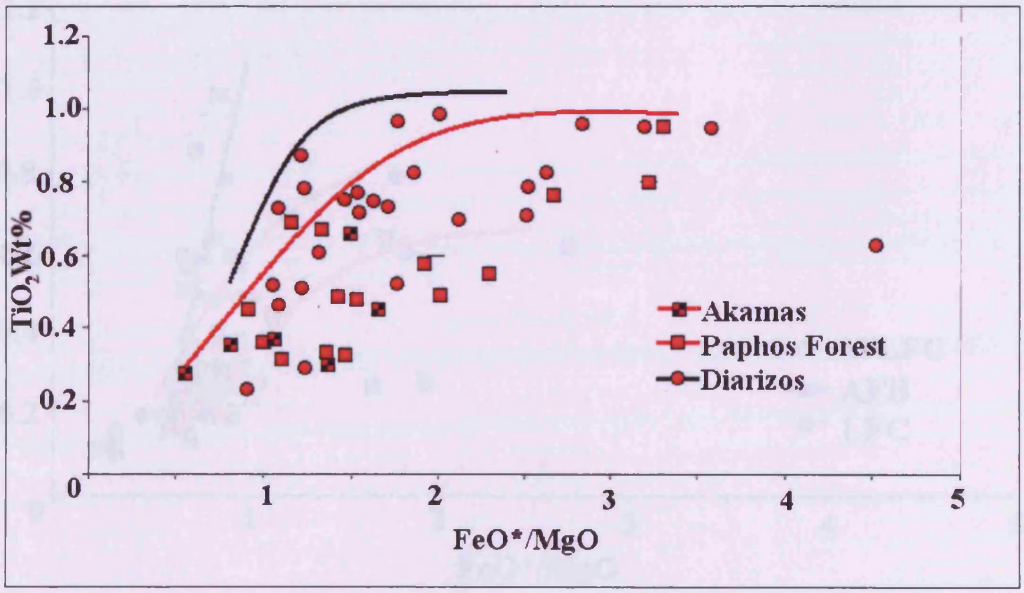

Limassol Forest Complex

Fig.3.1e-3 provides evidence for three distinct trends within lavas from the Limassol Forest Complex (LFC). The trend exhibited by lavas from the Arakapas Fault Belt (AFB) is near-vertical, with its base at a TiO_2 content of 0.2%, indicating substantial depletion of the source. Also, significant degrees of fractional crystallisation have taken place in some of the samples as shown by the relative TiO_2 content of those at the top of the fractionation curve compared with those at the base.

Samples from the general LFC area (southern and eastern LFC) lie on a trend similar to that shown by lavas from the Paphos Forest (Fig.3.1e-2), with lower degrees of fractional crystallisation. The maximum TiO_2 content is 0.8%. Lavas from the WLFC follow one of the shallowest FeO*/MgO v TiO_2 trends seen within the Troodos lavas. These lavas are extremely low in Ti, yet possess higher FeO*/MgO ratios than the rest of the LFC.

Fig.3.1e-3. FeO*/MgO v TiO_2 plot showing data-points and inferred trends for lavas from the Limassol Forest Complex (LFC) including Western LFC (WLFC) and Arakapas Fault Belt (AFB)

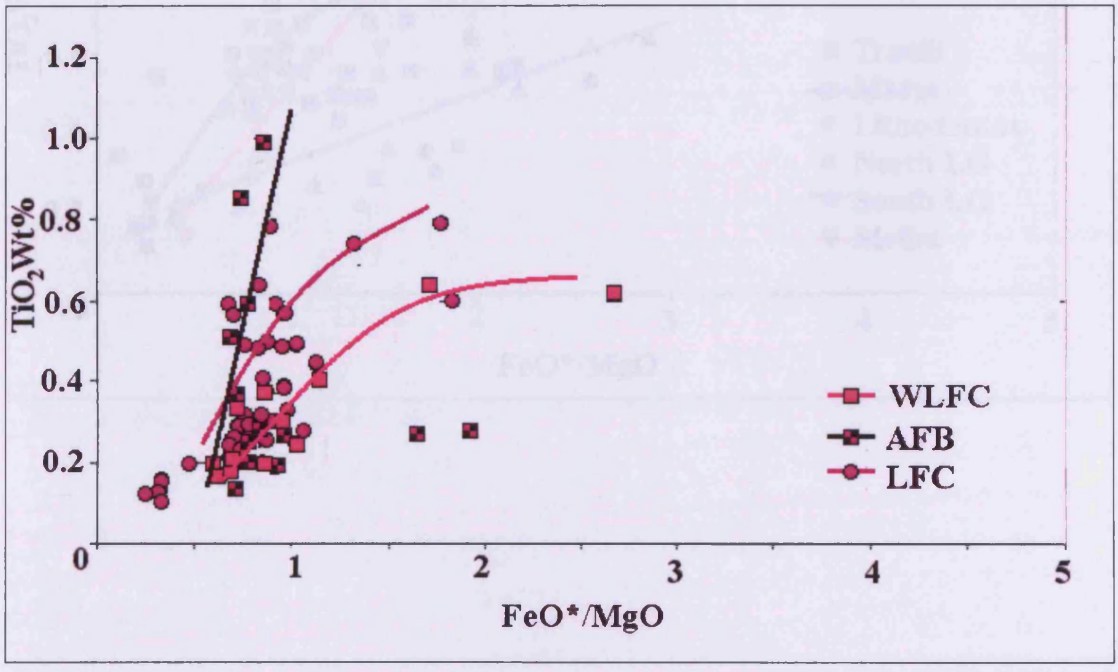

Larnaca Graben and Troulli

Fig.3.1e-4 shows TiO_2 v FeO*/MgO relationships of lavas within the Larnaca Graben and Troulli. Extensive alteration affecting the FeO*/MgO ratio (but not the Ti content) has resulted in a considerable scatter. Despite this, three trends are discernible. Lavas from Margi and Melini have similar trends, although all of the lavas from Margi are very primitive with TiO_2 content less than 0.8%. Lavas from Melini have a maximum TiO_2 of approximately 1%.

Lavas from the southern Larnaca Graben follow a much shallower trend, similar to that of the lavas from the WLFC. This is not unexpected, as both regions lie in close proximity to the AFB.

Fig.3.1e-4 FeO*/MgO v TiO_2 plot showing data-points and inferred trends for northern Troodos lavas

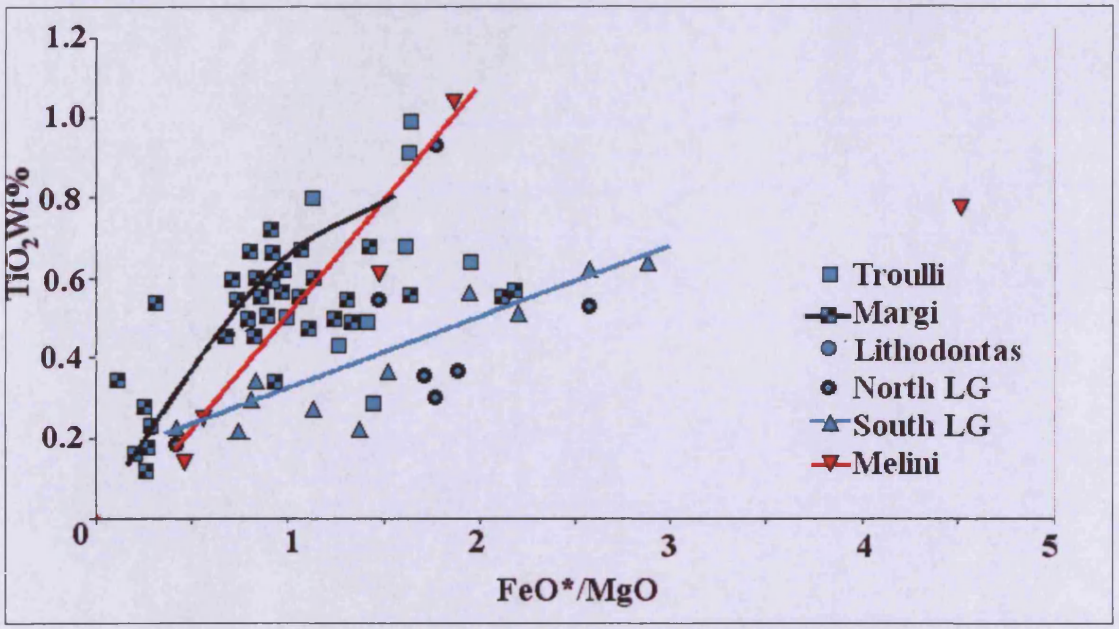

3.1f) Comparison of TiO_2 v FeO*/MgO trends from the Troodos Massif with trends from analogue regions

Northern Troodos

Fig.3.1f-1 depicts TiO_2 v FeO*/MgO trends for lavas from northern Troodos and the from analogue regions. The majority of lava samples from northern Troodos lie between the island arc tholeiite trend of Myashiro (1973) and the ELSC and Valu Fa trends using data from Pearce et al. (1995 and 2005). Only lavas from the axis of the Solea Graben (yellow trend) are substantially different. The trend for this group lies between that of the Tonga Arc and that of the combined Mariana Basin, ELSC and Valu Fa data.

Fig.3.1f-1. Ti v FeO* / MgO points and trends of lavas form the north of Troodos with average trends for MORB, island arc tholeiite (IAT), lavas form Tonga and calc-alkaline lavas from Myashiro (1973), Central Lau Spreading Centre (CLSC) and Eastern Lau Spreading Centre (ELSC) from Pearce et al. (1995), Valu Fa from Jenner et al. (1987), East Scotia Ridge (ESR) from Fretzdorff et al. (2002) and Leat et al.(2004)

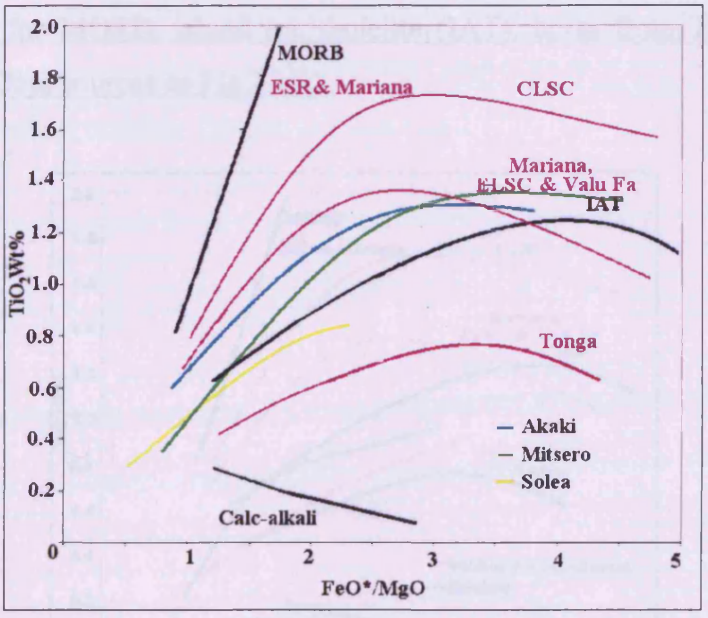

The northern Troodos lavas are also generally more depleted in TiO_2 than the analogue regions shown on Fig.3.1f-1, as shown by lower FeO*: MgO ratios and lower TiO_2 contents at the base of the fractionation curves. Comparison of the length of the Troodos lava trends with those of the analogue regions indicates that levels of fractional crystallisation are comparable. The fractionation curve for lavas from the axis of the Solea Graben is truncated, as there are too few fractionated samples to draw it reliably. However, the presence of some fractionated samples from the Solea Graben indicates that the degrees of fractional crystallisation may be comparable with degrees of fractionation elsewhere across the northern part of the Troodos Massif.

South West Troodos

Fig.3.1f-2 shows points and FeO*/MgO v Ti fractionation curves for the Diarizos and Paphos Forest regions within south western Troodos and selected analogue regions. The majority of lava samples from south western Troodos lie between the island arc tholeiite (IAT) and Tonga Arc trends of Myashiro (1973). The fractionation curve for lavas from the Diarizos area is closer to the IAT trend, with some samples plotting above IAT, whereas lavas form the Paphos Forest plot closer to the Tonga arc trend.

Fig.3.1f-2 FeO* / MgO v Ti trends for lavas from the south west of Troodos with average trends for MORB, island arc tholeiite (IAT), lavas from Tonga and calc-alkaline lavas. Data sources as Fig.3.1f-1.

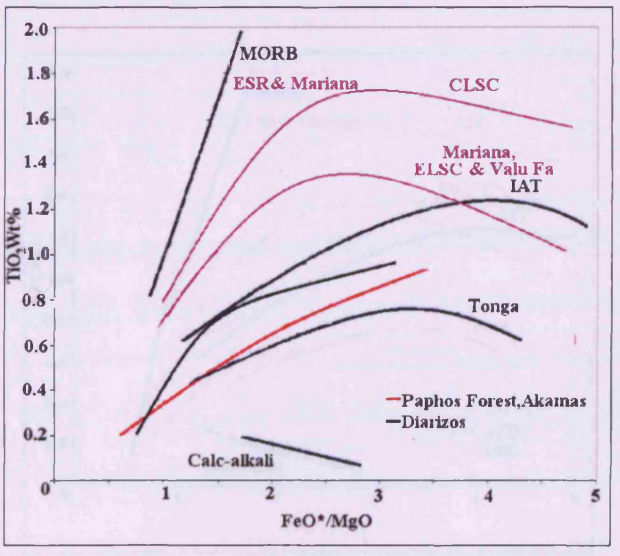

The south western Troodos lavas are also generally more depleted than the selected analogue lavas shown on Fig.3.1f-2, as shown by lower FeO*: MgO ratios and lower TiO_2 contents at the base of the fractionation curves. Unlike northern Troodos Lavas, the fractionation curves are shorter than the analogue curves, indicating that total overall degrees of fractionation were lower. Maximum fraction levels for the Diarizos area and the Paphos Forest are similar, indicating similar degrees of fractionation.

Limassol Forest Complex (LFC)

Fig.3.1f-3 shows points and FeO*/MgO v Ti fractionation curves for the Arakapas Fault Belt (AFB), parts of the LFC and of selected analogue regions. The majority of lava samples from LFC lie between the island arc tholeiite (IAT) and Tonga arc trends of Myashiro (1973). The fractionation curve for lavas from the AFB is most similar to the MORB trend of Myashiro (1973). The LFC fractionation trends most resemble the trends from south western Troodos. Therefore, it is likely that these lavas were sourced from mantle with a similar degree of subduction zone enrichment. The curve for the Western LFC, which exhibits a slightly greater subduction component than the rest of the LFC, lies almost along the curve for the Tonga Arc, indicating high levels of subduction enrichment and, by inference, high oxygen fugacities.

Fig.3.1f-3 FeO* / MgO v Ti profiles and trends of lavas from the Limassol Forest Complex (LFC) with average trends for MORB, island arc tholeiite (IAT), lavas from Tonga and calc-alkaline lavas. Data sources as Fig.3.1f-1.

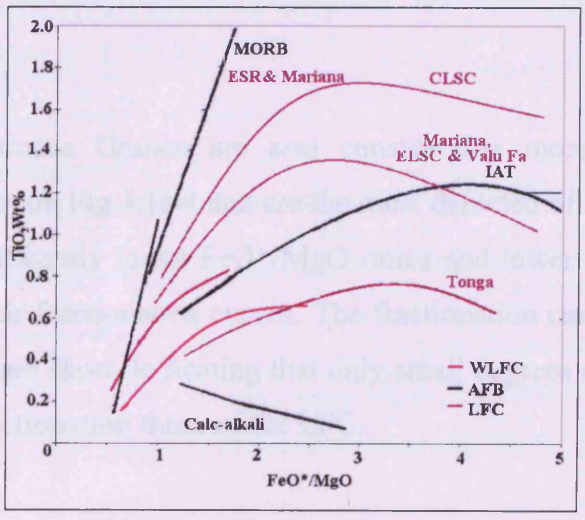

The trend produced by lavas from the AFB is unexpected, inasmuch that it is very different to the trends produced by neighbouring lavas from the LFC. The AFB lavas plot on the MORB array with no evidence (in this study) of subduction zone enrichment.

The LFC are also considerably more depleted than the analogue lavas, as shown by significantly lower FeO*/MgO ratios and lower TiO_2 contents at the primitive end of the fractionation curves. The fractionation curves or all regions of the LFC are short, indicating relatively low levels of fractional crystallisation.

Larnaca Graben and Troulli

Fig.3.1f-4 shows the compositions and FeO*/MgO v Ti fractionation curves for lavas from Margi, (the northern Larnaca Graben), the southern Larnaca Graben and Melini (located to the north of the AFB), together with selected analogue regions. The majority of lava samples from Margi and Melini lie near the island arc tholeiite (IAT) trend of Myashiro (1973). The fractionation curve for lavas from the southern Larnaca Graben is most similar to that of the Tonga arc trend of Myashiro (1973). The Margi and Melini fractionation trends are fairly similar to the trends from south western Troodos. Therefore, it is likely that these lavas were sourced from mantle with similar oxygen fugacities. The trend of the southern Larnaca Graben lavas, which indicates source oxygen fugacities higher than the rest of the Larnaca Graben and similar to those of the WLFC, lies almost along the curve for the Tonga arc.

Lavas from the Larnaca Graben are also considerably more depleted than the analogue lavas shown on Fig.3.1f-4 and are the most depleted of all Troodos lavas, as shown by their significantly lower FeO*/MgO ratios and lower TiO_2 contents at the primitive ends of their fractionation curves. The fractionation curves of all regions of the Larnaca Graben are short, indicating that only small degrees of fractionation took place. Degrees of fractionation those of the LFC.

Fig.3.1f-4 Ti v FeO*/MgO plot for lavas from the Larnaca Graben and Troulli with average trends for MORB, island arc tholeiite (IAT), lavas form Tonga and calc-alkaline lavas. Data sources as Fig.3.1f-1.

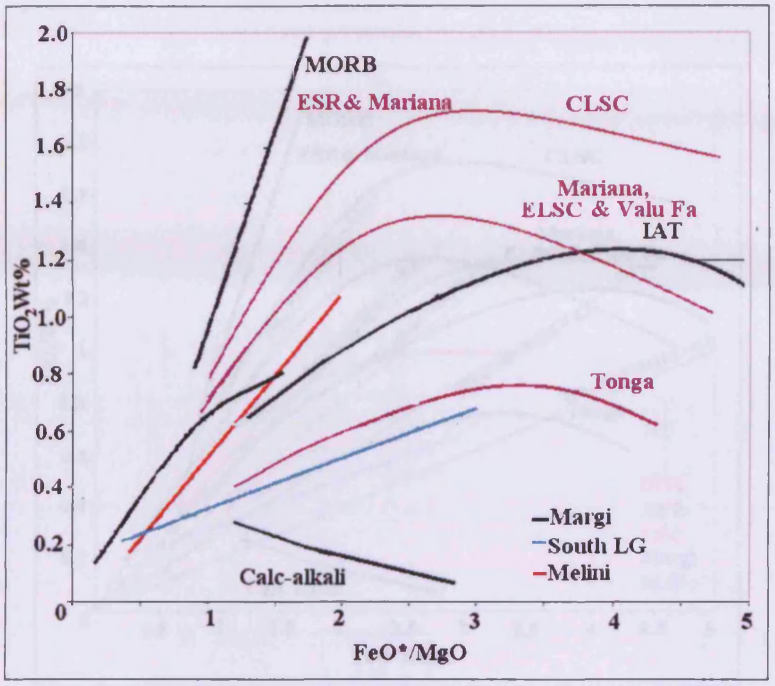

3.1g) Regional variation across the Troodos Massif and its analogues

Fig 3.1g-1 provides a comparison of TiO_2 v FeO*/MgO trends representative for the selected regions of the Troodos Massif together with selected analogue regions. Also drawn are TiO_2/(FeO*/MgO) ratios of 0.2, 0.3, 0.4, 0.5 and 0.7, corresponding approximately to TiO_2 v FeO*/MgO trends for Tonga, IAT, ELSC, CLSC and divisions between. As a result of the shape of the fractionation curves, the TiO_2 v FeO*/MgO contours discriminate best between lavas from the reported regions when FeO*/MgO values lie between 0.5 and 1.5 as, in this range, the fractionation curve maintains a roughly constant TiO_2/(FeO*/MgO) ratio. In this range, the value of TiO_2 at FeO*/MgO =1 can be deduced. This value, also equal to the gradient of the trend at this point will be referred to as Ti_1. The higher Ti_1 is, the lower the degree of partial melting and the higher the degree of source depletion are. Lavas from the north of the

Troodos Massif generally have the highest Ti_I values and lavas from the south and east have the lowest.

Fig.3.1g-1 Comparison of TiO_2 v FeO*/MgO trends from Troodos lava regions and analogues.

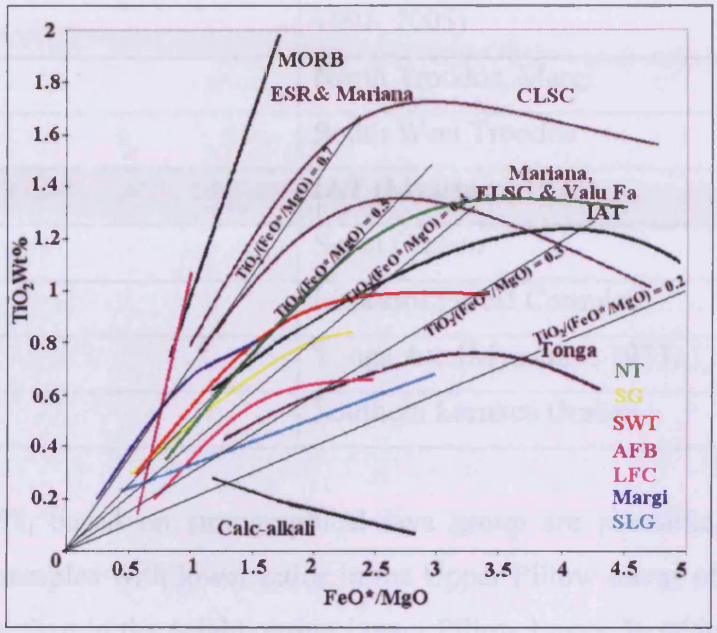

The relationship between locality and Ti_I is summarised in Table 3.1g-1. With the exception of lavas from the axis of the Solea Graben, lavas formed to the east of the Troodos Massif have lower Ti_I than lavas formed in the west. According to spreading models of Varga and Moores (1985) and MacLeod (1990), these lavas are also the youngest found within the Troodos Massif. This would indicate that either only lavas formed to the east of the Troodos Massif in its current orientation were strongly subduction-enriched or that subduction input increased with time during formation of the Troodos crust.

Fig 3.1g-2 is a map of the lavas of the Troodos Massif coloured according to Ti_I values. The contours are the same as in Fig 3.1g-1 with blue representing low ratios and red representing high ratios. This map complements Fig 3.1g-1 and Table3.1g-1. Lavas with MgO contents above 7% were excluded as lavas with high MgO content are generally primitive, having FeO*/MgO ratios less than 1. This explains why there are data gaps in the southern portion of the Troodos Massif, as many lavas from this area are primitive.

Table 3.1g-1 Ti_I values of Troodos lava regions and analogues

Ti_I	Location
0.75	CLSC (Pearce et al. 1995)
0.65	ELSC & selected Mariana Trough (Pearce et al. 1995, 2005)
0.5	North Troodos, Margi
0.5	South West Troodos
0.45	IAT (Myashiro, 1973)
0.42	Solea Graben
0.35	Limassol Forest Complex
0.3	Tonga Arc (Myashiro, 1973)
0.25	Southern Larnaca Graben

Variations in Ti_I based on stratigraphical lava group are plausible, based on the appearance of samples with lower ratios in the Upper Pillow Lavas of Margi and the Larnaca Graben than in the neighbouring Lower Pillow Lavas. In addition, the Lower Pillow Lavas in the Mitsero Graben area have lower Ti: FeO*/MgO ratios than their Basal Group counterparts.

Fig.3.1g-2 Map of Ti v FeO*/MgO ratios across the lavas with MgO content less than 7% of the Troodos Massif using the same divisions as Fig. 3.1f-1

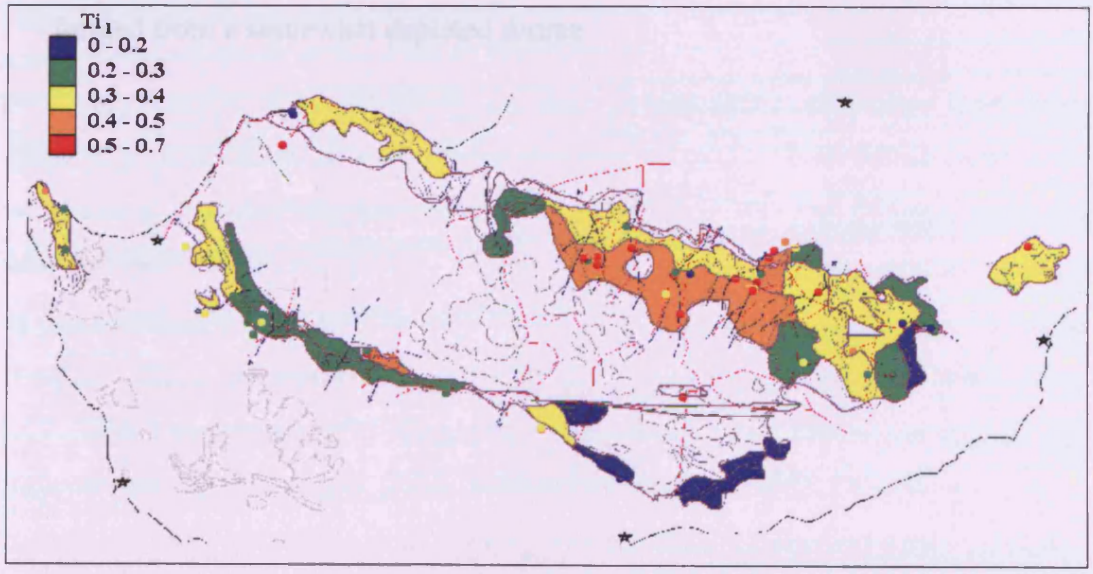

In conclusion :

- The difference in assumed oxygen fugacity between north and south Troodos is quite apparent. However the actual distance between the two outcrops is rarely more than 30km which, when compared to the distances involved in the Lau Basin and Tonga Arc, seems far too small to produce such a pronounced effect. Assuming that: *overall melt volume will affect the composition of a magma in two ways. Firstly, a high-volume melt will dilute an enriched component much more than a low-volume melt. Studies of incompatible elements have shown that the melt volumes decreased with proximity to the transform fault (Flower and Levine, 1987). Therefore, one would expect magma produced near the transform to have a higher f_{O2} than one produced to the north as the oxidising subduction input was less diluted by magma generated beneath the ridge. Secondly, differences in the compatibility of elements studied, even if small, may result in varying initial content if the melt volumes vary greatly.* Therefore roughly a constant input of oxidising subduction-derived fluid is incompletely diluted by the low melt volumes found at transform faults.
- Some lavas from Diarizos and Mandria in the south west of Troodos show FeO* v MgO trends similar to those from north Troodos. This effect cannot be explained as being as a result of reduced subduction input, as this area lies only a few km from the transform fault. It is more plausible that there was increased melt generation in the area. Although the titanium values are higher than those found elsewhere in the south west of Troodos, they are still considerably lower than those found in north Troodos. This would imply that the Diarizos area was still formed from a somewhat depleted source

3.2) Geochemical mapping using Titanium and Vanadium content to investigate variations in source depletion and enrichment.

3.2a) Theory

Variations in the Ti and V contents in lavas are dependent on a number of factors. These factors include source depletion or enrichment, the oxygen fugacity during melting and crystallisation and the incoming of magnetite as a crystallising phase. Systematic changes in these conditions in the zones of magmagenesis of boninites, island arc tholeiites (IAT) and MORBs result in lavas of these types having Ti/V ratios that are sufficiently different to allow Ti/V fingerprinting. Typically, boninites have Ti/V ratios less than 10, IAT's have Ti/V ratios between 10 and 20 and MORBs have Ti/V ratios between 20 and 50 (Shervais, 1982). Fields constructed by Shervais (1982) and Ti/V ratios of 10, 20 and 50 are shown in Fig.1. Mapping the lavas using the Ti/V ratio thus allows variations in the lava types to be discriminated on a regional basis.

Depletion of the magma source does not strip out Ti and V equally because of the different incompatibilities of the two elements. Ti is less compatible than V under upper mantle conditions so, during partial melting, Ti will be preferentially removed thus reducing the Ti/V ratio. The 'Bulk Earth' Ti/V ratio is 10, so magmas from depleted sources will have ratios less than 10. Conversely, enrichment of the upper mantle will increase Ti more strongly than V, as the more incompatible Ti is more readily transported in the enriching melt phase. The effects of depletion and enrichment are shown as vectors 1 and 2 on Fig 1.

Although titanium and vanadium are both incompatible elements, they behave differently in magmas because of the multiple valencies of vanadium have greater variations in compatibility than the various valencies of Ti. The different ionic states have different incompatibilities in a basic magma. As a result, the partition coefficient of vanadium, D_V can vary by two orders of magnitude depending on its oxygen fugacity. Where the magma has a low oxygen fugacity ($f_{O2} < 10^{-7}$), $V^{3+}/(V^{4+}+V^{5+})$ is high, with a partition coefficient above 1 (Shervais, 1982). Where the magma has a high oxygen fugacity ($f_{O2} > 10^{-4.5}$), $V^{3+}/(V^{4+}+V^{5+})$ is low, with a partition coefficient below 0.1. The process of partial melting will therefore release increasing amounts of

vanadium into the melt with increasing oxygen fugacity, resulting a smaller Ti/V ratio.

The final factor determining vanadium content in lava is crystallisation of magnetite. Crystallisation of magnetite removes both Ti and V from the magma. However, at lower oxygen fugacities, the partition coefficient of V into magnetite is far higher than the partition coefficient of Ti into magnetite. This preferentially strips V from the remaining melt. The eruptive products of this melt will have anomalously high Ti/V ratios and should not be used to discriminate tectonic setting on Ti-V plots. This effect is shown as vector 3 on Fig. 1

Fig. 3.2a-1 Ti/V plot based on Shervais (1982) showing fields for Boninite, island arc tholeiite and MORB with Ti/V ratios of 10, 20 and 50 marked. Also shown are vectors of source depletion, enrichment and magnetite fractionation.

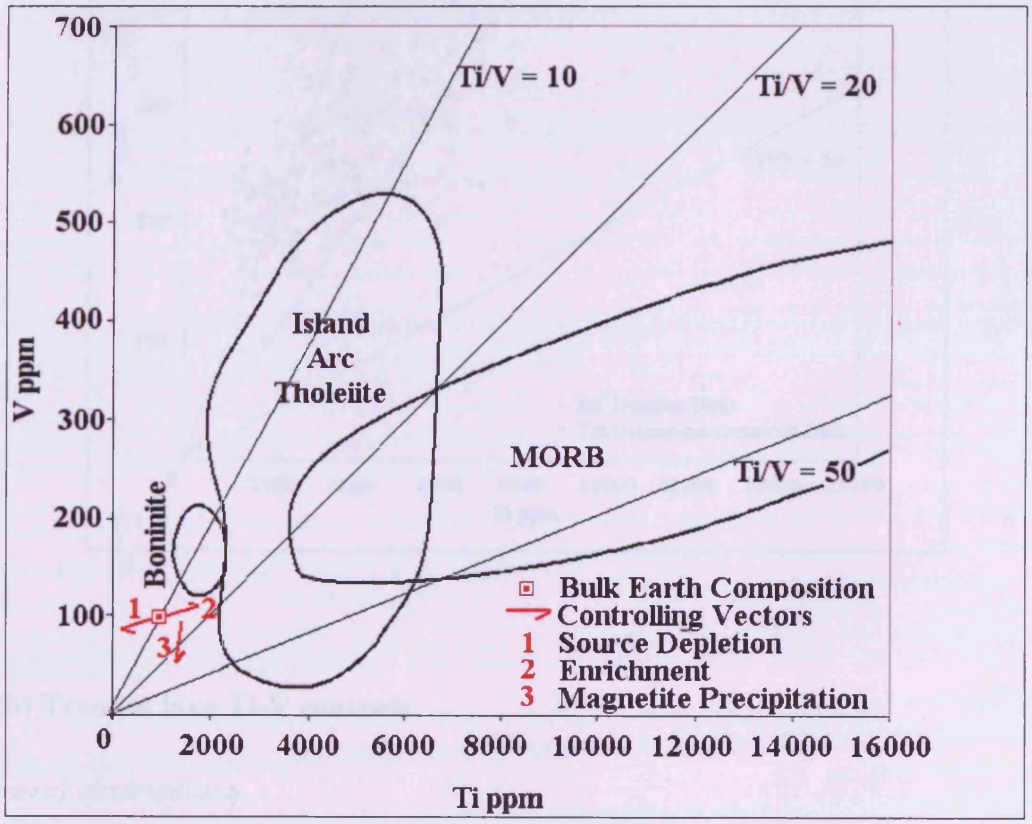

Two techniques are available to help discriminate between samples that are affected by magnetite fractionation and those that are not. Magnetite fractionation is linked to the silica content of the magma. Therefore, samples with high SiO_2 content can be discarded. Within Troodos lavas, silica contents above 55% are generally indicative

of magnetite fractionation. In addition, construction of a fractionation trend for a given region also shows which samples are affected by fractionation. Fig. 3.2a-2 shows the effect of removal of magnetite-fractionated samples from the total dataset. The original dataset is shown in pink, and overlaid in blue is the remaining dataset after fractionated samples are removed. The average Ti/V ratio and sample spread of the dataset is reduced.

Fig. 3.2a-2. Ti – V plot of all Troodos lava samples showing effect of removal of the magnetite-fractionated samples. Samples in blue are unfractionated. Samples in pink have been rejected.

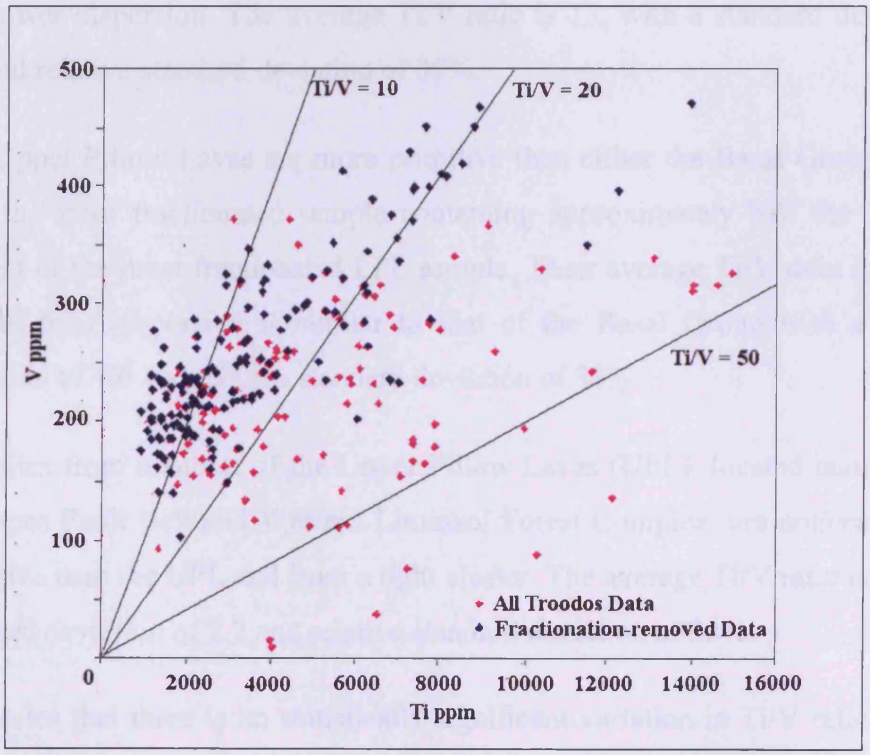

3.2b) Troodos lava Ti-V contents

General observations

Using fields determined by Shervais (1982) in Fig.1, virtually all Troodos lavas plot within SSZ compositional ranges. Some of the Ti-rich Lower Pillow Lava (LPL) samples from the north of the ophiolite plot just into the MORB field.

Stratigraphic variations

Fig. 3.2b-1 shows Troodos lavas divided on the basis of lava type. Lavas are divided into Basal Group, Lower Pillow Lavas, Upper Pillow Lavas and Boninites. The following properties are apparent:

- The Lower Pillow Lavas (LPL) have the highest range of fractionation and the highest average Ti/V ratio. The average Ti/V ratio is 14, with a standard deviation of 6.6 and relative standard deviation of 47%.

- The Basal Group has a slightly lower maximum fractionation level than the LPL and lower dispersion. The average Ti/V ratio is 13, with a standard deviation of 4.5 and relative standard deviation of 35%.

- The Upper Pillow Lavas are more primitive than either the Basal Group or LPL, with the most fractionated sample containing approximately half the Ti and V content of the most fractionated LPL sample. Their average Ti/V ratio is lower at 12 and their dispersion is similar to that of the Basal Group with a standard deviation of 4.6 and relative standard deviation of 38%.

- Boninites from a subset of the Upper Pillow Lavas (UPL), located mainly in the Arakapas Fault Belt and Western Limassol Forest Complex, are noticeably more primitive than the UPL and from a tight cluster. The average Ti/V ratio is 7, with a standard deviation of 2.2 and relative standard deviation of 33%.

This indicates that there is no statistically significant variation in Ti/V ratio between lavas of the three groups. Only the boninites, from a restricted area are different.

The lower degree of fractionation and lower dispersion of the Basal Group relative to the LPL supports the hypotheses of Sobolev et al. (1993), Portnyagin et al. (1997) and Pearce (pers. comm.) that the lowest section of the lava pile is generally more primitive than the LPL. Field observations supported this by revealing that the lavas of the Basal Group are usually in the form of smallish pillows, which is indicative of primitive lava. Some samples from the Basal Group are also olivine-phyric. LPL pillows are larger than most of those from the Basal Group and are not olivine-phyric.

Fig. 3.2b-1. Scatter plot of Ti-V contents for lavas from the Troodos Massif divided by lava unit.

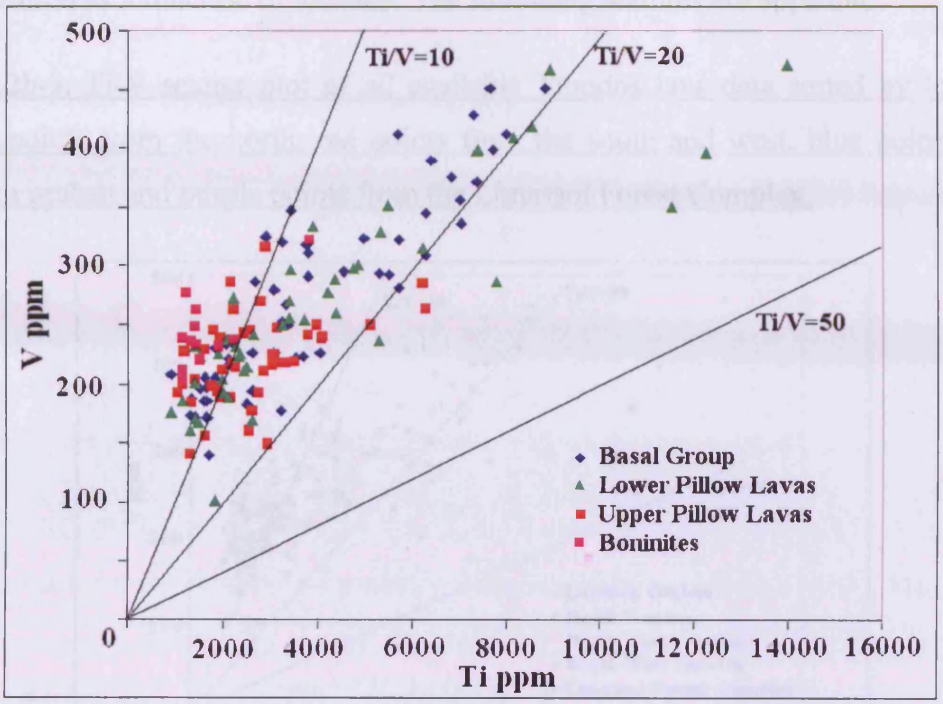

Spatial variations

Fig 3.2b-2 shows the boundaries of regions and locations of all localities referred to in this section.

Fig. 3.2b-2. Location map of localities mentioned in relation to Ti-V fingerprinting

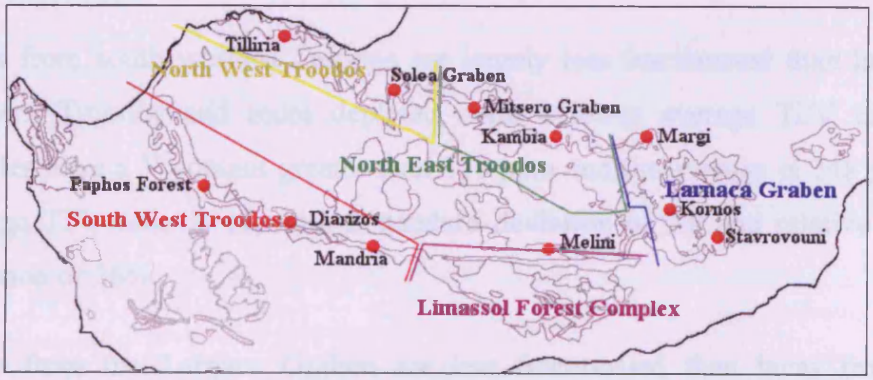

Fig 3.2b-3 is a Ti/V plot of that same selection of lavas shown in Fig3.2b-1 divided into regions rather than stratigraphical unit. This plot highlights differences in lava composition as a function of location. The following features are apparent:

Fig. 3.2b-3. Ti-V scatter plot of all available Troodos lava data sorted by locality. Green points from the north, red points from the south and west, blue points from Larnaca graben and purple points from the Limassol Forest Complex.

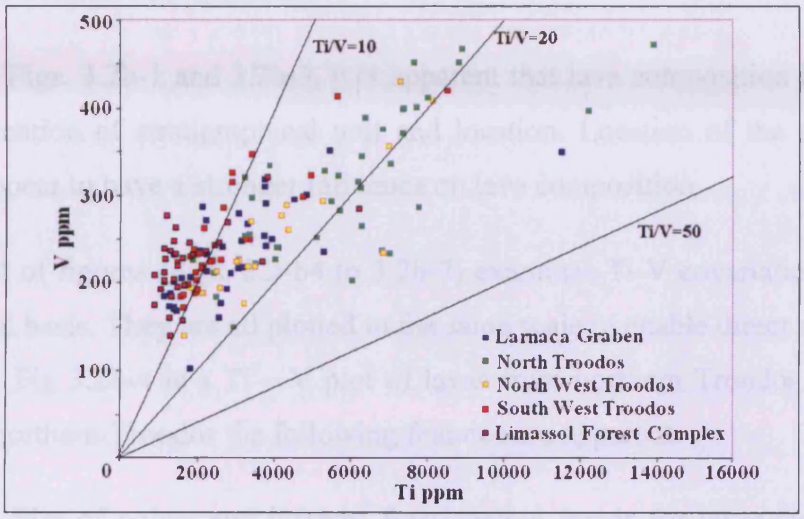

- There is very little difference in the spread of values from the eastern and western portions of northern Troodos. The average Ti/V ratio of lavas from the eastern section is 17, with a standard deviation of 3.5 and relative standard deviation of 20%. The average Ti/V ratio of lavas from the western section is 16, with a standard deviation of 4.5 and relative standard deviation of 28%. The average V content across northern Troodos is 290 ppm.

- Lavas from south western Troodos are largely less fractionated than lavas from northern Troodos and more depleted, with a lower average Ti/V ratio. Few samples have a V content greater than 350 ppm and the average is 248 ppm. The average Ti/V ratio is 11, with a standard deviation of 2.8 and relative standard deviation of 26%.

- Lavas from the Larnaca Graben are less fractionated than lavas from either northern or south western Troodos. The average V content is 232 ppm. They are however, more variable in composition, indicating that more than one lava type

may be involved. The average Ti/V ratio is 12.4, with a standard deviation of 5.3 and relative standard deviation of 43%.

- Lavas from the Limassol Forest Complex are the most depleted and least fractionated lavas found with the Troodos Massif. Most lavas have V content less than 300 and the average is 220 ppm. The average Ti/V ratio is 7.6, with a standard deviation of 2.6 and relative standard deviation of 34%. The are of a generally boninitic composition.

Contrasting Figs. 3.2b-1 and 3.2b-3, it is apparent that lava composition is controlled by a combination of stratigraphical unit and location. Location of the sample does however, appear to have a stronger influence on lava composition.

The next set of figures (Figs. 3.2-b4 to 3.2b-7) examines Ti-V covariations in detail, on a regional basis. They are all plotted to the same scale to enable direct comparisons to be made. Fig 3.2b-4 is a Ti – V plot of lavas from northern Troodos. Within the lavas from northern Troodos the following features are apparent:

Fig. 3.2b-4. Plot of points and inferred fractionation trends for lavas from northern Troodos. Inferred trends taken from lavas that show no evidence of magnetite fractionation.

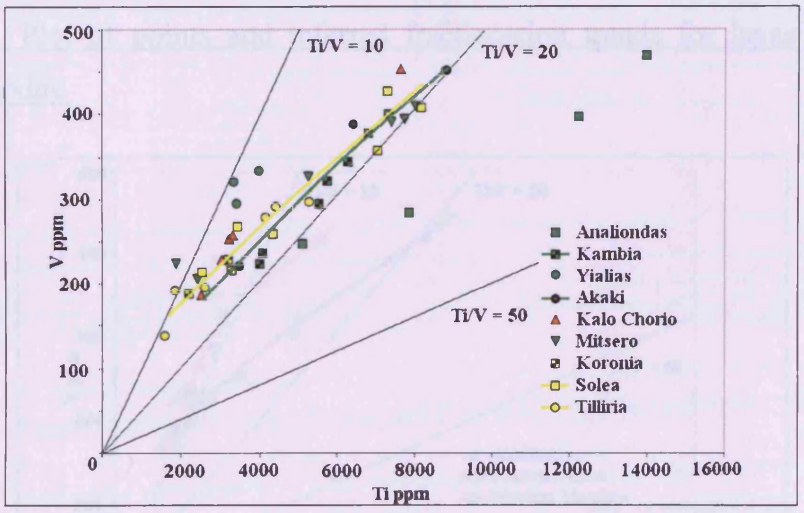

- Most of the lavas from northern Troodos lie on a single island arc tholeiite-type fractionation trend. The primitive end of this trend has a Ti/V ratio of 10 and the fractionated end of this trend has a Ti/V ratio of 20. The most primitive sample

has a V content of 130 ppm and Ti content of 1700 ppm. The most fractionated sample (Analiondas excluded) has a V content of 500 ppm and Ti content of 9000 ppm.

- The fractionation curve for lavas from the eastern section of north Troodos is based on lavas from Akaki and Kambia, although lavas from Mitsero and Kalo Chorio would produce a very similar trend.

- Lavas from the Solea Graben and Tilliria lie on the same trend as lavas from the eastern portion of the area. The lines are shown as parallel on Fig 3.2b-4 to aid clarity. The only difference between the trends is that the most primitive lavas from Solea and Tilliria are slightly more primitive than equivalent lavas from the eastern section.

- Lavas from Analiondas have a much flatter, MORB-like Ti–V fractionation curve than other lavas from northern Troodos. This is probably a reasonable interpretation as 1) the points form a relatively straight line and 2) they are all low in silica content.

Within the lavas from the south and west of Troodos, shown on Fig. 3.2b-5, the following features are apparent:

Fig. 3.2b-5. Plot of points and inferred fractionation trends for lavas from south western Troodos.

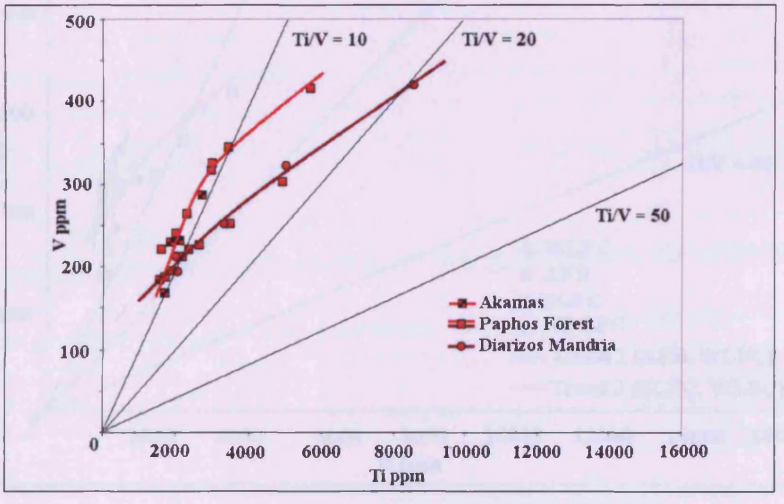

- Two clear fractionation trends are evident in lavas from south western Troodos. One is a steep, boninitic trend and the other is a depleted island arc tholeiite trend. The most primitive sample has a V content of 160 ppm and Ti content of 1700 ppm. The most fractionated sample has a V content of 420 ppm and Ti content of 8200 ppm.

- Lavas from Akamas are strongly depleted and boninitic and lavas from Diarizos and Mandria resemble depleted island arc tholeiites.

- Lavas from the Paphos Forest region are divided between both fractionation trends.

- The depleted island arc tholeiite lavas from Diarizos and Mandria have a fractionation curve similar to that obtained from northern Troodos

Within the lavas from the Limassol Forest Complex, including the Arakapas Fault Belt, shown on Fig. 3.2b-6, the following is noted:

Fig. 3.2b-6. Plot of points and inferred fractionation trends for lavas from the Limassol Forest Complex, including the Arakapas Fault Belt. Inferred trends taken from lavas that show no evidence of magnetite fractionation. AFB = Arakapas Fault Belt, W/S/NE LFC = Western / Southern / North Eastern Limassol Forest Complex.

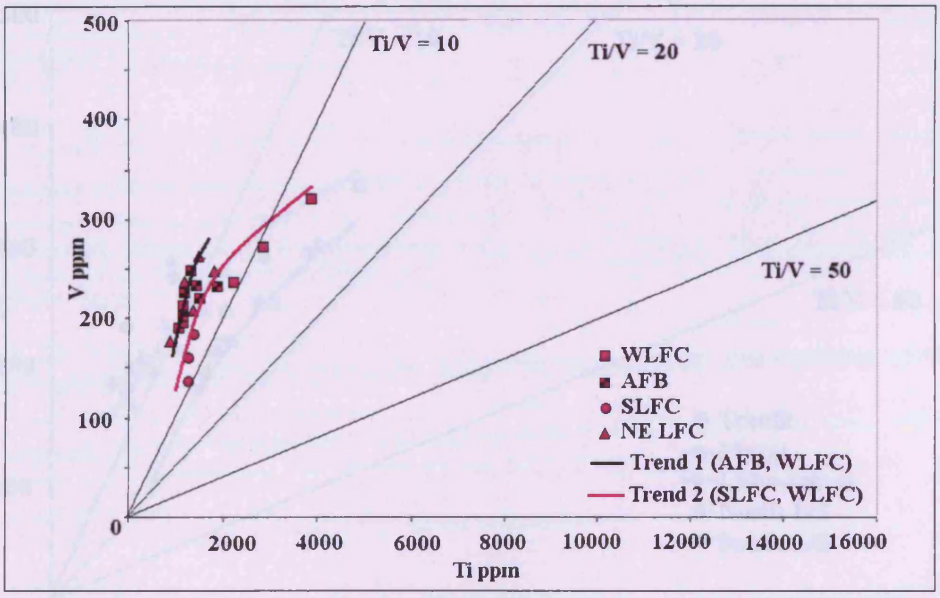

- Two separate fractionation curves are obtained from lavas from the Limassol Forest Complex. Both trends are boninitic and strongly depleted. The fractionation curves are also short compared to fractionation curves from northern Troodos, indicating that, overall, these lavas are much more primitive and less fractionated.
- The most primitive sample has a V content of 130 ppm and Ti content of 1400 ppm. The most fractionated sample has a V content of 320 ppm and Ti content of 4000 ppm.
- Lavas from the Arakapas Fault Belt and parts of the Western LFC lie on the most depleted trend.
- Lavas from the southern LFC and some form the western LFC lie on the less depleted trend. However, the base of this trend is more primitive.
- Lavas from the north eastern LFC are divided between both fractionation trends.

Lavas from the Larnaca Graben are shown on Fig. 3.2b-7. The following features are apparent:

Fig. 3.2b-7. Ti - V Plot of points and inferred fractionation trends for lavas from the Larnaca Graben. LG = Larnaca Graben.

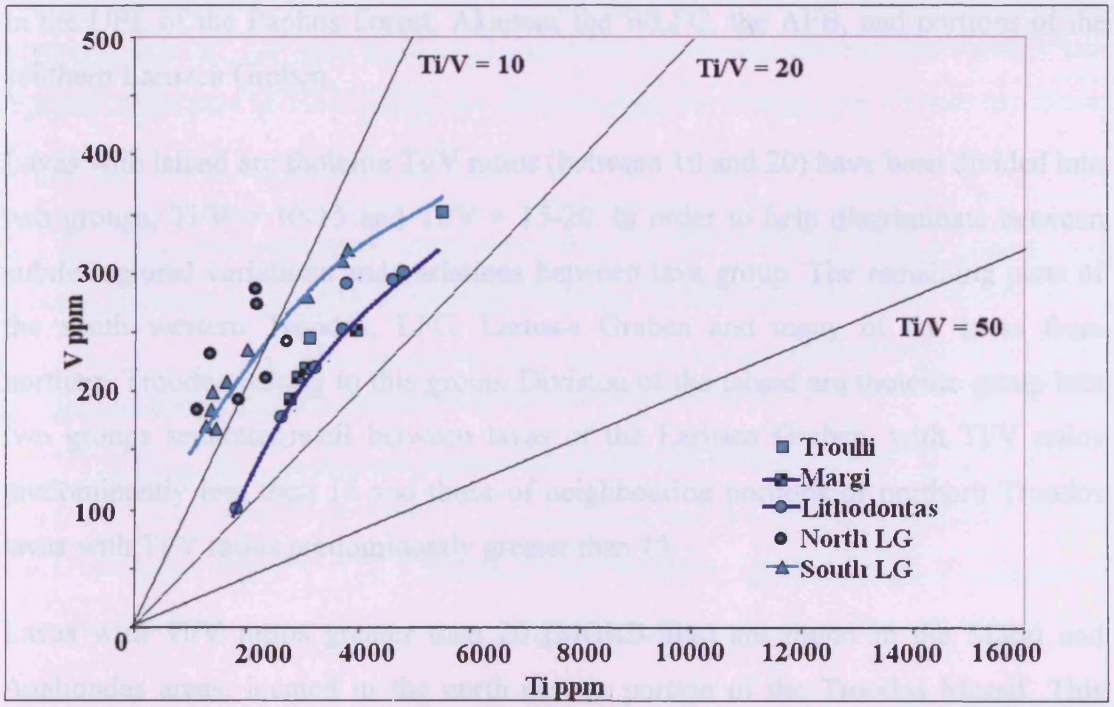

- Two distinct trends are apparent within lavas from the Larnaca Graben. One is a depleted and variably-fractionated island arc tholeiite-type and the other is a primitive, but non-depleted island arc tholeiite-type.

- The most primitive sample has a V content of 110 ppm and Ti content of 1800 ppm. The most fractionated sample has a V content of 350 ppm and Ti content of 5500 ppm.

- Lavas from the primitive trend originate from the Lithrodonda and Margi. This trend overlaps the primitive end of the northern Troodos trend.

- The lavas belonging to the depleted trend are mainly from the southern Larnaca Graben. Lavas from the northern Larnaca Graben are similar in composition though with a greater dispersion.

Mapping Ti-V variations within the Troodos Massif lava sequence

Mapping the Ti/V ratio across the Troodos Massif highlights variations resulting from both region and stratigraphical units. Fig.3.2b-8 shows the variation in Ti/V ratio across the Troodos Massif with contours based on the classification of Shervais (1982). Lavas with blue symbols have Ti/V ratios less than 10 and, using the classification of Shervais (1982), can be described as boninitic. Such lavas are found in the UPL of the Paphos Forest, Akamas, the WLFC, the AFB, and portions of the southern Larnaca Graben.

Lavas with island arc tholeiite Ti/V ratios (between 10 and 20) have been divided into two groups, Ti/V = 10-15 and Ti/V = 15-20, in order to help discriminate between subtle regional variations and variations between lava group. The remaining parts of the south western Troodos, LFC, Larnaca Graben and many of the lavas from northern Troodos belong to this group. Division of the island arc tholeiite group into two groups separates well between lavas of the Larnaca Graben, with Ti/V ratios predominantly less than 15 and those of neighbouring portions of northern Troodos lavas with Ti/V ratios predominantly greater than 15.

Lavas with Ti/V ratios greater than 20 (MORB-like) are found in the Margi and Analiondas areas, located in the north eastern portion of the Troodos Massif. This

area straddles the border between the Larnaca Graben and the older Solea Graben-derived lavas. These lavas have low silica content, and therefore are assumed to be unaffected by magnetite fractionation.

Fig. 3.2b-8. Contoured map of the lavas of the Troodos Massif showing variations in Ti/V ratio.

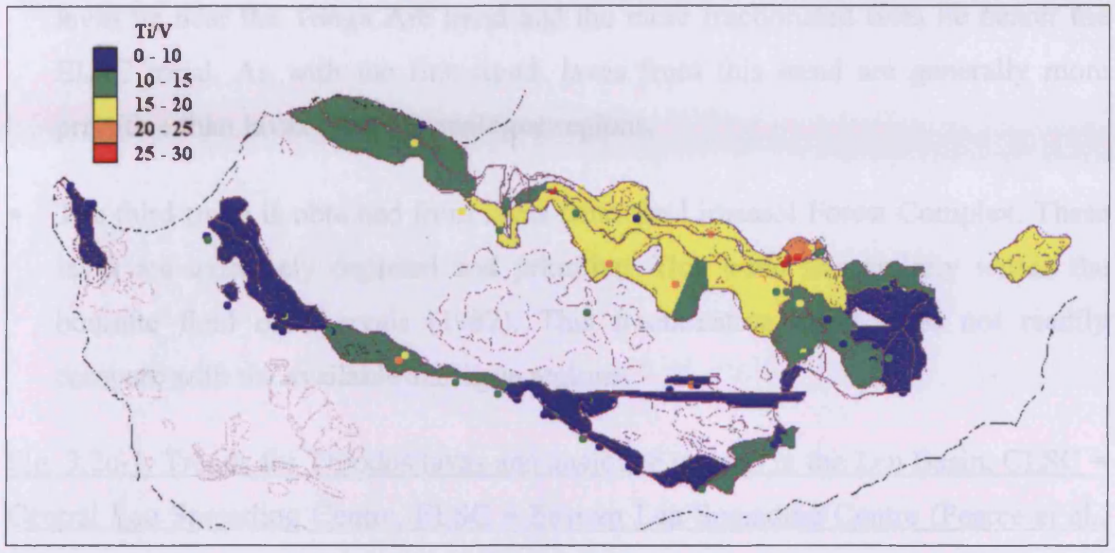

3.2c) Fractionation within the Troodos Massif and comparison with analogues

Fig. 3.2c-1 shows average Ti-V trends derived from the studied regions of the Troodos lava sequence (north Troodos, south west Troodos, the Limassol Forest Complex and the Larnaca Graben). In addition trends, for Central and Eastern Lau Spreading Centres and the Tonga arc are presented for comparison. Three trends are apparent.

- The first trend comprises lavas from Margi in the northern Larnaca Graben and the majority of lavas from northern Troodos. Lavas from Margi are found at the primitive end of the fractionation curve and lavas from northern Troodos are more fractionated. This fractionation curve lies approximately along that obtained from lavas from the Central Lau Spreading Centre (CLSC). However, lavas from the CLSC are more fractionated. The minimum and maximum V contents of the CLSC lavas are higher than the respective minimum and maximum V contents of Troodos lavas.

- The second trend is comprised of lavas from the Larnaca Graben, south western Troodos and some lavas from the Limassol Forest Complex (LFC). Lavas from the LFC are found at the primitive end of the trend and lavas from parts of south western Troodos (Diarizos) are at the upper end of the fractionation curve. This fractionation curve lies between the fractionation curves obtained from lavas from the Tonga Arc and the Eastern Lau Spreading Centre (ELSC). The more primitive lavas lie near the Tonga Arc trend and the more fractionated ones lie nearer the ELSC trend. As with the first trend, lavas from this trend are generally more primitive than lavas from the analogue regions.
- The third trend is obtained from lavas from the Limassol Forest Complex. These lavas are extremely depleted and primitive. This trend lies entirely within the boninite field of Shervais (1982). This fractionation curve does not readily compare with the available analogue regions

Fig. 3.2c-1. Trends for Troodos lavas and analogue regions in the Lau Basin. CLSC = Central Lau Spreading Centre, ELSC = Eastern Lau Spreading Centre (Pearce et al., 1995), Tonga arc from Shervais, 1982. Boninite, IAT and MORB fields omitted for clarity, see text.

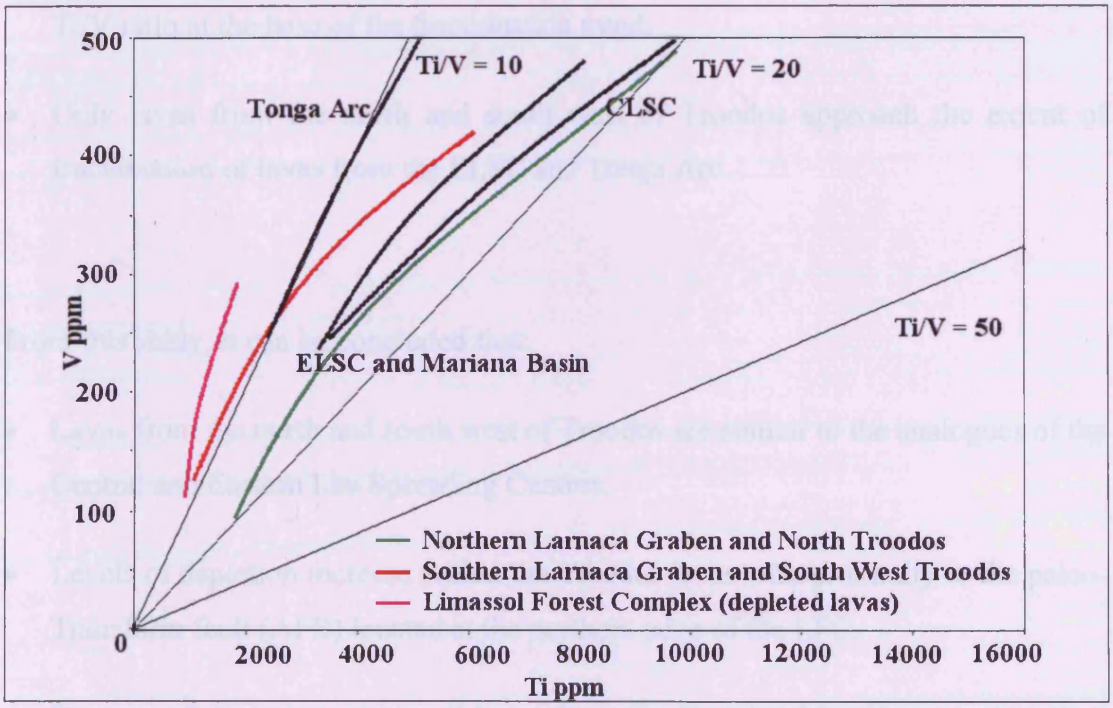

Fractionation trends based on Ti/V ratio for lavas from the Troodos Massif and selected analogue regions are shown in Fig. 8. Using classification fields devised by Shervais (1982) of Ti/V<10 – Boninite, Ti/V = 10-20 – IAT and Ti/V =20 – 50 – MORB, the following comparisons can be drawn:

- Mariana Trough and Central and Eastern Lau Spreading Centres plot within the IAT field.
- The Tonga Arc plots on the border between Boninite and IAT.
- Most of the lavas from northern Troodos and Margi plot within the IAT field.
- Lavas from the Troodos Massif are generally more depleted than lavas from most of the analogue regions, with lower Ti/V ratios at the base of the fractionation trend than the analogues. The only analogue with similar depletion is the Tonga Arc.
- Lavas from the remainder of the Larnaca Graben and south west Troodos have similar levels of depletion at the base of their fractionation trends.
- The most primitive lavas from the LFC are extremely depleted on the basis of the Ti/V ratio at the base of the fractionation trend.
- Only lavas from the north and south west of Troodos approach the extent of fractionation of lavas from the ELSC and Tonga Arc.

From this study, it can be concluded that:

- Lavas from the north and south west of Troodos are similar to the analogues of the Central and Eastern Lau Spreading Centres.
- Levels of depletion increase within the Troodos lavas with proximity to the paleo-Transform fault (AFB) located at the northern edge of the LFC.
- Degrees of depletion within all lavas from the Troodos Massif are greater than reported for lavas from the analogue regions.

- A large number of samples from the Troodos Massif, especially the northern section exhibit the effects of fractionation of magnetite and have been removed from the study. This reduces the density of valid data.

- Upper Pillow Lavas (UPL) are clearly less fractionated on average than the Lower Pillow Lavas (LPL) and Basal Group (Fig. 3.2b-1), although they lie on the same fractionation trends as the lower lavas appropriate for their location. This would imply that the lavas have the same source, albeit with different fractionation histories. Because the LPL are generally more fractionated than the UPL, a greater number of LPL samples were removed from the study as magnetite fractionation had taken place.

3.3) Measuring mantle source depletion, partial melting and fractional crystallisation using Cr and Y

3.3a) Theory

Incompatible vs. compatible element plots were first used by Pearce (1975) to differentiate between MORBs and island arc tholeiites, using Ti and Cr. These were later modified by Pearce (1982) using Y and Cr, both of which are also usually immobile during weathering and low-grade metamorphism.

The two main controlling factors determining the composition of a primitive melt are 1) source depletion and 2) degree of partial melting. Once a partial melt has been extracted, the composition of the final product is determined by fractional crystallisation of olivine, chrome-spinel clinopyroxene, and plagioclase. The use of two elements of differing compatibilities allows variations in source depletion, partial melting and fractional crystallisation to be separated. The controls on a melt composition and fertile mantle composition are shown in Fig. 3.3a-1.

Extraction of a partial melt has the following effects on the depleted residue:

- Y is reduced as this incompatible element is preferentially removed by the partial melt.
- Cr, as a compatible element remains preferentially in the mantle source and little is removed in the partial melt.
- Depleted mantle has lower a Y content and higher Cr content than fertile mantle, (see blue trend on Fig 3.3a-1)

The content of a partial melt is thus dependent on source depletion (as this dictates the location of the end of the partial melting curve) and the degree of partial melting.

- Y, being incompatible is highest in very low-degree partial melts, decreasing as the degree of melting increases.
- Although Cr, as a compatible element, remains preferentially in the mantle, it is still released in significant quantities during partial melting. A 5% partial melt from fertile mantle will contain about 600 ppm Cr, increasing slightly as the degree of melting increases.

Fig. 3.3a-1 Cr-Y diagram based on that of Flower and Levine (1987) showing controlling vectors of source depletion, partial melting fraction and clinopyroxene fractional crystallisation. Also shown is the composition of fertile mantle.

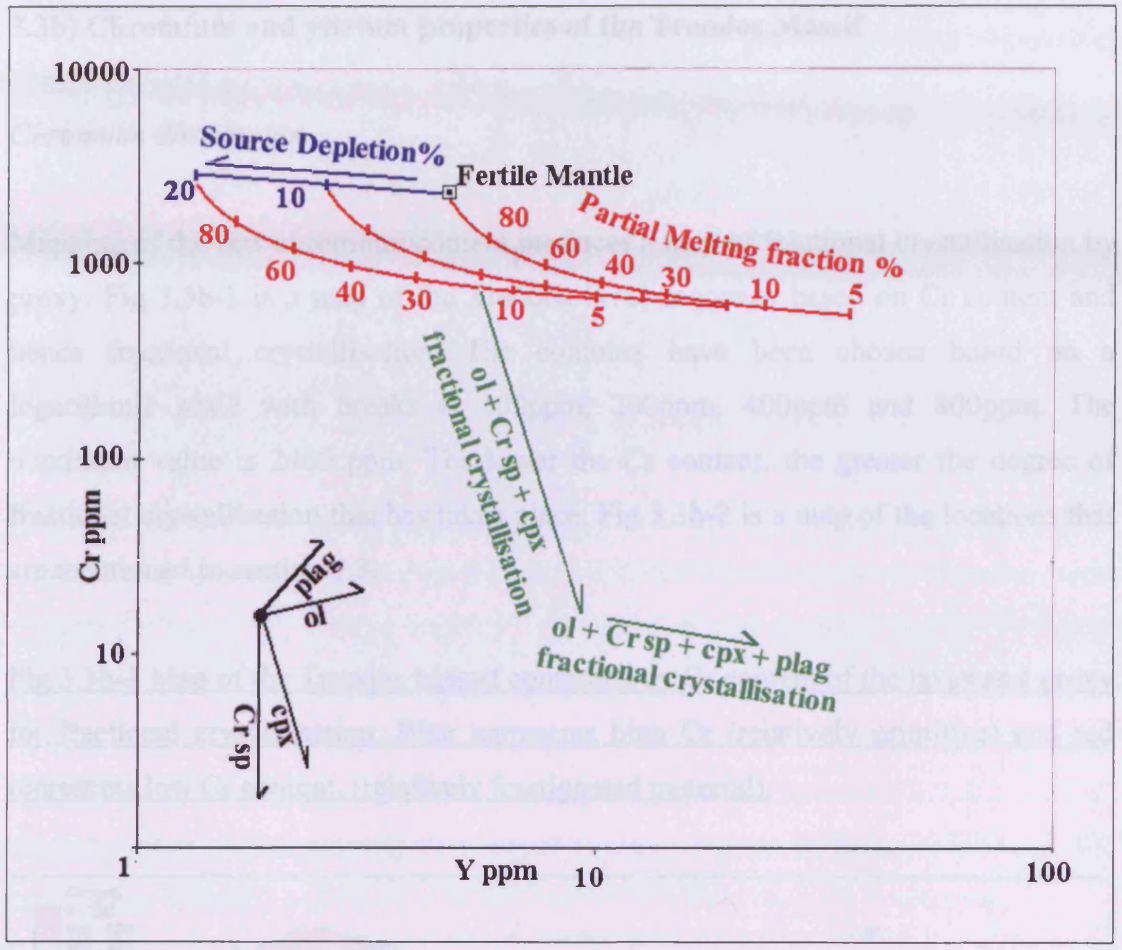

Fig. 3.3a-1 also shows the controls on composition resulting from the fractional crystallisation of olivine, chrome spinel, clinopyroxene and plagioclase. The individual fractionation vectors for these minerals are shown in black. During the first phase of fractional crystallisation, olivine, chrome spinel and clinopyroxene crystallise. The combination of the chrome spinel and olivine vectors roughly parallels the clinopyroxene vector. Therefore the combined fractionation vector reduces Cr greatly and slightly increases Y. Crystallisation of plagioclase strongly increases Y and Cr as both of these elements are incompatible in plagioclase. The addition of plagioclase to the combined ol + Cr Sp + Cpx vector results in a vector that slightly reduces Cr but increases Y. The combined vectors are shown in green.

The shifting of data-points to the right by crystallisation of plagioclase masks the clinopyroxene fractional crystallisation trend. In this study, samples with evidence of plagioclase crystallisation have been removed.

3.3b) Chromium and yttrium properties of the Troodos Massif

Chromium distribution

Mapping of the raw chromium content produces a map of fractional crystallisation by proxy. Fig 3.3b-1 is a map of the Troodos lavas sequence based on Cr content and hence fractional crystallisation. The contours have been chosen based on a logarithmic scale with breaks at 100ppm, 200ppm, 400ppm and 800ppm. The maximum value is 2400 ppm. The lower the Cr content, the greater the degree of fractional crystallisation that has taken place. Fig 3.3b-2 is a map of the locations that are mentioned in section 3.3.

Fig.3.3b-1 Map of the Troodos Massif contoured by Cr content of the lavas as a proxy for fractional crystallisation. Blue represents high Cr (relatively primitive) and red represents low Cr content, (relatively fractionated material).

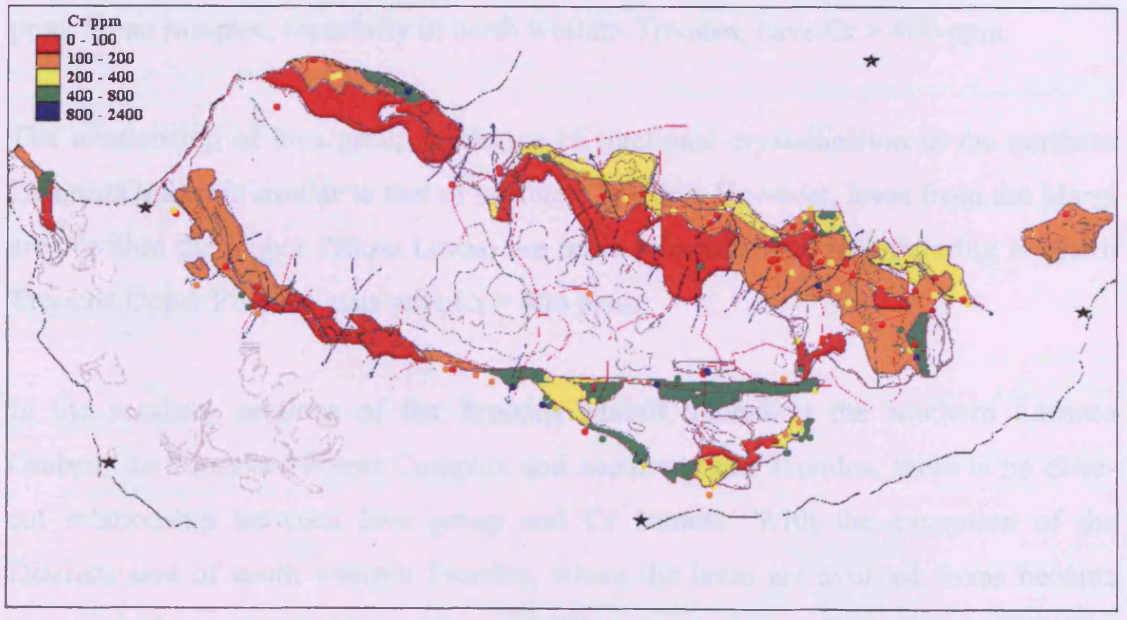

Fig. 3.3b-2. Location map of localities mentioned relating to Cr-Y geochemical fingerprinting

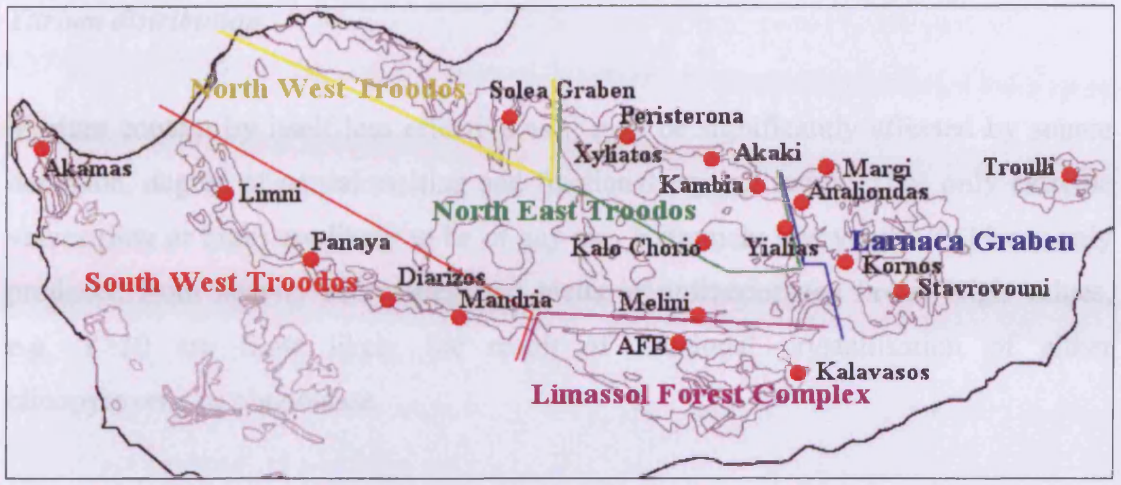

Within northern Troodos the Basal Group, Lower Pillow Lavas and the Upper Pillow Lavas are clearly distinguished by their Cr contents. The Basal Group has the lowest Cr content, hence is the most evolved. Most Basal Group samples had Cr<100 ppm. The Lower Pillow Lavas are only slightly less evolved, with the majority of samples having Cr content between 100 and 200 ppm. There are also a significant number of samples with Cr <100 ppm. The Upper Pillow Lavas of northern Troodos are less fractionated, with the majority of samples having Cr contents between 200 and 400 ppm. Some samples, especially in north western Troodos, have Cr > 400 ppm.

The relationship of lava group to degree of fractional crystallisation in the northern Larnaca Graben is similar to that of northern Troodos. However, lavas from the Margi area (within the Upper Pillow Lavas) are more primitive than neighbouring northern Troodos Upper Pillow Lavas with Cr > 400 ppm.

In the southern sections of the Troodos Massif, including the southern Larnaca Graben, the Limassol Forest Complex and south western Troodos, there is no clear-cut relationship between lava group and Cr content. With the exception of the Diarizos area of south western Troodos, where the lavas are evolved, lavas become progressively more primitive with proximity to the Arakapas Fault Belt (AFB). The most primitive lavas with the Cr > 800 ppm are located in the AFB and the Western Limassol Forest Complex. Other primitive lavas are found in the southern Larnaca

Graben (Stavrovouni area), the south western margin of the Limassol Forest complex and to the east of Mandria in south western Troodos.

Yttrium distribution

Yttrium content by itself less effective as it may be significantly affected by source depletion, degree of partial melting and fractional crystallisation. Thus only extreme values (low or high) are likely to be of any use. Extremely low values Y<10 are only produced from heavily source-depleted melts or unfractionated lavas. High values, e.g. Y>30 are most likely the result of fractional crystallisation of either clinopyroxene or plagioclase.

This problem can be negated if the yttrium content can be recalculated to a specific Cr content (i.e. degree of fractionation) taken here as 100ppm and referred to as Y_{100}. Cr value of 100 ppm is chosen as the yttrium recalculation value as this value lies approximately within the middle of the Cr value range. This was done graphically by regressing the ol+sp+cpx fractionation vector. This corrected value for each area under consideration gives an indication of source composition and partial melting for a given degree of fractional crystallisation. Fig. 3.3b-3 maps Y_{100} across the lavas of the Troodos Massif.

Fig. 3.3b-3. Map of calculated Y contents for 100 ppm Cr (Y_{100}). This largely negates the effect of fractional crystallisation. The only influences on Y content are source depletion and partial melting.

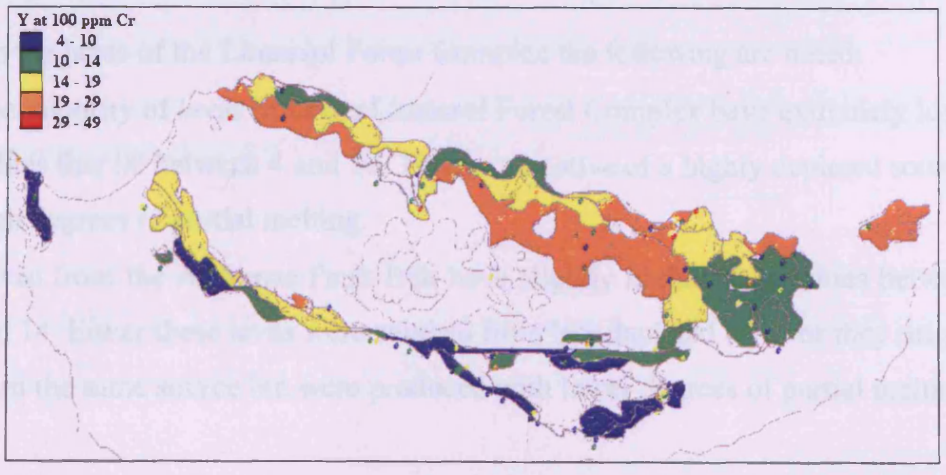

Within the lavas of northern Troodos the following are noted:

- Y_{100} values are generally constant across the northern Troodos lavas from east to west.
- Y_{100} values within the north of Troodos vary with respect to stratigraphic group. Lavas from the Basal Group have Y_{100} values between 19 and 29. Lower Pillow Lavas (LPL) have Y_{100} values between 14 and 19 and Upper Pillow Lavas (UPL) have Y_{100} values between 10 and 14. This would indicate either increasing depletion of the source during extrusion of the lavas or increasing levels of partial melting.
- Y_{100} values in the Kambia area are higher than Y_{100} values across the rest of the northern Troodos lavas, with the Lower and Upper Pillow Lavas having Y_{100} values between 19 and 29.

Within the lavas of south western Troodos the following are noted:

- There is considerable variation with lavas from south western Troodos.
- Lavas from Akamas and the UPL of the southern Paphos Forest have Y_{100} values less than 10, indicating a very depleted source.
- The majority of lavas from the south west of Troodos have Y_{100} values between 14 and 19, comparable with the LPL of the north. Some of the UPL have Y_{100} values between 10 and 14, comparable with UPL of the north of Troodos.
- A small area of lavas (Basal Group and LPL) in the Diarizos area have higher Y_{100} values, between 19 and 29, indicating a less depleted source or lower degrees of partial melting than neighbouring lavas.

Within the lavas of the Limassol Forest Complex the following are noted:

- The majority of lavas from the Limassol Forest Complex have extremely low Y_{100} values that lie between 4 and 10. This is indicative of a highly depleted source and high degrees of partial melting.
- Lavas from the Arakapas Fault Belt have slightly higher Y_{100} values between 10 and 14. Either these lavas were sourced from less depleted lavas or they originated from the same source but were produced with lower degrees of partial melting.

Within the lavas of the Larnaca Graben the following are noted:

- There is a wide spread of Y_{100} values across the Larnaca Graben from < 10 to 29.
- This spread in Y_{100} value is dependant on proximity to the Arakapas Fault Belt, with lavas from the southern Larnaca Graben having Y_{100} values generally between 10 ands 14, but a significant number of samples having Y_{100} values < 10.
- Lavas from the northern Larnaca Graben have Y_{100} values in both the 14 to 19 and 19 to 29 groups. This variation is unlikely to be a function of the lava group from where the lavas were sampled as most of the Larnaca Graben is composed of Upper Pillow Lavas.

3.3c) Troodos Lava Cr – Y profiles by region

Northern Troodos

Lavas from the north of Troodos form three distinct trends referred to in this section as Types 1, 2 and 3. The 'Type 1' lavas have the highest Y_{100} with a value of 22. These lavas are mainly from Akaki and the Mitsero Graben. A few lavas from the Solea Graben belong to this type. Lavas of all stratigraphic groups have Y_{100} values in the Mitsero and Akaki areas. Elsewhere in northern Troodos, Y_{100} is related to the lava group (Fig. 3.3b-3). Given that other geochemical fingerprinting methods (Sections 3.4, 3.5 and 3.6) reveal little variation in source composition between stratigraphical groups for northern Troodos lavas, the variation in Y_{100} is therefore related to the degree of partial melting involved in the genesis of these lavas.

Type 2 lavas have a Y_{100} value of 17, which is slightly lower than that of the Type 1 lavas. Lavas on this trend are mainly from Yialias, with some samples from Akaki Mitsero and Tilliria. Comparison with Fig. 3.3b-3 indicates that these are mainly Lower Pillow Lava samples.

Type 3 lavas are mainly found in the Solea Graben axis and Analiondas, although some Upper Pillow Lava samples from Koronia and Tilliria also fall on this trend. These lavas have an average Y_{100} of 12.

Fig. 3.3c-1. Logarithmic Cr-Y plot showing points and trends for lavas from northern Troodos. Samples showing plagioclase fractional crystallisation have been excluded.

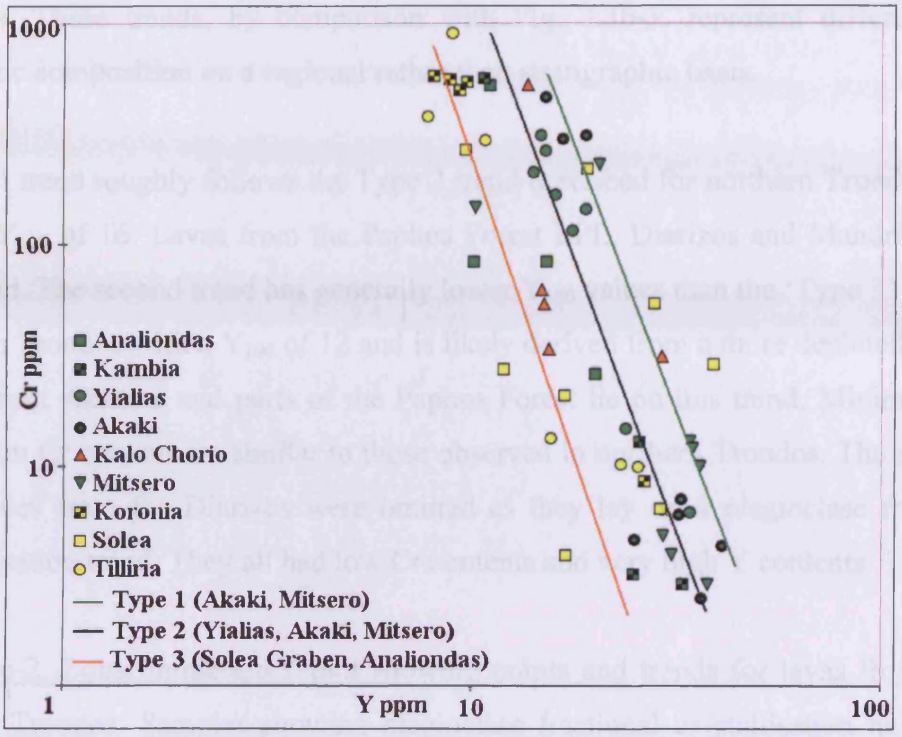

In addition, the wide range of Cr values indicates highly variable extents of fractional crystallisation. There is a significant cluster of UPL lavas with high Cr content, especially in the primitive lavas from Koronia. Similarly, there is a cluster of Basal Group and LPL lavas from Akaki, Mitsero and Kambia that are highly fractionated. A large number of samples, from all sections of the northern Troodos lavas, were omitted as they had elevated Y contents resulting from fractional crystallisation of plagioclase. These samples were removed on the basis of their elevated Y content compared to other lavas on the fractionation trend from a particular area. This particularly affects lavas from the Lower Pillow Lavas and Basal Group. Higher levels of plagioclase fractional crystallisation than those found in neighbouring areas probably cause the anomalous area around Kambia with high Y_{100} referred to in section 3.3b.

South west Troodos

There are two distinct trends shown on Fig. 3.3c-2 for lavas from south western Troodos. These trends, by comparison with Fig. 3.3b-3, represent differences in magmatic composition on a regional rather than stratigraphic basis.

The first trend roughly follows the Type 2 trend described for northern Troodos lavas with a Y_{100} of 16. Lavas from the Paphos Forest LPL, Diarizos and Mandria lie on this trend. The second trend has generally lower Y_{100} values than the 'Type 3' trend of northern Troodos with a Y_{100} of 12 and is likely derived from a more depleted source. Lavas from Akamas and parts of the Paphos Forest lie on this trend. Minimum and maximum Cr content are similar to those observed in northern Troodos. The majority of samples from the Diarizos were omitted as they lay on a plagioclase fractional crystallisation trend. They all had low Cr contents and very high Y contents.

Fig. 3.3c-2. Logarithmic Cr-Y plot showing points and trends for lavas from south western Troodos. Samples showing plagioclase fractional crystallisation have been excluded.

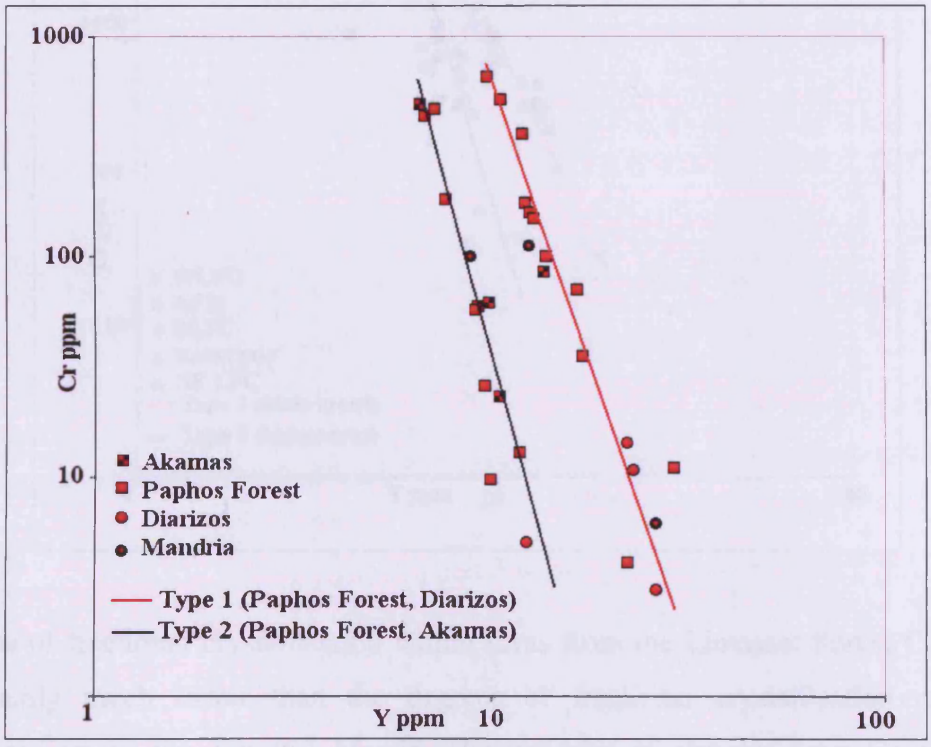

Limassol Forest Complex

Fig.3.3c-3 shows compositions and trends for lavas from the Limassol Forest Complex. The samples are divided into two trends, which are similar to the two trends observed in south western Troodos. The distribution of samples between the two trends is not dependent on location, so is more likely a result of samples originating from different lava groups. These compositional groups are not based on stratigraphy (Section 3.5). Rogers et al. (1989) reported that the sub-divisions of the Upper Pillow Lavas, as originally reported by McCulloch and Cameron (1983), were interleaved. This, however, masks correlation between lava type and location.

Fig. 3.3c-3. Logarithmic Cr-Y plot showing points and trends for lavas the Limassol Forest Complex. Samples showing plagioclase fractional crystallisation have been excluded.

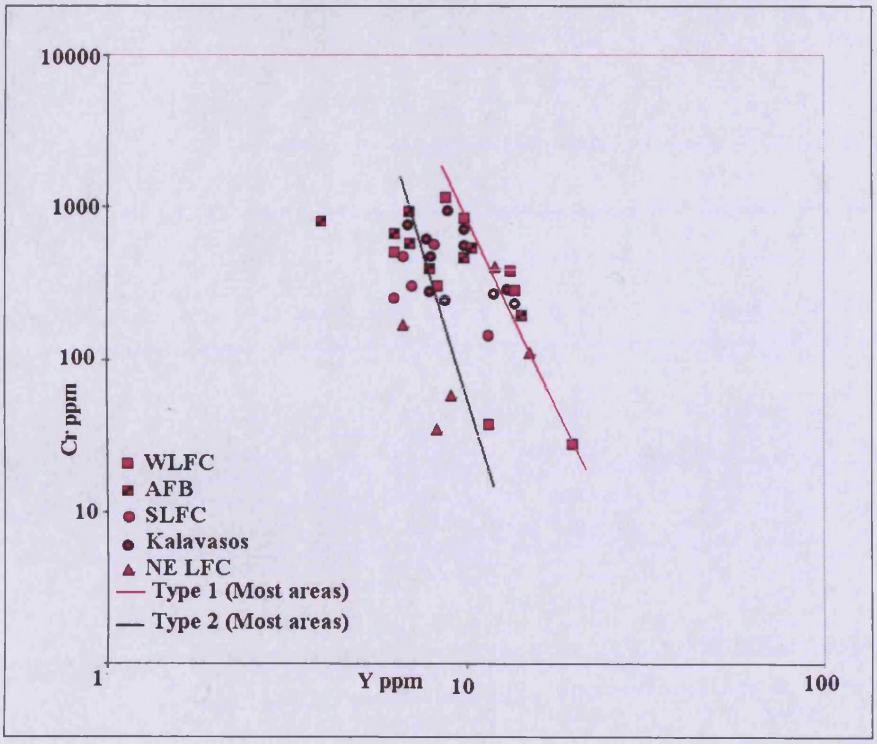

Degrees of fractional crystallisation within lavas from the Limassol Forest Complex are mainly much lower than the degrees of fractional crystallisation reported elsewhere across the Troodos Massif. The majority of samples have Cr contents

above 200 ppm. There is some correlation between location and fractional crystallisation, with lavas from the Arakapas Fault Belt being most primitive, and samples from north eastern LFC being the most fractionated. However, samples from the southern and western LFC have a wider range of Cr contents.

Larnaca Graben

There are three distinct Cr-Y trends within lavas from the Larnaca Graben shown on Fig.3.3c-4. Most of the lavas within the Larnaca Graben are mapped as Upper Pillow Lavas, although there are some inliers of lower stratigraphical units. On this basis, it is likely that the separation of lava types based on Cr-Y discrimination is a function of stratigraphy and location.

The 'Type 1' lavas, mainly found at Margi (within the Upper Pillow Lava outcrop area) with Y_{100} of 17, most resemble the Type 2 lavas of northern Troodos which are found in the Akaki and Yialias areas. The truncated fractionation trend indicates that fractionation of these lavas was not as extensive.

Fig. 3.3c-4. Logarithmic Cr-Y plot showing points and trends for lavas from the Larnaca Graben. Samples showing plagioclase fractional crystallisation have been excluded.

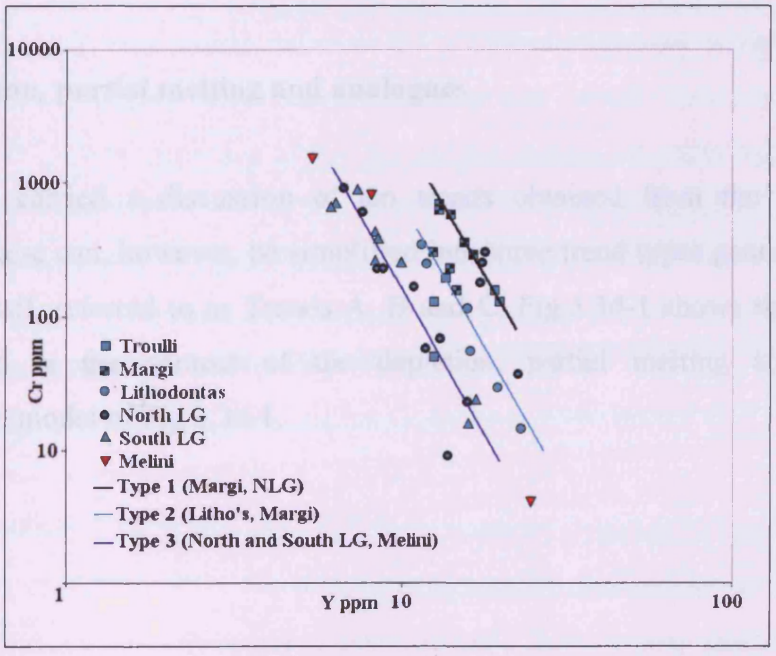

'Type 2' lavas, which are found at Margi and Lithrodonda (within the Lower Pillow Lava outcrop area) are similar to Type 3 lavas of northern Troodos, which are present across much of northern Troodos, especially within the Lower Pillow Lava outcrop and 'Type 2' lavas of south western Troodos. They are also more fractionated than the Upper Pillow Lavas from Margi but have a similar range of fractional crystallisation to the Lower Pillow Lava from northern Troodos. Lavas from Troulli lie on both 'Type 1' and 'Type 2' trends. This is to be expected as both Lower and Upper Pillow Lavas are found in the Troulli area, as shown on published geological maps (Cyprus Geological Survey, 1995).

'Type 3' lavas, found in the other parts of the Larnaca Graben, are represented by samples from all stratigraphic lava groups. These lavas have a low Y_{100} value of 11 and resemble 'Type 2' lavas from south western Troodos. The lavas at the primitive end of this trend also resemble primitive lavas from the Limassol Forest Complex and south western Troodos. These lavas are strongly depleted, hence the low Y_{100} value. This is most likely a function of the proximity of these lavas to the transform fault (note that lavas from the AFB are strongly depleted and primitive). In addition, many lavas within the Larnaca Graben, although sourced from depleted mantle, have become highly fractionated, unlike lavas from near the AFB. Degrees of fractional crystallisation are similar to those noted in northern Troodos. Lavas from the Melini inlier, although not strictly part of the Larnaca Graben also plot along the same trend.

3.3d) Depletion, partial melting and analogues

Section 3.3c carried a discussion of ten trends obtained from the four regions discussed. These can, however, be simplified into three trend types generic across the Troodos Massif, referred to as Trends A, B and C. Fig.3.3d-1 shows the three trend types plotted in the context of the depletion, partial melting and fractional crystallisation model of Fig 3.3a-1.

Fig.3.3d-1 Comparison of Troodos lava Cr-Y trends with calculated vectors of source depletion, partial melting and clinopyroxene fractional crystallisation.

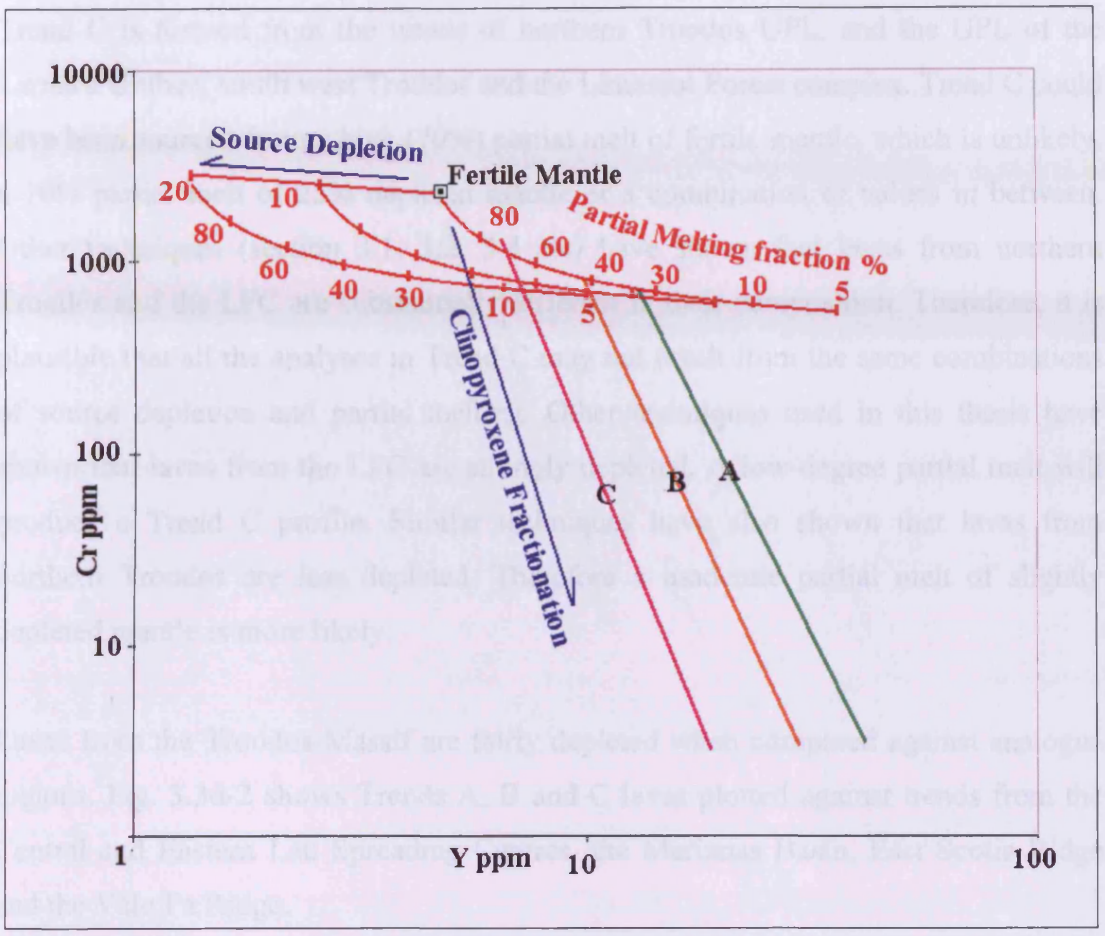

Trend A is formed from trends obtained from northern Troodos Basal Group lavas and lavas from the Upper Pillow Lavas of Margi and Troulli. These lavas show the lowest levels of source depletion and/or the lowest degrees of partial melting. Such a trend could be sourced from a 35% partial melt of fertile mantle or a 10% partial melt of 10% depleted mantle or a combination between these values. A 35% partial melt forming in a ridge environment is unrealistically high. Flower and Levine (1987) calculated that most lavas in the Troodos Massif were formed from approximately 20% partial melts.

Trend B is formed from trends obtained from northern Troodos Lower Pillow Lavas and Lower Pillow Lavas of the Larnaca Graben, south west Troodos and the Limassol Forest Complex. These lavas could have formed from higher degrees of partial

melting (40%) of a fertile mantle source than Trend A lavas or partial melting of a more depleted source (e.g. 10% partial melt of a 15% depleted source)

Trend C is formed from the trends of northern Troodos UPL, and the UPL of the Larnaca Graben, south west Troodos and the Limassol Forest complex. Trend C could have been sourced from a high (70%) partial melt of fertile mantle, which is unlikely, a 10% partial melt of 25% depleted mantle or a combination of values in between. Other techniques (section 3.1, 3.2, 3.4 etc) have shown that lavas from northern Troodos and the LFC are substantially different in their composition. Therefore, it is plausible that all the analyses in Trend C may not result from the same combinations of source depletion and partial melting. Other techniques used in this thesis have shown that lavas from the LFC are strongly depleted. A low-degree partial melt will produce a Trend C profile. Similar techniques have also shown that lavas from northern Troodos are less depleted. Therefore a moderate partial melt of slightly depleted mantle is more likely.

Lavas from the Troodos Massif are fairly depleted when compared against analogue regions. Fig. 3.3d-2 shows Trends A, B and C lavas plotted against trends from the Central and Eastern Lau Spreading Centres, the Marianas Basin, East Scotia Ridge and the Valu Fa Ridge.

Trend A lavas are most similar to those from the Mariana Basin and the Eastern Lau Spreading Centre. These are both back-arc spreading-centres located about 100 km behind their respective arcs. Trend B lavas are most similar to those from the Valu Fa Ridge and East Scotia Ridge. The Valu Fa Ridge is a spreading centre about 70km behind the Tonga Arc. However, the East Scotia Ridge is located nearer 150km behind the South Sandwich Arc.

Trend C lavas are lower in Y content than any of the analogues, with compositions more like arc-derived basalts than back-arc spreading centres.

Fig. 3.3d-2. Cr-Y diagram of Troodos lava trend types plotted against analogous regions. CLSC/ELSC = Central/Eastern Lau Spreading Centre (Pearce et al., 1995) MB = Marianas Basin (Pearce et al., (2005), ESR = East Scotia Ridge (Leat et al., (2004), VFR = Valu Fa Ridge (Peate et al., 2001)

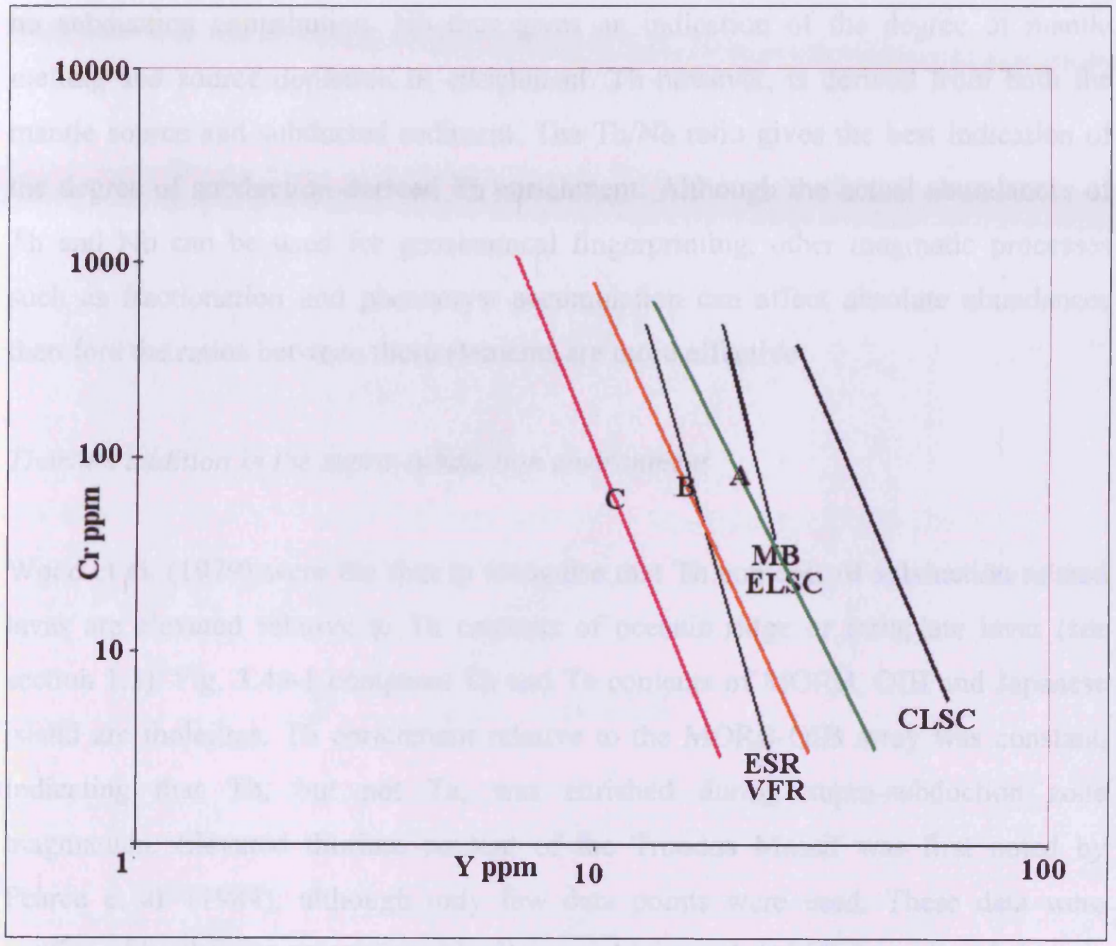

3.4) Measuring subduction input using Th-Nb and Th-Ta covariations

3.4a) Nb, Ta, Yb and their behaviour in subduction-related magmas and lavas

The Nb (and Ta) content of magmas is usually derived from the mantle with little or no subduction contribution. Nb thus gives an indication of the degree of mantle melting and source depletion or enrichment. Th however, is derived from both the mantle source and subducted sediment. The Th/Nb ratio gives the best indication of the degree of subduction-derived Th enrichment. Although the actual abundances of Th and Nb can be used for geochemical fingerprinting, other magmatic processes such as fractionation and phenocryst accumulation can affect absolute abundances therefore the ratios between these elements are more effective

Thorium addition in the supra-subduction environment

Wood et al. (1979) were the first to recognise that Th contents of subduction-related lavas are elevated relative to Th contents of oceanic ridge or intraplate lavas (see section 1.3). Fig. 3.4a-1 compares Th and Ta contents of MORB, OIB and Japanese island arc tholeiites. Th enrichment relative to the MORB-OIB array was constant, indicating that Th, but not Ta, was enriched during supra-subduction zone magmatism. Elevated thorium content of the Troodos Massif was first noted by Pearce et al. (1984), although only few data points were used. These data were confirmed by the dataset produced by Rautenschlein et al. (1985) from the Akaki area in north eastern Troodos.

The discrimination diagram of Wood et al. (1979) highlights subduction enrichment of Th but, by being based on absolute values of Th and Ta, is susceptible to variations in magma composition related to the degree of partial melting, source depletion and fractional crystallisation. Wood et al. (1979) also used the Th-Ta-Hf triangle, which effectively plots ratios between the elements.

Fig. 3.4a-1. Enriched thorium content of supra-subduction magmas (Japan used as example) compared to thorium contents of N-MORB, P-MORB (Iceland used as example) and ocean island basalt (OIB, with the Azores used as example). Diagram shows equal enrichment of thorium and tantalum as a result of increasing plume-enrichment. Lower end of Japan IAT field demonstrates that IATs may be sourced from mantle somewhat more depleted than the MORB source. (Wood et al., 1979)

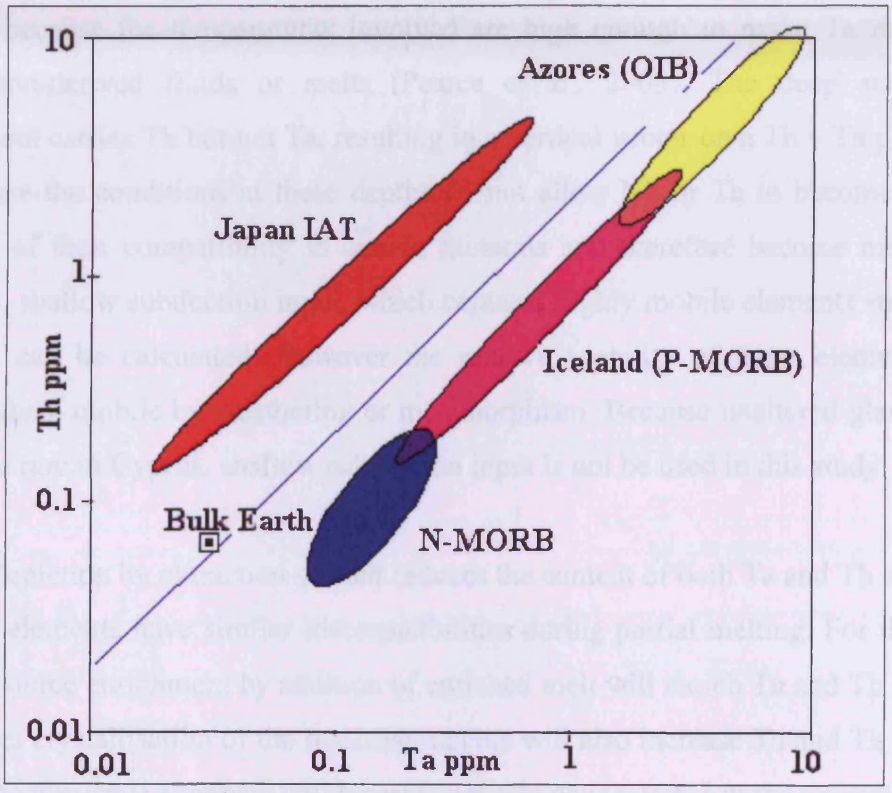

Pearce et al. (1981) improved the clarity of Th-Ta fingerprinting by normalising the data by an incompatible, immobile trace element so that variations due to partial melting and fractional crystallisation magmatic processes can be reduced. Yb was chosen as it strongly compatible in eclogitic assemblages so is therefore one of the most subduction-immobile incompatible elements. Over time, other modifications to the Th v Ta plot have been made. For example, Pearce et al. (1995) used Nb as the subduction-immobile element instead of Ta.

Pearce et al. (1995) produced a Th/Yb – Nb/Yb diagram with contours according to subduction content. These contours show the proportion of subduction-derived Th in

the mantle source. Where the content is listed as, e.g. 50% SZ, this indicates that 50% of the thorium content is derived from the subduction zone.

Fig.3.4a-2 is a Yb-normalised Th v Ta plot that shows two sample datasets for lavas from the Marianas area in order to demonstrate the effects of variable enrichment of both source and subduction content. The controlling vectors (marked in green) are source depletion/enrichment, ultra-deep subduction input and deep subduction input. The ultra-deep subduction component may carry a quantity of Ta in addition to Th. This is because the temperatures involved are high enough to make Ta mobile in subduction-derived fluids or melts (Pearce et al., 2005). The deep subduction component carries Th but not Ta, resulting in a vertical vector on a Th v Ta plot. This is because the conditions at these depths do not allow Nb or Ta to become soluble because of their compatibility in certain minerals and therefore become mobile. In addition, shallow subduction input, which contains highly mobile elements such as Sr and Pb, can be calculated. However the relative mobility of these elements also renders them mobile by weathering or metamorphism. Because unaltered glasses and rocks are rare in Cyprus, shallow subduction input is not be used in this study.

Source depletion by extraction of melt reduces the content of both Ta and Th similarly as these elements have similar incompatibilities during partial melting. For the same reason, source enrichment by addition of enriched melt will enrich Ta and Th equally. Fractional crystallisation of the resulting magma will also increase Ta and Th as these highly incompatible elements will be preferentially concentrated in the residual melt.

Variable supra-subduction zone enrichment of mantle a narrow vertical trend, as shown by lavas from the Mariana Trough (in blue). Partial melting of subduction-enriched mantle produces a trend parallel to the MORB array, as shown by lavas from the Mariana Northern Volcanic Tectonic Zone (in red).

Fig. 3.4a-2. Enrichment vectors and example datasets for Th/Nb v Yb/Nb plot. Example datasets from Mariana Trough and Mariana Northern Volcanic Tectonic Zone (NVTZ) from Pearce et al. (2005) used to demonstrate the differences in ratios produced by fractional partial melting of subduction-enriched mantle, shown in red, which is parallel to MORB array and variably enriched magma originating from variably subduction-enriched mantle.

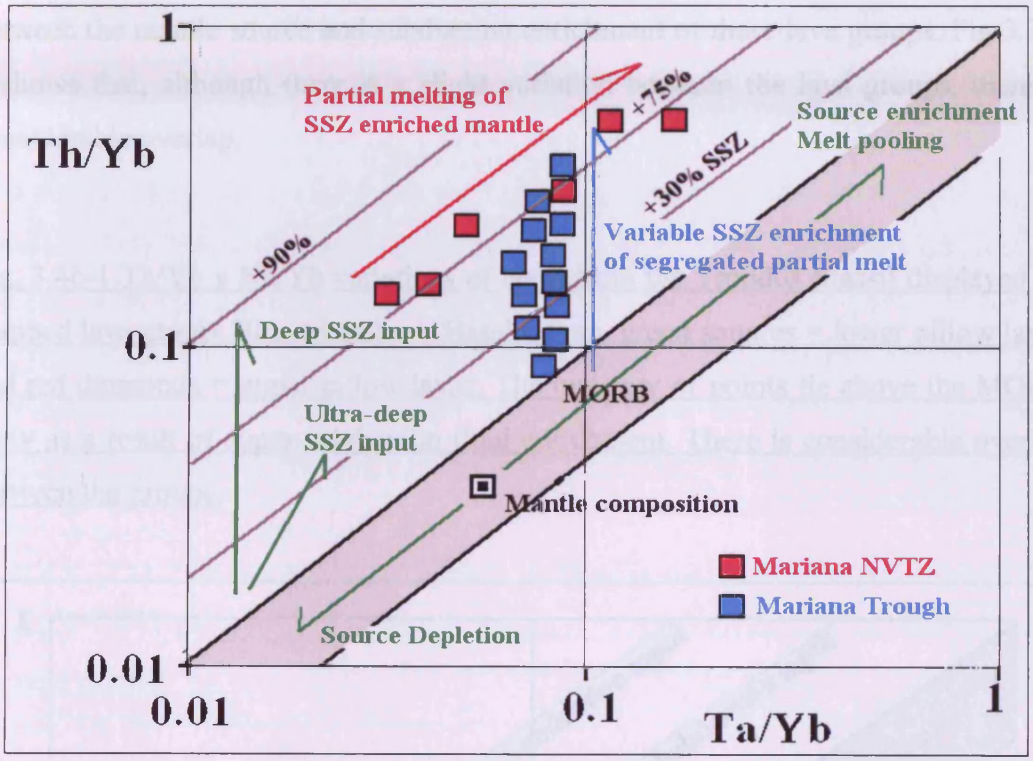

3.2b) Th/Nb variations within the Troodos Massif.

Variations between Basal Group, Lower Pillow Lavas and Upper Pillow Lavas

Variations between lava groups based on element content has previously been recognised by workers such as Cameron (1985), Flower and Levine (1987) and Taylor (1990). Sobolev (1993) and Portnyagin et al. (1997) also detected the difference in source between the LPL and Basal Group (BG) lavas by using multi-element spider diagrams, finding that the BG were more similar to the UPL than the LPL. Thus, if the lavas all had different sources, they should exhibit different levels of depletion and subduction-related enrichment. However, the Th-Ta-Hf plot of Pearce

(1984) was unable to distinguish between UPL and LPL. Variations between the spread of Th/Nb ratios of samples from each of the three lava groups should prove whether there was any fundamental source variation.

Plotting data for the Basal Group, Lower Pillow Lavas and Upper Pillow Lavas of the Troodos Massif on a logarithmic Th/Yb v Nb/Yb graph incorporating subduction input contours of Pearce et al. (2005) is an attempt to determine the relationship between the mantle source and subduction enrichment of these lava groups. Fig 3.2b-1 shows that, although there is a slight variation between the lava groups, there is considerable overlap.

Fig. 3.4b-1 Th/Yb v Nb/Yb variations of lavas from the Troodos Massif displayed by mapped lava group. Blue triangles = Basal Group, green squares = lower pillow lavas and red diamonds = upper pillow lavas. The majority of points lie above the MORB array as a result of supra-subduction fluid enrichment. There is considerable overlap between the groups.

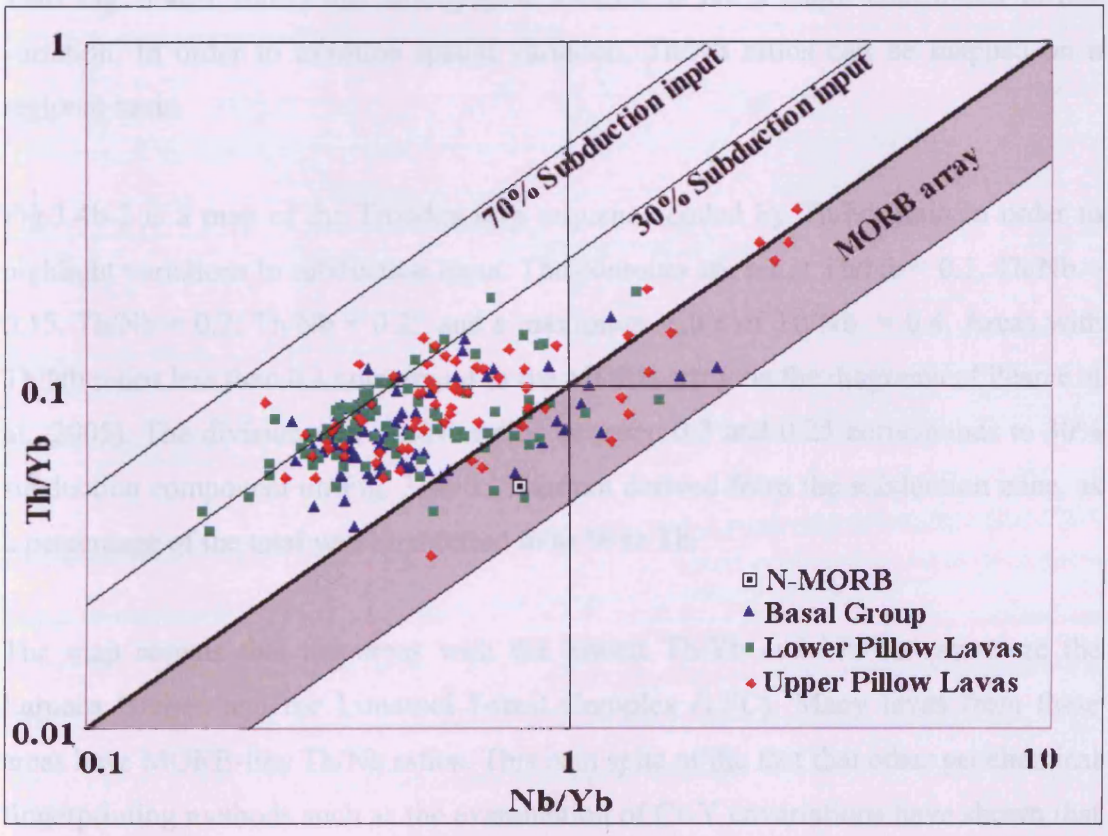

Subduction input between the groups is roughly constant. The mean values of Nb/Th are 0.16 for the Basal Group, 0.18 for the Lower Pillow Lavas and 0.16 for the Upper Pillow Lavas. The relative standard deviation is 36% for the Basal Group, 32% for the Lower Pillow Lavas and 37% for the Upper Pillow Lavas. This similarity between the groups indicates that subduction input is, although variable, not related to lava group.

The difference between the groups is highlighted when source depletion/enrichment is examined. The mean values of Nb/Yb are 0.55 for the Basal Group, 0.5 for the Lower Pillow Lavas and 0.73 for the Upper Pillow Lavas. The relative standard deviation is 63% for the Basal Group, 49% for the Lower Pillow Lavas and 80% for the Upper Pillow Lavas. These figures indicate that the Upper Pillow Lavas are derived, on average, from less depleted mantle than the Lower Pillow Lavas or the Basal Group. The high relative standard deviation also indicates that these lavas are very variable in their Nb/Yb ratios. The Lower Pillow Lavas and Basal Group, which have similar mean Nb/Yb ratios and standard deviation, are most likely to be probably cogenetic.

Thus Fig. 3.4a-1 shows that stratigraphic location is not a major contributor to this variation. In order to examine spatial variation, Th/Nb ratios can be mapped on a regional basis.

Fig.3.4b-2 is a map of the Troodos lava sequence coded by Th/Nb ratio in order to highlight variations in subduction input. The contours are set at Th/Nb = 0.1, Th/Nb = 0.15, Th/Nb = 0.2, Th/Nb = 0.25 and a maximum value of Th/Nb = 0.4. Areas with Th/Nb ratios less than 0.1 correspond to the MORB array on the diagrams of Pearce at al., 2005). The division with Th/Nb ratios between 0.2 and 0.25 corresponds to 30% subduction component on Fig. 3.4b-1. Thorium derived from the subduction zone, as a percentage of the total will be referred to as % sz Th.

The map reveals that the areas with the lowest Th/Yb and Nb/Yb ratios are the Larnaca Graben and the Limassol Forest Complex (LFC). Many lavas from these areas have MORB-like Th/Nb ratios. This is in spite of the fact that other geochemical fingerprinting methods such as the examination of Cr-Y covariations have shown that these lavas are not MORBs.

In detail, lavas from the southern Larnaca Graben, parts of the north eastern Larnaca Graben as well as lavas from the Arakapas Fault Belt, the western LFC and the Kalavasos area all have Th/Nb ratios less than 0.1 which places them within the MORB array. Locations of these sites, and all localities referred to in this section are shown later on Fig 3.4b-3.

Fig. 3.4b-2. Map of the Troodos Massif showing Th/Nb variations. A ratio of 0.1 (blue and green zones) approximates to the upper boundary of the MORB array. Higher ratios are the result of supra-subduction enrichment. Lavas from the AFB and Larnaca Graben have the lowest Th/Yb v Nb/Yb ratios. Highest ratios (highest SSZ input) are in the north and north west of the lava outcrop.

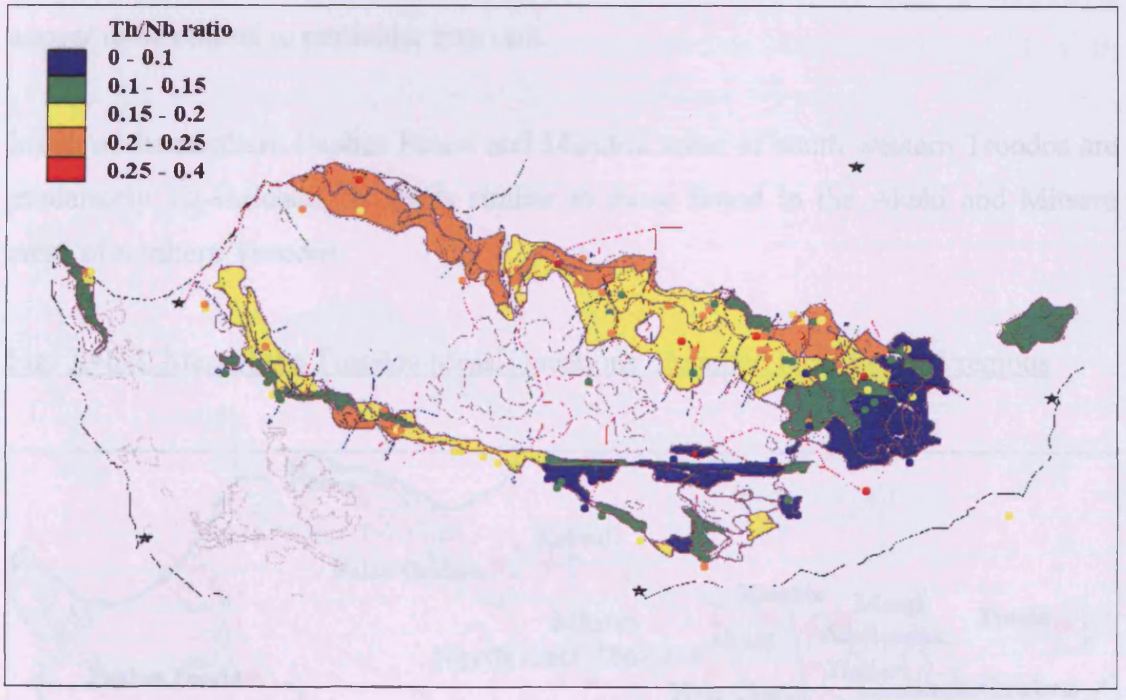

Other lavas that have low levels of Th addition are found within the Larnaca Graben, parts of the southern LFC and parts of south western Troodos. In detail, within the Larnaca Graben, these lavas with Th/Nb ratios between 0.1 and 0.15 are found in the central section and in the Troulli inlier. Within south west Troodos, low-Th/Nb lavas are found in the southern portion of the Paphos Forest and Akamas. Low Th/Nb lavas

are also found in the UPL of the Kambia area in north eastern Troodos. These Kambia UPL are in stark contrast to the high Th/Nb LPL and Basal Group from this area.

Lavas with the highest Th/Nb ratios (above 0.2, which approximates to about 30% subduction-derived Th content) are found across northern Troodos, the northern Larnaca Graben and in the Diarizos area of south western Troodos.

In detail, within the Larnaca Graben, high Th/Nb lavas are confined to the Margi and Lithrodonda areas. Within northern Troodos, high Th/Nb lavas appear to make up much of the Tilliria area but a smaller proportion of the central northern lavas. However, the Tilliria area was poorly sampled and there are many Th-enriched lavas within the Akaki and Mitsero areas which are shown as orange dots within the yellow (moderate Th-enrichment) field. The Th-enriched lavas from Diarizos in south western Troodos are confined to a small area. Th-enrichment in this area does not appear to be related to particular lava unit.

Much of the northern Paphos Forest and Mandria areas of south western Troodos are moderately Th-enriched, to levels similar to those found in the Akaki and Mitsero areas of northern Troodos.

Fig. 3.4b-3. Map of the Troodos Massif locations of named localities and regions

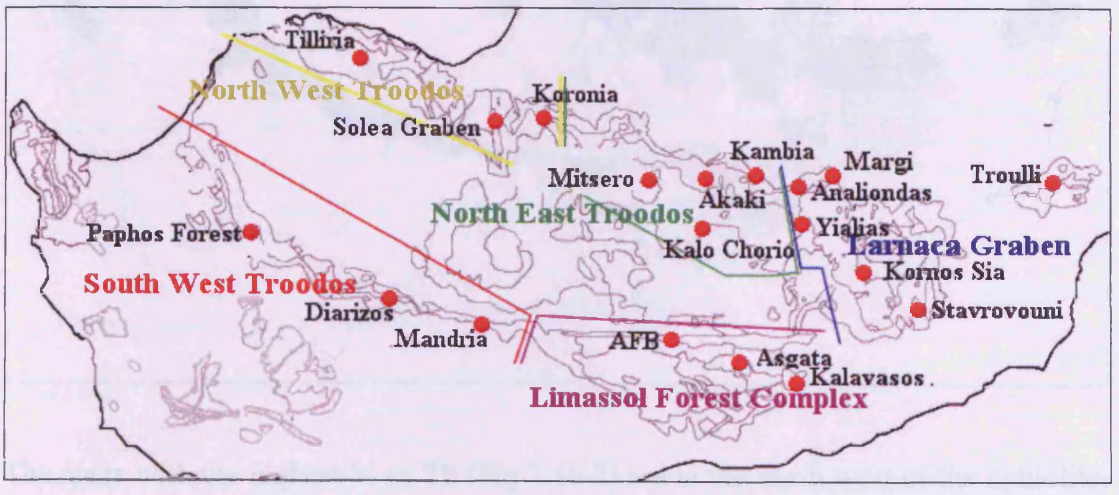

Fig.3.4b-4 is a map of the Troodos lava sequence showing variations in Nb/Yb ratios across the Troodos lavas in order to display variations in source depletion/enrichment.

Orange areas are most enriched, and blue areas are most depleted in Nb. Areas coloured blue or green have Nb/Yb ratios less than 0.75, indicating that they are depleted relative to N-MORB. The similarity of lavas in the Diarizos area to lavas from north Troodos is particularly clear using Nb/Yb. Much of the north and south west of the Troodos Massif is depleted relative to N-MORB. Some lavas from the northern portion of the Larnaca Graben and a few samples from the Limassol Forest Complex (LFC) are also depleted. The areas of greatest depletion are the Basal Group and much of the LPL of the north, together with lavas from Diarizos, Mandria and some of the UPL of the south west and lavas from the northern extremity of the Larnaca Graben.

Fig. 3.4b-4. Map of the Troodos Massif showing Nb/Yb variations. Nb/Yb variations are proxy for enrichment of the mantle source. Areas with Nb/Yb ratio lower than 0.75 are source depleted (blue and green on the map). Therefore most of the Troodos Massif is source-depleted. The southern portion of the Larnaca Graben, the AFB, parts of the LFC and some of the north Troodos UPL are Nb-enriched.

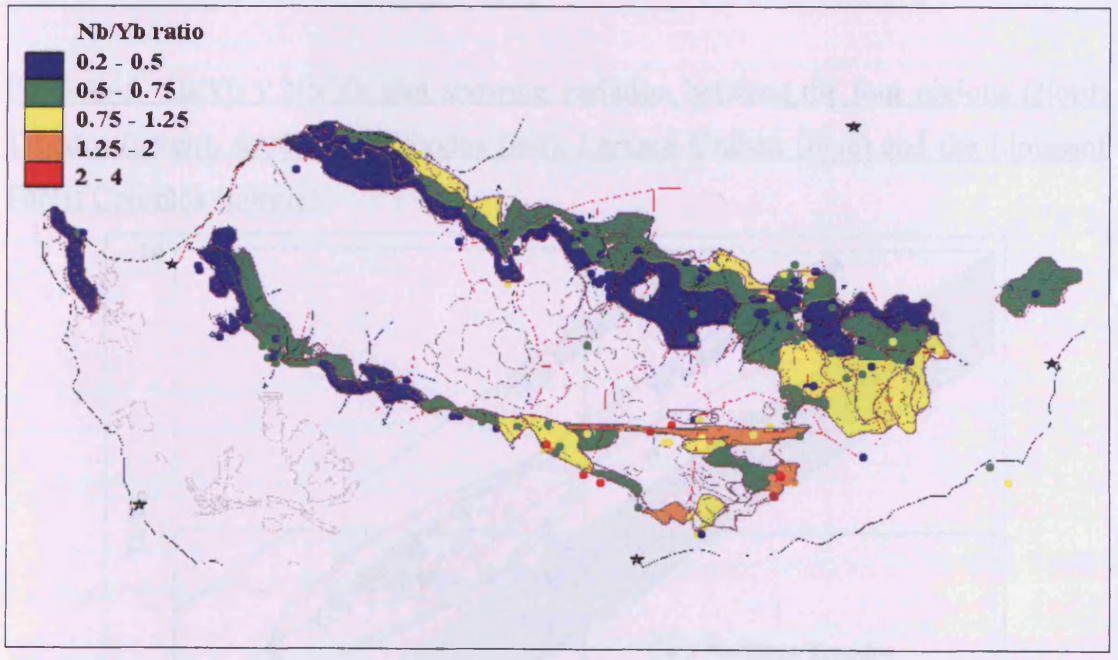

The areas with the highest % sz Th (Fig 3.4b-2) are to the north west of the ophiolite. This corresponds with the area of maximum source depletion shown on Fig 3.4b-4. Conversely, areas with the lowest subduction input (Southern Larnaca Graben and

LFC) correspond with areas of greatest Nb enrichment. However, a constant addition of Th added to variable mantle could also have this effect.

Fig 3.4b-5 is a Th/Yb v Nb/Yb plot of the Troodos lavas divided according to region. Although both the map (Fig 3.4b-4) and Fig 3.4b-5 distinguish the high-Nb lavas of the Larnaca Graben and AFB, the geochemical maps (both Th/Yb v Nb/Yb and Nb/Yb) do not clearly show the different ranges of compositions between north and south west Troodos. This is because there is one compositional group that encompasses lavas from northern, south western and some of the Larnaca Graben lavas. These lavas are all generally depleted and have between 10 and 40% $_{sz}$ Th.

Lavas from the Larnaca Graben and are found in two groups. One has a similar compositional range to lavas from the north and south west of the Troodos Massif, and the second group lies on the MORB array, indicating little or no subduction input. Most of the lavas from the LFC have little subduction input and generally higher Nb content than lavas from elsewhere around the Troodos Massif.

Fig 3.4b-5. Th/Yb v Nb/Yb plot showing variation between the four regions (North Troodos (green), south west Troodos (red), Larnaca Graben (blue) and the Limassol Forest Complex (purple).

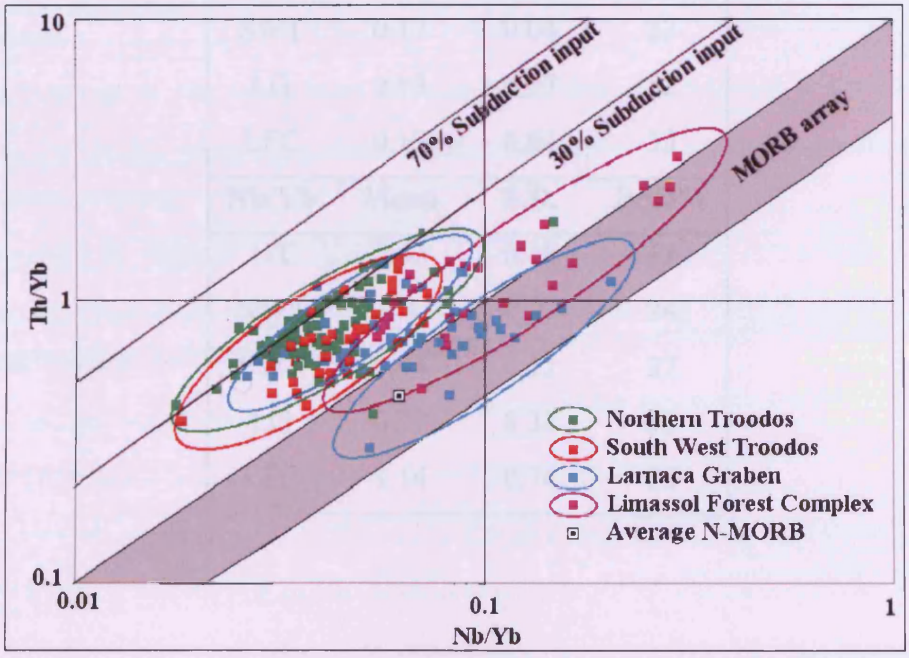

Although there is considerable overlap, lavas from the south west of Troodos are generally slightly less Nb-depleted than lavas from the north of Troodos as shown on Table 3.4b-1. The average lava from the Larnaca Graben is slightly enriched and lavas from the Limassol Forest Complex are considerably enriched. It should also be noted that there is generally a large spread of Nb/Yb ratios as indicated by the large relative standard deviations.

High standard deviations within the Larnaca Graben and Limassol Forest Complex lavas for both Nb/Th and Nb/Yb are caused by extensive variation in source enrichment and the presence of two distinct compositional fields.

Table 3.4b-1. Mean values, standard deviations and relative standard deviations of Nb/Th (subduction enrichment) and Nb/Yb (source depletion/enrichment) of lavas from selected regions of the Troodos lava sequence. NT = North Troodos, NWT = North western Troodos, SWT = South western Troodos, LG = Larnaca Graben, LFC = Limassol Forest Complex.

Nb/Th	**Mean**	**S.D.**	**RSD%**
NT	0.2	0.04	21
NWT	0.22	0.03	15
SWT	0.17	0.04	22
LG	0.13	0.07	52
LFC	0.12	0.04	33
Nb/Yb	**Mean**	**S.D.**	**RSD%**
NT	0.42	0.18	41
NWT	0.4	0.09	24
SWT	0.44	0.12	27
LG	0.71	0.38	53
LFC	1.14	0.74	65

North Troodos

Fig 3.4b-6 depicts lavas from northern Troodos plotted on a logarithmic Th/Yb v Nb/Yb diagram with trends drawn by eye. Two of the trends are parallel, with differing levels of Th-enrichment and the third is a curved trend between Th-enriched subduction-derived and Nb-enriched mantle-derived end-members. These trends are plotted on Fig 3.4b-6 as Trends 1, 2 and 3 respectively.

Lavas belonging to Trend 1 have the following properties:

- On average about 30% of the thorium content of the lavas of this trend is subduction-derived. As explained in Fig 3.4a-2, the MORB-parallel trend is likely the result of partial melting of SSZ-enriched mantle.
- Lavas on Trend 1 are found at Analiondas, Kambia (LPL and Basal Group only c.f. Fig 3.4b-2), the Solea Graben axis and Tilliria. The majority of lavas from northern Troodos lie on this trend.
- There is a substantial variation between the most and least depleted ends of this trend, although this may be related to the variations in pooling of melt fractions involved during formation of these lavas.

Lavas belonging to Trend 2 have the following properties:

- On average, about 15% of the thorium content of these lavas is subduction-derived.
- The majority of the lavas from the Akaki, Yialias and Mitsero areas lie on this trend. However, these are a small proportion of lavas relative to all samples from northern Troodos.
- The trend is shorter than Trend 1 and is less depleted is its 'low-Nb' end indicating that there was less variation in the source and melting conditions than Trend 1 lavas.

Lavas belonging to Trend 3 have the following properties:

- The Th-rich end-member of this trend has about 30-35% subduction-derived Th. The low-Th end-member of this trend has little or no subduction-derived Th.

- The trend could be explained by the mixing of mantle of the Trend 1 type and non subduction-enriched fertile mantle or addition of a constant subduction-derived component to variably depleted mantle
- Lavas on this trend originate from Akaki and Kambia. Comparison with the Th/Nb map (Fig 3.4b-2) indicates that these anomalous lavas belong to the Upper Pillow Lava sequence at Kambia and Akaki.
- Lavas with low and variable levels of subduction enrichment are also found at Kalo Chorio and Analiondas. As such, it is plausible that these lavas could either be 'overspill' from the Larnaca Graben or erupted from off-axis fissures during the opening of the Larnaca Graben. The boundary of the Larnaca Graben is located within 7 kilometres from this area.

Fig 3.4b-6. Plot of Th/Yb v Nb/Yb variation within lavas from the north of the Troodos Massif. Enrichment contours from Pearce et al. (1995). Although there are a few points that lie within the MORB array, the majority of samples plot with about 30% SSZ enrichment from variably depleted mantle sources. The average N-MORB composition is shown by the black and white nested square.

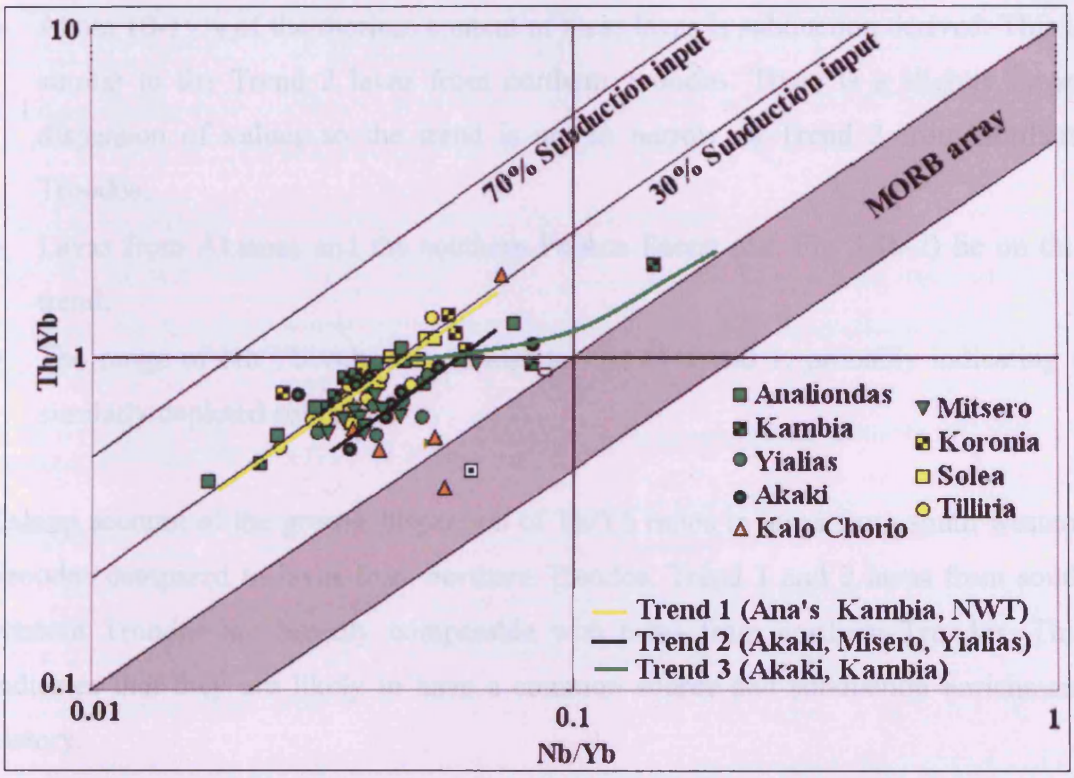

South west Troodos

Fig 3.4b-7 depicts lavas from south western Troodos plotted on a logarithmic Th/Yb v Nb/Yb diagram with trends drawn by eye. The trends are parallel, indicating differing levels of Th-enrichment. These trends are plotted as Trends 1 and 2 on Fig 3.4b-7 respectively.

Lavas belonging to Trend 1 have the following properties:

- About 25% of the thorium content of these lavas is subduction derived. This is slightly less than the equivalent value for the Trend 1 lavas from northern Troodos. There is a larger slightly dispersion of values of subduction component than Trend 1 northern Troodos in the south western lavas.
- Lavas from Diarizos, Mandria and the northern Paphos Forest (c.f. Fig 3.4b-2) lie on this trend.
- The 'low-Nb' end of the trend is less depleted than the 'low-Nb' end of the northern Troodos Trend 1. The trend is also shorter, indicating that the lavas originated from a less variable source.

Lavas belonging to Trend 2 have the following properties:

- About 10-15% of the thorium content of these lavas is subduction derived. This is similar to the Trend 2 lavas from northern Troodos. There is a slightly larger dispersion of values so the trend is not as narrow as Trend 2 from northern Troodos.
- Lavas from Akamas and the southern Paphos Forest (c.f. Fig 3.4b-2) lie on this trend.
- The range of Nb/Yb values is similar to that of Trend 1, probably indicating a similarly depleted source.

Taking account of the greater dispersion of Th/Yb ratios in lavas from south western Troodos compared to lavas from northern Troodos, Trend 1 and 2 lavas from south western Troodos are broadly comparable with lavas from northern Troodos. This indicates that they are likely to have a common source and subduction enrichment history.

Fig 3.4b-7. Plot of Th/Yb v Nb/Yb variation within lavas from the south west of Troodos. Enrichment contours from Pearce et al. (1995). Average N_MORB composition is shown by the black and white nested square. P.F. = Paphos Forest.

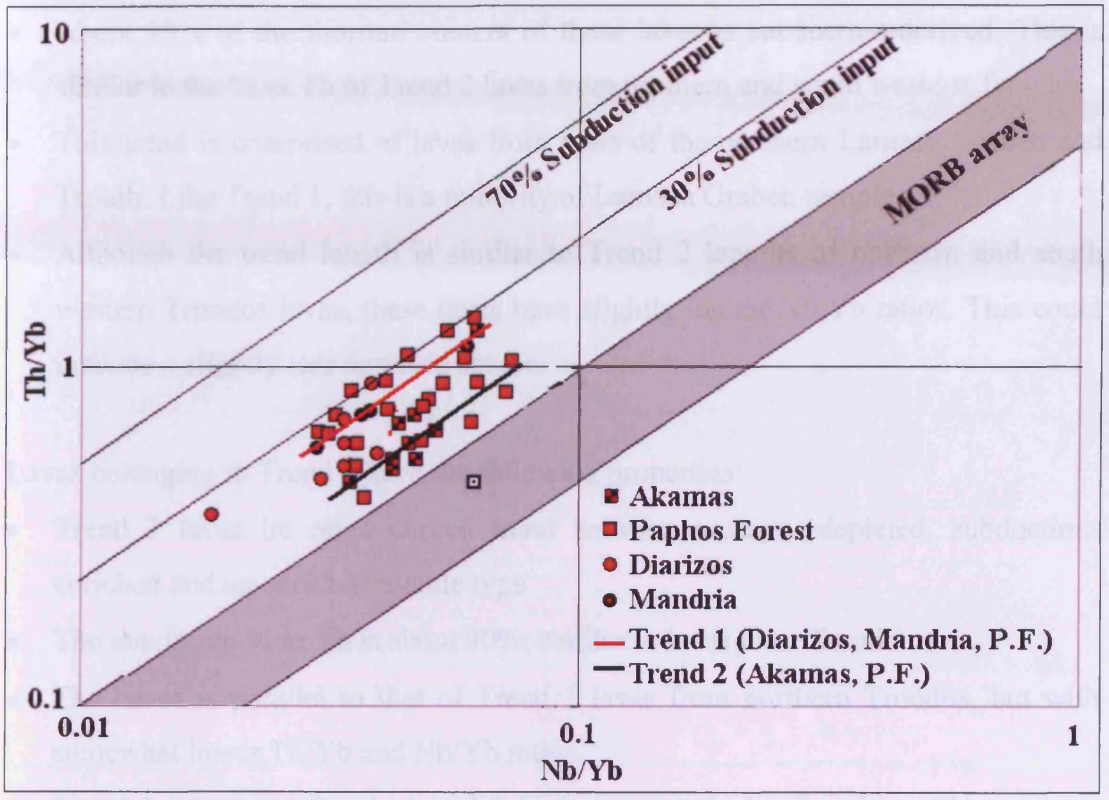

Larnaca Graben

Fig 3.4b-8 depicts lavas from northern Troodos plotted on a logarithmic Th/Yb v Nb/Yb diagram with best-fit trends. Two of the trends are parallel, with differing levels of Th-enrichment and the third curved trend between Th-enriched subduction-derived and Nb-rich magmas. These trends are plotted as Trends 1, 2 and 3 on Fig 3.4b-8 respectively.

Lavas belonging to Trend 1 have the following properties:

- About 25% of the thorium content of these lavas is subduction derived. This is similar to the % sz Th of Trend 1 lavas from northern Troodos.
- Only lavas from Margi and Lithrodonda lie on this trend, a minority of the Larnaca Graben sample suite.

- The range of Nb/Yb values is similar to that obtained from Trend 1 lavas from south western Troodos.

Lavas belonging to Trend 2 have the following properties:

- About 15% of the thorium content of these lavas is subduction-derived. This is similar to the % sz Th of Trend 2 lavas from northern and south western Troodos
- This trend is comprised of lavas from parts of the northern Larnaca Graben and Troulli. Like Trend 1, this is a minority of Larnaca Graben samples.
- Although the trend length is similar to Trend 2 lengths of northern and south western Troodos lavas, these lavas have slightly higher Nb/Yb ratios. This could indicate a slightly less depleted source.

Lavas belonging to Trend 3 have the following properties:

- Trend 3 lavas lie on a curved trend between a source-depleted, subduction-enriched and an enriched mantle type.
- The maximum % sz Th is about 30%, similar to lavas from Trend 1.
- The curve is parallel to that of Trend 3 lavas from northern Troodos, but with somewhat lower Th/Yb and Nb/Yb ratios.
- Trend 3 intersects Trends 1 and 2 at their most depleted ends, unlike northern Troodos Trend 3, which intersects the most Nb-enriched end of Trend 1.
- Lavas that lie on Trend 3 originate from a large portion of both the northern and southern Larnaca Graben and from the Melini inlier. The Melini inlier is not technically part of the Larnaca Graben, but is compositionally most similar to lavas from the graben.

The similarity between Trends 1 and 2 lavas of the Larnaca Graben and Trends 1 and 2 of northern and south western Troodos and may indicate that these lavas were formed in a similar way. Lavas belonging to Trend 3 may to be influenced by proximity to the LFC, including the paleo-transform fault referred to as the Arakapas Fault Belt (AFB). Proximity to the AFB during the formation of the Larnaca Graben may have allowed the introduction of small melt fractions into the source that were not present elsewhere. This is discussed in more detail in section 4.1.

Fig 3.4b-8. Plot of Th/Yb v Nb/Yb variation within lavas from Larnaca Graben. Enrichment contours from Pearce et al. (1995).

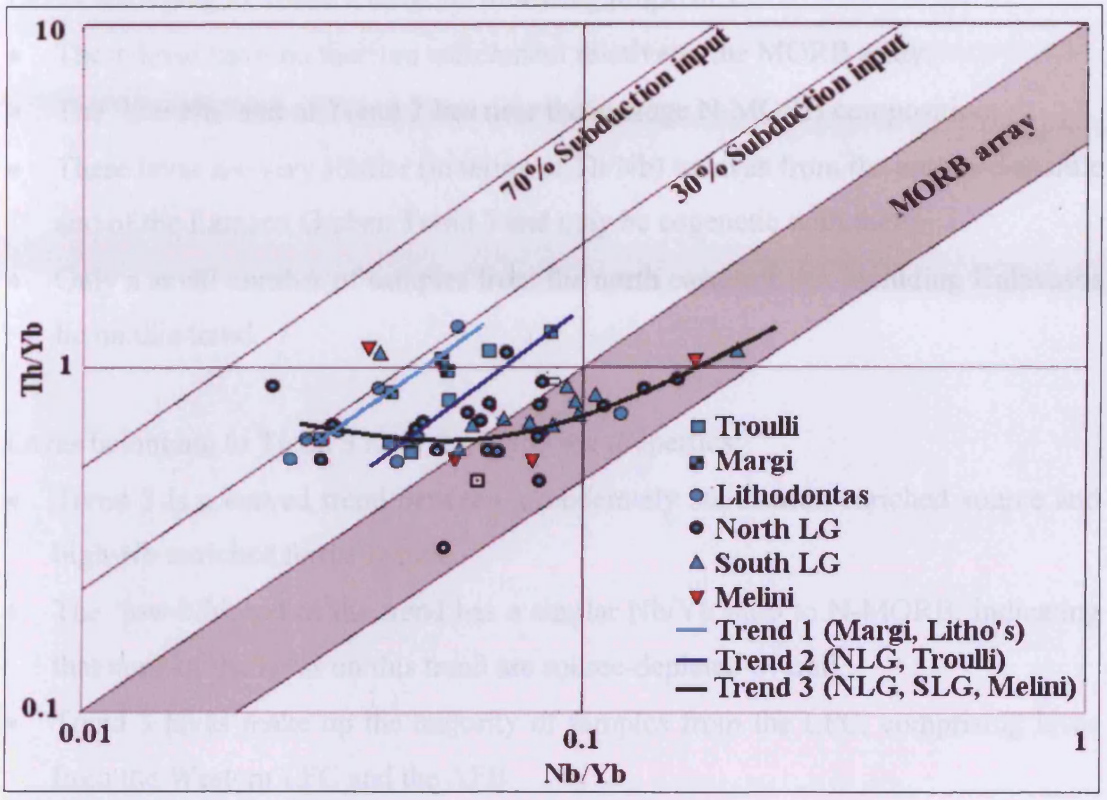

Limassol Forest Complex

Fig 3.4b-9 shows lavas from northern Troodos plotted on a logarithmic Th/Yb v Nb/Yb diagram with trends drawn by eye. Two of the trends are parallel, with differing levels of Th-enrichment and the third is a trend that connects Th-enriched subduction-derived and Nb-enriched mantle-derived sources. These trends are plotted as Trends 1, 2 and 3 on Fig 3.4b-9 respectively.

Lavas belonging to Trend 1 have the following properties:

- Lavas from Trend 1 have low % sz Th, at around 10%. This is comparable to Trend 2 lavas from south western Troodos.
- Unlike Trend 2 lavas from south western Troodos, Trend 1 lavas from the LFC have considerably higher Nb/Yb contents, indicating that they were not sourced from depleted mantle.

- Only a minority of samples lie on this trend – some from the southern and north eastern LFC.

Lavas belonging to Trend 2 have the following properties:

- These lavas have no thorium enrichment relative to the MORB array.
- The 'low-Nb' end of Trend 2 lies near the average N-MORB composition.
- These lavas are very similar (in terms of Th/Nb) to lavas from the enriched-mantle end of the Larnaca Graben Trend 3 and may be cogenetic with them.
- Only a small number of samples from the north eastern LFC, including Kalavasos lie on this trend.

Lavas belonging to Trend 3 have the following properties:

- Trend 3 is a curved trend between a moderately subduction-enriched source and high-Nb enriched fertile mantle.
- The 'low-Nb' end of the trend has a similar Nb/Yb ratio to N-MORB, indicating that none of the lavas on this trend are source-depleted overall.
- Trend 3 lavas make up the majority of samples from the LFC, comprising lavas from the Western LFC and the AFB.
- Trend 3 is similar to Trend 3 from northern Troodos although the maximum % sz Th is lower.

The similarity between Trends 1 and 2 lavas of the Limassol Forest Complex and Trends 2 and 3 of the Larnaca Graben may indicate that these lavas had a similar petrogenetic history. Most lavas from the Limassol Forest Complex had an enriched component containing high Nb added to their source. This entry of foreign mantle could have been linked to the change in tectonic layout as the Larnaca Graben opened up. This allowed the partial melting of fertile mantle, some of which was not subduction-enriched and mixing with the depleted, subduction-enriched mantle from which the rest of the Troodos Massif had been extracted. This mimics the model proposed by Leat et al. (2004) for non-subduction derived enrichment noted within the tips of the East Scotia Ridge.

Fig 3.4b-9 Plot of Th/Yb v Nb/Yb variation within lavas from the Limassol Forest Complex (LFC) Enrichment contours from Pearce et al. (1995). The bulk mantle composition is shown by the black and white nested square.

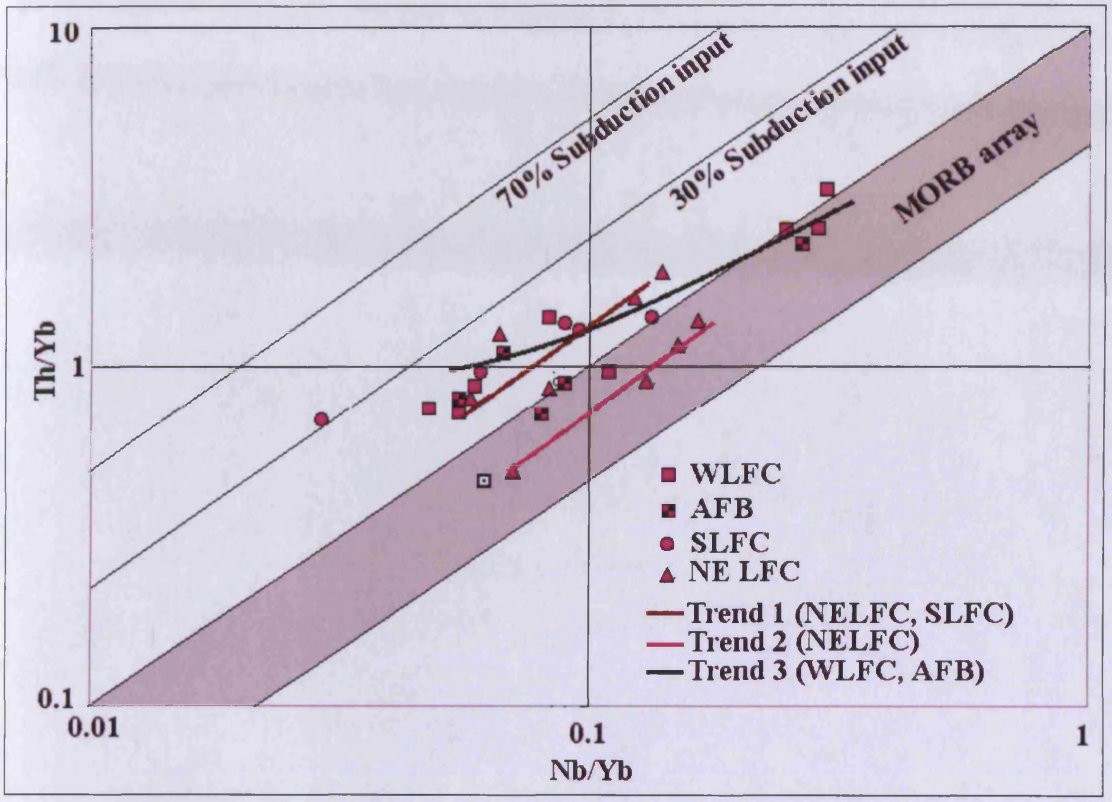

3.4c) Comparison of Troodos lavas Th/Nb properties with analogue regions

Comparison of four trends obtained from regional analysis of Troodos lavas with the analogue regions of Lau, Tonga, Marianas and the East Scotia Ridge allows direct comparisons to be made with areas for which the tectonic setting and magmagenesis are relatively well-known. The four trends obtained are:

- Trend 1: depleted source with about 30% of thorium being subduction-derived; obtained from the majority of northern Troodos lavas, from Margi in the Larnaca Graben and the northern Paphos Forest / Diarizos area in south western Troodos
- Trend 2: variably depleted source with about 15% of thorium being subduction-derived; obtained from some northern Troodos lavas (Akaki, Mitsero and Yialias) also Akamas and the southern Paphos Forest in south western Troodos, Troulli

and parts of the northern Larnaca Graben and also from parts of the southern and north eastern Limassol Forest Complex.

- Trend 3: This trend could either represent the addition of a constant amount of Th to variably depleted mantle or represent mixing of depleted, then 30% % sz Th source with enriched fertile mantle. Lavas on this trend are found in the majority of the Limassol Forest complex and some anomalous lavas from the Kambia and Akaki areas of northern Troodos.
- Trend 4: This trend could either represent the addition of a constant amount of Th to variably depleted mantle or mixing of 15% % sz Th, non-depleted source with enriched mantle. If the former, the addition of Th would be approximately half that of Trend 3 lavas. Lavas on this trend are found in the southern and central part of the Larnaca Graben and Kalavasos area of the Limassol Forest Complex.

Fig 3.4c-1 illustrates these trends, plotted together with compositions for analogue regions. From the Lau/Tonga area, of Central Lau Spreading Centre, Eastern Lau Spreading Centre, Valu Fa Ridge and Tonga Arc are plotted. As noted earlier, these regions lie progressively closer to the Tonga Arc, with increasing subduction component. The Central Lau Spreading Centre, which has almost MORB-like qualities, lies 200 km from the arc. The East Scotia Ridge and Mariana Arc/Basin system are also included. All three of these analogues vary between arc and MORB compositions. Lavas from the Lau basin vary form almost MORB-like in the CLSC, progressively becoming more subduction-enriched in the order: ELSC, Valu Fa Ridge and Tonga Arc. The East Scotia Ridge is a short ridge segment that lies above a strongly curved subduction zone. Therefore the lavas formed at the ends of the ESR are Arc-like, and those formed nearer the centre have very little subduction influence. The lavas used in this study are from segments 1, 9 and 10. Segment 1 is the northern tip of the ESR, situated close to the transform fault that delineates the end of the subduction / ridge system and segments 9 and 10 are situated at the southern tip, also in the proximity of a transform fault. These transform-proximal regions are structural analogues for the AFB and LFC. The Mariana Trough lies oblique to the Mariana Arc, with the northern section lying close to the arc, and the back-arc distance increases southward. Therefore, northern Mariana Basin lavas are arc-like and the

more southern lavas are more MORB-like. The Marian Basin lavas used in this study are from the regions lying between the MORB-like and Arc-like end-members/

Fig 3.4c-1. Comparison of trends obtained from Troodos lavas and analogue region distribution fields.

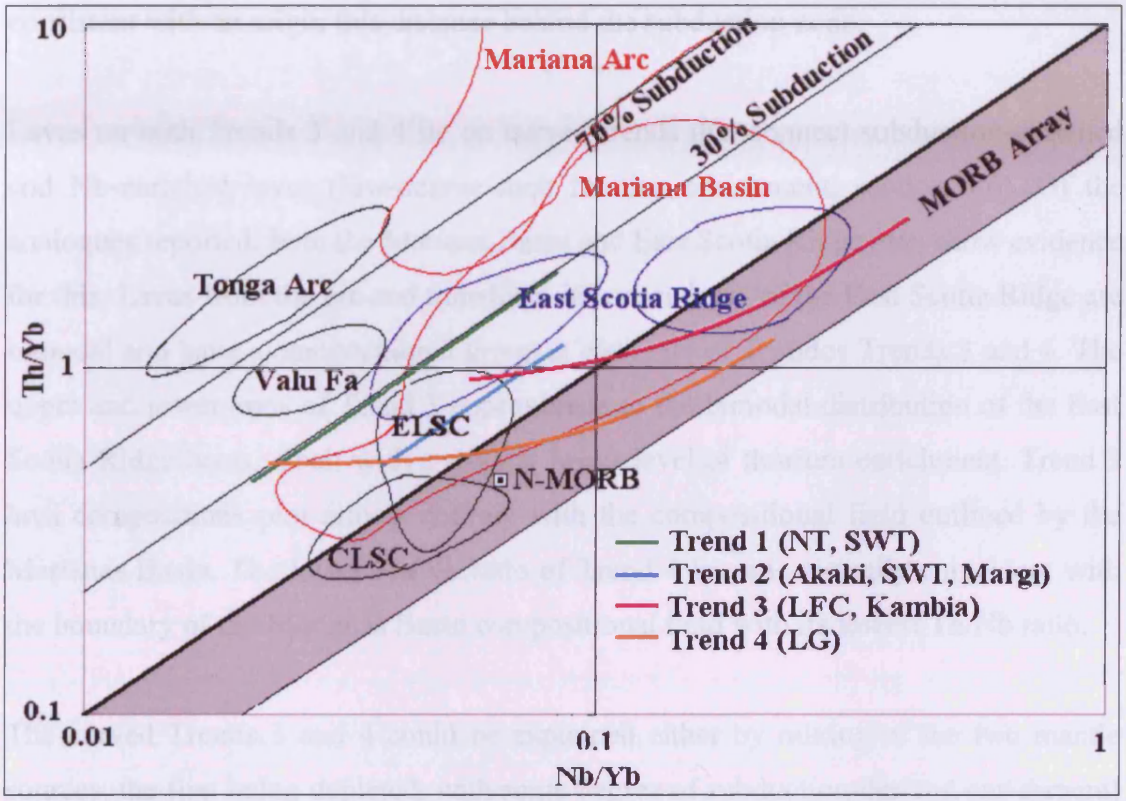

The degree of subduction-derived thorium enrichment of Trend 1 lavas is greater than that of the Eastern Lau Spreading Centre and depleted Mariana Basin lavas. Subduction-derived enrichment levels are lower than those of the Valu Fa Ridge and similar to those of the source-depleted East Scotia Ridge lavas. Their range of Nb/Yb ratios is similar to that of the combined range of Central and Eastern Lau Spreading Centre lavas. Some lavas with higher Nb/Yb ratios fall within the East Scotia Ridge compositional field.

The $\%_{Sz}$ Th of Trend 2 lavas is greater than that of the Central Lau Spreading Centre and less than that of the East Scotia Ridge. Their Th-enrichment levels are more similar to those of the Eastern Lau Spreading Centre. Their range of compositions lies

totally within the range of Mariana Basin lavas. Their range of Nb/Yb values is comparable to those of the Eastern Lau Spreading Centre and the East Scotia Ridge.

Thus, it is apparent that the Troodos lava types are typical for back-arc basin lavas located around 100 – 150 km behind the active arc (assuming normal dip of the subducted plate). Both their ranges of thorium enrichment and Nb/Yb ratio are consistent with an origin this distance behind the subduction zone.

Lavas on both Trends 3 and 4 lie on curved trends that connect subduction-enriched and Nb-enriched lavas (low-degree melt fraction enrichment, section 3.6). Of the analogues reported, both the Mariana Basin and East Scotia Ridge also show evidence for this. Lavas from the arc and transform-influenced tips of the East Scotia Ridge are bimodal and have a compositional group at each end of Troodos Trends 3 and 4. The upper and lower ends of Trend 3 approximate to the bimodal distribution of the East Scotia Ridge lavas, albeit with a slightly lower level of thorium enrichment. Trend 3 lava compositions plot almost entirely with the compositional field outlined by the Marianas Basin. The lower Nb/Yb ratio of Trend 4 lavas is virtually coincident with the boundary of the Marianas Basin compositional field with its lowest Th/Nb ratio.

The curved Trends 3 and 4 could be explained either by mixing of the two mantle sources, the first being depleted, with some degree of subduction-derived enrichment) and fertile mantle with enrichment by low-degree partial melts or the addition of a constant amount of subduction-derived Th to a variably depleted/enriched mantle.

3.5) Determining source depletion and subduction enrichment using rare earth element profiling

3.5a) Theory

Plotting and interpretation of rare earth element profiles

Chondrite-normalised REE profiles are affected in different ways by partial melting/fractional crystallisation and by source depletion/enrichment. Generally, pooled partial melting and fractional crystallisation affect the overall REE concentration. As with other incompatible elements, (section 3.3, Cr – Y relationships), low degrees of partial melting will result in lavas with high incompatible element contents. Higher degrees of partial melting (and source depletion) will produce lavas with low incompatible element contents. Fractional crystallisation serves to increase REE contents on lavas. The commonly used normalising factors are chondrite and MORB. Calculations and plots in this section will all be based on chondrite normalised values (Boynton, 1984).

Depletion and enrichment of the source affects the gradient of the profile. Lighter REE (LREE) are depleted preferentially relative to heavy REE (HREE) as they are the more incompatible. LREE, as a result of their lower ionic potential are also more readily transported in aqueous fluids. Slightly depleted lavas will have a REE profile that is flat at the HREE end and curving down towards the LREE. Strongly depleted lavas will have a profile that has high HREE but very low LREE. Lavas enriched by a subduction-derived component will have substantially elevated LREE contents. If depleted mantle has been enriched before melting, the resulting magmas may have a bowl-shaped REE profile.

Fig 3.5a-1 shows typical REE profiles from MORB, Japanese IAT and Troodos Basalts (Kay and Senechal, 1976). This figure shows how MORBs have a higher REE abundance than either IAT or Troodos basalts for a given degree of fractional crystallisation. This is a function of the higher degrees of partial and more depleted sources usually associated with arc magmatism. These lavas are also all slightly LREE-depleted.

The REE profile can be mathematically described using two ratios; Ce/Sm and Gd/Yb. Ce/Sm is the ratio of two LREE, that are affected by mantle depletion and subduction zone enrichment. The Gd/Yb ratio is predominantly affected by depletion. Where the Sm/Yb ratio is high relative to the Gd/Yb ratio, enrichment has taken place.

Fig. 3.5a-1 Sample REE profiles for MORB, Japanese Island Arc Tholeiite and basalt from the Troodos Massif (Kay and Senechal, 1976). Also shown are the positions of Ce, Sm, Gd and Yb, elements that have been chosen for REE ratio discrimination

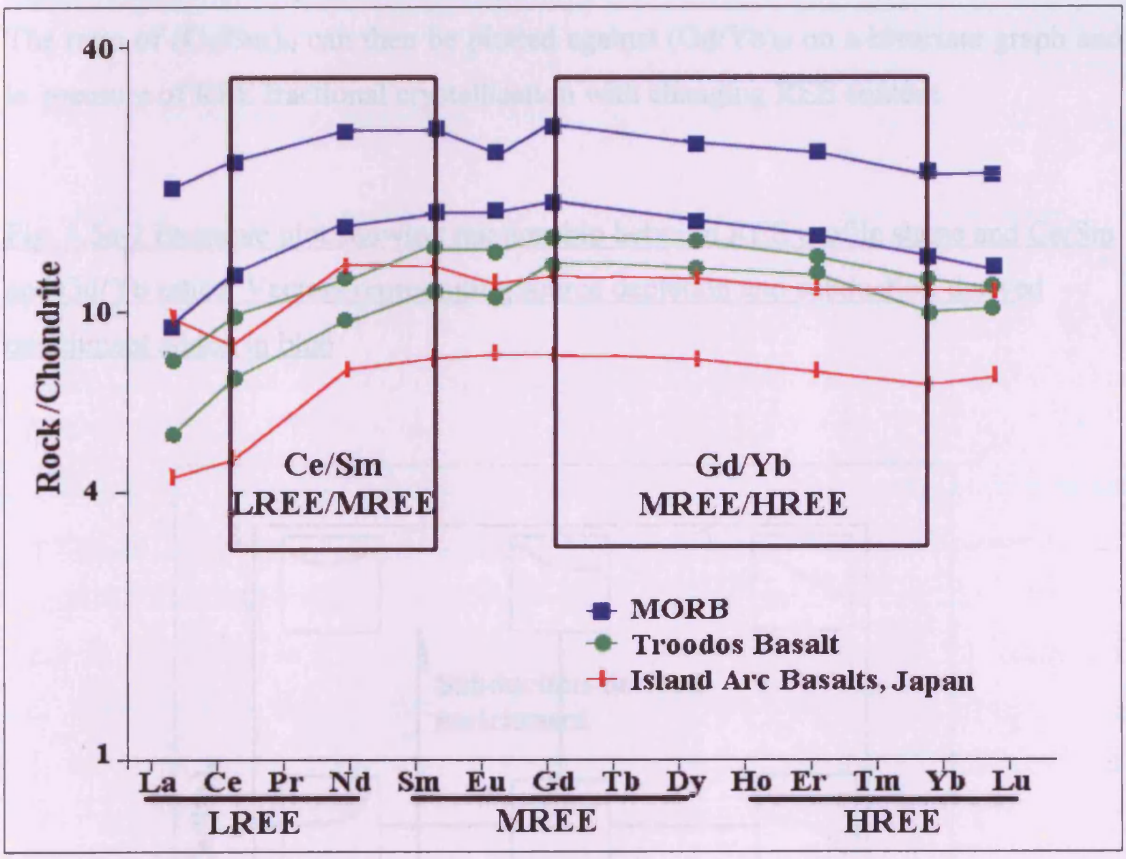

The effects of fractional crystallisation and partial melting can be greatly reduced, in the same way as with Th and Nb (section 3.4), by dividing values by Yb content. This allows the different profile shapes to be examined without the added complication of stacked, parallel curves that would be obtained from a suite of variably fractionated lavas form the same source. REE profile diagrams in this section will all be normalised by Yb (in addition to chondrite normalisation).

Humphries (1984) however showed that the REE, especially La, are not totally immobile, especially within heavily altered rocks. The fact that La is more mobile than Ce, combined with the fact that many of the lavas from the Troodos Massif are altered, means that Ce rather then La will be used to represent LREE in calculations.

REE Ratio diagrams

The shape of a REE profile can be expressed by the concentration of a light REE (Ce) divided by the concentration of a middle REE (Sm) and the concentration of a heavier MREE (Gd) divided by that of a heavy REE (Yb). Elements are chondrite-normalised. The ratio of $(Ce/Sm)_N$ can then be plotted against $(Gd/Yb)_N$ on a bivariate graph and is measure of REE fractional crystallisation with changing REE content.

Fig. 3.5a-2 Example plot showing relationship between REE profile shape and Ce/Sm and Gd/Yb ratios. Vectors representing source depletion and subduction-derived enrichment added in blue

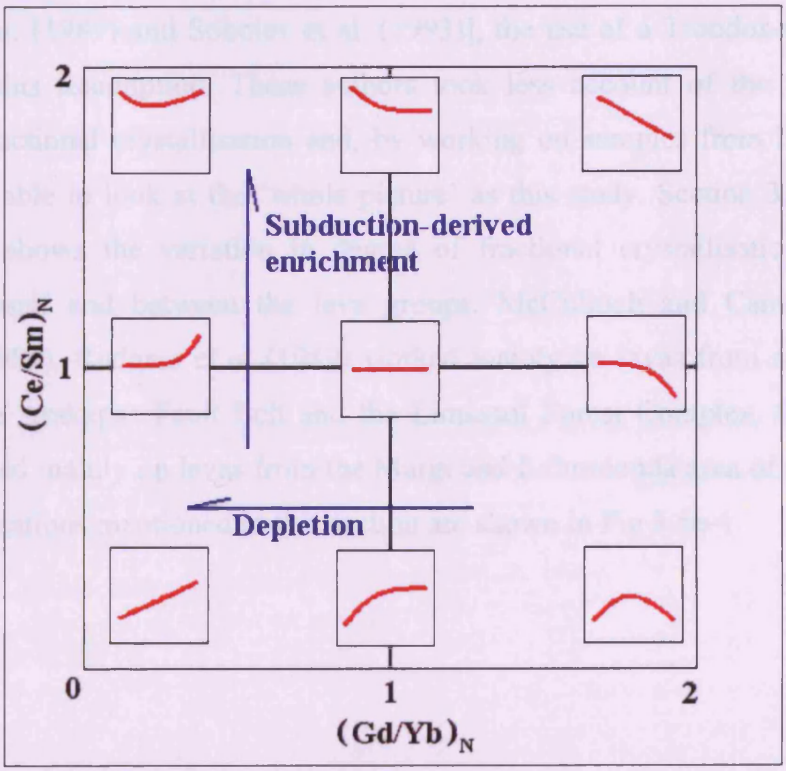

Where $(Ce/Sm)_N$ of a lava is less than 1, i.e. the lava is LREE-depleted, the source may be defined as depleted. The lower the $(Ce/Sm)_N$ ratio is, the more depleted the source is. Where $(Ce/Sm)_N$ is equal to 1, this can either be due to the addition of a subduction component to a depleted magma, an enriched mantle. Where $(Ce/Sm)_N$ is greater than 1, this is likely to indicate a mantle source which has undergone LREE addition by either a subduction component or a small melt fraction. Fig. 3.5a-2 illustrates the profiles that result in various $(Ce/Sm)_N$ and $(Gd/Yb)_N$ ratios are displayed in red. Unlike REE profile plots, this plot is linear and values have not been normalised by Yb. Also shown are vectors of depletion and subduction enrichment. Depletion reduces the Gd/Yb ratio and subduction-related/low melt fraction enrichment increases the Ce/Sm ratio.

3.5b) REE profiles of Troodos lava types

Variation between the Basal Group, Lower Pillow Lavas and Upper Pillow Lavas

Although much has been made of the differences in composition between the Basal Group (BG), Lower Pillow Lavas (LPL), and the Upper Pillow Lavas (UPL) in previous REE-based work [e.g. McCulloch and Cameron (1983), Cameron (1985), Rodgers et al. (1989) and Sobolev et al. (1993)], the use of a Troodos-wide data set contradicts this assumption. These authors took less account of the variations in degree of fractional crystallisation and, by working on samples from limited areas, were not as able to look at the 'whole picture' as this study. Section 3.3, especially Fig 3.3b-1, shows the variation in degree of fractional crystallisation across the Troodos Massif and between the lava groups. McCulloch and Cameron (1983), Cameron (1985), Rodgers et al (1989) worked mainly on lavas from south western Troodos, the Arakapas Fault Belt and the Limassol Forest Complex. Sobolev et al (1993) worked mainly on lavas from the Margi and Lithrodonda area of north eastern Troodos. Locations mentioned in this section are shown in Fig 3.5b-1.

Fig 3.5b-1 Locations of sites referred to in this section

Fig. 3.5b-2 shows the range of REE profiles obtained from the lavas of the Troodos Massif, divided into stratigraphical groups. The dataset is chondrite-normalised and further divided by Yb for reasons explained earlier. Profiles that have been normalised by chondrite and Yb will be referred to as Ch-Yb normalised. From this diagram, it is apparent that, although there is wide variation of REE profile within each lava group, there is very little difference between the lava groups.

Fig. 3.5b-2. Chondrite and Yb normalised REE profiles of the range of compositions exhibited by Basal Group (blue), Lower Pillow Lavas (green) and Upper Pillow Lavas (red)

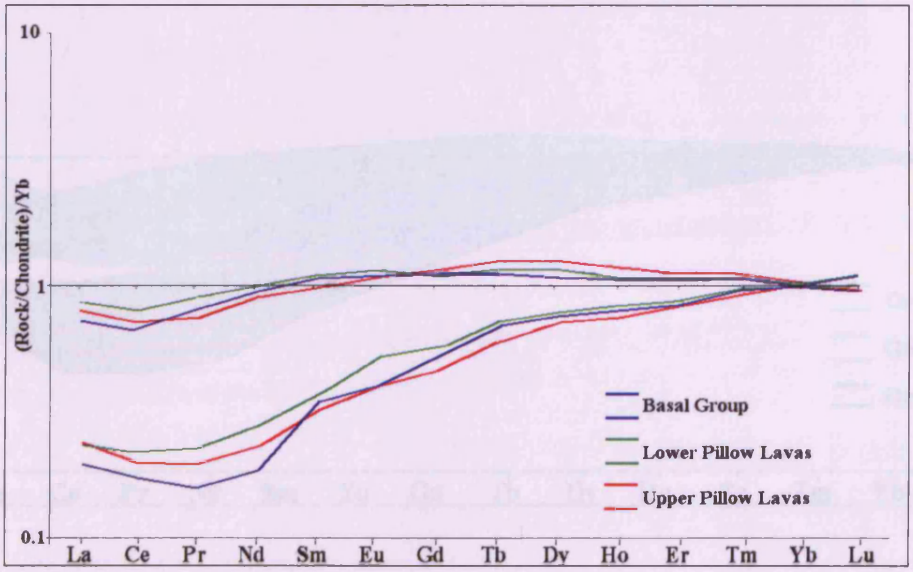

Division of lavas into three compositional groups based on chondrite and Yb normalised rare earth element profile

Although geochemical division of lava types by stratigraphic unit is not possible, the lavas can still be divided into three groups using geochemistry. These three groups correspond to those first reported within the UPL by McCulloch and Cameron (1983) and Cameron (1985). Fig. 3.5b-2 shows the relationship of these three chemical groups on a Ch-Yb normalised diagram. McCulloch and Cameron (1983) defined these groups as Group 1, with a slightly LREE-depleted profile; Group 2, with a slightly higher degree of depletion, but also a low amount of LREE enrichment from the subduction zone and Group 3 that are strongly depleted, providing evidence of variable and, at times, extensive supra-subduction enrichment.

Fig. 3.5b-2. Ch-Yb normalised REE profiles of range of compositions exhibited by Group 1 lavas from the Mitsero area (green), Group 2 lavas from the Paphos Forest (turquoise) and Group 3 lavas from the Limassol Forest Complex (blue). These lava groups correspond to the three subdivisions of the Upper Pillow Lavas reported by Cameron (1985)

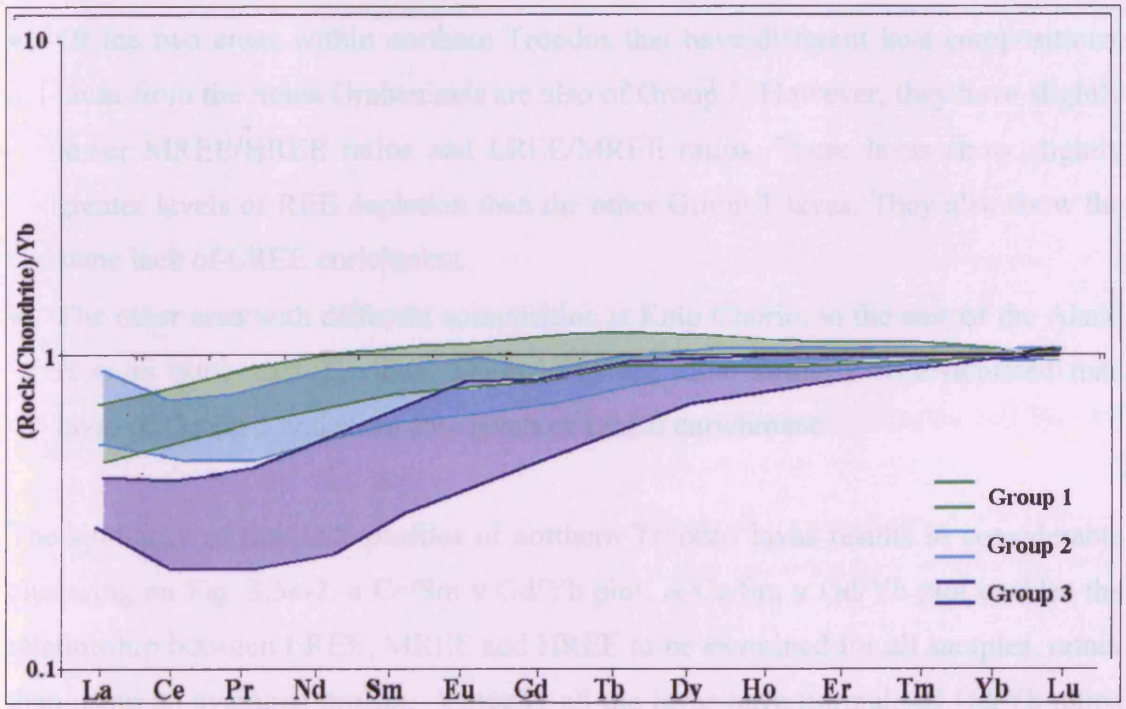

Group 1 lavas, shown in green, are slightly depleted and have Gd/Yb ratios greater than 0.8. They can be subdivided into Group 1A, with Gd/Yb ratios between 0.8 and 1 and Group 1B with Gd/Yb ratios greater than 1. Group 2 lavas are slightly more depleted however, with Gd/Yb ratios between 0.6 and 0.8 In addition, these lavas show a variable, but generally low degree of LREE enrichment. Group 3 lavas are strongly depleted, with Gd/Yb ratios lower than 0.6. They also show evidence of strong LREE enrichment with Ce/Sm ratios near or above 1, which is larger than the Gd/Yb ratio.

3.5c) REE profiles from selected regions of the Troodos Massif

Northern Troodos

Fig. 3.5c-1 is a Ch-Yb plot of REE profiles of lavas from northern Troodos. Within lavas from northern Troodos, the following are apparent:

- Lavas from most of northern Troodos are of Group 1 type. They have high Gd/Yb ratios and low LREE/MREE ratios. Their compositional range is narrow, indicating similar source compositions for most of the lavas.
- Of the two areas within northern Troodos that have different lava compositions, lavas from the Solea Graben axis are also of Group 1. However, they have slightly lower MREE/HREE ratios and LREE/MREE ratios. These lavas show slightly greater levels of REE depletion than the other Group 1 lavas. They also show the same lack of LREE enrichment.
- The other area with different composition is Kalo Chorio, to the east of the Akaki river in north east Troodos. These lavas are more strongly REE-depleted than lavas of Group 1 and show low levels of LREE enrichment.

The similarity of the REE profiles of northern Troodos lavas results in considerable clustering on Fig. 3.5c-2, a Ce/Sm v Gd/Yb plot. A Ce/Sm v Gd/Yb plot enables the relationship between LREE, MREE and HREE to be examined for all samples, rather than using an averaged profile. Virtually all the lavas have normalised Gd/Yb ratios between 0.8 and 1.2 and are of the Group 1 type.

Fig. 3.5c-1. Ch-Yb normalised REE profiles of lavas from northern Troodos (green), Solea Graben axis (Yellow) and anomalous lavas from Kalo Chorio are shown in orange.

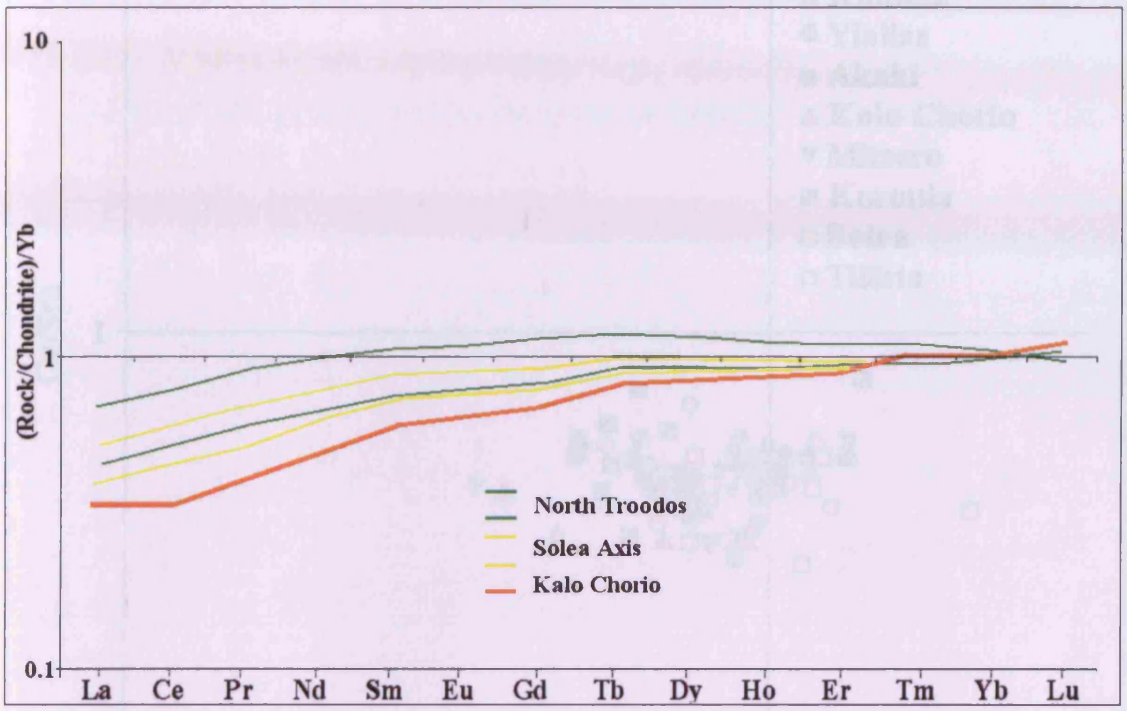

The majority of the northern Troodos lavas have Ce/Sm ratios between 0.5 and 0.8. This indicates that the Group 1 lavas are slightly LREE depleted relative to chondrite and that the levels of depletion are all similar. The range of Gd/Yb ratios within the few northern Troodos lavas that belong to Group 2 is narrower than the range seen within Group 1. The maximum LREE enrichment of Group 2 lavas produced Ce/Sm ratios of about 0.8. This shows the narrow spread of Ce/Sm ratios of lavas from the majority of the eastern portion of the section. Lavas from Analiondas and the Solea Graben are more diverse in their compositions, with higher Ce/Sm ratios but a similar range of Gd/Yb ratios. Lavas from Tilliria have a similar spread of Ce/Sm and Gd/Yb ratios as the north east of Troodos

Fig. 3.5c-2. Ce/Sm v Gd/Yb plot for northern Troodos lavas.

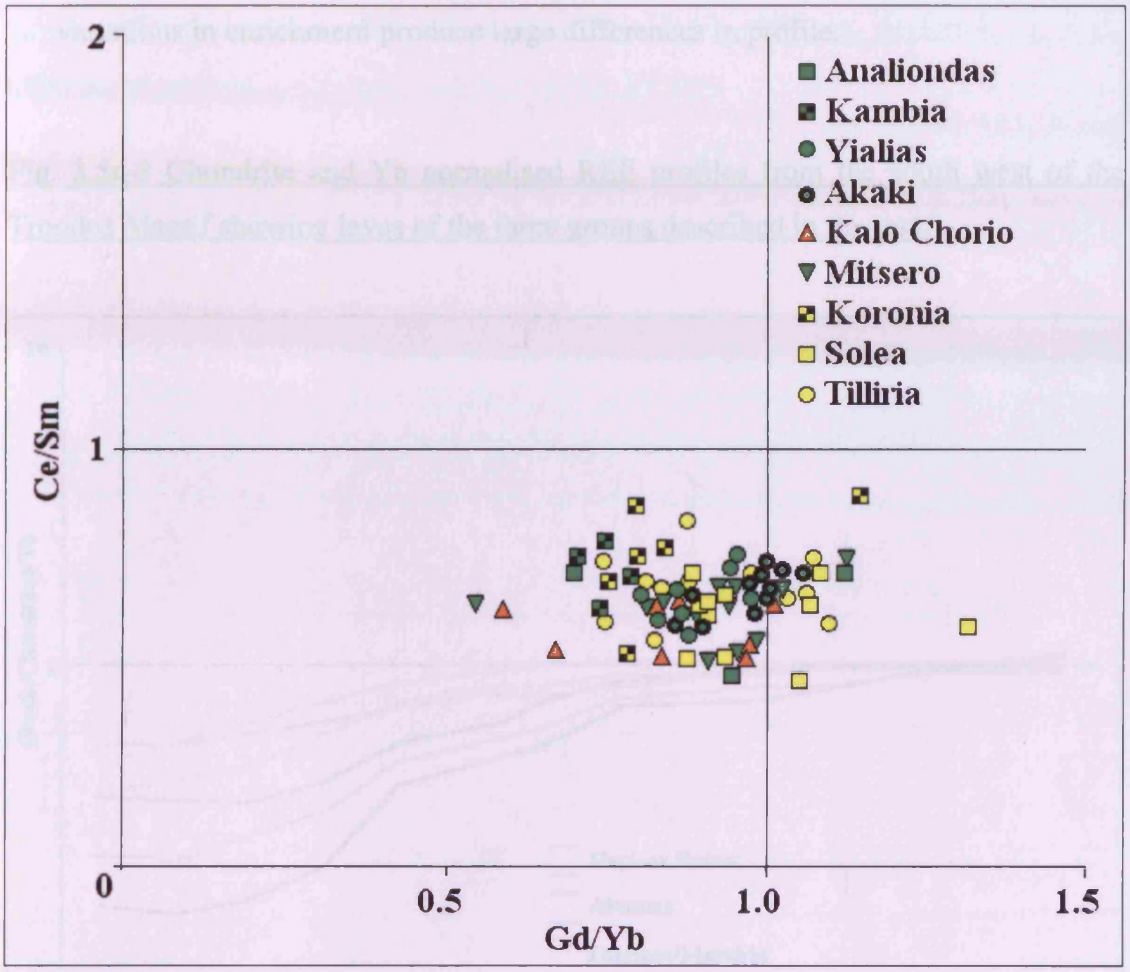

South West Troodos

Fig. 3.5c-3 is a Ch-Yb normalised plot of REE profiles of lavas from south western Troodos. Within lavas from south western Troodos, the following are apparent:

- Lavas from all three compositional groups are found in south western Troodos.
- Group 1 lavas with similar REE profiles to those from northern Troodos are found in the Diarizos and Mandria areas.
- Group 2 lavas, with a steeper positive REE gradient (therefore more depleted) profiles than Group 1 lavas, are found within the Paphos Forest area There is a continuous spectrum of lava compositions between Groups 2 and 3.
- Group 3 lavas, with low MREE/HREE ratios (strongly depleted) and highly variable LREE contents are found in the Akamas area and parts of the Paphos

Forest. Ce/Sm ratios are variable because the degree of LREE depletion prior to enrichment was high. Where the mantle source was strongly depleted, slight variations in enrichment produce large differences in profile.

Fig. 3.5c-3 Chondrite and Yb normalised REE profiles from the south west of the Troodos Massif showing lavas of the three groups described in the text.

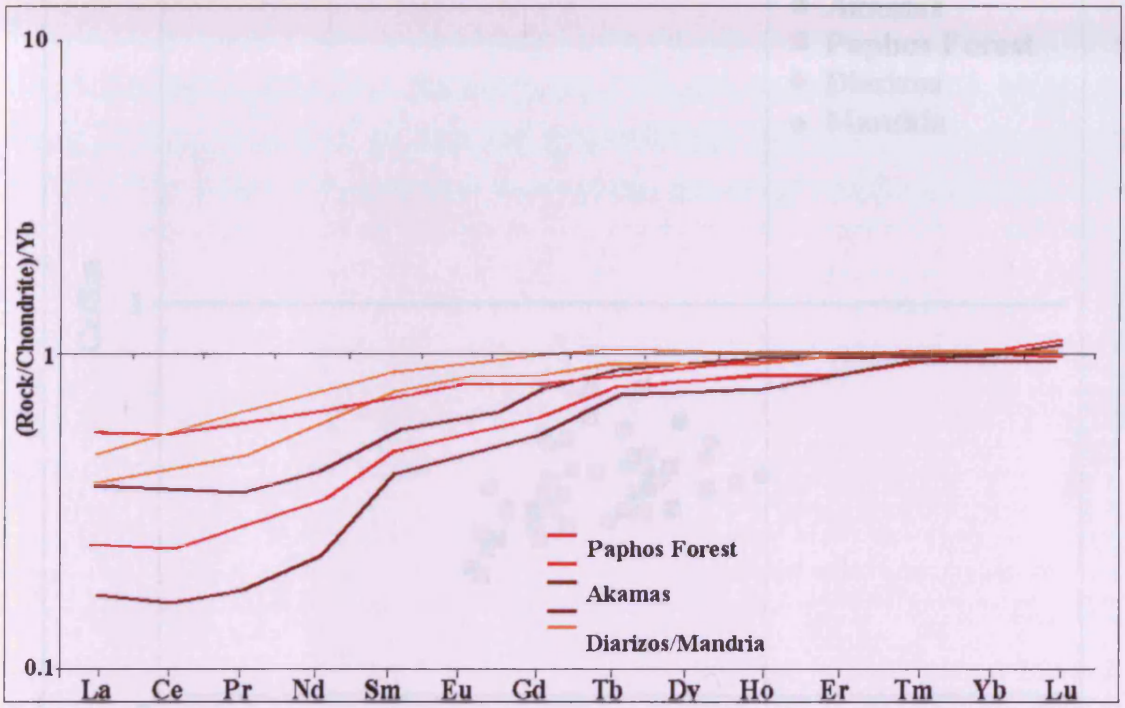

Fig. 3.5c-4 shows that lavas from the south west of the Troodos Massif form a continuous spectrum between Groups 1, 2 and 3. The Group 1 lavas from Diarizos and Mandria plot within very similar Ce/Sm v Gd/Yb space as Group 1 lavas from northern Troodos with Gd/Yb ratios between 0.7 and 0.9 and Ce/Sm ratios around 0.6. The Gd/Yb ratios of Group 2 lavas vary from 0.5 to 0.7, implying substantial but variable depletion of the mantle source. This is similar to the maximum Group 2 LREE enrichment measured in lavas from the Solea Graben. Ce/Sm ratios are variable. Group 3 lavas have Gd/Yb ratios between 0.5 and 0.6, with generally low Ce/Sm ratios indicating that although depleted, the mantle source of these lavas received little secondary enrichment.

Fig. 3.5c-4. Ce/Sm v Gd/Yb plot for south western Troodos lavas showing progression from Group 1 lavas (Diarizos) with Gd/Yb ratios greater than 0.8, to Group 3 lavas with Gd/Yb ratios less than 0.6. Although depletion is high, subduction-derived LREE enrichment is generally low.

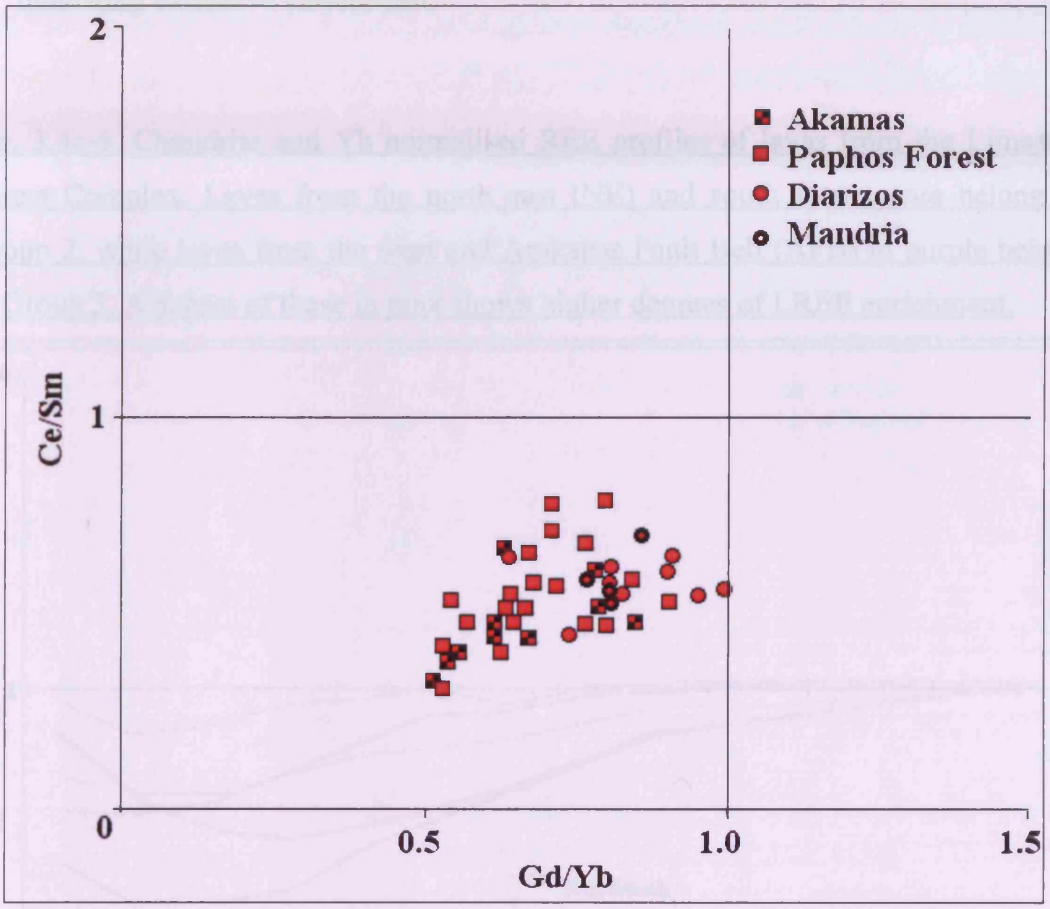

Limassol Forest Complex

Fig. 3.5c-5 is a Ch-Yb normalised plot of REE profiles of lavas from the Limassol Forest Complex (LFC). Within lavas from northern Troodos, the following are apparent:

- There appear to be no Group 1 lavas within this data set. Lavas are restricted to Groups 2 and 3.
- Lavas from the north east (including Kalavasos) and the south of the LFC are slightly depleted with fairly high MREE/HREE ratios and LREE/MREE ratios similar to their MREE/HREE (i.e. fairly straight profiles, albeit LREE depleted)

- Two types of Group 3 lavas are found elsewhere across the LFC. One type of Group 3 lavas has REE profiles very similar to those obtained from Akamas and the southern Larnaca Graben.
- The other type of Group 3 lavas, also found in the western LFC and AFB show lower are the most depleted of the Group 3 lavas and have high Ce/Sm ratios, indicating extensive enrichment.

Fig. 3.5c-5. Chondrite and Yb normalised REE profiles of lavas from the Limassol Forest Complex. Lavas from the north east (NE) and south in magenta belong to Group 2, while lavas from the west and Arakapas Fault Belt (AFB) in purple belong to Group 3. A subset of these in pink shows higher degrees of LREE enrichment.

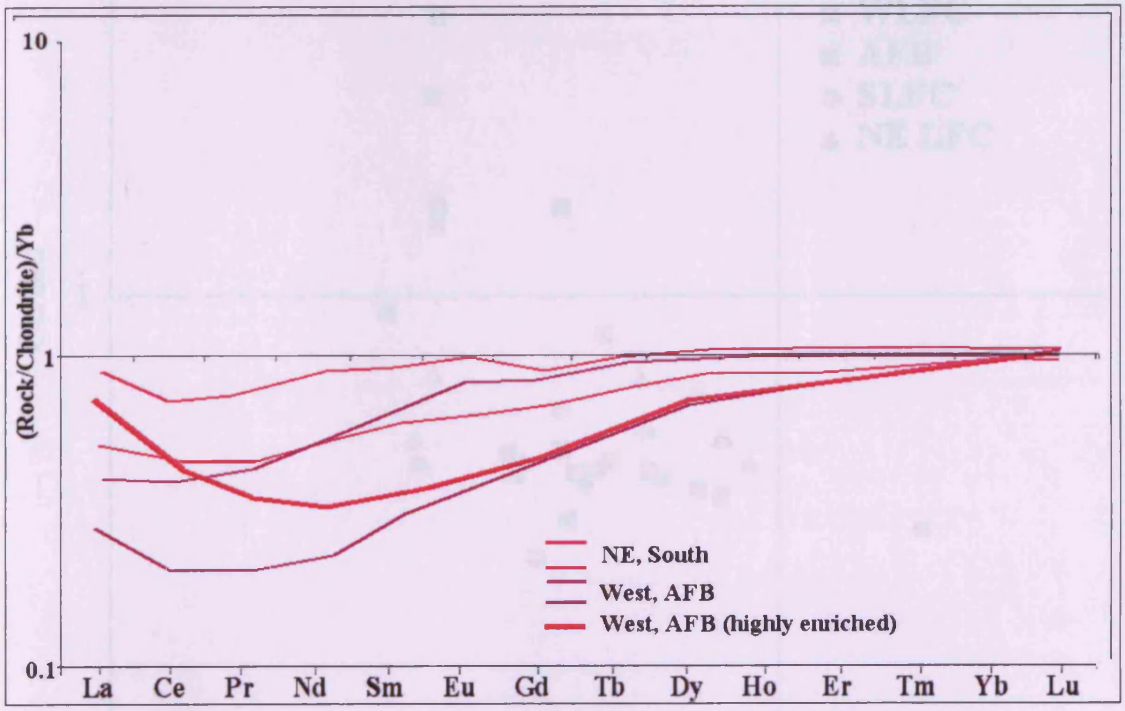

Lavas from the Limassol Forest Complex are widely scattered on a Ce/Sm v Gd/Yb plot (Fig. 3.5c-6). Group 2 lavas have a range of Gd/Yb ratios between 0.6 and 0.9, with Ce/Sm ratios between 0.5 and 1.2 (Fig. 3.5c-6). Group 3 lavas have Gd/Yb ratios around 0.5, with Ce/Sm ratios between 0.3 and 2.7. This plot also shows how the LREE enrichment of the Group 3 lavas is extremely variable, lending credence to the hypothesis that the LREE enriched component could be a low volume, low-degree partial melt. This, would variably enrich the mantle sources and so lead to extensive regional variability. Also, when considering a very depleted source, small absolute

additions of an enriched component will produce large effects on some element ratios. Lavas with Ce/Sm ratios much above 1 correspond to the highly enriched lavas from the WLFC and AFB shown on Fig 3.5c-5.

Fig. 3.5c-6 Ce/Sm v Gd/Yb plot for lavas from the Limassol Forest Complex showing variation between Groups 2 and 3 lavas in their maximum depletion level (minimum Ce/Sm and Gd/Yb value) and maximum enrichment level (maximum Ce/Sm value).

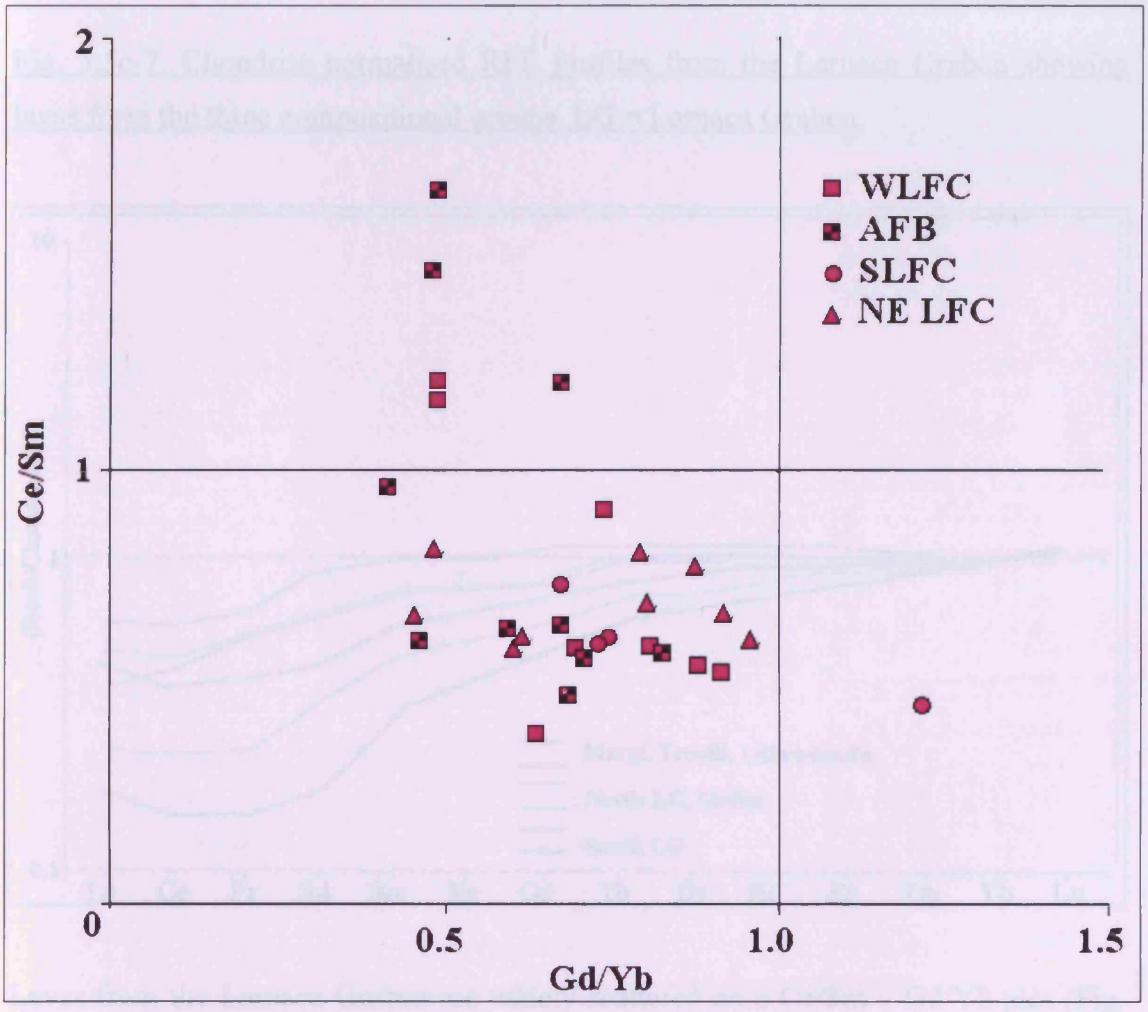

Larnaca Graben

Fig. 3.5c-7 is a Ch-Yb normalised plot of REE profiles of lavas from the Larnaca Graben. Within these lavas, the following are apparent:

- Lavas from the three compositional groups are found within the Larnaca Graben

- Group 1 lavas are found at Margi, Troulli and Lithrodonda in the far north of the Larnaca Graben
- Group 2 lavas are found within other parts of the northern Larnaca Graben and Melini. The northern Larnaca Graben also has some lavas that belong to Group 3.
- Group 3 lavas are found in parts of the northern Larnaca Graben and the Southern Larnaca Graben.
- There is a clear relationship between proximity to the AFB and depletion and subsequent enrichment of the mantle source.

Fig. 3.5c-7. Chondrite normalised REE profiles from the Larnaca Graben showing lavas form the three compositional groups. LG = Larnaca Graben.

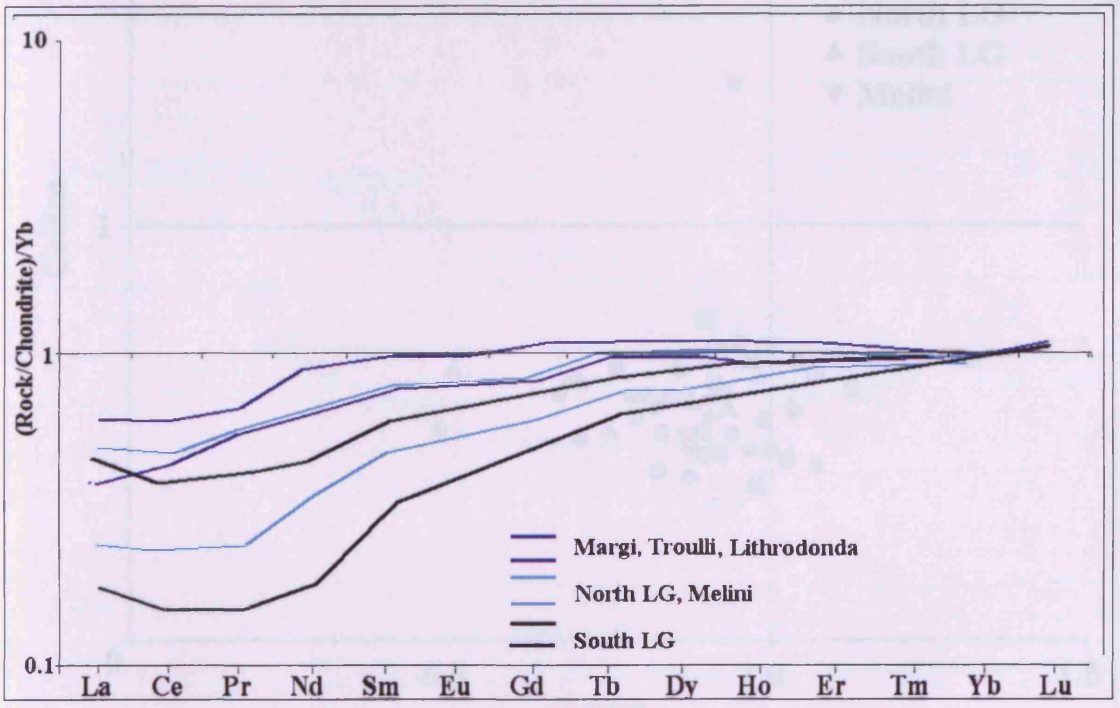

Lavas from the Larnaca Graben are widely scattered on a Ce/Sm v Gd/Yb plot (Fig. 3.5c-8). The Group 1 lavas have Gd/Yb ratios between 0.8 and 1.2, with Ce/Sm ratios between 0.4 and 0.8 (Fig. 3.5c-8). Group 2 lavas have Gd/Yb ratios between 0.7 and 0.8, with Ce/Sm ratios between 0.5 and 0.8. Group 3 lavas have Gd/Yb ratios between 0.5 and 0.7, with Ce/Sm ratios between 0.3 and 0.9. These lavas are L/MREE depleted, but the level of secondary LREE enrichment is low. The Ce/Sm ratio ranges are similar to those found in lavas from the south west of Troodos. Correlation

between distance from the AFB and lava group is less clear on this plot than Fig. 3.5c-7

Fig. 3.5c-8 Ce/Sm v Gd/Yb plot for lavas from the Larnaca Graben showing a lack of a clear correlation between Sm/Yb ratio and distance from the AFB. Lavas from both north and south of the graben share Ce/Sm v Gd/Yb space.

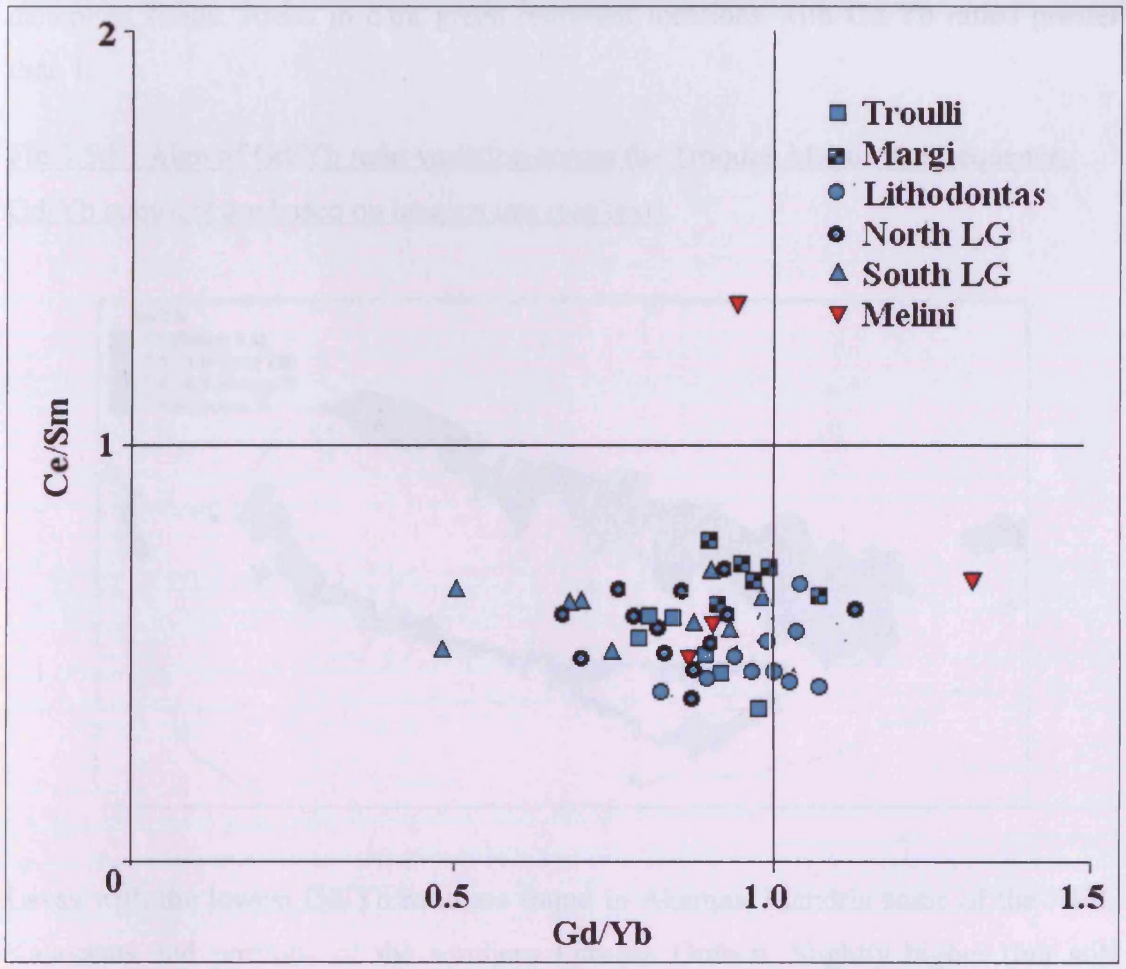

3.5d) REE variation across the Troodos Massif and comparison with analogue regions

Variations in the Gd/Yb ratio are mainly the result of the degree of depletion of the mantle source. A non-depleted source, such as a MORB source, will have a Gd/Yb ratio near or just greater than 1. This is because Gd is more incompatible than Yb and

little affected by subduction. A slightly depleted source will cause a magma to have a Gd/Yb ratio of just below 1 and a heavily depleted source will produce a magma with a low Gd/Yb ratio. Fig 3.5d-1 shows Gd/Yb ratio variations across the Troodos Massif. Blue areas show locations with Gd/Yb less than 0.6, indicating strongly L/MREE -depleted areas. Turquoise areas show locations where the Gd/Yb ratio is between 0.6 and 0.8, indicating moderate M/HREE depletion. Green areas show locations with Gd/Yb ratios between 0.8 and 1, indicating slight M/HREE depletion, which would result from slight LREE enrichment from subduction or low-degree melt generated fluids. Areas in dark green represent locations with Gd/Yb ratios greater than 1.

Fig 3.5d-1 Map of Gd/Yb ratio variation across the Troodos Massif lava sequence. Gd/Yb contours are based on lava groups (see text)

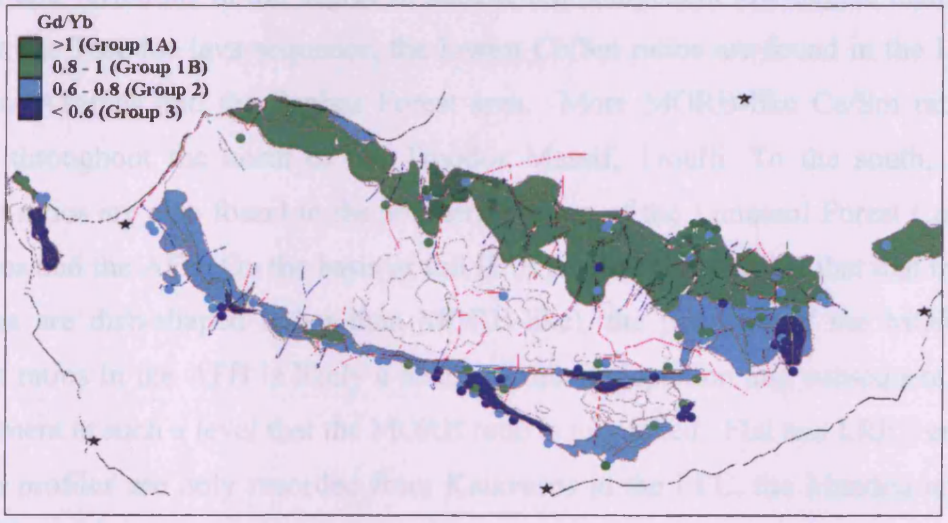

Lavas with the lowest Gd/Yb ratio are found in Akamas, Mandria some of the AFB, Kalavasos and portions of the southern Larnaca Graben. Slightly higher (but still M/HREE depleted), Gd/Yb ratios are found in lavas from the rest of the south west of the Troodos Massif (with the exception of Diarizos and a few samples from Kapilio that are highly enriched by subduction-derived fluids) and the southern Larnaca Graben. Lavas from the north west of Troodos, Troulli and the Basal Group in the Yialias and Lithrodonda areas have slightly depleted Gd/Yb ratios. The area between Peristerona Canyon and Margi and the Diarizos area have Gd/Yb ratios of about 1,

indicating a non-depleted source. The only lavas with Gd/Yb ratios greater than 1 are found near Koronia, Xyliatos and some from Akaki and Kambia.

Fig. 3.5d-2 is a map of variations in the Ce/Sm ratio within the lavas of the Troodos Massif. Blue areas are locations with Ce/Sm less than 0.5, indicating strongly LREE - depleted areas. Green areas are locations where the Ce/Sm ratio is between 0.5 and 0.8, indicating slightly LREE-depleted (MORB-like) profiles. Yellow areas are locations with Ce/Sm ratios between 0.8 and 1.1, indicating slight LREE enrichment from subduction or low-degree melt generated fluids added to depleted source magma. Areas in orange and red denote Ce/Sm ratios above 1.1, indicating strong LREE enrichment.

Variations of the Ce/Sm ratio in basalts result from variations in the depletion of the source and variations in the degree of subduction component low-degree melt, input. Within the Troodos lava sequence, the lowest Ce/Sm ratios are found in the Larnaca Graben, Akamas and the Paphos Forest area. More MORB-like Ce/Sm ratios are found throughout the north of the Troodos Massif, Troulli. To the south, similar Ce/Sm ratios are also found in the southern portion of the Limassol Forest Complex, Diarizos and the AFB. On the basis of full REE profiles (i.e. the fact that that the REE patterns are dish-shaped rather than MORB-like), the presence of the MORB-like Ce/Sm ratios in the AFB is likely a result of source depletion and subsequent LREE enrichment at such a level that the MORB ratio is mimicked. Flat and LREE enriched Ce/Sm profiles are only recorded from Kalavasos in the LFC, the Mandria area and parts of the AFB.

Fig. 3.5d-2 Map of normalised Ce/Sm ratio variation across the Troodos Massif lava sequence.

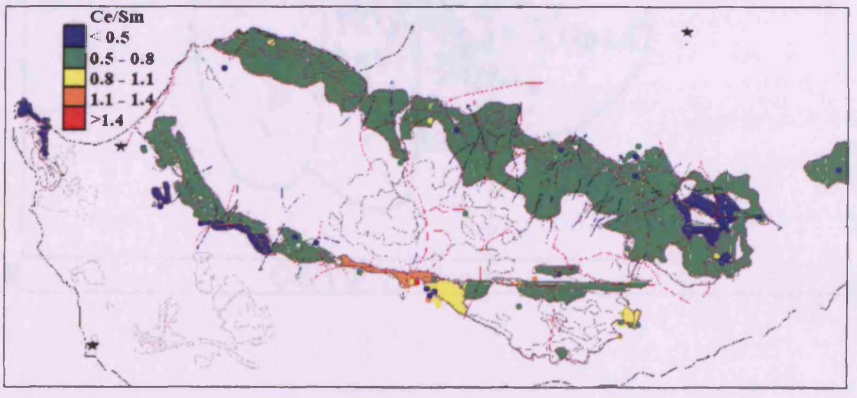

Fig 3.5d-4 displays Ce/Sm b Gd/Yb data for all Troodos lavas overlaid with the boundaries of Groups 1A and B, 2 and 3. Group 1 lavas are found from Margi to Tilliria in the north of Troodos with a few small isolated areas of Group 2 lava and at Diarizos and Mandria in the south west. Group 2 lavas are found sporadically in the north of the Troodos Massif, the north of Larnaca Graben except Margi, Troulli, and the Paphos Forest area in the south west of the Troodos Massif. They also are found in parts of the Limassol Forest Complex, especially to the south. Group 3 (Boninitic) lavas are found extensively in the south of the Larnaca Graben, the AFB and in much of the LFC. They are found sporadically in the Paphos Forest area.

Fig 3.5d-4. Ce/Sm v Gd/Yb plot of Troodos lavas coloured by location within the Troodos Massif Green points represent northern Troodos, red points indicate samples from south western Troodos, blue points are or samples from the Larnaca Graben and purple points indicate samples from the Limassol Forest Complex

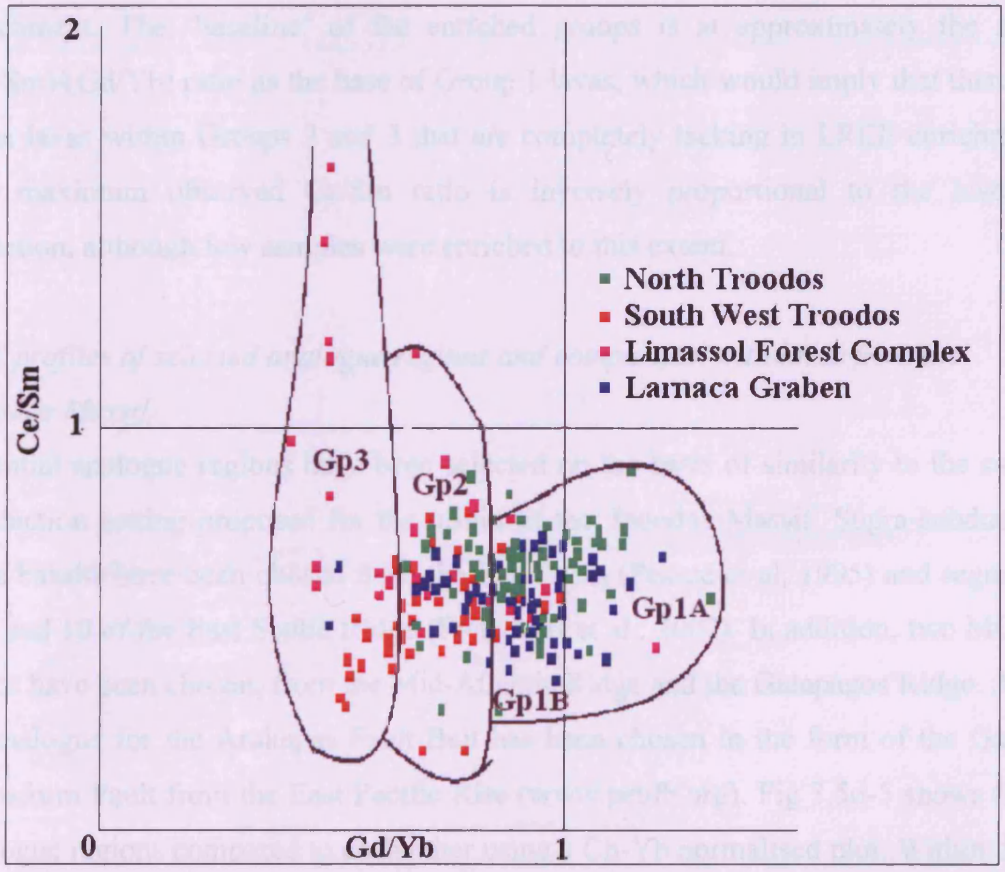

Comparing the general distribution of Ce/Sm v Gd/Yb values for each region reveals that the clear divide between them is in source depletion (Gd/Yb ratio). Northern Troodos lavas (green) exhibit very little overlap with the more depleted south west Troodos and Limassol Forest Complex lavas (purple and red). This variation in the level of source depletion is likely a function of the proximity to the transform fault. Although there are Group 1 lavas present in the south western region, the low overall abundances of REE, especially LREE, indicate depleted sources. Thus, these lavas are lacking subsequent enrichment in LREE for some reason. In the south west of the Troodos Massif, faulting breaks the lava outcrop, and the separation from the northern outcrop prevents complete comparison between distance and depletion. Lavas from the Larnaca Graben (blue) and south western Troodos (red) have a wide spread of source composition, a function of increasing distance from the transform fault. This gradual change can be mapped because there is a continuous outcrop of lavas.

Throughout the Troodos Massif, the Group 1 lavas have a narrow range of compositions (Fig 3.5d-4): Groups 2 and 3 both exhibit wider ranges of LREE enrichment. The 'baseline' of the enriched groups is at approximately the same (Ce/Sm)/(Gd/Yb) ratio as the base of Group 1 lavas, which would imply that there are some lavas within Groups 2 and 3 that are completely lacking in LREE enrichment. The maximum observed Ce/Sm ratio is inversely proportional to the level of depletion, although few samples were enriched to this extent.

REE profiles of selected analogue regions and comparison with lavas from the Troodos Massif.

Potential analogue regions have been selected on the basis of similarity to the supra-subduction setting proposed for the origin of the Troodos Massif. Supra-subduction zone basalts have been chosen from the Lau Basin (Pearce et al, 1995) and segments 1, 9 and 10 of the East Scotia Ridge (Fretzdorff et al., 2002). In addition, two MORB suites have been chosen, from the Mid-Atlantic Ridge and the Galapagos Ridge. Also, an analogue for the Arakapas Fault Belt has been chosen in the form of the Garrett Transform Fault from the East Pacific Rise (www.petdb.org). Fig 3.5d-5 shows these analogue regions compared to each other using a Ch-Yb normalised plot. Within these analogue regions, the following is apparent:

- Lavas from the Mid-Atlantic Ridge and the Galapagos Ridge, both MORBs have very similar REE profiles. The REE profiles of these two regions fall within the somewhat wider compositional range of lavas from the Lau Basin.
- Lavas from the Lau basin have a wide range of levels of depletion and enrichment, somewhat wider than that of MORBs.
- Lavas from the East Scotia Ridge, although they provide evidence of extensive LREE enrichment, show no evidence of depletion as Gd/Yb values are greater than 1. This is unlike lavas from the Troodos Massif, so this analogue, which in other sections (e.g. Section 3.4) mirrors the Troodos Massif well, will be discarded as it does not reflect the generally depleted nature of Troodos lavas.
- Lavas from the Garrett Transform have a bimodal distribution, one set of lavas having MORB characteristics and the other set being strongly depleted with no LREE enrichment.

Fig 3.5d-5. Chondrite normalised REE profiles of the chosen analogue areas. Garrett Transform, Mid-Atlantic Ridge, Lau Basin, East Scotia Ridge and Galapagos Ridge. All data from www.petdb.org

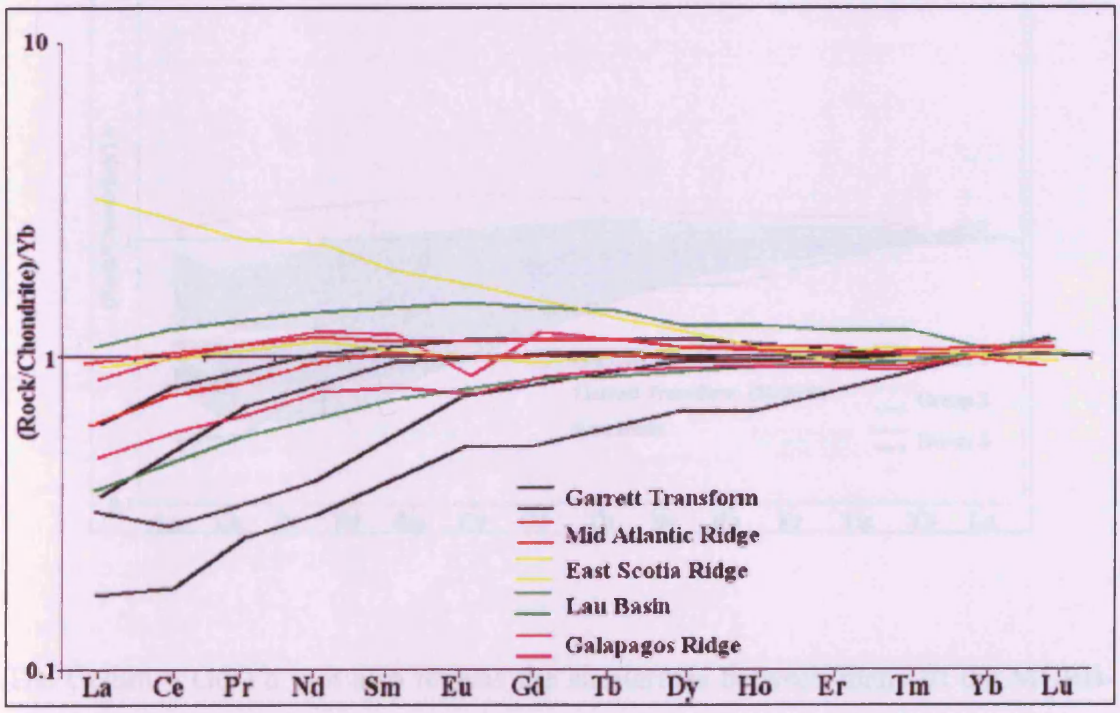

Fig 3.5d-6 is a Ch-Yb normalised plot of the analogue regions of Lau Basin and the Garrett Transform (both MORBs and depleted lavas) overlain with the compositional ranges of Groups 1,2 and 3 lavas from the Troodos Massif. For clarity, overlapping MORB lava types shown on Fig 3.5d-5 are removed. Within these lavas, the following is apparent:

- Troodos Group 1 lavas lie totally within the compositional field of Lau Basin lavas and approximately within the same boundaries as the MORB-like Garrett Transform Lavas.
- Troodos Group 3 lavas have a similar level of depletion to the depleted Garrett Transform Lavas. The Garrett Transform lavas do not show significant LREE enrichment. This may not be surprising considering that Troodos Group 3 lavas are only found in the proximity to the AFB
- There are no direct analogues for Troodos Group 2 lavas; however, the compositional range is only slightly more depleted than that of the Lau Basin.

Fig 3.5d-6. Comparison of Troodos lava Groups 1,2 and 3 with analogue regions of the Garrett Transform and the Lau Basin.

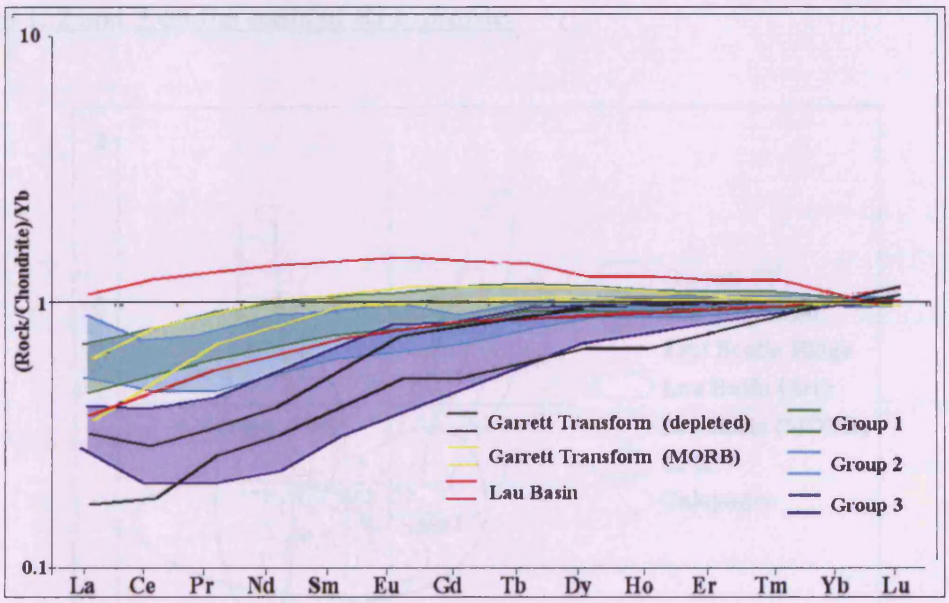

The Ce/Sm v Gd/Yb plot also reveals the similarities between many of the MORB-like analogue regions. Fig 3.5d-7 shows the selected analogue areas of Garrett

Transform Fault, Mariana Basin, East Scotia Ridge, Lau Basin (arc and MORB), East Pacific Rise and the Galapagos Ridge. This plot shows how lavas from the Mariana Basin, East Scotia Ridge, Lau (Arc-like) and the East Pacific Rise all have similar ranges in Ce/Sm v Gd/Yb space.

In relation to Troodos lavas, the least enriched lavas from all the MORB-like analogue regions lie within the field occupied by Group 1 lavas. The compositional range of the Group 1 lavas also virtually matched the MORB-like Lau Basin lavas. The nearest analogue on this plot for the Group 2 lavas is the Galapagos Ridge. However, these lavas are not quite as depleted as Troodos Group 2 lavas, although the levels of LREE enrichment are similar. There are no direct analogues for Group 3 lavas using the Ce/Sm v Gd/Yb plot. However, the range of Gd/Yb ratios seen within lavas from the Garrett Transform is the best match for the range of Gd/Yb ratios found within lavas from the Troodos Massif.

Fig 3.5d-7. Ce/Sm v Gd/Yb plot for lavas from selected analogue areas of Garrett Transform Fault, Mariana Basin, East Scotia Ridge, Lau Basin (arc and MORB), East Pacific Rise and the Galapagos Ridge. Troodos lavas are divided into enrichment Groups 1, 2 and 3 on the basis of REE profile.

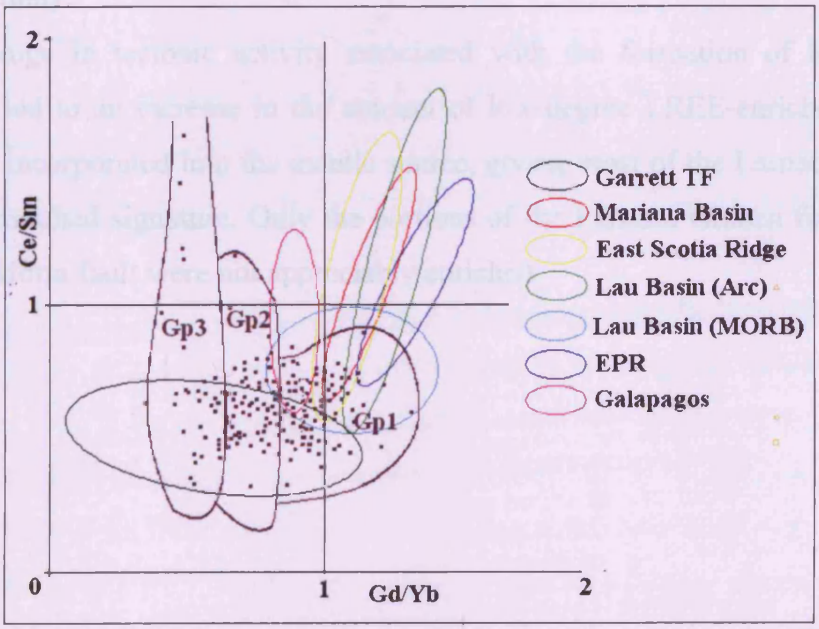

- Troodos lavas are variably depleted; the level of LREE depletion is generally dependent on the distance from the transform fault.
- The depletion level of transform-distal lavas is similar to that observed in the Lau basin.
- The most depleted lavas, from near the transform, are far more depleted than any lavas recorded in the analogue regions except the Garrett Transform
- LREE enrichment levels that give a Ce/Sm ratio of around 2 may be seen in the Mariana Trough, Lau Basin and the East Scotia Ridge as well as some of the Troodos lavas, confirming that substantial LREE enrichment is likely in a supra-subduction environment.
- LREE enrichment is highly localised, but restricted to the most depleted lavas. Many of the strongly depleted lavas have not undergone subsequent enrichment. This restriction of LREE enrichment signatures to the most depleted lavas may be partially a dilution effect. A small LREE-rich input will not alter the chemistry of a relatively incompatible-element rich mantle, but will markedly alter the chemistry of strongly depleted mantle.
- The localised nature of the LREE enrichment could indicate the presence of low volume, low-degree partial melts. (this is also indicated by Th/Nb fingerprinting)
- Any low-degree partial melts are concentrated in the area around the transform fault initially.
- The change in tectonic activity associated with the formation of the Larnaca Graben led to an increase in the amount of low-degree LREE-enriched melts to become incorporated into the mantle source, giving most of the Larnaca Graben a LREE-enriched signature. Only the portions of the Larnaca Graben furthest from the transform fault were not appreciably enriched.

3.6) Determining mantle, lithospheric and subduction-derived source components from extended incompatible element profiles (Spider diagrams)

3.6a) Theory

Multi-element spider diagrams have been used for some time to depict relative concentrations of incompatible elements. Over time, the concept has been expanded and refined. The diagrams are often plotted normalised to N-MORB, although primitive mantle and chondrite are also in common use. The profile can then easily be broken down into its components (Pearce et al., 1983). The components that will be discussed in this section are mantle-derived, low-degree partial melts and subduction-derived fluids and hydrous melts.

Conservative vs. non-conservative behaviour

The terms of 'conservative' or 'non-conservative' behaviour during subduction are based on mobility of the selected element during the subduction and magmatism process (Pearce and Peate, 1995). Conservative elements are those where there is no detectable slab input into the volcanic products. Non-conservative elements are those where there is a detectable slab input into the volcanic products. Generally, LIL elements are non-conservative and HFS elements are conservative in a supra-subduction setting. This gives a characteristic LILE enrichment when compared to HFS elements. A simple measure of non-conservative behaviour can be obtained from geochemical patterns by taking the abundance of the element under scrutiny above a baseline extrapolated from the abundances of the conservative elements. This value, expressed as a percentage of the total concentration gives the percentage of subduction component in the lava. For most volcanic arc magmas, non-conservative elements can be divided as follows (Pearce and Peate, 1995). Highly non-conservative elements are those where the subduction component comprises at least 80% of the content. These elements are Rb, Ba K, Pb, Th, U and Sr. Non-conservative elements are those where the subduction component comprises 40 - 80% of the content. These elements are P and LREE. Slightly non-conservative elements are those where the subduction component comprises less than 40% of the content. These elements are

MREE and Na. Conservative elements (where any subduction enrichment is below detection limit) are Zr, Hf, Ti, HREE, Y and Sc.

Several types of component can be defined.

- *Mantle Component* - The mantle component is the component of the magma derived purely from partial melting of the mantle asthenosphere. The shape of the mantle component curve reflects the degree of source depletion. A MORB mantle source will have a flat profile. The profile of a depleted lava will dip to the left with very low values of the most incompatible elements.

- *Low-degree partial melt component* - This component is strongly enriched in highly incompatible elements. This strong enrichment in also these elements, but lack of enrichment in less incompatible elements is indicative of very low degrees of partial melting of a fertile or enriched mantle source. Such a source could be depleted mantle that has reacted with infiltrating melts

- *Subduction Component* - Of the subduction-mobile elements, some are mobile only under deep-subduction processes, and some are mobile under all subduction processes. Elements mobile under shallow subduction processes are typically mobile under weathering also. Therefore these elements, such as Rb, Ba, U, Pb and Sr, cannot be used where the rocks are altered. Some elements, such as Th are immobile at low temperatures, so therefore are only mobile in the deeper parts of the subduction zone. The latter elements are also weathering-immobile. The subduction input of thorium and LREE can be determined empirically from an extended incompatible element suite.

3.6b) Variations in extended incompatible element profiles across the Troodos Massif

Incompatible element profiles have been collated from a large number of samples as explained in Section 2.1. For the purposes of this study, the Troodos Massif lava

outcrop is divided into four regions (northern Troodos, south western Troodos, the Larnaca Graben and the Limassol Forest Complex). These regions are subdivided. A total of 23 subdivisions within the Troodos lavas were chosen. The incompatible, immobile element profiles within each subdivision were then averaged. The average profiles for each division were then compared with their neighbours to produce regional profiles. The regions and subdivisions are shown in Fig. 3.6b-1.

Fig 3.6b-1. Locations mentioned within text and constituent regions of the Troodos Massif. AFB = Arakapas Fault Belt, W/S/NE LFC = Western / Southern / North eastern Limassol Forest Complex, Lith'da = Lithrodonda, Ana's = Analiondas, KC = Kalo Chorio.

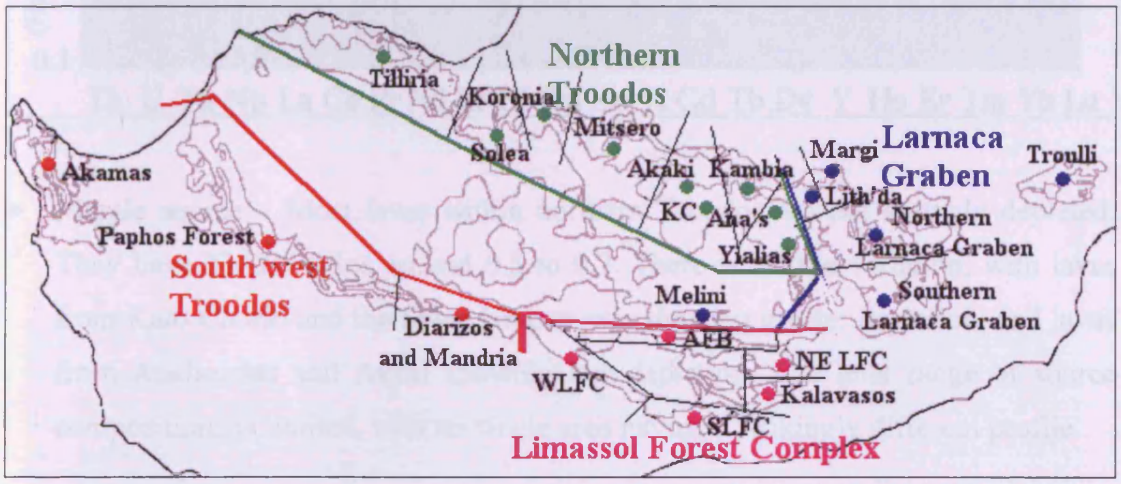

Northern Troodos

Fig 3.6b-2 is a multi-element spider diagram that shows a representative profile of lavas from the Akaki area in northern Troodos. However, most profiles obtained from northern Troodos are similar with only minor differences in depletion and subsequent enrichment. The profile has been normalised to N-MORB (Sun and McDonough, 1989) and Yb to reduce the effects of variations in partial melting and fractionation. The following features are apparent within northern Troodos lavas:

Fig 3.6b-2 MORB and Yb normalised incompatible element spider diagram showing source components for for an average lava from northern Troodos. Blue represents asthenospheric mantle component and yellow represents the deep subduction component.

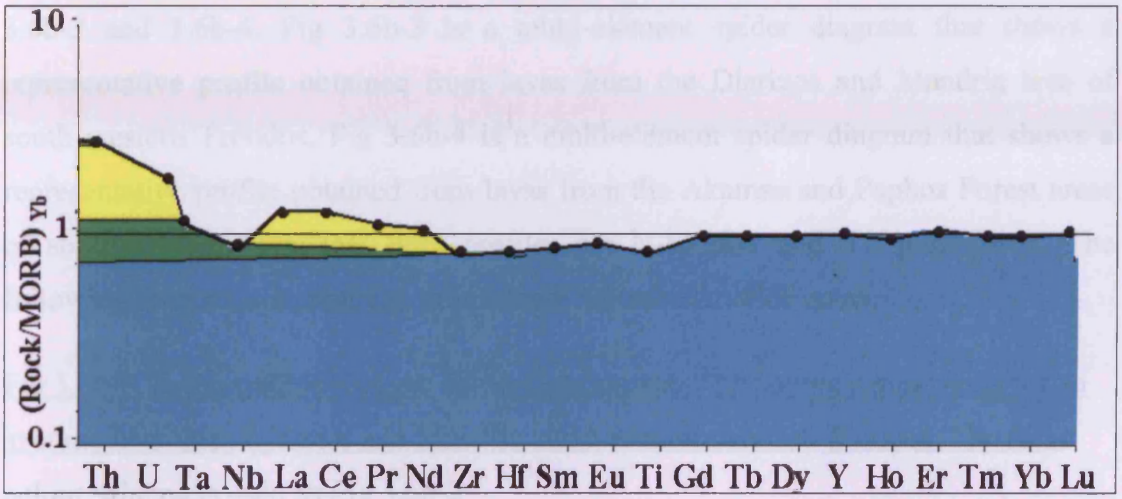

- Mantle source – Most lavas within northern Troodos are not strongly depleted. They have Th/Yb ratios around 0.5 to 0.7. There is a little variation, with lavas from Kalo Chorio and the Solea Graben axis showing greater depletion, and lavas from Analiondas and Akaki showing less depletion. The total range of source compositions is limited, with no single area having a strikingly different profile.

- Low-degree partial melt input – Levels of this enriched component are generally very low throughout northern Troodos. The lowest levels of low-degree partial melt input are found at Analiondas, Kambia, Tilliria and Akaki. Higher levels are found at Kalo Chorio and in the Solea Graben axis.

- Subduction Input - Enrichment of Th and LREE is fairly consistent across the north of Troodos when overall variations on profile shape resulting from source depletion are taken into account. Mitsero has the lowest level of subduction enrichment and the Solea Graben has the highest. However, the variations between the end-members are small. Variations in profiles between samples in each location were of similar size.

South western Troodos

Two distinct lava types are apparent in south western Troodos based on depletion and enrichment patterns. The difference in composition between lavas from Diarizos and Mandria compared to lavas from Akamas and the Paphos Forest is shown by Figs. 3.6b-3 and 3.6b-4. Fig 3.6b-3 is a multi-element spider diagram that shows a representative profile obtained from lavas from the Diarizos and Mandria area of south western Troodos. Fig 3.6b-4 is a multi-element spider diagram that shows a representative profile obtained from lavas from the Akamas and Paphos Forest areas of south western Troodos. Both profiles are N-MORB and Yb normalised. The following features are apparent within south western Troodos lavas:

Fig 3.6b-3. Incompatible element spider diagram showing source components for an average lava from Diarizos and Mandria areas of south western Troodos. The same colour scheme is used as Fig 3.6b-2

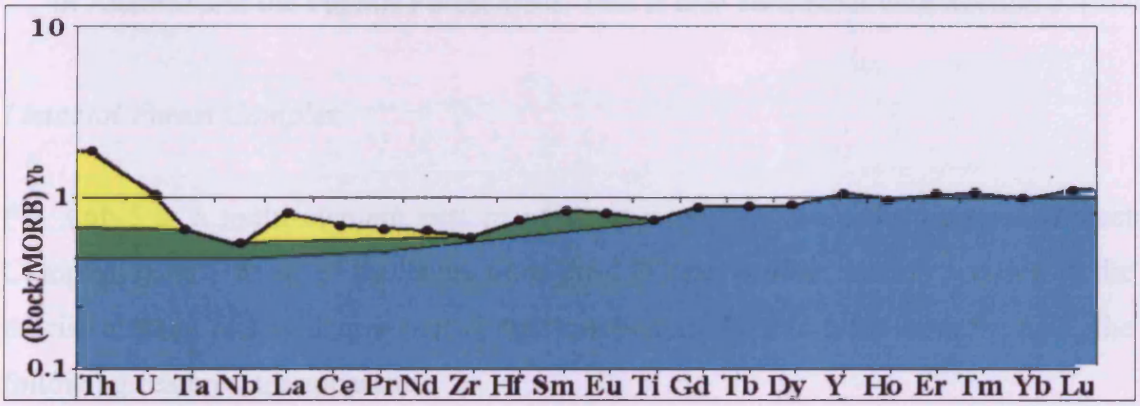

Fig 3.6b-4 Incompatible element spider diagram showing source components for an average lava from the Paphos Forest and Akamas area of south western Troodos. The same colour scheme is used as Fig 3.6b-2

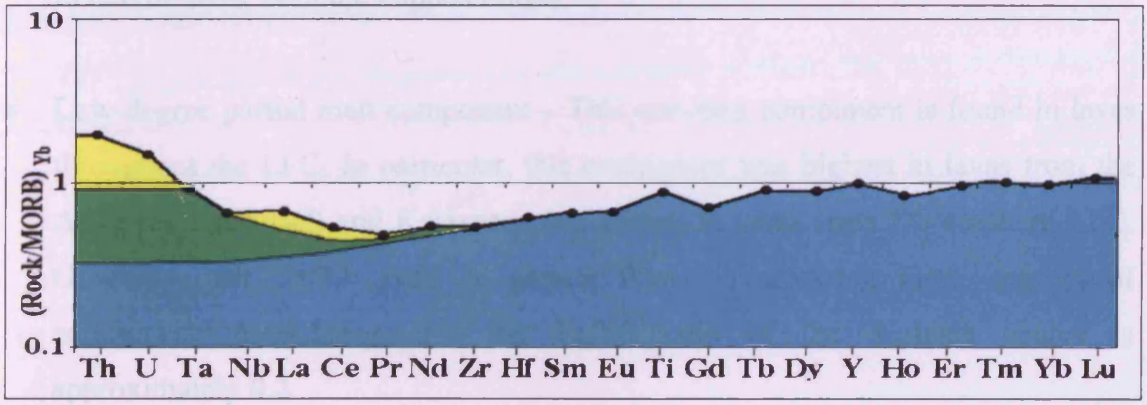

- Mantle Source – The extent of depletion of lavas from Diarizos and Mandria is similar to that recorded in lavas of the Mitsero-type from northern Troodos. Lavas from Akamas and the Paphos Forest have greater levels of incompatible element depletion. The normalised Zr/Yb ratio of the mantle component is about 0.4.
- Low-degree partial melt input – Low levels of this component are found in lavas from Diarizos and Mandria, highlighting their similarity with lavas from northern Troodos. However, lavas from the Paphos Forest and Akamas exhibit a considerable input of incompatible element-rich component. Only elements more incompatible than Zr are enriched. This component is characterised by high Ta/Yb and Nb/Yb ratios compared to Zr/Yb.
- Subduction Input - Enrichment of Th and LREE of lavas from Diarizos and Mandria is fairly similar to the degree of enrichment observed within northern Troodos. This is consistent with Section 3.4, where Th/Nb ratios were similar to northern Troodos. The contribution of the subduction-derived component is lower in Akamas and the Paphos Forest areas. This is also consistent with Section 3.4.

Limassol Forest Complex

Fig 3.6b-5 is a multi-element pattern of an average lava from the Limassol Forest Complex (LFC). Most of the lavas from the LFC are similar, mainly varying in the precise amount of low-degree partial melt component. Within lavas from the LFC, the following features are apparent:

- Mantle component – The mantle component of lavas from the LFC is strongly depleted. The normalised Zr/Yb ratio of these lavas is about 0.3, which is similar to that of lavas from the Paphos Forest.

- Low-degree partial melt component – This enriched component is found in lavas throughout the LFC. In particular, this component was highest in lavas from the Arakapas Fault Belt and Kalavasos and lowest in lavas from the southern LFC. Generally, the Ta/Yb ratio is greater than 1, indicating large degrees of enrichment, considering that the Ta/Yb ratio of the depleted source is approximately 0.2.

- Subduction Input - Enrichment of Th and LREE is fairly low across the LFC, with the highest levels in the southern LFC and the lowest near the Arakapas Fault Belt and Kalavasos. Degrees of subduction-derived enrichment are similar to those from the Paphos Forest and Akamas. Generally, degrees of enrichment are lower than those recorded within the lavas of northern Troodos.

Fig 3.6b-5 Incompatible element spider diagram showing source components for an average lava from the Limassol Forest Complex. The same colour scheme is used as Fig 3.6b-2

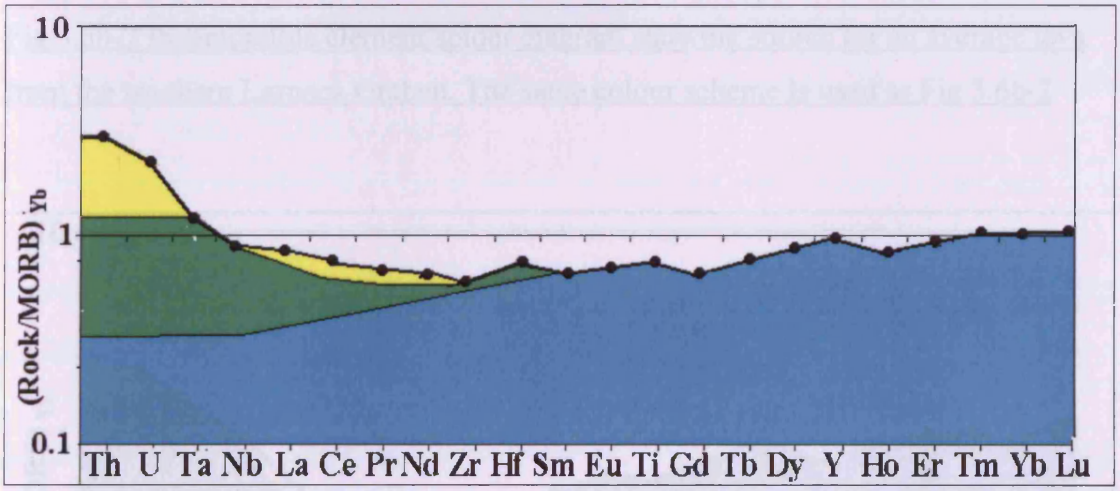

Larnaca Graben

Two distinct lava types are apparent in the Larnaca Graben based on depletion and enrichment patterns. Figs. 3.6b-6 and 3.6b-7 highlights the difference in composition between lavas from Margi and Troulli in the far north of the Larnaca Graben compared to lavas from the south of the Larnaca Graben. Fig 3.6b-6 presents a representative profile obtained from Margi and Troulli in the northern Larnaca Graben. Fig 3.6b-7 is an equivalent diagram that depicts a representative profile obtained from lavas from the southern Larnaca Graben. The following features are apparent within lavas from the Larnaca Graben:

Fig 3.6b-6 Incompatible element spider diagram showing source for an average lava from the Margi and Troulli areas. The same colour scheme is used as Fig 3.6b-2

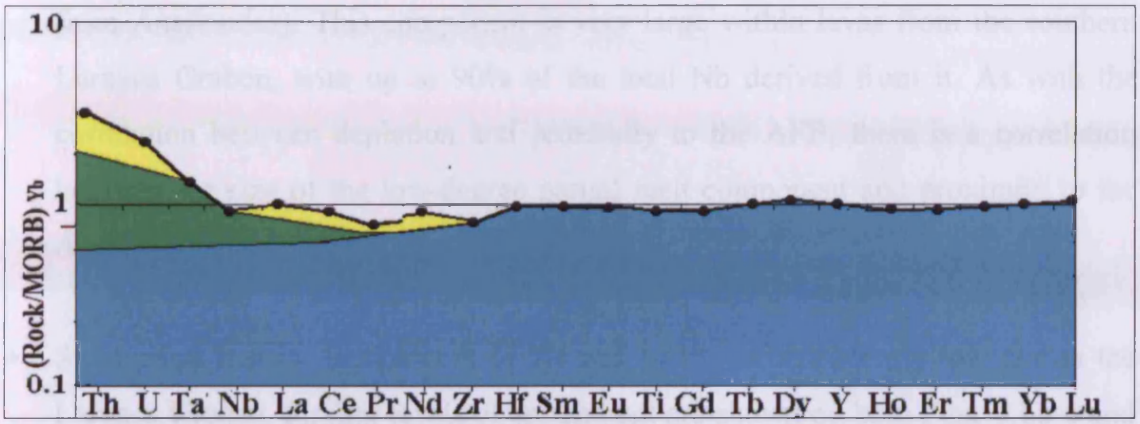

Fig 3.6b-7 Incompatible element spider diagram showing source for an average lava from the southern Larnaca Graben. The same colour scheme is used as Fig 3.6b-2

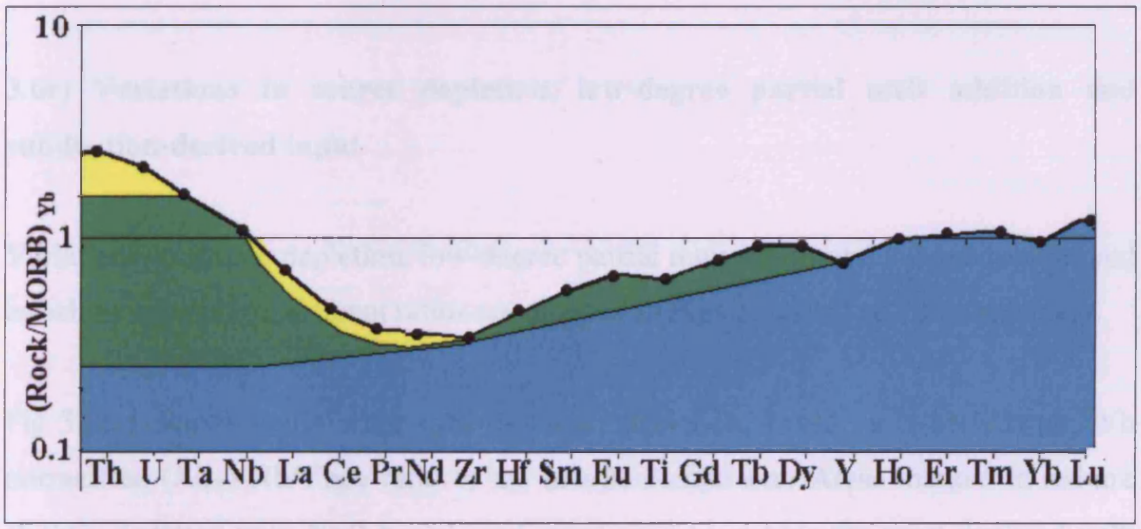

- Mantle Component – The mantle component of lavas from Margi in the north of the Larnaca Graben is very slightly depleted with an almost flat profile. This is in contrast to the mantle component of lavas from the southern Larnaca Graben, where the mantle is strongly depleted. The extrapolated Nb/Yb of the mantle source of the southern Larnaca Graben lavas is 0.3, compared to 0.7 for lavas from Margi and Troulli. This is strong evidence for progressive depletion of the source with proximity to the AFB.

- Low-degree partial melt component – This is moderate in lavas from Margi and slightly higher in these lavas than in neighbouring northern Troodos lavas (e.g. from Analiondas). This component is very large within lavas from the southern Larnaca Graben, with up to 90% of the total Nb derived from it. As with the correlation between depletion and proximity to the AFB, there is a correlation between the size of the low-degree partial melt component and proximity to the AFB.

- Subduction Input - Enrichment of Th and LREE is consistently low across the Larnaca Graben. Similar levels of enrichment are shown on both Figs. 3.6b-6 and 3.6b-7 of Margi and southern Larnaca Graben Lavas respectively. The extent of subduction-derived enrichment is lower than that observed within lavas from northern and south western Troodos but equal to, or higher than, levels observed in the Limassol Forest Complex.

3.6c) Variations in source depletion, low-degree partial melt addition and subduction-derived input

Variations in source depletion, low-degree partial melt inputs and subduction-derived enrichment based on element ratios are mapped in Figs 3.6c-1, 2 and 3 respectively.

Fig 3.6c-1 shows spatial variations in source depletion, based on N-MORB and Yb normalised (X_{NY}) Nb/Yb_{NY} ratio of the mantle component. Areas marked in red are slightly depleted with $Nb/Yb_{NY}>1$, and areas marked in blue the most depleted with $Nb/Yb_{NY}<0.2$. The other contours are at Nb/Yb_{NY} = 0.4, 0.6 and 0.8. Most of northern Troodos is mildly depleted, with source depletion increasing with proximity to the transform fault. There are two anomalous areas that show greater levels of source depletion. These are the Solea Graben axis and Kalo Chorio. Lavas in the proximity of the Solea Graben axis would have been the last lavas produced when magmatism ceased and therefore it would be logical to assume that input of partial melt beneath the graben ceased before the magma chamber emptied, leaving a batch of increasingly depleted lavas as melt was extracted without replenishment.

Fig 3.6c-1. Map of the lava sequence of the Troodos Massif degrees of mantle source depletion based on Nb/Yb_{NY} ratio of the mantle component. Red areas are least depleted and blue areas are the most depleted (see text for details).

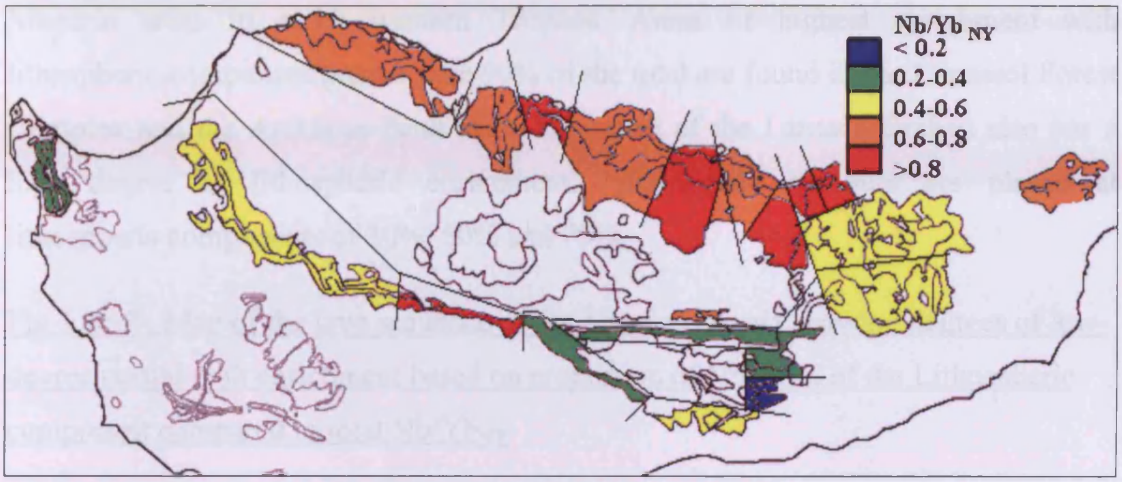

In the Larnaca Graben, the depletion of Troulli and Margi lavas is greater than depletion of northern Troodos lavas, but is lower than the depletion of lavas from the central and southern Larnaca Graben. This increase in depletion is probably a function of proximity to the transform fault.

In the south west of Troodos, lavas from the Paphos Forest area are depleted. However, lavas from Diarizos and Mandria have depletion levels more similar to those found in the north of Troodos. The proximity of lavas from Diarizos and Mandria to the Arakapas Fault Belt does not correspond well with the evidence from the Larnaca Graben that depletion increases with proximity to a transform fault.

Lavas from the Limassol Forest and the Arakapas Fault Belt are the most depleted lavas from the Troodos Massif. In addition, lavas from the southern Limassol Forest Complex are less depleted than lavas from the northern portions of the region, indicating, in the same manner as lavas from the Larnaca Graben, that proximity to a transform fault has a strong influence on mantle depletion.

Fig 3.6c-2 depicts spatial variation in low-degree partial melt components, also interpreted as lithospheric or OIB-type enrichments, calculated by subtracting the Nb/Yb_{NY} of the mantle component the total Nb/Yb_{NY} and dividing by the total

Nb/Yb_{NY}, which is then converted to a percentage. Areas marked in blue have a low degree of lithospheric enrichment, and areas marked in red have a high degree of lithospheric enrichment. Areas of lowest enrichment with lithospheric component less than 10% of the total are the entirety of northern Troodos and the Diarizos and Mandria areas in south western Troodos. Areas of highest enrichment with lithospheric component greater than 90% of the total are found in the Limassol Forest Complex and the Arakapas Fault Belt. The much of the Larnaca Graben also has a high degree of lithospheric enrichment. Intermediate contours are placed at lithospheric components of 30%, 50% and 70%.

Fig 3.6c-2 . Map of the lava sequence of the Troodos Massif showing degrees of low-degree partial melt enrichment based on proportion of Nb/Yb_{NY} of the Lithospheric component compared to total Nb/Yb_{NY}

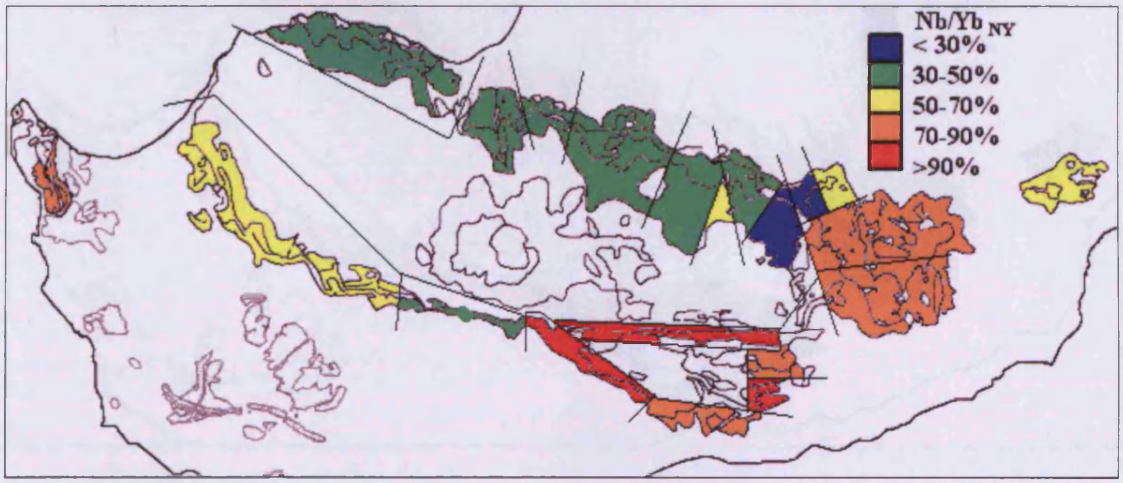

The enrichment of the lavas from the Larnaca Graben could be explained as a function of the movement of the centre of magmatism and the change in the direction of plate movement allowing 'fresh' mantle to be drawn into the zone of magmagenesis as discussed in detail in Section 4.1. Although lavas from Diarizos and Mandria are anomalous, there appears to be a correlation between low-degree partial melt enrichment and proximity to the Arakapas Fault Belt.

Fig 3.6c-3 shows the spatial variation in subduction-derived enrichment derived by subtracting Nb/Yb_{NY} from Th/Yb_{NY} and dividing by Th/Yb_{NY}, which is then converted to a percentage. Areas marked in blue have a low degree of enrichment ($\%Th_{SZ}$ less

than 20%), and areas marked in red have a high degree of enrichment (%Th_{sz} greater than 60%). The highest degrees of subduction-derived enrichment are found across the northern Troodos lavas and in the south west of Troodos, especially the Diarizos and Mandria areas. Enrichment is lowest in the Limassol Forest Complex and Larnaca Graben. Both of these areas were formed at a graben axis that lay to the east of the Troodos Massif. Therefore, enrichment in the eastern areas was less influenced by subduction than the crust formed at the Solea Graben axis. Intermediate contours are at %Th_{sz} = 30%, 40% and 50%.

Fig 3.6c-3 Map of the lava sequence of the Troodos Massif showing calculated levels of SSZ enrichment. Blue areas are least enriched and orange areas are the most enriched.

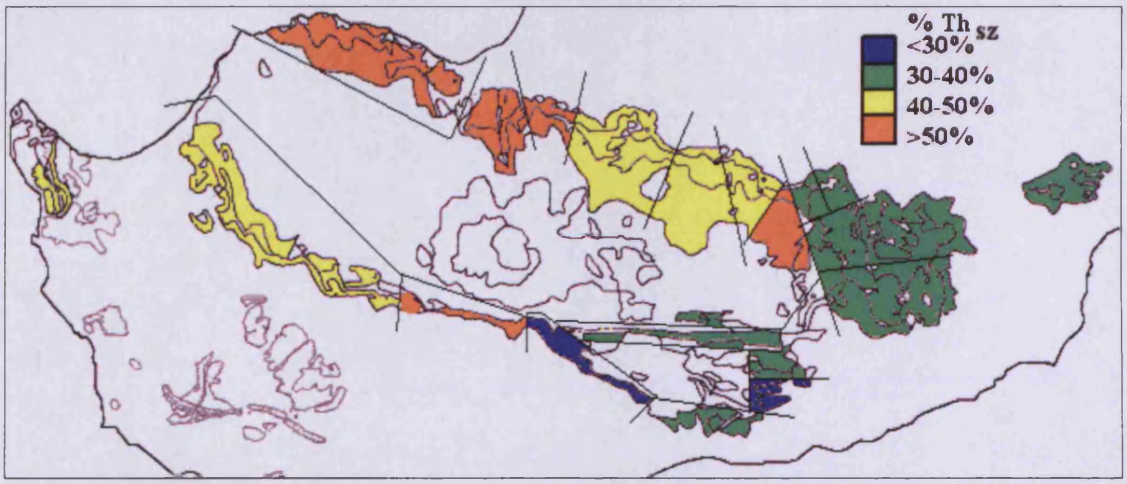

3.6d) Comparison with analogue regions to the Troodos Massif (Lau Basin and the Garrett Transform in the East Pacific Rise)

Northern Troodos

Lavas from northern Troodos are most similar to lavas from the Eastern Lau Spreading Centre (ELSC) as shown in Fig 3.6d-1. The mantle and lithospheric enrichment components are virtually identical. However the lavas from northern Troodos are somewhat higher in their subduction component than the lavas from the ELSC. This indicates that the environments of formation of the two regions are

similar, with the exception that the Troodos Massif was perhaps slightly closer to the subduction zone than the average distance of the ELSC to the Tonga subduction zone.

Fig 3.6d-1. Comparison of MORB normalised element profiles for northern Troodos with the Eastern Lau Spreading Centre (ELSC) overlain in red. These profiles display very similar levels of mantle depletion and lithospheric input. The profile from northern Troodos displays a higher degree of subduction input than the profile from the ELSC

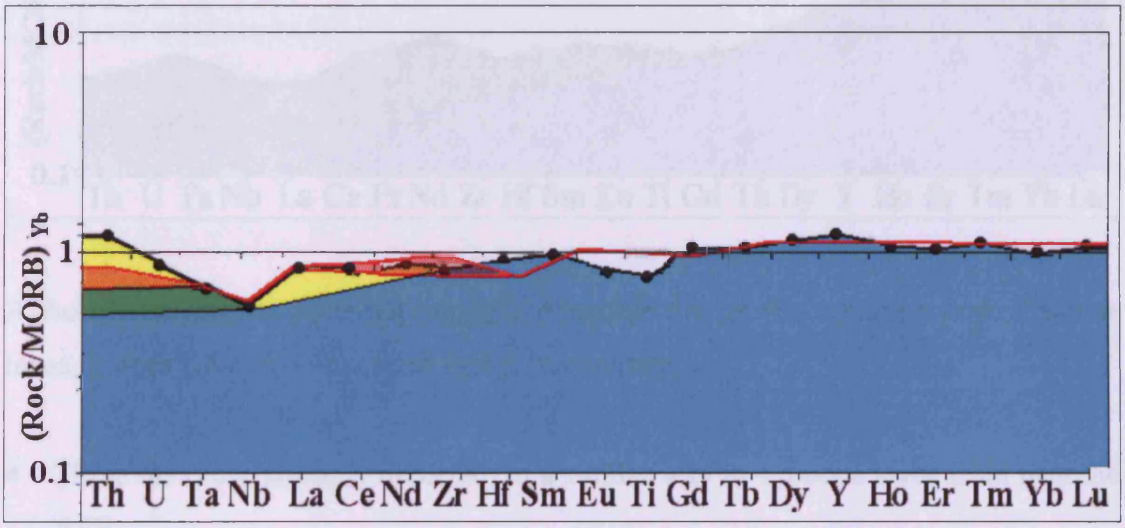

South West Troodos, Limassol Forest Complex and Larnaca Graben

These three regions all show a broadly similar pattern of extensive source depletion, variable, and sometimes high, levels of low-degree partial melt enrichment and low to moderate subduction-derived enrichment. The main variation between these areas is in the degree of depletion and low-degree partial melt input. The degree of depletion and low-degree partial melt enrichment appears to be related to the proximity to the Arakapas Fault Belt, a transform zone. As an analogue, Fig 3.6d-2 is an incompatible element plot for lavas from the Garrett Transform in the East Pacific Rise. Two types of lava are reported from the Garrett Transform: one is MORB-like with low levels of low-degree partial melt enrichment and the other type, shown on Fig. 3.6d-2 is strongly depleted with moderate degrees of lithospheric enrichment.

Fig 3.6d-2. MORB and Yb normalised extended incompatible element profile for depleted lavas from the Garrett Transform, East Pacific Rise (Hekinian, 1995) Blue shows mantle component and green shows low-degree partial melt component.

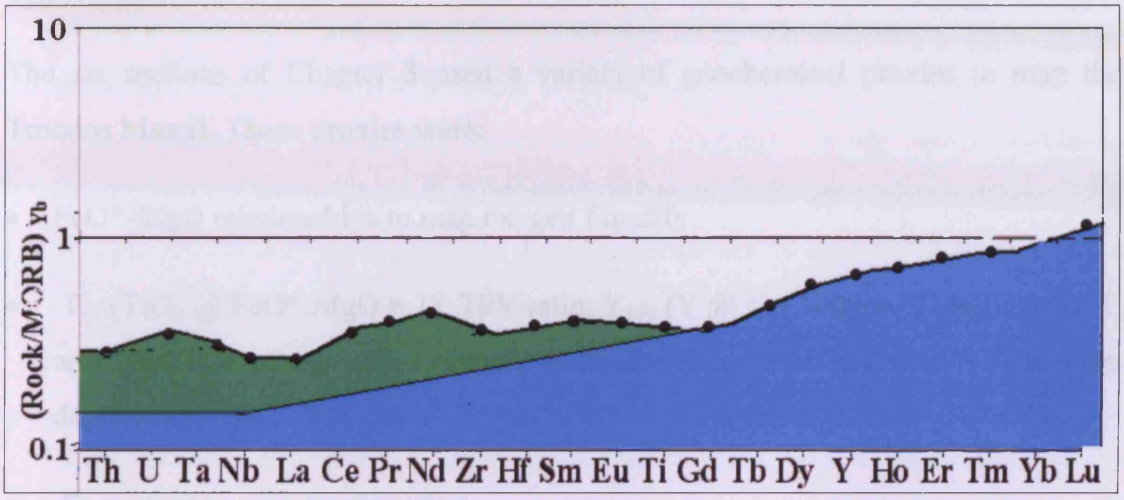

Although the profile does not strongly resemble the profile obtained from Troodos lavas, it does have two important things in common:

- These lavas are strongly depleted, in a similar way to Troodos lavas from near the AFB.
- These lavas show low-degree partial melt enrichment that, although less than that observed within the Troodos Massif, may also be associated with proximity to the transform fault.

4) Implications for Petrogenesis and Tectonic setting of the Troodos Massif

4.1) Summary of results

The six sections of Chapter 3 used a variety of geochemical proxies to map the Troodos Massif. These proxies were:

- FeO*-MgO relationships to map oxygen fugacity.
- Ti_1 (TiO_2 @ FeO*/MgO = 1), Ti/V ratio, Y_{100} (Y @ Cr=100ppm), MREE/HREE, and Nb/Yb_{NY} of the asthenosphere (normalised to N-MORB and Yb) to map depletion.
- Cr content to map fractionation.
- Th/Nb ratios, LREE/MREE and Th/Nb_{NY} of the subduction component to map subduction contribution.

In order to ensure consistency and accuracy and to be able to draw conclusions based on all available data, maps summarising Chapter 3 have been created. Summary maps are presented for distribution of depleted mantle, distribution of subduction component, distribution of evolved and primitive lavas and distribution of lithospheric component. Note that 'lithospheric component' refers to the component with an OIB-type of geochemical signature, or uncertain origin, which is interpreted here as having enriched ocean lithosphere and become incorporated in some Troodos magmas.

4.1a) Distribution of depleted mantle

Fig 4.1a-1 provides comparison of five proxies used in this thesis to map source depletion. Maps of a) Ti/V ratio, b) Y_{100}, c) Ti_1, d) MREE/HREE ratio (Gd/Yb) and e) Nb/Yb_{NY} ratio of the mantle component are shown. There is a strong similarity between the areas of strong depletion shown on all the maps (in the south and the Limassol Forest Complex) and also between the areas of little depletion (Mitsero Graben and northern Larnaca Graben) that will be discussed below. There are also some differences between the maps that need to be addressed.

- Ti/V ratio mapping indicates that lavas from the Tilliria region have a depleted source. This contradicts the other methods that indicate a less depleted source. It also indicates greater depletion of the southern Larnaca Graben and south western Troodos than the other methods. Because the Ti/V ratio is affected by fractional crystallisation, this may be the cause of this discrepancy.
- Y_{100} and Ti_I broadly agree. However, Ti_I mapping reveals lower levels of depletion for lavas from the central Larnaca Graben and Akamas than Y_{100} mapping. This may be explained by small differences in the partition coefficients of Ti and Y may explain inconsistencies between the lava groups in northern Troodos.
- MREE/HREE mapping contradicts Ti/V, Y_{100} and Ti_I by indicating a non-depleted source for lavas from the axis of the Solea Graben. However, it broadly agrees with Nb/Yb_{NY}.

Fig 4.1a-1 comparison of methods used to map source depletion across the lavas of the Troodos Massif. Individual maps are: a) Ti/V ratio, b) Y_{100}, c) Ti_I, d) MREE/HREE ratio (Gd/Yb) and e) Nb/Yb_{NY} ratio of the mantle component

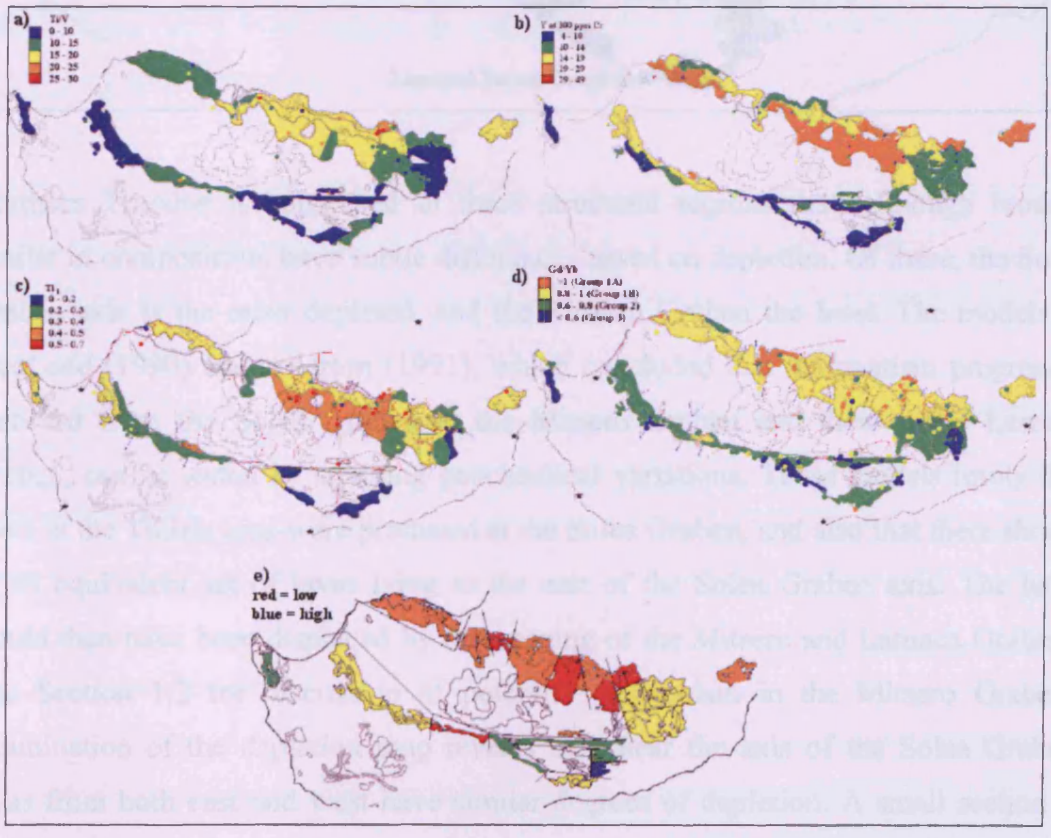

Fig. 4.1a-2 displays variations in source depletion across the Troodos Massif based on depletion patterns observed in Fig. 4.1a-1. The summary map was built up by overlaying the five maps in a graphics program as partially transparent layers. The resulting map was then smoothed and re-coloured. Degrees of depletion may vary abruptly across a structural boundary, indicating that the boundary marks the change between lavas of different sources, or they may vary gradually over a distance. Gradual variation would indicate either a temporal change or a progressive change related to proximity to a feature that influenced the composition of the lavas.

Fig. 4.1a-2 Summary depletion map derived from the methods described above.

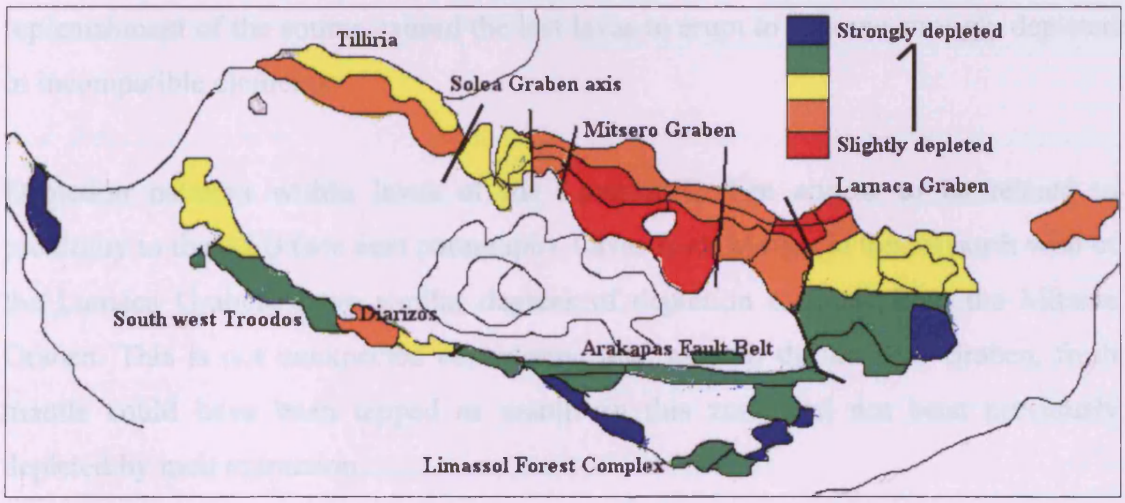

Northern Troodos is composed of three structural regions that, although broadly similar in composition, have subtle differences based on depletion. Of these, the Solea Graben axis is the most depleted, and the Mitsero Graben the least. The models of MacLeod (1990) and Allerton (1991), which concluded that magmatism progressed eastward from the Solea Graben to the Mitsero Graben and then to the Larnaca Graben, can be tested by studying geochemical variations. These models imply that lavas in the Tilliria area were produced at the Solea Graben, and also that there should be an equivalent set of lavas lying to the east of the Solea Graben axis. The latter would then have been displaced by the opening of the Mitsero and Larnaca Grabens. (see Section 1.2 for discussion of potential magmatism in the Mitsero Graben). Examination of the depletion map reveals that, near the axis of the Solea Graben, lavas from both east and west have similar degrees of depletion. A small section of

lavas between the Mitsero and Larnaca Grabens also has similar levels of depletion. There are sharp boundaries between lavas of the Solea, Mitsero and Larnaca Grabens.

On the basis of this pattern in Fig. 4.1a-2, I therefore propose that lavas originally generated at the Solea Graben, which were slightly depleted, are to be found at Tilliria, Koronia (between the Mitsero and Solea Grabens) and Kambia (between the Mitsero and Larnaca Grabens). Following eastward migration of the spreading centre, the Mitsero Graben opened within Solea Graben-generated crust. Tapping mantle that had not been significantly depleted by melt extraction during flow and mixing in a mantle wedge may have meant that these lavas were less depleted than lavas from the Solea Graben. In addition, as magmatism ceased at the Solea Graben, lack of replenishment of the source caused the last lavas to erupt to become strongly depleted in incompatible elements.

Depletion patterns within lavas of the Larnaca Graben appear to be related to proximity to the AFB (see next paragraph). Lavas from Margi (in the far north west of the Larnaca Graben) have similar degrees of depletion to lavas from the Mitsero Graben. This is not unexpected considering that, as with the Mitsero Graben, fresh mantle could have been tapped as mantle in this zone had not been previously depleted by melt extraction

The increase in depletion with proximity to the paleo-transform fault is more difficult to explain. Theories of melt propagation along ridge segments towards transform faults (Schouten and Keleman, 2002) indicate that the nearer to a transform fault the mantle migrates, the greater the depletion. This is because the mantle would already experience some preconditioning (melt extraction) at the ridge crest, losing some of its incompatible element content. However, the mantle also cools towards a transform fault, reducing the degree of partial melting and so increasing incompatible element content in the lavas produced.

Given that the Troodos Massif formed in a supra-subduction zone environment, it is reasonable to expect that hydrous subduction-derived fluids increased the degree of partial melting. In addition, decompression-related melting of mantle passing beneath the transform fault and rising on the side where the lithosphere was thinner and

younger could also have increased the degree of partial melting in this location. If the degree of partial melting were increased in such a manner, there would be little appreciable enrichment of incompatible elements, allowing the depleted character of the mantle to remain. Assuming this scenario, the two areas in the southern Troodos lavas that are noticeably less depleted (at the far northern end of the south western lava outcrop and Diarizos) can be explained. The northern lavas of the south western lava outcrop are located at a similar distance from the paleo-transform fault as lavas from the eastern part of the northern Troodos region (crust generated as the Solea and Mitsero Grabens). Therefore, they were probably too far from the paleo-transform fault to be affected by localised depletion effects. The absence of depleted lavas from Diarizos, which also lies to the paleo-transform fault, can perhaps best be explained by lower degrees of partial melting of depleted mantle.

The mantle source is depleted throughout the ophiolite, and the level of depletion increases with proximity to the transform fault. This could be explained if asthenosphere rises near the centre of a ridge segment, then migrates towards the margins, becoming more depleted and cooler as it does so, undergoing lower degrees of partial melting.

4.1b) Distribution of the subduction-derived component

Fig 4.1b-1 provides comparison of three proxies used in this thesis to map subduction-derived input. The proxies used are: a) Th/Nb ratio, b) $\%Th_{sz}$ and c) oxygen fugacity relative to QFM. Th/Nb and $\%Th_{sz}$ maps are similar, as would be expected. However, the oxygen fugacity map, Fig 4.1b-1(c), displays pattern inverse to that of the other maps. The oxygen fugacity map gives similar patterns to the map of lithospheric component distribution (Fig 4.1d-2, thus indicating that, in the case of the Troodos Massif, oxidising fluids were carried in the lithospheric component, rather than just in the subduction-derived component as is usually assumed (Parkinson and Arculus, 1999).

Fig 4.1b-1 comparison of methods used to map subduction-derived enrichment across the lavas of the Troodos Massif. Individual maps are: a) Th/Nb, b) $\%Th_{sz}$ and c) oxygen fugacity relative to QFM.

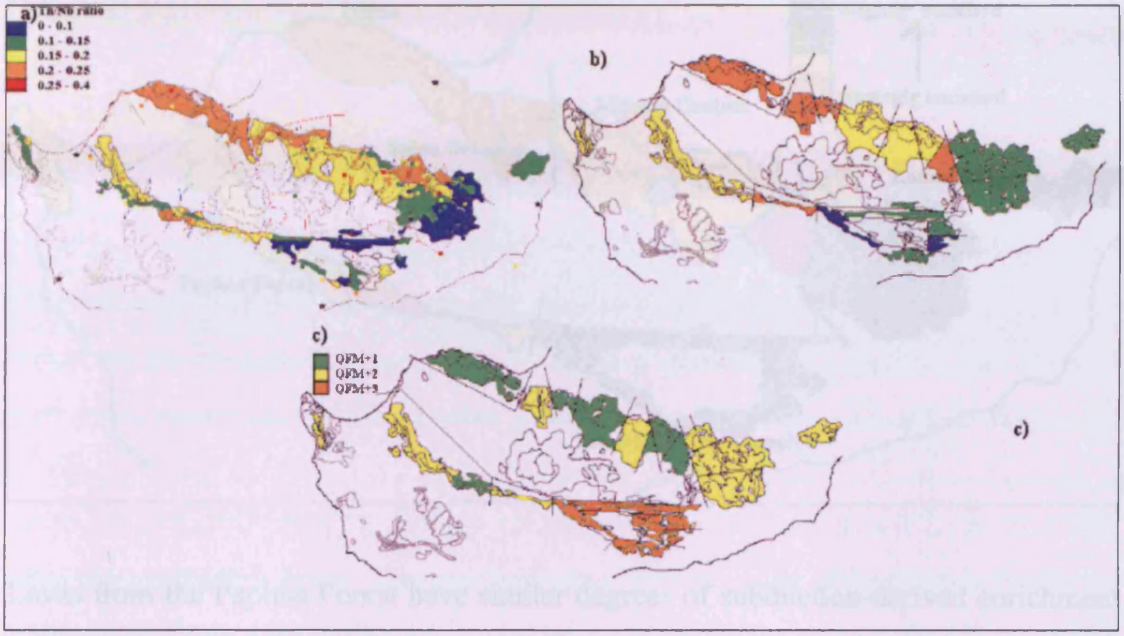

Fig. 4.1b-2 summarises both Th/Nb and $\%Th_{sz}$ maps to produce a summary of subduction-derived enrichment. On the basis of the proportion of subduction-derived Th in the source, lavas of the Troodos Massif may be divided into two parts. One part has a moderate proportion of subduction-derived Th (about 40% - see section 3.4) and the other part has a very low proportion of subduction-derived Th (<20%)

The enriched portion comprises Tilliria, the Solea and Mitsero Grabens, and the Paphos Forest. Lavas from Tilliria, the Solea Graben and Kambia (between the Mitsero Graben and the Larnaca Graben) have the greatest subduction enrichment. This supports the model proposed in Section 4.1a, that these sections of crust were all formed at the Solea Graben. Lavas within the Mitsero Graben have slightly lower degrees of subduction-derived enrichment. Just as their lower degree of depletion indicated that they were not co-genetic with lavas from the Solea Graben, their clearly lower subduction component also supports this theory.

Fig. 4.1b-2 Summary subduction component map derived from the methods described above.

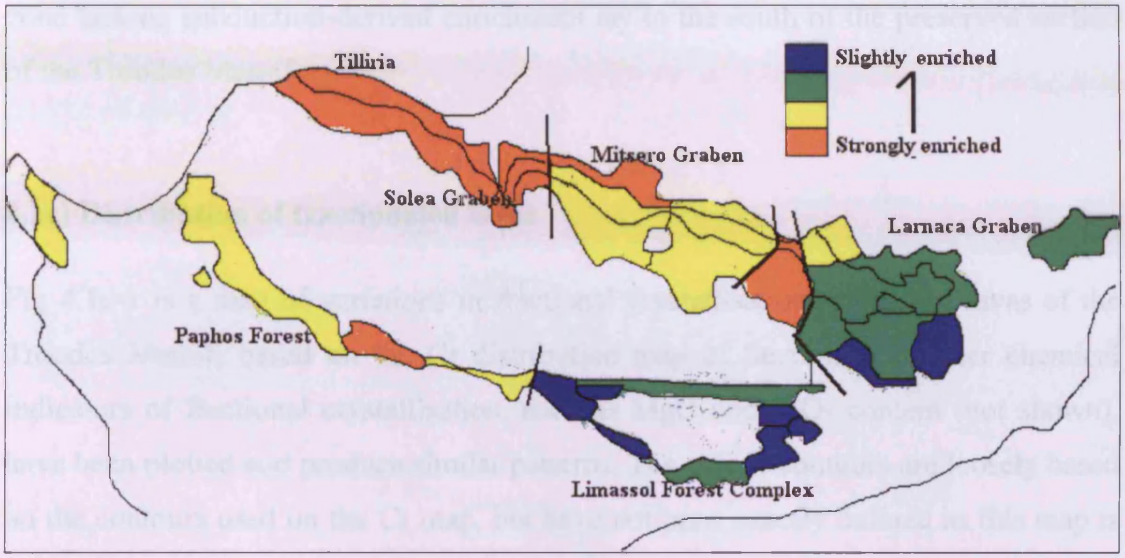

Lavas from the Paphos Forest have similar degrees of subduction-derived enrichment to lavas from the Mitsero Graben, with the exception of lavas from Diarizos where enrichment is more comparable with that seen in Solea Graben lavas. Most noteworthy is the considerable difference between Diarizos and lavas from the nearby AFB. This indicates that proximity to the paleo-transform fault is not a driving factor for subduction-derived enrichment. If proximity to the paleo-transform fault were a factor, a gradual change with proximity would be expected.

Lavas with little subduction-derived enrichment are located within the Limassol Forest Complex and the majority of the Larnaca Graben. Although some subduction-derived enrichment is evident in lavas from Margi in the northern Larnaca Graben, the remainder of the Larnaca Graben exhibits little subduction-derived enrichment. Lavas from the southern Larnaca Graben have less enrichment than the AFB. This could indicate that, as with the enriched lavas from the Paphos Forest discussed earlier, proximity to the AFB does not affect the degree of subduction-derived enrichment. Compared to lavas from the Paphos Forest, Solea Graben and Mitsero Graben, lavas from the Limassol Forest Complex and the Larnaca Graben formed further east. The reduction in subduction-derived enrichment eastwards, over a relatively short distance, indicates a sharp drop-off in subduction-derived enrichment of the mantle

source. Within the lavas of northern Troodos, those from the Mitsero Graben (to the east of the Solea Graben axis) have a smaller subduction component than lavas from the Solea Graben. Thus, before the anticlockwise rotation of the Troodos plate, the zone lacking subduction-derived enrichment lay to the south of the preserved section of the Troodos Massif.

4.1c) Distribution of fractionated lavas

Fig 4.1c-1 is a map of variations in fractional crystallisation within the lavas of the Troodos Massif, based on the Cr distribution map of Section 3.3. Other chemical indicators of fractional crystallisation, such as MgO and TiO_2 content (not shown), have been plotted and produce similar patterns. The colour contours are loosely based on the contours used on the Cr map, but have not been exactly defined as this map is based on a combination of factors. Orange represents fractionated lavas and blue represents primitive lavas. This colour-coding shows a clear distinction between the stratigraphic lava groups (Basal Group, Lower Pillow Lavas and Upper Pillow Lavas) within northern Troodos and the northern part of the Larnaca Graben. Lavas from the Upper Pillow Lavas are the most primitive and lavas from the Basal Group are the most evolved. Field evidence and previous research by Pearce (pers. comm.) and Sobolev et al. (1993) indicate that, in some places, lavas of the Basal Group are primitive. This new evidence indicates that primitive lavas are not common on a Troodos-wide scale.

Most lavas throughout the Troodos Massif are evolved, and only the Upper Pillow Lavas are primitive in regions away from the Limassol Forest Complex and the paleo-transform fault (a.k.a. the AFB). Most lavas from the Limassol Forest Complex and the southern Larnaca Graben are primitive. Eruption of primitive lavas indicates a relatively short residence time in any magma chamber. This would be therefore true of both the Upper Pillow Lavas of northern Troodos and lavas from the Limassol Forest Complex. Schouten and Kelemen (2002) proposed that the Upper Pillow Lavas were erupted directly from off-axis vents, a model that this study does not contradict.

Structural studies (e.g. Murton, 1986) have shown that the Limassol Forest Complex crustal sequence is thin compared to other parts of the Troodos Massif. Evidence that

the paleo-transform fault was trans-tensional (MacLeod, 1990) provides a mechanism for a combination of decompression-related melting and rapid transference of melt to the surface.

Fig. 4.1c-1 Summary map of fractional crystallisation derived from the methods described above.

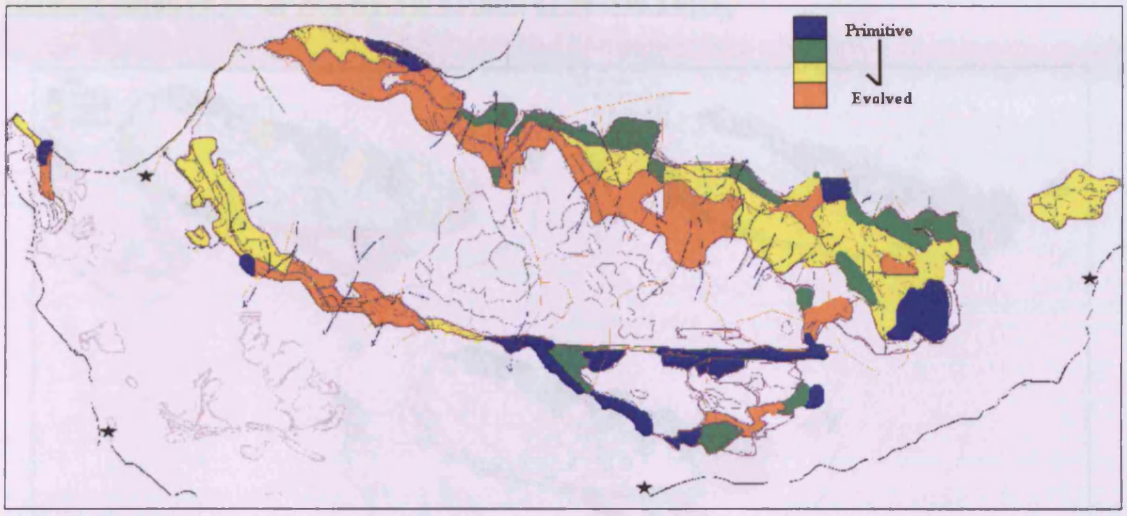

4.1d) Distribution of lithospheric component.

Fig. 4.1d-1 illustrates the three proxies used to map this component. These proxies are: a) oxygen fugacity relative to QFM, b) Nb/Yb and c) % Nb/Yb_{Litho} (% lithospheric Nb/Yb compared to total Nb/Yb). Generally, the three maps correspond well with only a few minor differences. They all show the lowest lithospheric component in northern Troodos and Diarizos, with a moderate component in the Larnaca Graben and high component in the Limassol Forest Complex. In addition, the Nb/Yb map indicates that the UPL have a higher Nb/Yb ratio than the LPL or BG in the Tilliria and Kambia areas. However, the resolution of the other maps is too low to show this. Other features are:

- Nb/Yb mapping indicates that Akamas has low Nb/Yb but the other methods indicate higher proportions of lithospheric component.

- Strong Nb enrichment (Fig 4.1d-1(b)) is, within in the Larnaca Graben, restricted to the southern portion. The other maps indicate uniform distribution across the graben.

- The oxygen fugacity map shows areas of slightly higher oxygen fugacity within the axis of the Solea Graben. The lithospheric component is not shown in the other maps in this location.

Fig 4.1d-1 comparison of methods used to map enriched lithosphere (or OIB) component.across the lavas of the Troodos Massif. Individual maps are: a) oxygen fugacity relative to QFM., b) Nb/Yb and c) % $Nb/Yb_{L\,itho}$

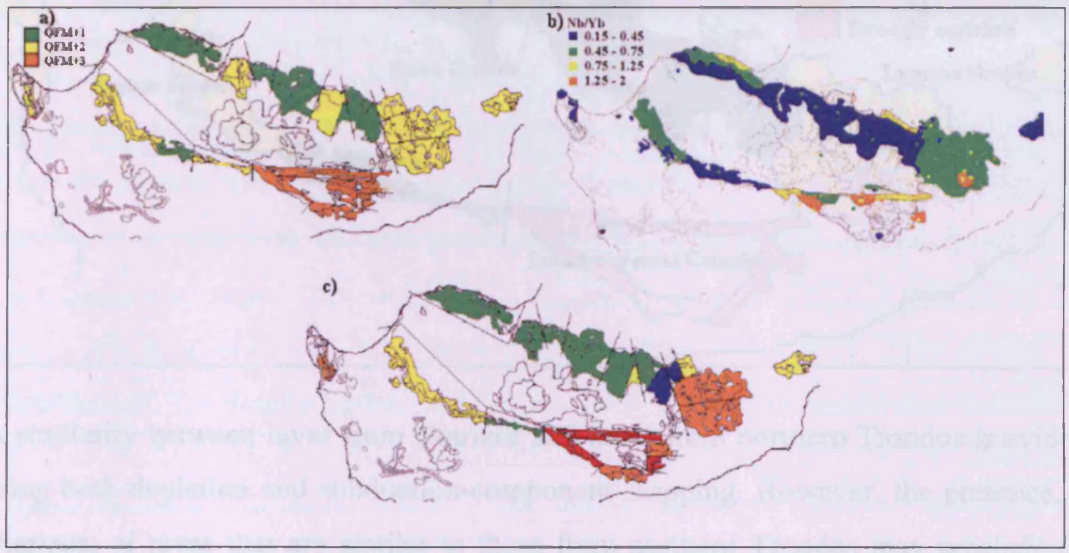

Fig.4.1d-2 indicates lithospheric component based on the proxies shown in Fig.4.1d-1. The lavas of the Troodos Massif are split into two types based on lithospheric input. Generally, lavas from the north of Troodos have a small lithospheric component and lavas from the south and east of Troodos a high lithospheric component.

Lavas with little enriched lithosphere (or OIB) component are found across northern Troodos and in the Diarizos area of south western Troodos. There is slight variation between lavas formed at the Solea Graben and those formed within the Mitsero Graben. Lavas from Tilliria, the Solea Graben axis and Kambia have small components. In contrast, lavas from the Mitsero Graben have very small components. However, variation between stratigraphic units in the Tilliria area and the presence of lavas with very small lithospheric components to the south east of Kambia does not fit the model established using depletion and subduction input mapping that there is no fundamental difference between the lava groups in terms of the lava source. This could indicate either that the model of two magmatic grabens is not entirely correct or

that the actual variations are so slight that the placement of colour contours creates a false pattern or masks the true pattern.

Fig. 4.1d-2 Summary lithospheric-derived enrichment map derived from the methods described above.

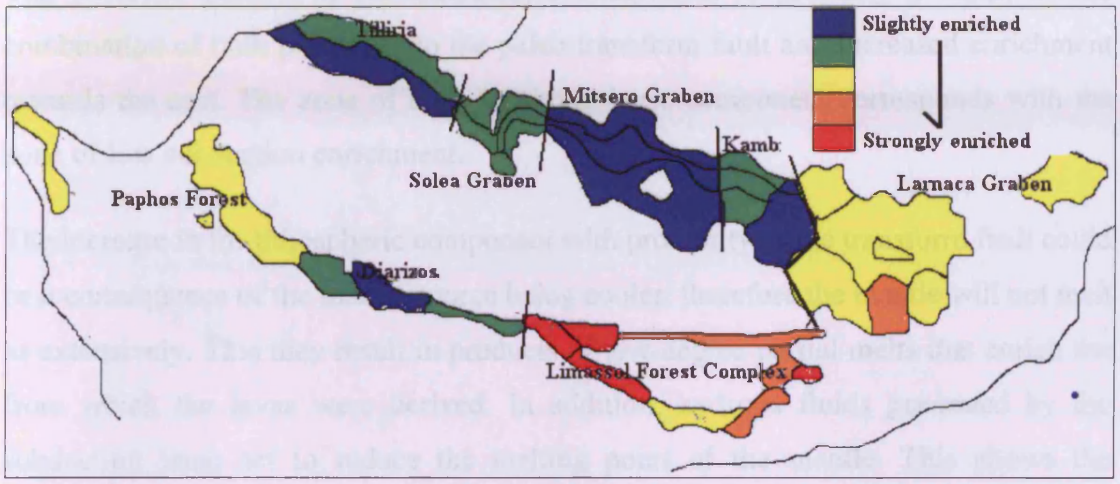

A similarity between lavas from Diarizos and those from northern Troodos is evident using both depletion and subduction-component mapping. However, the presence, in Diarizos, of lavas that are similar to those from northern Troodos may preclude the formation of a general model associating the lithospheric component with proximity to the Arakapas Fault Belt.

The distribution of the lithospheric component indicates that the source of this component was local to the east of the Troodos Massif and/or related to proximity to the paleo-transform fault. The evidence that lithospheric component was greatest to the east is that most of the Larnaca Graben is enriched and the Limassol Forest Complex is strongly enriched. However, this model does not explain enriched lavas in the Paphos Forest and Akamas areas. The evidence that the enrichment was related to transform fault proximity is that the southern part of the Larnaca Graben is more enriched than the north, that the north and west of the Limassol Forest Complex is enriched. This model could also explain enrichment of the Paphos Forest region. However, this does not answer the problem posed by lavas from Diarizos have little enrichment.

Enrichment of lavas resulting from proximity to transform faults is apparent in analogue lavas from the Garrett Transform in the East Pacific Rise, the northern Lau

Basin and also the tips of the East Scotia Ridge. The models provided for lithospheric component addition in these environments is that decompression melting of asthenospheric mantle takes place as material rises beneath the younger, thinner side of the a transform fault.

The observed pattern of for lithospheric component is probably a result of the combination of both proximity to the paleo-transform fault and increased enrichment towards the east. The zone of high for lithospheric component corresponds with the zone of low subduction enrichment.

The increase in for lithospheric component with proximity to the transform fault could be a consequence of the mantle source being cooler; therefore the mantle will not melt as extensively. This may result in products of low-degree partial melts that enrich the from which the lavas were derived. In addition, hydrous fluids generated by the subduction zone act to reduce the melting point of the mantle. This allows the production of low-degree partial melts, even where the mantle is too cool to partially melt otherwise. Away from the transform fault, where the mantle is hotter, addition of hydrous fluids will serve to increase the degree of partial melting. Although the mantle source is already depleted (see above), low-degree partial melts will still be enriched in highly incompatible elements, partially negating the effect of asthenospheric depletion.

4.1e) Source and component variations between the Basal Group, Lower Pillow Lavas and the Upper Pillow Lavas.

The debate over geochemical variation between the three lava groups has been ongoing since the early 1970's and this debate was covered in more detail in Section 1.3. Chemical differences between the lava groups are most pronounced within the lavas of northern Troodos. Fig. 4.1e-1 focuses on lavas from the Solea and Mitsero Grabens in order to illustrate differences between the stratigraphically-defined lava groups. The groups can usually be distinguished using Y at 100 ppm Cr (Y_{100}), 'OIB' type enrichment and in the degree of fractional crystallisation (Cr content). The quantity of subduction-derived enrichment, depletion using Gd/Yb and depletion/fractionation using Ti/V do not show significant variation with lava unit.

Fig. 4.1e-1 maps of depletion, partial melting, subduction-derived enrichment and Nb-enrichment within the Basal group, Lower Pillow Lavas and Upper Pillow Lavas of northern Troodos.

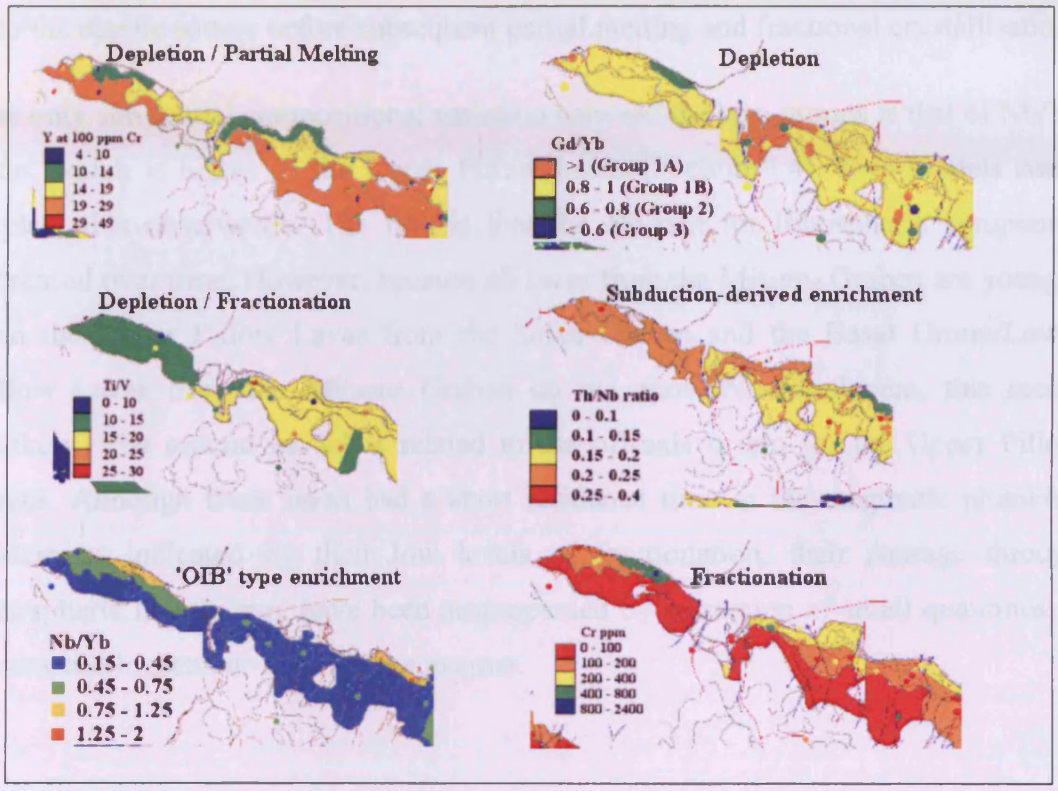

Given that Ti/V is more strongly affected by depletion than fractional crystallisation (fractionated samples were removed from the dataset – section 3.2) and that Gd/Yb-based depletion mapping shows little variation in source depletion between tha lava groups, the large differences between the lava units using Y_{100} could be, at least partially, due to variations in partial melting. If true, the Basal Group lavas must have formed from a lower degree of partial melting than the Upper Pillow Lavas or Upper Pillow Lavas are the least fractionated and the Basal Group are the most fractionated. The primitive nature of the Upper Pillow Lavas indicates a short residence time in the magmatic plumbing system before eruption. This agrees with previous theories, such as those of Thy and Xenophontos (1987) and Schouten and Keleman (2002) that the Upper Pillow Lavas were erupted via off-axis fissures that bypassed the main magma chamber. A small number of Upper Pillow Lava samples from Tilliria are more depleted than nearby Lower Pillow Lava and Basal Group samples. This could be

explained by partial melting of mantle that had already lost small melt fractions during the extraction of the Lower Pillow Lavas and Basal Group.

Because there is no difference in the contribution of the subduction-derived component in the lava groups, it is likely that the subduction component was added into the mantle source before subsequent partial melting and fractional crystallisation.

The only substantial compositional variation between the lava groups is that of Nb/Yb ratio, which is higher in the Upper Pillow Lavas (Section 3.4). Two models could explain this observation. The first is that the Nb-rich for lithospheric component increased over time. However, because all lavas from the Mitsero Graben are younger than the Upper Pillow Lavas from the Solea Graben and the Basal Group/Lower Pillow Lavas from the Mitsero Graben do not show Nb-enrichment, this seems unlikely. The second model is related to the off-axis origin for the Upper Pillow Lavas. Although these lavas had a short residence time in the magmatic plumbing system as indicated by their low levels of fractionation, their passage through lithospheric mantle may have been accompanied by extraction of small quantities of incompatible element-rich into the magma.

4.2) Implications for petrogenesis

Unlike the analogue regions of the Lau Basin, Mariana arc-basin system and the East Scotia Ridge, the exposed area of the Troodos Massif is small. Also, within the Troodos Massif, there are significant changes in composition over small distances. Therefore, the location of the Troodos Massif within any arc-basin-transform system must allow for considerable variations within small areas. Alternatively, if there is no exact modern-day analogue, a model for the origin of the Troodos Massif can be constructed based on the closest available data. In addition, previous models for the origin of the Troodos Massif will be tested.

4.2a) Comparison with models provided by analogue regions

Chapter 3 compared the geochemistry of lavas from the Troodos Massif with the geochemistry of lavas from the analogue regions of the Lau Basin, the East Scotia

Ridge, the Mariana Basin and the Garrett Transform. Comparisons can be made between the analogues and the Troodos Massif by overlaying a geochemical map of the Troodos Massif over a geochemical map of the analogue region. Geochemical maps of analogue regions are taken from Pearce et al. (in press).

Lau Basin

Fig. 4.2a-1 depicts the variation in Nb/Yb and Ba/Yb ratios within the Lau arc-basin system. The Ba/Yb subduction component proxy cannot be used for the Troodos Massif because of Ba mobility though it should resemble the Th/Yb proxy to some extent. A cartoon of the Troodos Massif has been overlain at the same scale. This cartoon is coloured by Nb/Yb or Th/Yb ratio. The Th/Yb contours have been adjusted to take account of the different variances of Th and Ba.

Chapter 3 showed some similarities between geochemical patterns within the Lau Basin and the Troodos Massif. Much of the Lau Basin (southern Peggy Ridge, Central and Eastern Lau Spreading Centres) has a depleted source (using Nb/Yb) and overall degrees of subduction-derived enrichment in these regions are similar to the northern part of the Troodos Massif. Areas of significant Nb-enrichment are found within lavas of the Northern Lau Spreading Centre and the northern portion of the Peggy Ridge. Nb-enrichment in these zones is a combination of proximity to a major transform fault (that turns into the Tonga Trench) and also the presence of a mantle plume in the Samoa area. The Nb/Yb ratio in these areas is similar to or higher than the Nb/Yb ratios within lavas from southern Troodos, Larnaca Graben and the Limassol Forest Complex. The Northern Lau Spreading Centre, because of its proximity to the Tofua Arc as well as the transform fault has very high Ba (Th)/Yb ratios. These ratios are much higher than those recorded within the Troodos Massif. In addition, lavas from parts of the Eastern Lau Spreading Centre and the Valu Fa Ridge have higher subduction-derived content than the Troodos Massif.

Two regions within the Lau arc-basin system (Northern Lau Spreading Centre and the Central/Eastern Lau Spreading Centres) could be considered similar to the two parts of the Troodos Massif (northern Troodos and south/east Troodos). However, the distances involved within the Lau Basin are much greater as is indicated by the small

size of the Troodos Massif cartoon in the bottom left of the figures. Therefore, although some of the processes involved must be similar, dynamics during the formation of the Troodos lavas must have been different.

Fig 4.2a-1 Distribution of depleted source and subduction-enriched zones within the Lau Basin with the Troodos Massif for comparison. (from Pearce et al., 2005)

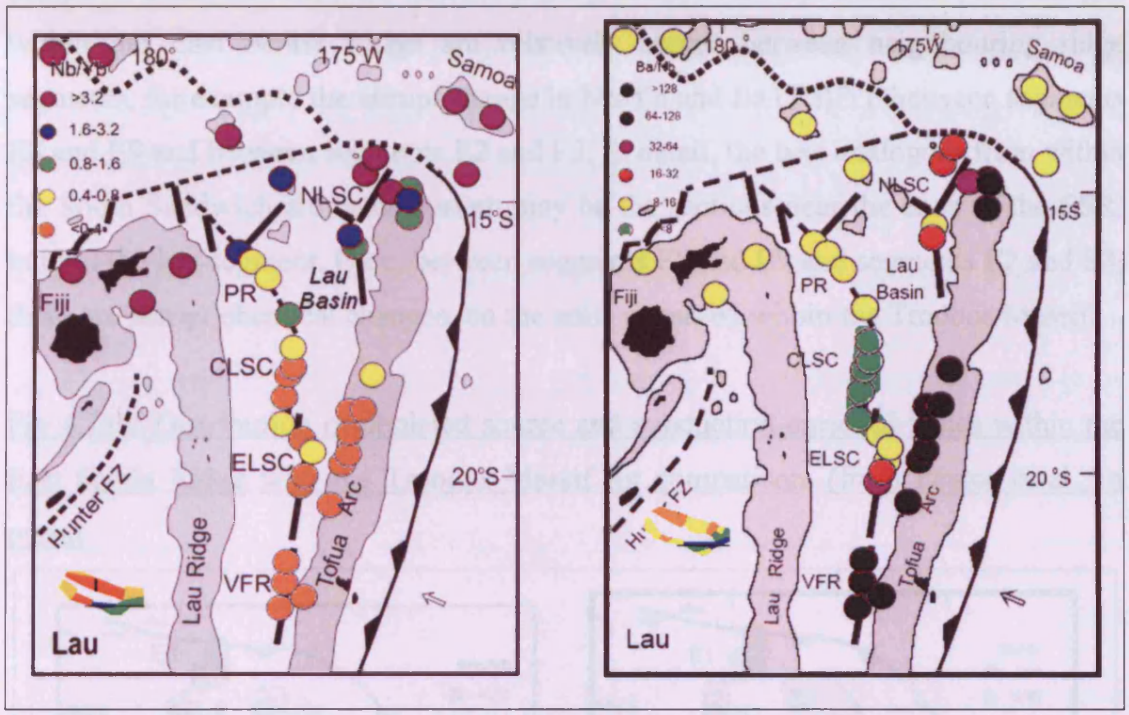

East Scotia Ridge

Fig. 4.2a-2 depicts the variation in Nb/Yb and Ba/Yb within the East Scotia Ridge. Overlain is a cartoon of the Troodos Massif at the same scale. Unlike the Troodos Massif, lavas from the East Scotia Ridge (ESR) are generally derived from asthenosphere that is enriched relative to N-MORB. In detail, lavas from the ridge-transform intersections at each end of the ESR are strongly enriched in Nb and lavas from the central section of the ESR are mildly enriched. The reduction in the degree of enrichment of the central ESR lavas is a function of the mantle flow regime within the mantle wedge. Fertile mantle onlys enter the mantle wedge from each end. As it flows towards the centre it becomes progressively more depleted. Therefore the overall abundances of incompatible elements within the end segments (labelled E1, E2, E9 and E10 on Fig. 4.2a-2) are much higher than those within the Troodos

Massif. The flow towards the centre, combined with increased distance from the subduction zone causes a similar drop-off in Th/Yb ratios toward the centre.

Comparing the relative sizes of the South Sandwich arc-basin system and the Troodos Massif, the South Sandwich arc-basin system is a better analogue for the Troodos Massif than the Lau Basin in terms of the degree of variation recorded over short distances. Changes within the Lau basin are gradual, over large distances, but changes within the East Scotia Ridge are relatively abrupt between neighbouring ridge segments, for example the abrupt change in Nb/Yb and Ba (Th)/Yb between segments E8 and E9 and between segments E2 and E3. In detail, the best analogues from within the South Sandwich arc-basin system may be the sections near the ends of the ESR, but not the last segment. Here, between segments E8 and E9 and segments E2 and E3, there are abrupt chemical changes on the scale observed within the Troodos Massif.

Fig 4.2a-2 Distribution of depleted source and subduction-enriched zones within the East Scotia Ridge with the Troodos Massif for comparison. (from Pearce et al., in press)

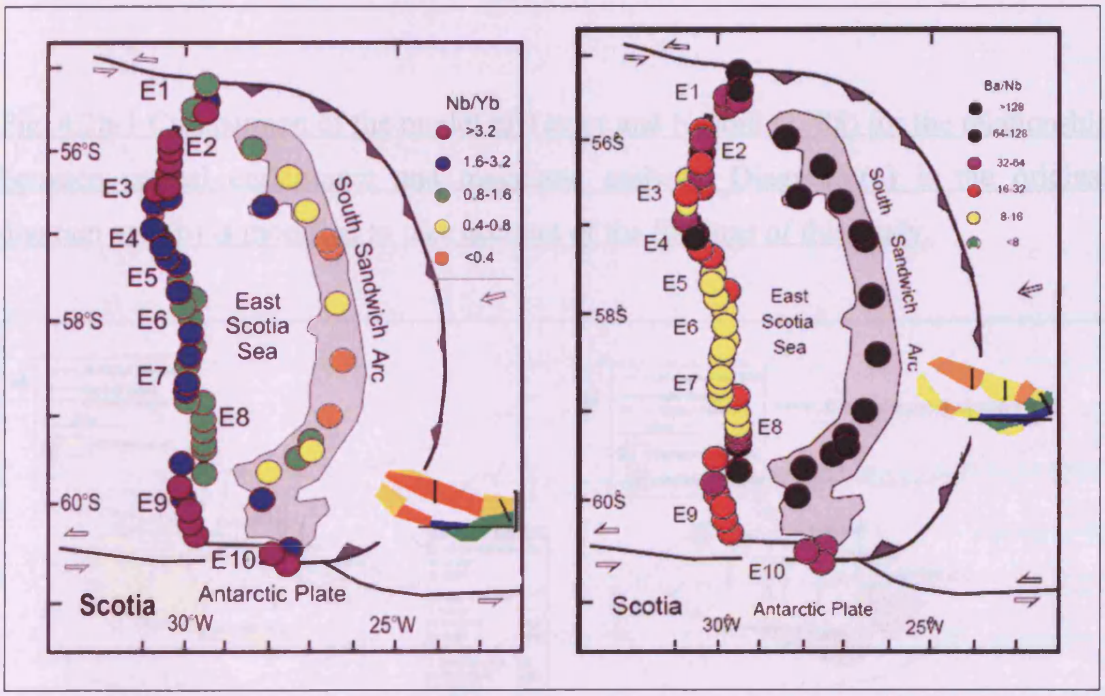

4.2b) Comparison of previous Troodos Massif Models

Taylor and Nesbitt (1988)

Fig. 4.2b-1 (a) reproduced from Fig. 1.4-29 is an early attempt by Taylor and Nesbitt (1988) to produce a geochemical map of the Troodos Massif based on trace element enrichment Their enrichment parameters were rare-earth element profiles, Zr/P and εNd. Using this diagram, Taylor and Nesbitt (1988) argued that the Troodos Massif lay to the north east of the paleo-subduction zone on the basis that the south and west portions of the Troodos Massif were the most enriched.

This model can be further developed using the research described here. The enrichment parameters used by Taylor and Nesbitt (1988) can be produced by both subduction and lithospheric enrichment, a distinction that was not made at the time. Zr enrichment is lithospheric-derived and LREE enrichment can be derived from both subduction and an lithospheric component (Pearce et al. 2005). Fig. 4.2b-1 (b) shows the enrichment pattern split into OIB-type and subduction-derived.

Fig. 4.2b-1 Comparison of the model of Taylor and Nesbitt (1988) for the relationship between crustal enrichment and magmatic grabens. Diagram (a) is the original diagram and (b) is modified to take account of the findings of this study.

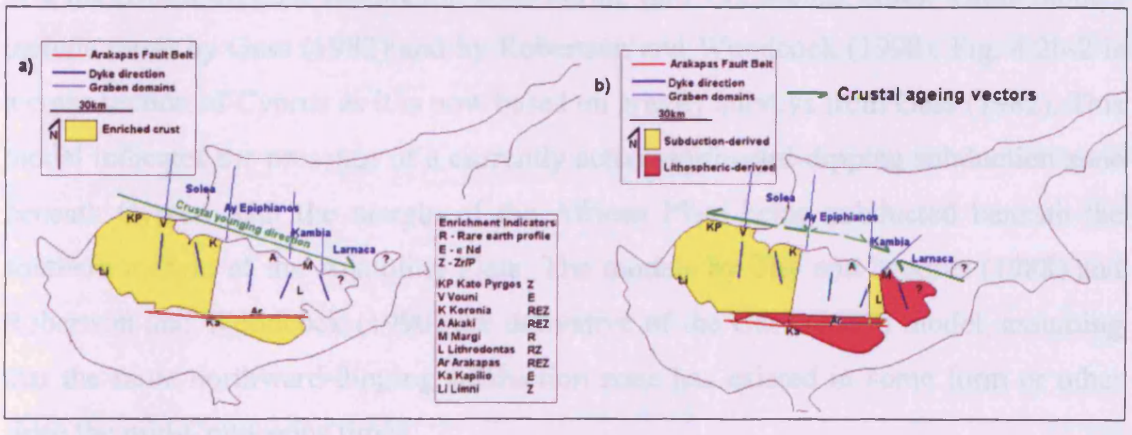

Structural studies by authors such as Allerton and Vine (1991) and Hurst et al. (1994), as well as the chemical mapping in this thesis (Section 4.1), indicate that the original crustal younging vector (in green) shown on the left-hand diagram of Fig. 4.2b-1 (a) needs modification. A series of crustal ageing vectors have been applied to the righ-hand diagram (b) in green. The area referred to by Taylor and Nesbitt (1988), as the Kambia Graben appears to be a slice of crust, originally formed at the Solea Graben, within which the Mitsero (Ayios Epiphianos) Graben later formed. This is shown on diagram (b) as a narrow yellow (subduction-enriched) band. The Mitsero Graben, which has little enrichment (either subduction-derived or lithospheric) is left uncoloured.

The modifications to this diagram do not greatly contradict the original findings of Taylor and Nesbitt (1988). Fig. 4.2b-1 (b) still indicates that western Troodos (lavas formed at the Solea Graben) has the highest subduction component and that the Larnaca Graben and Limassol Forest Complex areas, although enriched, lack significant subduction-derived enrichment. What the original figure (a) does not show is the distribution of lithospheric enrichment compared to subduction-derived enrichment.

Comparison with structural models

Structural models for the eastern Mediterranean region typically invoke the presence of a northward-dipping subduction zone during mid-Cretaceous times. These models include those by Gass (1982) and by Robertson and Woodcock (1990). Fig. 4.2b-2 is a cross section of Cyprus as it is now based on gravity surveys from Gass (1982). This model indicates the presence of a currently active northward-dipping subduction zone beneath Cyprus with the margin of the African Plate being subducted beneath the southern margin of the Anatolian Plate. The models by Thy and Moores (1988) and Robertson and Woodcock (1990) are derivative of the Gass (1982) model, assuming that the same northward-dipping subduction zone has existed in some form or other since the mid-Cretaceous times.

Fig. 4.2b-2 Model of Gass (1980) based on gravity measurements placing the Troodos Massif above a northerly-dipping subduction zone located to the south of Cyprus.

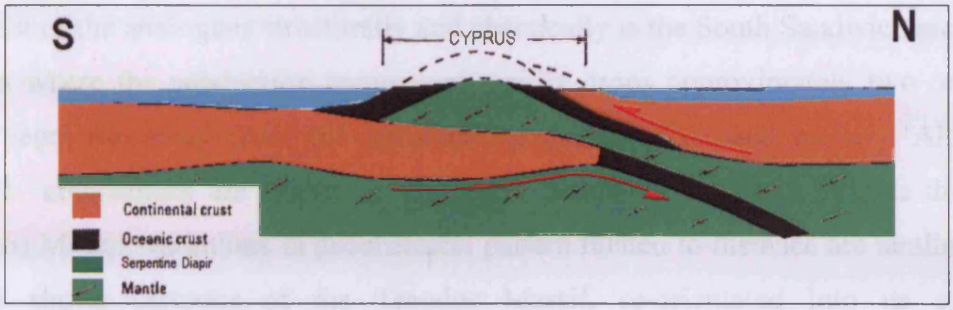

The structural models of Gass (1980) and MacLeod (1990) cause a problem because their includes a north-dipping subduction zone is not obviously compatible with the distribution of subduction component within the Troodos Massif. The result of the 90o anticlockwise rotation of Cyprus is that the Larnaca Graben originally lay to the south (near to the subduction zone) and that the Solea Graben originally lay to the north (further from the subduction zone) using the models of Gass (1982), Thy and Moores (1988) and Robertson and Woodcock (1990). This would mean that subduction influence is strongest further away from the subduction zone and this is not consistent with evidence from analogue regions (discussed in detail in Section 4.2a).

Dilek et al. (1990)

The model of Dilek et al. (1990) includes the presence of multiple and short-lived subduction zones in the Tethys Ocean during the Cretaceous period and so allows the possibility of the existence of a southward-dipping subduction zone. Dilek et al. (1990) proposed that the plate being subducted was the Paleotethys oceanic plate, and that the basin which opened up above the subduction zone was Neotethys. The Neotethys mid-ocean ridge was aligned approximately east-west. Only later, during the closure of the Neotethys, did the present northward-dipping subduction zone form.

This model has advantages over the model of Taylor and Nisbett (1988). By allowing a southward-dipping subduction zone to the north of the Troodos Massif in the mid-Cretaceous, it eliminates the problem of the most subduction-enriched lavas from the

Solea Graben, lavas having formed further from the subduction zone than the non-enriched lavas of the Larnaca Graben.

The best of the analogues structurally and chemically is the South Sandwich arc-basin system where the subduction component rapidly drops approximately two or three ridge segments away from the terminal transforms (discussed earlier). Although overall abundances are higher in the South Sandwich arc-basin system than the Troodos Massif, variations in geochemical pattern related to distance are similar. Fig. 4.2b-3 shows cartoons of the Troodos Massif, re-orientated into its original configuration overlaid onto the South Sandwich arc-basin system. The South Sandwich arc-basin system has been re-orientated to provide the best match for the chemical variations observed within the Troodos Massif. In this model, the Troodos Massif corresponds to an area comprising two spreading segments near to, but not at the tip of the spreading centre. If the Troodos Massif was a remnant of the segment adjacent to the major transform fault, one would expect a higher input of fertile mantle across the transform. Also, one could expect a higher degree of OIB-type component throughout the ophiolite. However, the higher OIB-type component within the entirety of the Limassol Forest Complex would indicate that this part of the Troodos Massif was closer to any possible terminal transform fault than the northern section of Troodos.

Fig. 4.2b-3 comparison of the Troodos Massif with the East Scotia Ridge (from Pearce, in press) for Nb/Yb and Th/Nb. the Troodos Massif has been returned to its original orientation and the East Scotia Ridge and arc system has been reorientated to best fit the geochemistry of the Troodos Massif.

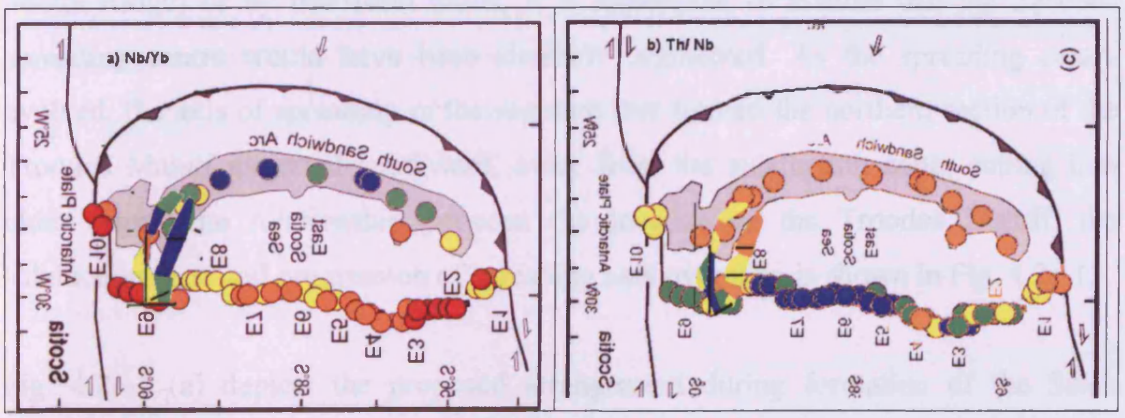

4.2c) Relationship between the Troodos Massif, the paleo-subduction zone, the Neotethys basin and the Paleotethys Ocean.

The majority of the accepted structural models for the formation of the Troodos Massif (e.g. Gass, 1982; Robertson and Woodcock, 1990, as well as models proposed by MacLeod, 1990 and MacLeod and Murton, 1993), indicate that the Troodos Massif formed as a section of Neotethys ocean floor to the north of a northwards-dipping subduction zone, the remnants of which form the Hellenic and Cyprus Trenches. Geochemical models (e.g. Taylor and Nisbett, 1988) for the formation of the Troodos Massif favour the formation of the Troodos Massif above a southwards-dipping subduction zone on the basis of increased subduction enrichment in lavas originally formed to the north. The geochemical maps produced in this study concur with these previous findings. Models resulting from the two methods (geochemical mapping and structural analysis) contradict each other. Only one structural model (Dilek et al., 1990) favours the existence of a southward-dipping subduction zone during the formation of the Troodos Massif. . Using a combination of the Dilek et al. (1990) model and the geochemical evidence, the following model for the formation of the Troodos Massif is proposed.

According to this model, the Troodos Massif formed as a section of Neotethys oceanic crust, above a southward-dipping subduction zone with the Paleotethys oceanic plate being subducted. The opening of the Neotethys was accompanied by the formation of a major transform fault at the western end of the spreading centre. Considering that the majority of spreading centres are segmented, with segments separated either by overlapping spreading centres (as in the Lau Basin and the East Scotia Ridge) or by transform faults, it is reasonable to assume that the Troodos spreading centre would have been similarly segmented. As the spreading centre evolved, the axis of spreading in the segment that formed the northern section of the Troodos Massif migrated southward, away from the subduction zone, cutting into older crust. The relationship between the location of the Troodos Massif, the subduction zone and progression of spreading axis over time is shown in Fig. 4.2c-1.

Fig. 4.2c-1 (a) depicts the proposed arrangement during formation of the Solea Graben, while (b) illustrates the effect of the opening of the Mitsero Graben, cutting

into pre-existing Solea Graben-generated crust (the inactive Solea Graben is shown in grey). (c) illustrates the final layout with the active Larnaca Graben in black and the other grabens being inactive. Again, this graben cut into Solea Graben-genrated crust, rather than into Mitsero Graben-generated crust. Although there is no evidence about its location, the location of the Limassol Forest Complex spreading axis is being assumed to be stationary for the purposes of this model.

The migration of spreading away from the subduction zone resulted in the reduced subduction component of lavas from the Mitsero and Larnaca Grabens. In addition, the migration of the spreading axis allowed the tapping of mantle sources that were less depleted or had been refreshed by inflow of mantle from the end of the subduction zone. Within this model, it is also plausible that migration of the spreading axis was linked to the input of fertile mantle across the terminal transform fault that over time propagated as far as the Troodos spreading centre.

Fig. 4.2c-1 General layout of the Troodos Massif with respect to the paleo-subduction zone. Cartoons (a) to (c) show progression of magmatism away from the subduction zone as snapshots in time. The approximate boundary of the Troodos Massif is shown by the red rectangle. Black ridge axes are active and grey ridge axes are relicts.

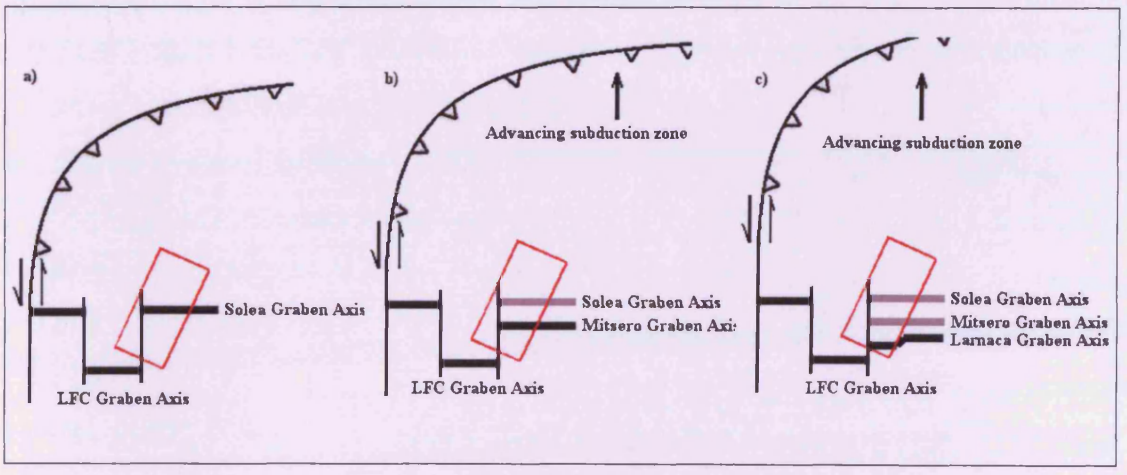

The general arrangement in cross-section during the formation of the Larnaca Graben is depicted in Fig. 4.2c-2. This model is based on that of Dilek et al. (1990) with refinements. The relationship between the shrinking Paleotethys, surrounded on both

sides by subduction zones and the expanding Neotethys is clear. Although there is no direct proof, on the basis of analogue subduction systems (e.g. Mariana, South Sandwich, Tonga) it is likely that the southern Paleotethys subduction zone underwent roll-back, so producing the extension necessary to generate oceanic crust.

Fig. 4.2c-2. Cross section through the Eastern Mediterranean during mid-Cretaceous times showing the relationship of the opening Neotethys basin to the subducting Paleotethys plate. Also shown is the relationship between the three magmatic grabens within northern Troodos.

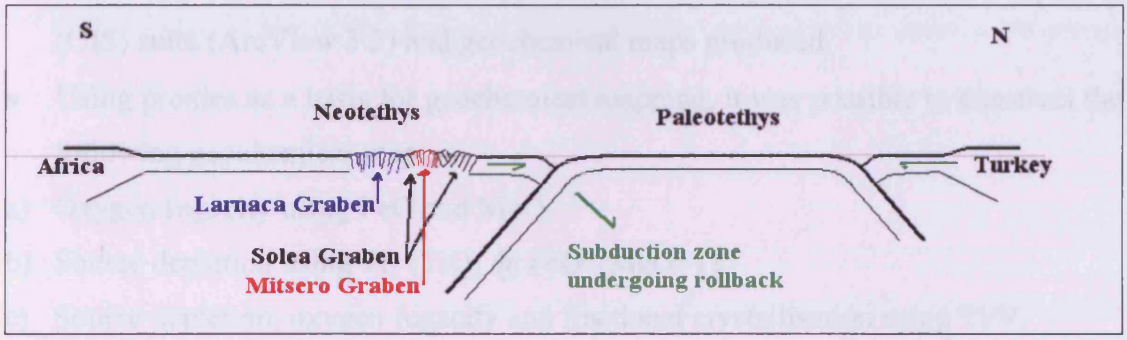

5) Conclusions

5.1) Data collection and geochemical mapping

- The existing geochemical database for lavas form the Troodos Massif has been expanded considerably. 240 samples have been analysed for an extensive suite of major and trace elements. This has significantly improved the sample density.
- The elements Fe, Mg, Ti, V, Cr, Y, Nb, Ta, Th and REE were studied most closely.
- The Troodos Massif has been mapped within a Geographic Information Systems (GIS) suite (ArcView 3.2) and geochemical maps produced.
- Using proxies as a basis for geochemical mapping, it was possible to construct the following geochemical maps:

a) Oxygen fugacity using FeO and MgO.
b) Source depletion using Ti_1 (TiO_2 @ FeO*/MgO=1).
c) Source depletion, oxygen fugacity and fractional crystallisation using Ti/V.
d) Partial melting and source depletion using Y_{100} (Y@ Cr=100ppm)
e) Fractional crystallisation using Cr content
f) Subduction-derived input using Th/Nb
g) Source depletion using Nb/Yb
h) Source depletion and combined subduction-derived and OIB-type enrichment using LREE/MREE and MREE/HREE
i) Mantle source depletion, OIB-type and subduction-derived components by splitting multi-element spider diagrams

- Maps of the proxies were combined to produce maps for mantle source depletion, OIB-type component, fractional crystallisation and subduction-derived component.
- The resulting maps were used to highlight variations in the petrogenesis of lavas within the Troodos Massif as summarised below. On the basis of the evidence presented in Chapters 3 and 4 of this study, the following conclusions can be drawn.

5.2) Implications for the relationship between the stratigraphic lava groups

- Compositional variations between the Basal Group, Lower Pillow Lavas and the Upper Pillow Lavas in a single region are a result of variations in degree of partial melting of the mantle source and fractional crystallisation that the resulting magma underwent.
- Within the majority of lavas from the Solea and Mitsero Grabens in the north of the Troodos Massif, the degree of partial melting decreases upwards through the lava pile.
- Within the majority of lavas from the Solea and Mitsero Grabens in the north of the Troodos Massif, the degree of fractionation decreases upwards through the lava pile.

5.3) Implications for graben development

- Variations in source depletion and subduction derived and OIB-type enrichment has proved that the three structurally-defined grabens (Solea, Mitsero and Larnaca) also have distinctive geochemical compositions and so formed by crustal accretion rather than amagmatic extension.
- Geochemical mapping allows the boundaries of the grabens to be accurately defined on the basis of lateral change in lava compositions. Thus it has been found that the Larnaca Graben was formed within crust generated at the axis of the Solea Graben rather than within Mitsero Graben-generated crust as previously assumed.
- Geochemical mapping reveals that a sliver of Solea Graben-type crust exists in the Kambia area, sandwiched between the Mitsero and Larnaca Grabens. This sliver was recognised as not belonging to the Mitsero or Larnaca Grabens by Taylor and Nesbitt (1988) and was referred to as the Kambia Graben.
- Subduction input decreases in the order Solea Graben, Mitsero Graben and Larnaca Graben, indicating that the subduction input decreased either in space or time during the formation of the Troodos Crust.

5.4) Implications for the effect of a transform fault on lava composition

- The composition of lavas of the Troodos Massif is strongly influenced by proximity to the paleo-transform fault also known as the Arakapas Fault Belt.
- Lavas are more primitive in close proximity to the fault.
- The mantle source becomes more depleted in incompatible elements within 10 km of the fault
- In addition, proximity to the transform fault increases the enrichment by a lithospheric or OIB-type component.
- Enrichment of the mantle source by subduction-derived components is independent of proximity to the paleo-transform fault.

5.5) Implications for the tectonic setting of the Troodos Massif within the Eastern Mediterranean

- Assuming subduction-derived components increase with proximity to the paleo-subduction zone, the approximate location of the paleo-subduction zone may be determined.
- The Neotethys at least began life as a supra-subduction zone spreading centre.
- The increase in subduction component northwards (assuming the original orientation of the Troodos Massif) favours models that place the subduction zone to the north of Cyprus.

Appendix 1) Data tables

Abbreviations used:

BG - Basal Group

LPL – Lower Pillow Lavas

UPL – Upper Pillow Lavas

SDC – Sheeted Dyke Complex

Bon - Boninite

Stavr'ni - Stavrovouni

Lith'da – Lithrodonda

Kat'as – Kataliondas

AOP – Ayios Onouphrios Potamos (Kambia)

Note that iron content given as total (FeO*), rather than individual oxide contents

Sample Naming Conventions

CC2/xxx – Collected by the author, February 2002

CC5/xxx - Collected by the author, February 2005 (No major element data)

Samples with the prefixes A, E, G, K, M and X collected by Taylor, 1985, analysed by the author, 2005. Previously reported as XRF analyses (Taylor, 1987)

91CCxx – Collected by MacLeod, 1991, analysed by the author, 2005

97CCxx – Collected by MacLeod, 1997, analysed by the author, 2005

85-xx - Collected by MacLeod, 1985, analysed by the author, 2005

YL-x – Collected by Pearce, date unknown, analysed by the author, 2005

	CC2/001	CC2/002	CC2/003	CC2/004	CC2/005	CC2/006	CC2/007	CC2/008	CC2/009	CC2/013	CC2/014	CC2/015	CC2/016	CC2/018
Lava	BG	BG	BG	BG	BG	BG	BG	LPL	BG	BG	BG	BG	BG	BG
	Akaki	*Akaki*	*Akaki*	*Akaki*	*Akaki*	*Akaki*	*Akaki*	*Akaki*	*Kambia*	*Kambia*	*Kambia*	*Kambia*	*Kambia*	*Kapedes.*
X	11917	11917	11935	12311	12313	12686	12948	13078	22670	22542	22211	22195	22148	22836
Y	70911	70911	70985	72665	72670	73005	73260	73560	71569	71436	71280	71394	71575	70553
SiO_2	64.28	59.87	52.00	52.80	54.71	54.39	58.49	57.63	57.98	55.62	51.26	51.84	53.61	53.38
TiO_2	1.09	1.28	1.18	0.59	1.47	1.07	1.10	0.68	1.05	1.14	0.68	1.05	0.92	0.95
Al_2O_3	13.26	13.75	14.01	13.44	14.54	13.24	13.35	13.34	14.31	13.90	15.87	13.98	13.68	15.07
FeO*	9.25	11.01	12.25	8.47	13.81	16.19	11.72	8.15	9.34	12.59	9.47	10.19	9.41	8.74
MnO	0.13	0.15	0.28	0.19	0.23	0.22	0.33	0.11	0.05	0.12	0.07	0.12	0.11	0.07
MgO	2.99	3.13	6.94	8.67	4.59	3.94	5.55	2.49	3.05	5.54	8.08	5.74	3.20	3.76
CaO	1.74	2.34	2.19	7.54	3.66	1.17	1.31	4.44	3.43	4.43	3.13	4.89	6.61	5.94
Na_2O	5.63	5.88	4.14	4.34	5.32	2.92	3.45	3.88	3.24	2.20	4.94	2.60	2.49	1.91
K2O	0.02	0.10	0.02	0.05	0.08	0.03	0.03	0.56	0.41	0.81	0.23	0.45	0.50	0.16
P_2O_5	0.17	0.15	0.99	0.06	0.12	0.10	0.13	0.29	0.09	0.11	0.07	0.10	0.09	0.09
LOI	2.45	2.60	4.50	3.89	3.22	7.31	4.15	8.74	7.68	4.81	7.04	9.06	7.81	8.39
Tot	101.01	100.26	98.49	100.04	101.74	100.56	99.61	100.31	100.62	101.27	100.84	100.02	98.45	98.46
Sc	27	30	35	41	35	31	28	19	34	32	35	35	36	42
Ti	6549	7683	7062	3540	8827	6395	6596	4077	6283	6839	4052	6300	5516	5712
V	37	165	336	222	451	389	215	10	309	375	227	344	293	322
Cr	4	2	7	455	6	2	3	1	3	3	73	4	13	9
Co	16	14	34	36	34	31	15	9	11	34	36	35	34	20
Ni	2	2	7	395	217	3	4	1	4	4	158	6	11	9
Cu	35	24	7	93	30	247	30	8	141	7	110	98	70	115
Zn	69	34	151	62	102	171	268	101	187	108	54	88	183	262
Ga	14	17	19	11	19	16	17	18	16	17	14	18	16	18
Rb	0	1	0	0	1	0	0	9	1	3	1	2	3	1
Sr	30	104	14	161	28	53	50	131	161	111	114	112	86	122
Y	41	41	32	15	32	25	34	61	25	34	19	35	26	29
Zr	76	69	50	27	58	48	65	137	59	69	33	61	52	54
Nb	1.80	1.65	1.06	0.59	0.89	1.26	1.42	2.34	1.15	1.06	0.77	1.46	0.96	0.94
Cs	0.00	0.01	0.00	0.01	0.01	0.00	0.00	0.06	0.00	0.00	0.01	0.00	0.01	0.01
Ba	3	10	1	13	28	5	6	25	29	23	12	14	21	13
La	3.70	3.56	2.19	0.98	2.71	1.95	2.62	5.33	2.21	2.68	1.38	2.73	2.61	2.43
Ce	11.94	10.69	6.98	2.97	7.48	5.65	8.14	15.93	4.60	7.79	3.76	7.30	6.72	6.15
Pr	1.91	1.86	1.28	0.54	1.34	0.99	1.48	2.80	1.09	1.41	0.68	1.38	1.17	1.24
Nd	10.29	10.21	7.16	3.01	7.33	5.47	8.19	15.18	5.83	7.68	3.76	7.50	6.29	6.72
Sm	3.81	3.71	2.71	1.20	2.71	2.01	3.08	5.37	2.18	2.82	1.48	2.71	2.34	2.42
Eu	1.20	1.34	0.96	0.38	1.00	0.72	0.95	1.77	0.86	1.01	0.55	1.03	0.90	0.94
Gd	5.31	5.29	3.90	1.67	3.79	2.93	4.27	7.56	3.12	4.10	2.05	4.07	3.34	3.52
Tb	0.99	0.98	0.74	0.35	0.76	0.56	0.82	1.39	0.61	0.78	0.42	0.75	0.62	0.66
Dy	6.46	6.35	4.87	2.37	5.07	3.73	5.43	9.11	4.04	5.11	2.88	4.84	4.11	4.31
Ho	1.42	1.38	1.06	0.53	1.07	0.83	1.19	2.01	0.89	1.14	0.65	1.08	0.91	0.93
Er	4.12	4.03	3.05	1.53	3.26	2.41	3.46	5.85	2.60	3.34	1.88	3.08	2.64	2.69
Tm	0.64	0.63	0.48	0.25	0.52	0.38	0.54	0.93	0.41	0.52	0.31	0.48	0.42	0.42
Yb	4.09	4.02	3.12	1.58	3.30	2.42	3.47	5.96	2.59	3.39	1.97	3.01	2.73	2.67
Lu	0.64	0.63	0.48	0.25	0.52	0.38	0.50	0.93	0.39	0.54	0.31	0.48	0.44	0.41
Hf	2.33	2.24	1.56	0.84	1.85	1.42	1.94	3.87	1.79	2.01	1.04	1.77	1.51	1.56
Ta	0.12	0.11	0.07	0.04	0.08	0.07	0.10	0.15	0.09	0.08	0.05	0.09	0.06	0.07
Pb	1.05	0.44	2.32	1.01	0.29	3.11	0.84	2.25	8.71	0.77	1.79	0.88	5.21	2.96
Th	0.32	0.28	0.17	0.14	0.26	0.23	0.23	0.48	0.25	0.24	0.16	0.25	0.19	0.23
U	0.13	0.11	0.09	0.08	0.13	0.31	0.15	0.25	0.37	0.13	0.16	0.19	0.12	0.26

	CC2/112	CC2/115	CC2/110	CC2/111	CC2/116	CC2/076	CC2/077	CC2/078	CC2/079	CC2/080	CC2/081
Lava	BG	BG	BG	BG	LPL	LPL	LPL	LPL	LPL	LPL	LPL
	Kalo	*Kalo*	*Kalo*	*Kalo*	*Kalo*	*Peristerona*	*Peristerona*	*Peristerona*	*Peristerona*	*Peristerona*	*Peristerona*
	Chorio	*Chorio*	*Chorio*	*Chorio*	*Chorio*	*canyon*	*canyon*	*bridge*	*bridge*	*bridge*	*bridge*
X	13710	13816	14954	13710	13860	7719	7719	7021	7021	7021	7021
Y	68586	70609	73438	68586	71503	76688	76688	79211	79211	79211	79211
SiO_2	52.64	53.46	61.86	45.08	57.35	55.86	49.30	48.22	50.47	46.55	57.67
TiO_2	1.28	0.51	0.42	0.54	1.16	1.10	1.23	1.54	0.40	0.31	1.32
Al_2O_3	14.29	13.88	12.24	14.83	12.59	14.12	13.80	15.80	12.97	14.47	14.13
FeO*	13.07	8.44	10.13	11.23	10.47	10.33	11.24	11.70	7.90	8.58	7.77
MnO	0.16	0.15	0.22	0.17	0.06	0.13	0.14	0.17	0.13	0.21	0.24
MgO	5.33	9.85	2.57	7.78	10.13	3.86	5.60	3.41	6.76	10.59	1.65
CaO	4.65	4.52	9.57	8.21	0.19	5.45	6.47	7.60	13.34	6.29	8.25
Na_2O	3.96	4.64	0.01	0.45	0.32	2.41	2.26	3.05	1.54	2.06	3.09
K_2O	0.95	0.01	0.00	0.15	0.02	0.94	0.59	0.51	0.85	1.13	0.89
P_2O_5	0.10	0.06	0.05	0.05	0.06	0.07	0.10	0.13	0.05	0.03	0.13
LOI	4.50	5.56	3.47	11.08	7.04	7.20	7.63	9.23	5.47	11.09	4.19
Tot	100.93	101.08	100.54	99.57	99.39	101.46	98.37	101.35	99.89	101.31	99.34
Sc	40	38	25	37	25	32	33	38	41	45	25
Ti	7662	3082	2520	3240	6951	6619	7404	9219	2424	1884	7935
V	451	226	183	253	281	317	399	368	211	225	180
Cr	31	505	61	33	2	4	6	1	375	235	3
Co	39	34	7	25	32	26	38	38	32	38	22
Ni	60	107	1	37	10	6	29	7	18	29	16
Cu	100	65	271	25	7	79	62	53	12	76	23
Zn	54	72	21	74	20	99	72	115	46	61	112
Ga	17	11	13	14	14	17	16	21	12	11	17
Rb	5	0	0	0	0	12	7	13	32	16	15
Sr	139	69	95	27	5	100	96	143	69	39	106
Y	29	14	15	16	9	32	31	43	14	6	38
Zr	51	25	17	20	54	59	70	104	22	14	98
Nb	1.11	0.53	0.51	0.82	1.02	1.06	1.01	1.59	0.74	0.53	1.45
Cs	0.02	0.02	0.00	0.01	0.02	0.05	0.03	0.36	1.72	0.24	0.16
Ba	26	9	3	2	9	45	45	13	13	14	31
La	2.07	0.96	1.09	0.72	0.76	2.32	2.42	3.89	0.90	0.22	3.23
Ce	6.24	2.88	2.54	1.80	2.12	7.05	7.35	11.86	2.53	0.79	9.66
Pr	1.15	0.52	0.52	0.34	0.38	1.24	1.31	2.06	0.45	0.08	1.72
Nd	6.37	2.84	2.89	1.94	2.09	6.77	7.17	11.14	2.54	0.48	9.36
Sm	2.41	1.09	1.17	0.86	0.84	2.50	2.66	3.90	1.03	0.30	3.42
Eu	0.97	0.39	0.56	0.36	0.12	0.97	0.97	1.41	0.41	0.16	1.23
Gd	3.52	1.56	1.77	1.34	1.07	3.62	3.50	5.51	1.56	0.57	4.36
Tb	0.67	0.32	0.33	0.30	0.22	0.69	0.72	1.01	0.30	0.14	0.88
Dy	4.40	2.16	2.26	2.13	1.50	4.48	4.82	6.52	2.09	1.01	5.74
Ho	0.98	0.46	0.50	0.50	0.35	1.00	1.08	1.41	0.46	0.23	1.26
Er	2.83	1.41	1.48	1.47	1.12	2.97	3.17	4.05	1.40	0.71	3.64
Tm	0.44	0.22	0.23	0.25	0.21	0.47	0.52	0.63	0.23	0.12	0.59
Yb	2.82	1.44	1.47	1.60	1.46	3.08	3.29	3.97	1.49	0.85	3.68
Lu	0.44	0.23	0.22	0.26	0.26	0.49	0.54	0.60	0.24	0.14	0.58
Hf	1.55	0.79	0.61	0.66	1.74	1.75	1.96	2.79	0.75	0.54	2.70
Ta	0.07	0.03	0.03	0.07	0.08	0.07	0.08	0.11	0.05	0.04	0.11
Pb	0.41		1.74	0.22	3.42	1.12	0.81	1.42	0.45	2.06	0.71
Th	0.15	0.12	0.09	0.09	0.26	0.22	0.20	0.28	0.08	0.08	0.30
U	0.08	0.09	0.10	0.04	0.25	0.15	0.10	0.19	0.11	0.05	0.77

Sample	CC2/024	CC2/026	CC2/027	CC2/029	CC2/031	CC2/030	CC2/082	CC2/083	CC2/084	CC2/085	CC2/129	CC2/129a
Lava	BG	BG	BG	BG	LPL	BG	BG	BG	BG	BG	LN	LN
	Xyliatos	*Xyliatos*	*Xyliatos*	*Xyliatos*	*Xyliatos*	*Xyliatos*	*Xyliatos*	*Xyliatos*	*Xyliatos*	*Xyliatos*	*Nikitari core*	*Nikitari village*
X	3647	3612	3508	1824	3445	3475	2633	3567	2641	2385	-500	-600
Y	73457	73549	74520	75402	76116	75525	75629	75585	75586	75015	80500	80000
SiO_2	54.79	60.48	55.55	53.14	60.22	57.82	58.12	58.12	59.26	59.13	55.08	53.36
TiO_2	1.04	0.96	1.29	1.34	1.21	1.34	1.24	1.24	1.23	1.28	1.36	0.57
Al_2O_3	16.14	13.11	13.49	13.90	12.56	13.92	13.65	13.65	11.33	13.82	14.38	15.56
FeO*	11.67	12.09	11.77	13.08	10.49	12.37	10.74	10.74	14.07	10.09	11.20	8.43
MnO	0.23	0.32	0.13	0.15	0.12	0.22	0.13	0.13	0.16	0.06	0.11	0.21
MgO	4.34	5.27	5.13	4.98	3.75	5.00	3.83	3.83	3.53	2.26	3.26	6.80
CaO	5.59	2.13	2.55	2.56	3.43	3.66	1.82	1.82	1.23	2.16	7.22	0.70
Na_2O	5.57	3.62	4.88	5.14	3.22	3.38	5.03	5.03	3.94	5.80	2.98	1.82
K_2O	0.02	0.01	0.12	0.07	0.64	0.97	0.15	0.15	0.04	0.17	0.75	2.14
P_2O_5	0.11	0.09	0.10	0.10	0.17	0.12	0.11	0.11	0.10	0.14	0.11	0.06
LOI	1.83	3.03	5.35	3.35	4.17	3.86	5.67	6.76	3.91	6.30	4.12	10.92
Tot	101.32	101.11	100.35	97.82	99.98	102.65	100.49	101.58	98.81	101.21	100.57	100.58
Sc	36	38	32	34	24	32	30	33	33	29	36	45
Ti	6233	5744	7743	8031	7286	8056	7440	7440	7383	7656	8150	3411
V	315	282	399	411	76	279	186	168	370	236	408	270
Cr	3	14	1	10	1	12	13	1	5	4	54	28
Co	28	29	39	17	20	33	26	22	35	28	39	25
Ni	6	55	6	38	2	42	43	5	22	22	122	39
Cu	38	9	56	46	16	8	33	59	8	43	18	97
Zn	69	126	74	26	96	47	112	119	37	83	80	858
Ga	16	12	17	15	18	17	16	18	15	15	19	13
Rb	0	0	1	8	6	5	1	4	0	1	24	11
Sr	71	10	63	88	72	92	119	127	22	80	112	48
Y	29	24	37	36	47	35	35	41	30	33	28	12
Zr	55	38	77	73	119	76	72	89	47	79	71	28
Nb	0.95	0.82	1.28	1.26	2.01	1.46	1.46	1.26	1.01	1.22	1.20	0.54
Cs	0.00	0.00	0.00	0.01	0.02	0.03	0.02	0.05	0.00	0.01	1.17	0.01
Ba	3	1	10	28	29	26	12	35	2	6	19	40
La	1.52	1.80	3.00	2.51	4.32	2.89	2.67	2.63	2.48	2.66	2.57	1.12
Ce	5.40	5.45	9.21	7.83	13.49	8.56	7.54	6.19	7.38	6.18	7.67	2.20
Pr	1.03	1.00	1.62	1.43	2.36	1.52	1.45	1.35	1.33	1.47	1.38	0.64
Nd	5.94	5.51	8.93	8.00	12.80	8.33	7.98	7.59	7.21	8.03	7.52	3.72
Sm	2.37	2.07	3.25	3.00	4.38	3.08	2.98	2.92	2.67	2.97	2.67	1.19
Eu	0.95	0.81	1.19	1.03	1.46	1.11	1.06	1.21	0.99	1.08	1.07	0.39
Gd	3.48	2.75	4.67	3.98	6.11	4.15	4.05	4.51	3.52	3.84	3.70	1.44
Tb	0.67	0.57	0.86	0.80	1.12	0.83	0.81	0.87	0.72	0.79	0.68	0.26
Dy	4.42	3.78	5.61	5.37	7.27	5.59	5.48	5.85	4.75	5.21	4.42	1.64
Ho	0.97	0.83	1.23	1.20	1.58	1.17	1.16	1.31	1.03	1.14	0.95	0.37
Er	2.84	2.38	3.57	3.46	4.59	3.58	3.55	3.79	2.92	3.30	2.76	1.08
Tm	0.45	0.39	0.56	0.56	0.72	0.57	0.58	0.60	0.46	0.54	0.44	0.18
Yb	2.86	2.36	3.54	3.52	4.59	3.63	3.66	3.78	2.76	3.40	2.78	1.11
Lu	0.44	0.36	0.54	0.56	0.71	0.57	0.59	0.54	0.41	0.52	0.43	0.18
Hf	1.70	1.28	2.21	2.13	3.18	2.31	2.27	2.45	1.50	2.20	1.97	0.88
Ta	0.06	0.06	0.08	0.09	0.13	0.09	0.09	0.10	0.08	0.09	0.08	0.04
Pb	0.66	0.49	1.16	0.20	1.28	0.52	2.28	2.43	0.46	0.94	0.90	3.03
Th	0.19	0.17	0.22	0.23	0.31	0.26	0.26	0.27	0.17	0.24	0.19	0.13
U	0.12	0.08	0.16	0.13	0.19	0.12	0.14	0.16	0.08	0.13	0.16	0.06

Sample	CC5/022	CC5/017	CC5/018	CC5/006	CC5/007	CC5/008	CC5/009	CC5/010	CC5/011	CC5/012	CC5/013	CC5/014	CC5/015	CC5/016
Lava	UPL	LPL	UPL	LPL	UPL	BG	LPL	LPL	BG	BG	BG	UPL	BG	UPL
	Yialias	*Mitsero*	*Agrokipia*	*Linou*	*Lemonas*	*Ayios Theodoros*	*Flasou*	*Korakou*	*Temvira*	*Linou*	*Koutrafas*	*Vyzakia*	*Ayia Marina*	*Ayia Marina*
X	28865	10635	13145	-9430	-8109	-8038	-8707	-10275	-9040	-6904	-36	535	2477	1352
Y	71208	77116	77874	81499	81660	79287	79875	77831	76824	80759	83015	81343	78857	76410
SiO_2														
TiO_2	0.49	0.89	0.36	0.35	1.02	1.19	0.73	0.42	1.40	1.22	0.54	0.59	1.17	1.03
Al_2O_3														
FeO*														
MnO	0.11	0.12	0.07	0.15	0.09	0.13	0.16	0.09	0.13	0.19	0.34	0.36	0.19	0.04
MgO														
CaO														
Na_2O														
K_2O														
P_2O_5														
LOI														
Sc	29	26	25	26	25	21	27	31	32	34	28	30	31	25
Ti	2952	5322	2172	2112	6120	7122	4386	2508	8394	7290	3222	3516	7002	6168
V	149	328	155	189	265	154	260	213	341	429	177	219	356	246
Cr	255	233	149	32	4	6	21	264	29	15	218	135	2	1
Co	29	20	23	24	27	18	32	29	26	38	32	31	30	28
Ni	67	870	30	26	32	6	65	78	14	36	59	42	7	1
Cu	35	10	26	13	57	13	248	56	40	20	55	45	14	7
Zn	58	201	44	52	128	212	56	53	91	101	68	59	97	13
Ga	11	14	9	10	17	14	14	15	19	18	13	14	17	14
Rb	26	4	13	4	10	5	3	4	1	1	15	9	3	6
Sr	75	72	77	41	63	105	111	259	118	99	144	46	98	15
Y	15	21	10	9	17	30	17	10	39	30	19	16	32	27
Zr	25	40	19	13	53	76	43	22	82	62	30	33	69	51
Nb	0.42	0.86	0.39	0.29	0.86	1.29	0.82	0.44	1.37	1.09	0.59	0.53	1.08	0.94
Cs	0.38	0.08	0.11	0.02	0.15	0.02	0.04	0.11	0.05	0.03	0.28	0.10	0.04	0.07
Ba	53	23	15	29	10	35	13	8	16	15	38	27	23	8
La	1.74	1.69	0.75	0.48	1.35	3.09	1.72	0.79	3.16	2.36	2.13	1.35	2.45	1.63
Ce	3.07	4.56	2.17	1.46	5.04	7.78	4.83	1.83	8.63	7.08	4.16	3.85	7.46	4.92
Pr	0.58	0.75	0.35	0.25	0.87	1.42	0.79	0.38	1.52	1.16	0.75	0.62	1.24	0.89
Nd	3.43	4.66	2.23	1.67	5.54	8.72	4.83	2.38	9.31	7.16	4.46	3.79	7.57	5.81
Sm	1.17	1.76	0.84	0.70	2.13	2.97	1.76	0.89	3.32	2.64	1.53	1.36	2.77	2.34
Eu	0.45	0.72	0.34	0.30	0.87	1.06	0.66	0.35	1.21	0.93	0.60	0.54	0.97	0.74
Gd	1.56	2.42	1.13	0.98	2.71	3.82	2.28	1.16	4.43	3.44	2.10	1.79	3.63	3.16
Tb	0.30	0.48	0.23	0.21	0.51	0.72	0.44	0.23	0.87	0.68	0.41	0.35	0.72	0.62
Dy	2.10	3.32	1.62	1.47	3.30	4.80	2.97	1.56	6.09	4.71	2.87	2.45	4.98	4.31
Ho	0.47	0.73	0.35	0.32	0.66	1.02	0.63	0.34	1.34	1.03	0.63	0.54	1.09	0.94
Er	1.39	2.19	1.07	0.96	1.83	2.95	1.79	1.02	3.98	3.03	1.88	1.59	3.21	2.76
Tm	0.23	0.36	0.18	0.16	0.28	0.47	0.29	0.17	0.64	0.48	0.30	0.26	0.52	0.44
Yb	1.41	2.31	1.11	1.01	1.67	2.88	1.75	1.07	3.99	2.95	1.82	1.63	3.20	2.71
Lu	0.22	0.37	0.18	0.17	0.26	0.44	0.27	0.17	0.64	0.45	0.29	0.26	0.48	0.40
Hf	0.80	1.33	0.63	0.49	1.64	2.27	1.38	0.70	2.45	1.89	0.95	1.02	2.11	1.66
Ta	0.04	0.06	0.04	0.03	0.07	0.10	0.07	0.04	0.12	0.09	0.05	0.05	0.09	0.08
Pb	1.02	9.78	0.35	0.42	1.00	1.60	0.42	0.59	0.56	1.52	0.97	0.71	1.17	0.19
Th	0.09	0.18	0.07	0.06	0.19	0.23	0.17	0.11	0.26	0.22	0.13	0.12	0.26	0.17
U	0.09	0.20	0.06	0.05	0.09	0.20	0.50	0.09	0.15	0.12	0.09	0.13	0.17	0.15

Sample	CC2/090	CC2/093	CC2/130	CC2/091	CC2/131	CC5/001	CC5/002	CC5/003	CC5/004	CC5/005
Lava	LPL	LPL	LPL	BG	LPL	LPL	BG	UPL	LPL	BG
	Kato	*Kokkina*	*Mansoura*	*Kokkina*	*Galini core*	*Pano*	*Pyrgos*	*Katydata*	*Lefka Road*	*Ayios*
	Pyrgos		*core*		*MR/15/72*	*Pyrgos*				*Epifianos*
X	-30968	-35099	-34000	-33845	-21000	-28728	-27920	-9624	-15049	-11744
Y	94785	89222	93400	93064	89000	92705	89080	82181	80202	80804
SiO_2	48.26	53.04	65.14	67.85	49.08					
TiO_2	0.78	1.15	0.67	0.95	0.70	0.28	0.43	0.60	0.73	0.88
Al_2O_3	17.99	14.30	13.14	12.84	15.65					
FeO*	10.29	10.80	6.54	5.43	9.72					
MnO	0.13	0.10	0.27	0.03	0.17	0.09	0.09	0.10	0.04	0.13
MgO	5.21	5.74	1.43	0.33	5.40					
CaO	6.22	0.67	3.68	4.21	9.97					
Na_2O	1.41	4.60	0.68	3.00	0.21					
K_2O	1.74	0.40	3.37	0.44	2.09					
P_2O_5	0.11	0.09	0.21	0.12	0.09					
LOI	8.88	8.22	3.07	3.23	5.31					
Tot	101.02	99.09	98.20	98.44	98.39					
Sc	44	36	19	28	35	29	18	24	18	24
Ti	4656	6874	4026	5672	4213	1674	2598	3624	4350	5292
V	350	292	15	238	277	140	194	157	288	294
Cr	23	16	4	10	10	296	14	15	13	-4
Co	31	26	9	11	46	29	25	21	13	24
Ni	18	20	10	9	37	91	26	49	68	-8
Cu	48	67	10	52	109	21	61	29	111	39
Zn	64	90	867	106	78	40	53	64	126	52
Ga	21	15	21	14	16	9	12	10	13	13
Rb	22	2	4	4	6	3	0	12	0	1
Sr	168	76	123	89	91	52	26	31	55	84
Y	29	42	61	26	24	11	10	23	16	25
Zr	50	60	168	58	41	16	21	33	36	49
Nb	0.92	0.98	2.32	0.83	0.80	0.39	0.53	0.85	0.69	0.74
Cs	0.21	0.00	0.02	0.02	0.14	0.03	0.01	0.25	0.01	0.02
Ba	26	14	51	31	6	2	1	20	13	10
La	3.32	2.60	6.12	2.60	1.97	1.03	0.63	3.27	1.11	1.94
Ce	6.36	3.64	18.58	5.77	4.85	2.66	1.95	4.58	3.58	5.61
Pr	1.23	1.40	3.30	1.27	0.83	0.44	0.33	0.91	0.58	0.91
Nd	6.51	7.80	17.70	6.72	4.48	2.72	2.12	5.30	3.63	5.55
Sm	2.30	2.88	6.03	2.39	1.72	0.97	0.87	1.66	1.42	2.03
Eu	0.91	1.07	1.95	0.96	0.66	0.35	0.32	0.52	0.49	0.73
Gd	3.41	4.28	8.41	3.35	2.39	1.30	1.19	2.25	1.87	2.70
Tb	0.65	0.83	1.53	0.62	0.49	0.24	0.24	0.41	0.38	0.53
Dy	4.33	5.65	9.92	4.05	3.32	1.61	1.74	2.85	2.71	3.70
Ho	0.98	1.31	2.16	0.89	0.76	0.35	0.38	0.64	0.60	0.82
Er	2.96	3.92	6.24	2.51	2.22	1.00	1.13	1.87	1.77	2.47
Tm	0.48	0.62	0.99	0.39	0.37	0.16	0.19	0.29	0.29	0.39
Yb	3.24	4.04	6.32	2.47	2.36	0.98	1.16	1.72	1.80	2.46
Lu	0.52	0.65	0.99	0.38	0.38	0.16	0.18	0.27	0.28	0.39
Hf	1.54	1.76	4.47	1.67	1.27	0.55	0.75	1.10	1.17	1.50
Ta	0.06	0.07	0.16	0.06	0.06	0.04	0.05	0.06	0.06	0.06
Pb	1.53	1.37	3.28	2.52	0.75	0.42	0.67	1.20	0.26	0.40
Th	0.21	0.22	0.48	0.20	0.18	0.09	0.10	0.16	0.15	0.16
U	0.23	0.08	0.28	0.17	0.55	0.04	0.07	0.08	0.11	0.11

Sample	CC2/033	CC2/038	CC2/036	CC2/037	CC2/032	CC2/034	CC2/039	CC2/040	CC2/041
Lava	BG	BG	SDC	SDC	BG	BG	BG	BG	BG
	Akamas	*Akamas*	*Akamas*	*Akamas*	*Akamas*	*Akamas*	*Akamas*	*Akamas*	*Akamas*
X	-61679	-61670	-61695	-61488	-61679	-61246	-61246	-61246	-61246
Y	81291	81281	78244	76262	81291	81270	81270	81270	81270
SiO_2	57.32	53.02	56.18	54.44	46.03	57.41	54.04	56.66	50.41
TiO_2	0.45	0.35	0.36	0.30	0.27	0.34	0.33	0.34	0.26
Al_2O_3	13.71	13.75	15.37	14.71	11.78	13.86	13.84	13.54	11.65
FeO*	10.16	7.93	7.45	8.36	9.14	8.12	7.77	8.19	8.35
MnO	0.11	0.15	0.08	0.08	0.21	0.12	0.08	0.19	0.13
MgO	6.16	9.83	7.17	6.06	16.43	9.25	8.61	8.08	13.18
CaO	4.40	8.76	10.46	9.49	3.53	2.59	3.40	4.29	6.47
Na_2O	2.57	1.62	1.70	1.35	2.38	2.18	3.77	3.60	2.29
K_2O	1.29	0.63	0.30	0.48	0.26	2.30	1.77	1.70	0.77
P_2O_5	0.04	0.04	-0.02	-0.02	0.03	-0.02	0.05	0.04	0.04
LOI	4.49	4.41	2.89	5.39	8.16	4.83	6.18	3.53	5.92
Tot	100.71	100.48	101.96	100.66	98.23	100.99	99.84	100.16	99.49
Sc	40	39	38	41	37	20	32	34	36
Ti	2696	2119	2182	1818	1639	2040	1980	2040	1576
V	286	220	234	230	171	182	190	233	185
Cr	85	360	86	24	477	180	61	63	465
Co	30	31	20	20	46	29	32	30	38
Ni	53	118	73	47	324	266	62	59	213
Cu	223	141	4	32	148	200	26	52	3
Zn	81	140	6	21	262	68	41	103	63
Ga	12	11	13	12	10	10	10	10	10
Rb	8	4	2	5	1	7	7	9	4
Sr	92	72	84	80	48	32	70	70	104
Y	14	12	12	11	7	9	10	10	7
Zr	12	15	9	7	13	13	12	12	13
Nb	0.81	0.72	0.59	0.45	0.44	0.46	0.50	0.51	0.41
Cs	0.05	0.06	0.03	0.04	0.00	0.00	0.01	0.01	0.01
Ba	23	16	3	5	6	12	10	14	9
La	0.44	0.47	0.38	0.24	0.49	0.36	0.38	0.45	0.51
Ce	1.08	1.14	0.89	0.66	1.16	1.19	0.97	1.03	1.31
Pr	0.18	0.19	0.16	0.12	0.20	0.17	0.17	0.19	0.20
Nd	1.06	1.11	0.97	0.79	1.07	1.06	1.05	1.10	1.11
Sm	0.63	0.59	0.54	0.47	0.46	0.55	0.54	0.57	0.48
Eu	0.27	0.25	0.24	0.20	0.25	0.19	0.19	0.19	0.20
Gd	1.20	1.09	0.96	0.84	0.70	0.99	0.89	0.92	0.76
Tb	0.28	0.25	0.23	0.20	0.15	0.20	0.21	0.21	0.16
Dy	2.10	1.79	1.71	1.51	1.06	1.45	1.49	1.51	1.15
Ho	0.48	0.40	0.41	0.37	0.24	0.34	0.34	0.35	0.26
Er	1.52	1.29	1.25	1.13	0.69	1.01	1.02	1.07	0.82
Tm	0.26	0.21	0.22	0.20	0.11	0.16	0.17	0.18	0.14
Yb	1.74	1.42	1.44	1.30	0.72	1.01	1.07	1.19	0.97
Lu	0.28	0.23	0.24	0.22	0.11	0.15	0.17	0.19	0.16
Hf	0.55	0.57	0.39	0.32	0.47	0.49	0.49	0.47	0.46
Ta	0.05	0.05	0.04	0.03	0.03	0.04	0.04	0.05	0.03
Pb	0.97	2.04	0.01	1.56	2.45	0.45	1.23	1.20	3.91
Th	0.10	0.09	0.08	0.06	0.09	0.06	0.08	0.08	0.07
U	0.09	0.07	0.02	0.04	0.10	0.09	0.12	0.10	0.10

Sample	CC2/019	CC2/021	CC2/020	CC2/022	CC2/023	CC2/086	CC2/087	CC2/088	CC2/101	CC2/102	CC2/104	CC2/105	CC2/121
Lava	BG	BG	BG	BG	SDC	UPL	UPL	LPL	BG	BG	LPL	BG	LPL
	Stavros Tis Psokas	*Stavros river*	*Stavros Tis Psokas*	*Panaya rd*	*Polystipos road*	*Limni mine*	*Limni*	*Limni*	*Milikori*	*Milikori*	*Panaya*	*Panaya*	*Anadhiou*
X	-39300	-41000	-39500	-33500	837	-46977	-46996	-46786	-24544	-24764	-24755	-31532	-37680
Y	71650	70500	71750	66500	67377	77144	77123	76721	63402	62307	63130	65022	66597
SiO_2	53.66	49.69	55.28	61.56	51.62	50.70	43.20	44.09	51.63	57.51	52.33	50.72	49.49
TiO_2	0.45	0.35	0.35	0.54	0.44	0.33	0.37	0.40	0.67	0.76	0.69	0.27	0.33
Al_2O_3	16.71	15.65	13.82	14.44	14.98	11.67	12.42	15.53	15.24	14.27	14.72	12.63	14.67
FeO*	8.71	6.64	7.94	9.62	9.07	8.66	8.41	7.88	9.14	9.55	10.44	6.97	8.17
MnO	0.22	0.11	0.21	0.13	0.14	0.17	0.19	0.11	0.10	0.13	0.21	0.21	0.07
MgO	9.56	5.69	7.92	4.18	9.38	11.03	11.39	6.60	6.85	3.57	9.01	9.53	5.92
CaO	1.05	11.29	4.96	3.22	7.65	11.01	10.20	10.51	0.75	0.64	2.21	5.33	12.05
Na_2O	4.30	0.56	3.69	4.37	2.49	0.76	1.55	1.28	4.16	5.27	4.73	2.67	1.42
K_2O	0.05	0.04	0.04	0.17	0.16	0.23	0.39	0.71	0.08	0.01	0.09	0.89	0.80
P_2O_5	0.06	0.04	0.05	0.06	0.05	0.04	0.04	0.08	0.05	0.08	0.07	0.04	0.05
LOI	5.00	9.87	4.50	2.87	5.10	6.13	10.67	13.86	10.72	7.69	7.39	7.74	8.47
Tot	99.78	99.93	98.76	101.16	101.08	100.72	98.83	101.04	99.39	99.48	101.89	97.01	101.44
Sc	32	29	37	34	40	41	45	35	39	33	36	36	36
Ti	2698	2116	2099	3233	2617	1958	2204	2374	4027	4556	4129	1639	1980
V	211	216	193	317	226	212	262	225	239	261	254	186	203
Cr	211	56	169	36	149	605	622	99	13	4	73	183	96
Co	25	28	29	28	37	47	52	28	21	29	36	28	32
Ni	398	110	112	60	68	237	293	64	4	27	47	76	19
Cu	157	68	257	132	65	93	102	42	129	50	4	45	54
Zn	156	32	253	101	33	64	55	52	556	66	29	117	49
Ga	13	14	12	14	12	9	7	13	17	15	12	9	13
Rb	0	1	0	1	1	6	6	12	1	0	1	3	27
Sr	61	19	59	98	55	51	242	1465	55	55	112	47	52
Y	10	9	13	17	13	9	10	14	12	22	16	8	11
Zr	18	11	25	31	19	9	11	15	33	41	22	8	14
Nb	0.77	0.41	0.81	1.17	0.65	0.54	0.58	0.62	0.63	0.75	1.20	0.35	0.42
Cs	0.00	0.03	0.01	0.06	0.02	0.39	0.10	0.30	0.01	0.01	0.02	0.02	0.29
Ba	2	1	2	10	2	31	42	36	2	4	5	17	8
La	0.51	0.45	1.01	1.32	0.89	0.39	0.23	0.73	1.13	1.81	0.85	0.32	0.66
Ce	1.82	1.11	2.74	3.26	2.38	0.90	0.82	1.48	1.24	3.93	2.24	0.82	1.45
Pr	0.28	0.18	0.42	0.51	0.41	0.14	0.14	0.24	0.70	0.85	0.41	0.15	0.23
Nd	1.63	1.03	2.13	2.69	2.30	0.82	0.83	1.43	4.02	4.68	2.44	0.87	1.36
Sm	0.75	0.49	0.84	1.11	0.93	0.41	0.46	0.69	1.60	1.80	1.08	0.42	0.61
Eu	0.16	0.22	0.27	0.42	0.43	0.17	0.20	0.27	0.64	0.62	0.43	0.18	0.28
Gd	1.17	0.80	1.29	1.72	1.33	0.72	0.80	1.14	1.95	2.40	1.61	0.68	1.07
Tb	0.24	0.18	0.27	0.36	0.28	0.17	0.19	0.25	0.37	0.49	0.35	0.15	0.22
Dy	1.66	1.29	1.80	2.57	1.95	1.25	1.41	1.81	2.47	3.27	2.40	1.08	1.54
Ho	0.37	0.30	0.40	0.57	0.44	0.30	0.34	0.43	0.52	0.72	0.55	0.26	0.36
Er	1.10	0.91	1.24	1.80	1.30	0.93	1.04	1.31	1.58	2.10	1.61	0.78	1.11
Tm	0.18	0.16	0.20	0.30	0.21	0.16	0.18	0.22	0.28	0.34	0.27	0.13	0.18
Yb	1.13	1.01	1.32	1.98	1.37	1.07	1.20	1.46	2.02	2.18	1.69	0.85	1.21
Lu	0.17	0.17	0.22	0.32	0.22	0.18	0.20	0.24	0.31	0.35	0.27	0.14	0.19
Hf	0.62	0.40	0.85	1.10	0.59	0.34	0.40	0.57	1.08	1.23	0.74	0.29	0.51
Ta	0.05	0.03	0.05	0.07	0.04	0.04	0.04	0.05	0.04	0.06	0.09	0.02	0.03
Pb	0.30	2.41	0.58	0.94	0.49	1.95	1.60	2.08	13.15	1.06	0.10	2.16	0.74
Th	0.12	0.07	0.18	0.21	0.08	0.08	0.09	0.11	0.13	0.19	0.14	0.05	0.07
U	0.07	0.08	0.14	0.17	0.02	0.04	0.06	0.10	0.12	0.11	0.04	0.04	0.08

Sample	CC2/108	CC2/117	CC2/122	CC2/123	CC2/128	CC2/124	CC2/118	CC2/119	CC2/119a	CC2/120	CC2/127	CC2/103	CC2/126
Lava	BG	UPL	LPL	LPL	LPL	SDC	UPL	UPL	UPL	UPL	BG	BG	BG
	Panaya	*Sarama*	*Anadhiou*	*Kannaviou*	*Kannaviou*	*Anadhiou*	*Anadhiou*	*Anadhiou*	*Anadhiou*	*Anadhiou*	*Kannaviou*	*Panaya*	*Anadhiou*
X	-31732	-44452	-37410	-37338	-37495	-37445	-39203	-38481	-38481	-37520	-37858	-24564	-37558
Y	65111	68400	67011	67108	65007	68128	67144	65808	65808	67221	65936	63752	68238
SiO_2	54.76	44.77	53.33	57.73	43.35	56.71	41.97	34.86	46.90	53.59	57.43	57.55	55.47
TiO_2	0.56	0.48	0.39	0.79	0.25	0.49	0.29	0.32	0.32	0.36	0.48	0.95	0.57
Al_2O_3	13.99	15.06	13.61	12.46	14.33	14.61	11.78	10.34	13.64	14.59	13.28	14.02	13.76
FeO*	9.57	8.89	7.57	8.89	8.38	8.91	8.12	7.33	7.98	8.60	12.29	11.59	10.52
MnO	0.13	0.14	0.11	0.09	0.12	0.13	0.15	0.12	0.06	0.12	0.26	0.08	0.12
MgO	7.47	6.19	7.15	2.78	11.74	4.45	6.58	5.01	7.30	7.35	8.12	3.52	5.45
CaO	1.27	11.38	4.85	2.33	3.29	3.54	9.92	19.26	9.62	2.97	0.71	2.14	4.32
Na_2O	4.45	1.72	2.49	4.96	0.26	4.92	2.23	0.46	0.87	3.26	2.47	4.95	3.67
K_2O	0.52	1.02	0.98	0.75	3.21	0.03	2.81	2.16	1.70	1.30	0.32	0.05	0.02
P_2O_5	0.05	0.05	0.05	0.06	0.04	0.06	0.09	0.10	0.05	0.04	0.05	0.08	0.06
LOI	6.74	11.97	8.50	7.40	13.79	5.12	15.16	18.75	9.69	7.92	4.77	6.43	5.02
Tot	99.51	101.67	99.03	98.25	98.76	98.97	99.11	98.73	98.13	100.10	100.19	101.35	98.98
Sc	40	41	32	33	41	35	33	33	46	34	42	34	38
Ti	3379	2899	2340	4769	1500	2940	1754	1946	1917	2172	2890	5679	3420
V	250	316	224	298	223	290	198	188	238	218	325	412	347
Cr	22	161	25	1	142	4	464	439	534	10	1	11	9
Co	32	34	28	25	38	30	39	32	40	28	35	31	35
Ni	34	59	28	11	55	20	241	184	222	7	1	49	35
Cu	153	68	87	146	31	121	38	35	38	90	925	156	146
Zn	123	54	55	80	56	70	61	56	47	61	145	84	91
Ga	13	12	13	15	10	15	6	8	12	12	14	16	14
Rb	3	21	6	6	26	0	38	35	26	7	3	0	0
Sr	47	672	100	54	64	65	76	54	28	91	21	72	20
Y	15	13	10	24	4	15	7	7	10	10	9	29	15
Zr	15	11	25	30	5	28	8	11	10	22	11	40	18
Nb	0.56	0.58	0.63	0.77	0.33	0.76	0.46	0.55	0.51	0.67	0.47	0.87	0.61
Cs	0.02	0.72	0.14	0.12	0.33	0.07	0.98	0.69	0.35	0.06	0.02	0.02	0.07
Ba	8	15	12	15	18	10	35	32	6	19	20	5	3
La	0.72	0.53	0.96	1.30	0.08	1.23	0.80	0.65	2.31	0.69	0.31	1.83	0.79
Ce	1.52	1.08	2.41	3.06	0.25	3.10	0.94	0.93	0.49	1.79	0.92	4.00	1.97
Pr	0.28	0.19	0.39	0.54	0.05	0.51	0.18	0.19	0.41	0.28	0.13	0.89	0.33
Nd	1.71	1.16	2.00	3.06	0.29	2.71	0.98	1.04	1.87	1.56	0.78	4.94	1.91
Sm	0.82	0.64	0.75	1.30	0.20	1.11	0.40	0.48	0.60	0.66	0.46	2.01	0.91
Eu	0.32	0.26	0.31	0.49	0.10	0.41	0.16	0.19	0.23	0.29	0.24	0.81	0.37
Gd	1.32	1.08	1.03	2.01	0.36	1.59	0.65	0.72	0.91	1.04	0.89	2.88	1.41
Tb	0.29	0.25	0.22	0.43	0.09	0.33	0.14	0.15	0.19	0.21	0.20	0.60	0.32
Dy	2.10	1.79	1.52	3.02	0.68	2.29	0.98	1.07	1.33	1.51	1.53	4.13	2.23
Ho	0.50	0.42	0.34	0.73	0.16	0.52	0.23	0.24	0.30	0.35	0.36	0.94	0.51
Er	1.49	1.28	1.03	2.23	0.47	1.56	0.69	0.70	0.98	1.09	1.11	2.76	1.52
Tm	0.25	0.21	0.18	0.37	0.08	0.26	0.11	0.12	0.16	0.18	0.19	0.46	0.26
Yb	1.64	1.41	1.18	2.41	0.55	1.70	0.74	0.76	1.06	1.25	1.29	2.93	1.70
Lu	0.27	0.23	0.19	0.42	0.09	0.28	0.12	0.12	0.18	0.21	0.19	0.48	0.28
Hf	0.58	0.47	0.79	1.08	0.22	0.95	0.32	0.39	0.45	0.75	0.46	1.42	0.72
Ta	0.04	0.04	0.04	0.06	0.02	0.06	0.03	0.04	0.03	0.04	0.03	0.06	0.05
Pb	2.31	0.99	1.28	1.73	0.88	1.33	2.05	1.54	4.90	1.14	0.87	1.80	1.90
Th	0.09	0.09	0.15	0.17	0.04	0.18	0.07	0.08	0.08	0.11	0.05	0.19	0.12
U	0.07	0.17	0.12	0.12	0.05	0.13	0.04	0.08	0.06	0.11	0.04	0.08	0.07

Sample	CC2/094	CC2/095	CC2/096	CC2/098	CC2/099	CC2/100	CC5/060	CC5/061	CC5/062
Lava	LSW	LSW	LSW	DSW	DSW	SDC	LPL	UPL	LPL
	Diarizos	*Diarizos*	*Diarizos*	*Diarizos*	*Diarizos*	*Diarizos.*	*Kouka*	*Pera Pedi*	*Mandria West*
X	-22999	-22968	-22643	-22195	-22195	-21494	-10493	-12238	-15818
Y	61026	61026	61595	61969	61969	62949	57056	57836	58578
SiO_2	60.08	61.28	50.10	62.74	59.17	48.10			
TiO_2	0.95	0.94	0.74	0.83	0.83	0.99	0.54	0.61	0.34
Al_2O_3	13.86	12.92	14.33	12.29	13.38	15.24			
FeO*	10.91	8.91	11.01	8.77	10.92	14.29			
MnO	0.08	0.17	0.19	0.11	0.23	0.17	0.20	0.28	0.15
MgO	3.83	2.78	7.48	3.33	5.90	7.14			
CaO	3.75	4.51	2.85	4.18	4.13	8.79			
Na_2O	2.71	2.68	3.52	2.10	1.59	1.41			
K_2O	0.25	0.16	0.88	0.11	0.10	0.29			
P_2O_5	0.12	0.09	0.07	0.11	0.07	0.05			
LOI	4.64	5.66	7.45	3.91	6.14	2.99			
Tot	101.18	100.11	98.62	98.48	102.46	99.46			
Sc	30	30	38	26	36	49	33	39	28
Ti	5720	5668	4450	4970	4972	5940	3264	3654	2010
V	142	111	372	113	323	825	250	117	193
Cr	3	12	3	1	11	5	111	101	109
Co	24	21	36	20	30	47	35	33	22
Ni	17	29	3	10	28	30	74	41	26
Cu	89	40	108	31	194	6	39	72	7
Zn	90	98	104	88	91	18	70	104	96
Ga	16	17	15	14	15	16	14	15	11
Rb	1	1	6	1	1	1	12	30	5
Sr	66	94	86	82	63	62	80	76	78
Y	26	32	22	36	23	13	13	9	11
Zr	53	57	32	64	40	9	21	30	15
Nb	1.03	1.12	0.73	1.20	0.91	0.40	0.52	0.65	0.34
Cs	0.01	0.01	0.04	0.03	0.03	0.03	0.19	0.43	0.03
Ba	30	19	78	9	5	5	40	93	36
La	2.00	2.30	1.39	2.22	1.74	0.47	0.87	0.68	0.62
Ce	5.74	6.43	3.72	6.18	4.49	1.43	2.29	2.45	1.76
Pr	1.03	1.15	0.69	1.18	0.89	0.27	0.39	0.33	0.30
Nd	5.81	6.59	4.01	6.71	5.04	1.68	2.47	2.04	1.93
Sm	2.24	2.46	1.63	2.68	1.91	0.78	0.96	0.85	0.79
Eu	0.82	0.95	0.62	0.95	0.77	0.34	0.44	0.45	0.34
Gd	3.00	3.70	2.56	3.73	2.87	1.22	1.34	1.17	1.13
Tb	0.61	0.70	0.48	0.78	0.54	0.26	0.28	0.24	0.23
Dy	4.04	4.70	3.27	5.31	3.57	1.86	1.98	1.73	1.64
Ho	0.89	1.06	0.72	1.20	0.79	0.42	0.43	0.37	0.37
Er	2.58	3.10	2.14	3.52	2.29	1.26	1.33	1.10	1.11
Tm	0.42	0.50	0.33	0.58	0.36	0.21	0.22	0.18	0.18
Yb	2.69	3.31	2.18	3.67	2.34	1.34	1.40	1.10	1.15
Lu	0.43	0.53	0.34	0.59	0.37	0.22	0.23	0.17	0.18
Hf	1.67	1.82	1.07	1.94	1.30	0.37	0.76	1.00	0.53
Ta	0.08	0.07	0.05	0.09	0.06	0.03	0.04	0.05	0.03
Pb	0.80	0.94	4.27	0.65	1.33	0.02	0.77	1.51	2.15
Th	0.25	0.23	0.11	0.26	0.13	0.06	0.10	0.13	0.07
U	0.13	0.14	0.10	0.12	0.13	0.00	0.06	0.10	0.05

Sample	CC2/042	CC2/043	CC2/044	CC2/045	CC2/046	CC2/047	CC2/049	CC2/052	CC2/053	CC2/054	CC2/055	CC2/056
Lava	BG	BG	BG	LPL	BG	LPL	BG	UPL	UPL	LPL	UPL	UPL
	Melini	*Melini*	*Melini*	*Melini*	*Melini*	*Melini*	*Melini*	*Ayia Anna*	*Ayia Anna*	*Ayia Anna*	*Ayia Anna*	*Ayia Anna*
X	14525	14716	14726	14122	1323	12170	1323	44765	44769	44269	44269	40893
Y	58391	58240	58244	58145	56543	56356	54833	66428	66425	66925	66925	67387
SiO_2	48.99	51.17	50.50	46.23	64.76	55.75	45.33	48.59	48.89	48.54	42.21	55.36
TiO_2	0.15	0.25	0.30	1.04	0.77	0.56	0.62	0.53	0.36	0.37	0.37	0.30
Al_2O_3	8.54	9.31	13.29	15.69	12.55	13.91	15.60	16.28	15.60	14.12	13.89	11.89
FeO*	9.28	8.22	8.23	12.77	9.25	8.95	15.77	9.39	8.48	9.74	8.10	9.43
MnO	0.18	0.20	0.24	0.20	0.13	0.23	0.08	0.05	0.04	0.13	0.13	0.10
MgO	18.94	14.99	10.15	6.79	2.06	7.66	10.74	3.61	4.86	5.05	5.29	5.27
CaO	7.69	7.76	5.86	4.68	2.09	6.12	3.25	7.61	7.03	8.44	10.03	1.83
Na_2O	0.41	1.78	3.69	4.81	4.96	4.85	3.77	0.78	0.72	2.03	2.40	2.92
K_2O	0.01	-0.04	0.10	1.43	0.12	0.04	0.03	4.03	4.03	2.43	1.97	0.25
P_2O_5	0.03	-0.04	0.04	0.09	0.08	0.05	0.06	0.24	0.04	0.05	0.07	0.07
LOI	5.87	6.65	6.56	7.98	2.96	4.61	4.88	8.56	9.40	7.73	13.99	13.59
Tot	100.09	100.25	98.96	101.70	99.75	102.73	100.12	99.67	99.45	98.63	98.46	101.01
Sc	35	44	33	42	25	41	40	49	44	39	37	38
Ti	898	1494	1825	6243	4636	3385	3704	3172	2140	2213	2244	1810
V	208	195	206	285	169	255	224	216	287	272	213	147
Cr	1544	835	428	30	4	52	300	298	288	68	36	236
Co	56	45	29	39	22	35	120	12	48	33	27	30
Ni	371	125	340	23	16	18	39	51	23	12	7	17
Cu	88	38	202	50	154	42	4	32	38	21	104	87
Zn	71	53	1244	128	83	74	14	67	125	54	55	51
Ga	7	8	8	16	10	13	14	13	14	13	12	9
Rb	0	0	1	8	1	0	0	58	50	50	31	20
Sr	17	30	69	42	68	70	42	67	84	813	229	1344
Y	5	8	8	25	24	15	18	19	6	13	22	9
Zr	4	11	9	34	43	11	22	14	13	18	15	12
Nb	1.27	0.70	0.70	0.84	2.25	0.87	1.02	0.95	0.97	1.23	1.15	0.58
Cs	0.01	0.00	3.72	0.01	0.01	0.00	0.00	0.90	0.51	0.62	0.54	0.48
Ba	2	1	8	109	9	6	2	18	17	26	20	19
La	0.36	0.39	0.48	2.00	1.83	0.75	1.02	4.71	0.41	0.56	1.22	0.41
Ce	0.68	1.03	1.18	5.11	4.34	2.21	3.04	2.29	1.03	1.44	1.97	1.45
Pr	0.08	0.19	0.21	0.89	0.77	0.41	0.56	0.98	0.14	0.25	0.38	0.22
Nd	0.26	1.13	1.24	4.81	4.23	2.47	3.18	4.64	0.83	1.51	2.26	1.31
Sm	0.12	0.52	0.60	1.81	1.70	1.07	1.31	1.42	0.42	0.75	0.99	0.60
Eu	0.07	0.22	0.30	0.75	0.58	0.47	0.29	0.50	0.22	0.32	0.41	0.28
Gd	0.34	0.88	1.05	2.72	2.42	1.72	2.03	2.08	0.71	1.30	1.79	1.01
Tb	0.09	0.18	0.23	0.51	0.50	0.34	0.41	0.40	0.15	0.27	0.36	0.20
Dy	0.71	1.26	1.64	3.36	3.46	2.32	2.81	2.65	1.03	1.91	2.64	1.36
Ho	0.17	0.29	0.36	0.76	0.79	0.53	0.64	0.59	0.23	0.44	0.64	0.30
Er	0.61	0.85	1.13	2.25	2.34	1.58	1.86	1.67	0.68	1.35	1.99	0.88
Tm	0.11	0.14	0.18	0.35	0.39	0.25	0.29	0.25	0.11	0.22	0.33	0.14
Yb	0.75	0.90	1.24	2.26	2.47	1.64	1.86	1.50	0.73	1.51	2.20	0.87
Lu	0.13	0.14	0.21	0.36	0.40	0.27	0.28	0.23	0.11	0.25	0.36	0.14
Hf	0.15	0.39	0.49	1.09	1.40	0.50	0.69	0.54	0.53	0.62	0.58	0.41
Ta	0.08	0.04	0.04	0.05	0.14	0.05	0.06	0.07	0.06	0.07	0.07	0.04
Pb	0.25	0.80	247.70	2.34	1.19	0.48	0.09	4.61	1.09	0.39	0.59	0.70
Th	0.08	0.05	0.07	0.26	0.28	0.07	0.10	0.09	0.06	0.07	0.07	0.05
U	0.05	0.05	0.06	0.08	0.17	0.05	0.07	0.22	0.19	0.14	0.12	0.08

Sample	CC2/057	CC2/058	CC2/058b	CC2/060	CC2/061	CC2/062	CC2/063	CC2/064	CC2/065	CC2/066	CC2/067	CC2/068	CC2/069	CC2/070
Lava	LPL	LPL	LPL	BG	BG	BG	BG	BG	BG	BG	BG	UPL	LPL	LPL
	Sia	*Sia*	*Sia*	*Stavrovouni*	*Stavr'ni*	*Stavr'ni*	*Stavr'ni*	*Stavr'ni*	*Stavr'ni*	*Stavr'ni*	*Stavr'ni*	*Kornos*	*Kornos*	*Kornos*
X	38633	38633	38633	38119	38766	38766	39076	39074	38637	38518	38518	37003	36613	34814
Y	68003	68003	68003	61024	60045	60045	61105	61105	61588	61582	61582	63252	61385	63912
SiO_2	57.90	48.78	53.17	54.37	46.72	61.05	54.74	50.88	56.76	55.31	60.14	41.46	48.46	53.22
TiO_2	0.93	0.19	0.54	0.27	0.21	0.51	0.22	0.33	0.63	0.55	0.63	0.23	0.37	0.69
Al_2O_3	12.44	8.90	16.58	13.84	8.34	13.14	14.40	11.34	14.08	14.78	14.28	10.68	15.37	15.71
FeO*	9.86	8.60	8.89	8.67	9.06	10.41	10.40	9.08	10.32	10.56	11.50	7.24	8.35	8.33
MnO	0.07	0.18	0.19	0.13	0.16	0.09	0.10	0.21	0.15	0.20	0.15	0.10	0.10	0.13
MgO	5.51	19.21	5.95	7.55	20.28	4.71	7.62	10.88	3.58	5.39	4.43	9.93	8.70	5.01
CaO	1.92	7.45	7.12	8.30	8.41	5.77	4.65	6.64	1.09	7.44	2.97	12.73	12.04	10.28
Na_2O	3.05	0.52	4.92	2.25	0.17	2.39	3.69	2.96	4.65	2.19	4.85	0.25	1.75	2.09
K_2O	0.26	0.02	0.03	0.01	0.02	0.44	0.23	0.24	0.03	0.30	0.21	2.35	0.37	0.25
P_2O_5	0.07	0.03	0.05	0.04	0.03	0.05	0.05	0.04	0.06	0.05	0.06	0.03	0.05	0.07
LOI	6.73	7.23	4.35	5.95	6.20	3.17	4.63	5.53	7.29	3.22	2.47	14.34	5.45	4.00
Tot	98.73	101.11	101.79	101.38	99.60	101.73	100.72	98.13	98.64	99.99	101.68	99.35	101.03	99.79
Sc	31	34	39	43	34	38	41	43	37	39	38	39	42	37
Ti	5572	1138	3212	1607	1273	3079	1316	1972	3777	3325	3772	1381	2242	4147
V	305	185	280	206	172	279	187	236	310	267	318	171	231	262
Cr	1	901	23	246	902	16	657	575	1	38	23	703	167	11
Co	26	57	27	34	59	31	30	30	25	33	32	31	34	33
Ni	1	488	45	92	312	49	40	82	2	61	65	142	67	5
Cu	95	63	444	9	57	79	29	5	156	35	117	35	19	35
Zn	88	61	86	78	59	43	44	286	106	87	48	52	58	76
Ga	14	8	15	12	8	12	10	11	17	15	13	10	12	17
Rb	1	1	0	0	0	2	21	1	0	2	2	24	7	6
Sr	80	25	64	33	12	91	35	53	79	105	101	33	58	74
Y	24	7	16	10	7	16	6	9	23	16	17	6	11	23
Zr	42	4	19	8	5	13	7	9	29	23	22	7	17	38
Nb	1.57	1.20	1.99	2.52	1.03	2.77	1.04	1.08	2.37	1.81	1.68	0.90	1.02	1.16
Cs	0.00	0.01	0.00	0.01	0.00	0.03	0.19	0.02	0.00	0.04	0.05	0.28	0.12	0.14
Ba	10	3	3	2	1	11	37	7	12	21	13	40	13	23
La	2.16	0.39	0.71	0.77	0.26	0.54	0.32	0.28	1.21	0.90	0.87	0.32	0.93	1.47
Ce	5.74	0.65	1.69	1.36	0.55	1.12	0.70	0.71	2.23	2.23	2.37	0.67	2.20	4.29
Pr	1.03	0.09	0.29	0.17	0.08	0.19	0.13	0.13	0.47	0.39	0.43	0.13	0.36	0.77
Nd	5.67	0.48	1.70	0.76	0.46	1.13	0.76	0.78	2.77	2.17	2.47	0.77	1.90	4.48
Sm	2.13	0.26	0.85	0.38	0.29	0.68	0.38	0.42	1.29	1.00	1.11	0.37	0.77	1.80
Eu	0.78	0.13	0.26	0.17	0.12	0.26	0.17	0.16	0.52	0.43	0.38	0.16	0.32	0.71
Gd	3.09	0.48	1.37	0.76	0.61	1.31	0.69	0.72	2.20	1.60	1.72	0.64	1.12	2.71
Tb	0.59	0.12	0.31	0.18	0.14	0.31	0.14	0.17	0.45	0.35	0.37	0.15	0.24	0.51
Dy	3.97	0.89	2.26	1.39	1.07	2.32	1.03	1.26	3.14	2.47	2.57	1.02	1.66	3.49
Ho	0.86	0.22	0.53	0.32	0.26	0.53	0.23	0.30	0.73	0.55	0.57	0.24	0.38	0.78
Er	2.51	0.68	1.63	1.06	0.81	1.72	0.68	0.92	2.21	1.73	1.77	0.68	1.14	2.27
Tm	0.40	0.12	0.28	0.18	0.14	0.29	0.11	0.16	0.36	0.29	0.29	0.11	0.19	0.36
Yb	2.56	0.78	1.83	1.24	0.91	1.94	0.71	1.02	2.41	1.91	1.91	0.73	1.22	2.32
Lu	0.39	0.13	0.30	0.20	0.15	0.32	0.11	0.17	0.38	0.31	0.31	0.12	0.20	0.36
Hf	1.34	0.17	0.70	0.32	0.21	0.60	0.28	0.36	1.06	0.88	0.86	0.29	0.57	1.23
Ta	0.10	0.09	0.16	0.16	0.07	0.17	0.07	0.08	0.16	0.11	0.11	0.07	0.07	0.07
Pb	1.83	1.28	1.85	0.48	0.95	0.07	0.35	0.50	0.82	0.28	0.37	0.58	0.61	0.75
Th	0.18	0.07	0.15	0.14	0.04	0.12	0.03	0.09	0.18	0.15	0.13	0.05	0.11	0.14
U	0.12	0.04	0.10	0.07	0.03	0.07	0.05	0.06	0.17	0.10	0.08	0.03	0.09	0.13

Sample	CC5/031	CC5/032	CC5/033	CC5/034	CC5/035	CC5/036	CC5/037	CC5/039	CC5/039a	CC5/041	CC5/042
Lava	UPL	LPL	LPL	Bg	LPL	LPL	LPL	LPL	LPL	LPL	UPL
	Psevdas	*Sia South*	*Pyrga*	*Moni Panyias*	*Anglisese*	*Delikipos*	*Kornos*	*Delikipos*	*Dhypotamos Dam*	*Lefkara*	*Kato Drys*
X	40952	36360	40649	34913	40349	32897	36034	30928	33010	25527	27203
Y	69454	66673	65645	53727	57273	63458	64918	66566	56920	58709	56198
SiO_2											
TiO_2	0.52	0.69	0.56	0.40	0.23	0.25	0.67	0.23	0.49	0.15	0.43
Al_2O_3											
FeO*											
MnO	0.17	0.10	0.10	0.09	0.09	0.06	0.08	0.12	0.08	0.20	0.16
MgO											
CaO											
Na_2O											
K_2O											
P_2O_5											
LOI											
Sc	28	27	28	27	21	30	25	27	21	34	29
Ti	3120	4140	3342	2382	1380	1470	3996	1398	2922	900	2580
V	166	259	222	168	201	168	249	170	189	175	155
Cr	9	34	63	254	14	383		247	-6	612	392
Co	37	25	29	29	20	28	21	26	17	29	31
Ni	10	2	7	132	16	50		263	-21	55	222
Cu	42	58	56	32	52	28	24	79	30	14	25
Zn	77	53	48	46	46	37	65	44	67	759	47
Ga	13	14	12	11	8	8	11	8	11	7	8
Rb	27	37	22	10	1	10	15	3	4	14	7
Sr	60	78	582	59	43	822	70	36	71	36	46
Y	14	26	16	11	10	9	22	8	14	9	12
Zr	20	29	29	21	8	10	26	8	21	4	20
Nb	0.85	1.27	0.49	0.45	1.02	0.53	0.90	0.66	1.43	0.60	0.72
Cs	0.40	1.60	0.54	0.86	0.02	0.37	0.25	0.12	0.02	0.22	0.28
Ba	38	30	17	12	29	21	13	14	19	213	20
La	0.80	1.68	1.40	0.96	0.70	0.64	1.49	0.33	0.76	0.48	1.28
Ce	1.78	3.53	3.27	2.58	1.10	1.13	3.26	0.79	1.76	0.80	2.65
Pr	0.35	0.64	0.60	0.41	0.18	0.20	0.58	0.13	0.31	0.10	0.49
Nd	2.36	4.00	3.69	2.50	1.08	1.29	3.71	0.84	2.06	0.66	2.95
Sm	1.02	1.55	1.35	0.93	0.47	0.54	1.42	0.42	0.93	0.32	1.08
Eu	0.44	0.60	0.52	0.37	0.19	0.21	0.55	0.20	0.37	0.19	0.41
Gd	1.52	2.33	1.82	1.25	0.82	0.83	2.07	0.70	1.37	0.65	1.48
Tb	0.30	0.48	0.36	0.25	0.18	0.17	0.41	0.16	0.29	0.14	0.29
Dy	2.13	3.48	2.49	1.75	1.34	1.24	2.92	1.19	2.13	1.06	2.02
Ho	0.46	0.81	0.54	0.38	0.32	0.28	0.66	0.28	0.48	0.26	0.43
Er	1.36	2.51	1.61	1.14	1.03	0.86	2.01	0.88	1.48	0.82	1.27
Tm	0.21	0.41	0.26	0.18	0.17	0.14	0.32	0.15	0.24	0.13	0.20
Yb	1.30	2.67	1.63	1.16	1.16	0.90	2.03	0.96	1.56	0.86	1.25
Lu	0.21	0.44	0.26	0.19	0.20	0.15	0.34	0.16	0.25	0.15	0.20
Hf	0.77	1.03	0.91	0.66	0.33	0.39	0.89	0.34	0.84	0.16	0.68
Ta	0.07	0.10	0.04	0.03	0.08	0.04	0.07	0.06	0.10	0.05	0.05
Pb	0.72	0.42	0.54	0.21	0.27	0.35	0.60	0.75	0.33	0.29	0.66
Th	0.10	0.19	0.10	0.13	0.08	0.06	0.13	0.07	0.14	0.04	0.10
U	0.11	0.15	0.09	0.08	0.05	0.08	0.15	0.04	0.09	0.03	0.05

Sample	CC2/074	CC2/073	CC2/075	CC5/021	CC5/023	CC5/024	CC5/025	CC5/026	CC5/027	CC5/028	CC5/029	CC5/030	CC5/038
Lava	BG	BG	LPL	UPL	LPL	UPL	UPL	UPL	BG	UPL	UPL	UPL	LPL
	Lith'da	*Lith'da*	*Lith'da*	*Kata'as*	*Mathiatis*	*Ayia Varvara*	*Gerakies*	*Sia*	*Xylias*	*Alampra*	*Lympia*	*Lympia*	*Lith'da*
X	28013	27967	28806	27731	31478	34130	29622	34699	35180	37155	38090	40014	25463
Y	62316	61803	62496	71328	69734	72746	68095	68212	66455	71526	70380	71692	66997
SiO_2	45.40	56.71	51.58										
TiO_2	0.76	0.63	0.62	0.73	0.81	0.53	0.44	0.70	0.40	0.64	0.31	0.62	0.24
Al_2O_3	14.30	13.46	14.58										
FeO*	11.23	10.10	9.15										
MnO	0.26	0.18	0.17	0.13	0.05	0.11	0.10	0.10	0.18	0.11	0.18	0.14	0.12
MgO	7.20	4.00	4.75										
CaO	6.49	3.57	6.45										
Na_2O	4.35	4.09	4.77										
K_2O	0.00	0.33	0.01										
P_2O_5	0.07	0.05	0.06										
LOI	8.82	5.00	6.23										
Tot	98.88	98.13	98.36										
Sc	41	36	39	35	32	21	21	27	26	29	33	30	29
Ti	4561	3790	3740	4398	4854	3198	2616	4194	2370	3834	1854	3702	1422
V	295	291	254	256	301	218	176	204	200	180	194	194	173
Cr	29	14	54	83	9	114	247	51	58	253	233	300	198
Co	38	31	31	40	25	23	28	27	25	31	32	38	28
Ni	12	45	8	49	-3	13	85	28	84	67	42	141	37
Cu	55	194	66	98	89	41	58	33	560	40	32	44	24
Zn	96	97	63	77	70	40	47	54	129	64	52	76	40
Ga	15	14	15	12	14	12	9	11	7	12	10	12	9
Rb	0	2	0	3	1	26	3	10	1	25	8	24	0
Sr	59	101	23	273	72	63	48	141	35	108	44	132	109
Y	20	23	19	19	18	16	12	16	12	17	9	18	7
Zr	32	24	29	39	39	24	23	38	15	37	10	37	7
Nb	0.55	2.89	0.85	0.52	0.71	0.52	0.39	0.38	0.95	0.55	0.44	0.54	0.54
Cs	0.00	0.02	0.00	0.09	0.01	0.47	0.05	0.12	0.03	0.46	0.19	0.37	0.01
Ba	2	22	1	6	20	5	8	19	10	52	27	46	25
La	1.37	1.26	1.19	1.41	1.43	1.26	0.80	1.20	0.96	1.62	0.49	1.38	0.39
Ce	3.91	2.70	3.48	4.07	3.98	2.95	2.49	3.86	2.09	4.10	1.27	4.15	0.84
Pr	0.70	0.48	0.62	0.70	0.68	0.48	0.42	0.66	0.34	0.70	0.21	0.68	0.14
Nd	3.91	2.81	3.54	4.34	4.25	3.00	2.64	4.13	2.12	4.27	1.36	4.13	0.90
Sm	1.50	1.27	1.43	1.64	1.56	1.13	1.00	1.50	0.87	1.48	0.57	1.52	0.40
Eu	0.60	0.53	0.56	0.60	0.62	0.44	0.40	0.60	0.32	0.58	0.25	0.59	0.18
Gd	2.28	2.09	2.18	2.17	2.11	1.63	1.36	1.94	1.26	1.99	0.85	2.05	0.62
Tb	0.44	0.45	0.42	0.44	0.41	0.33	0.27	0.38	0.26	0.39	0.18	0.40	0.13
Dy	2.96	3.15	2.88	3.04	2.88	2.39	1.87	2.60	1.90	2.69	1.31	2.77	0.95
Ho	0.66	0.70	0.65	0.66	0.62	0.54	0.41	0.55	0.42	0.58	0.30	0.60	0.22
Er	1.93	2.24	1.93	1.96	1.86	1.64	1.22	1.61	1.26	1.72	0.90	1.81	0.67
Tm	0.31	0.37	0.31	0.31	0.30	0.26	0.20	0.25	0.21	0.27	0.15	0.28	0.11
Yb	2.00	2.46	2.01	1.97	1.83	1.61	1.23	1.59	1.35	1.71	0.97	1.80	0.70
Lu	0.31	0.41	0.32	0.31	0.28	0.26	0.20	0.25	0.20	0.27	0.16	0.28	0.11
Hf	0.99	0.96	0.90	1.18	1.23	0.80	0.70	1.15	0.55	1.11	0.39	1.11	0.26
Ta	0.04	0.18	0.05	0.05	0.07	0.05	0.04	0.04	0.08	0.05	0.04	0.05	0.05
Pb	0.45	0.72	1.02	1.02	0.68	1.31	0.55	0.46	1.07	0.61	0.58	0.65	0.39
Th	0.12	0.18	0.11	0.11	0.16	0.11	0.08	0.14	0.15	0.12	0.06	0.10	0.05
U	0.07	0.11	0.07	0.04	0.37	0.12	0.04	0.08	0.11	0.13	0.10	0.06	0.03

Sample	CC5/043	CC5/044	CC5/064	CC5/045	CC5/047	CC5/048	CC5/049	CC5/050
Lava	UPL	LPL	LPL	LPL	BG	UPL	LPL	UPL
	Parsada	*Drapia*	*Drapia*	*Platies*	*Kellaki*	*Pyrgos*	*Parekkilksha*	*Armenokouri*
X	23480	25322	52780	21694	14932	15407	13731	12421
Y	57453	52526	50547	49802	47830	44939	46152	46409
SiO_2								
TiO_2	0.52	0.30	0.43	0.23	0.32	0.27	0.21	0.22
Al_2O_3								
FeO*								
MnO	0.11	0.06	0.14	0.07	0.10	0.08	0.11	0.14
Sc	26	30	27	17	23	31	24	30
Ti	3108	1812	2604	1362	1944	1608	1284	1332
V	195	240	169	92	173	156	160	184
Cr	109	159	85	35	58	321	298	452
Co	27	23	33	16	23	25	34	30
Ni	26	221	46	3	22	62	268	172
Cu	195	97	48	47	77	65	61	32
Zn	72	73	63	24	62	42	47	61
Ga	11	13	13	7	9	9	8	9
Rb	5	6	23	10	6	24	4	20
Sr	66	73	94	118	207	34	58	39
Y	15	7	12	8	9	5	7	7
Zr	21	13	29	15	21	11	11	11
Nb	1.24	0.98	1.10	0.58	1.30	0.61	0.72	0.92
Cs	0.02	0.07	0.27	0.08	0.12	0.25	0.14	0.18
Ba	12	41	42	18	30	20	9	39
La	1.34	0.56	1.48	1.14	1.05	0.39	0.67	0.96
Ce	3.37	1.38	3.52	2.43	2.55	0.92	1.41	1.00
Pr	0.53	0.19	0.53	0.39	0.37	0.16	0.21	0.21
Nd	3.22	1.13	3.06	2.19	2.11	0.94	1.18	1.11
Sm	1.24	0.49	1.10	0.75	0.77	0.39	0.46	0.40
Eu	0.55	0.23	0.45	0.28	0.30	0.16	0.19	0.17
Gd	1.72	0.71	1.43	0.98	1.05	0.56	0.67	0.63
Tb	0.35	0.15	0.28	0.19	0.21	0.12	0.14	0.13
Dy	2.39	1.09	1.96	1.31	1.49	0.88	1.04	0.97
Ho	0.53	0.24	0.43	0.29	0.33	0.19	0.24	0.22
Er	1.53	0.72	1.26	0.87	1.01	0.59	0.73	0.67
Tm	0.25	0.12	0.21	0.14	0.17	0.10	0.12	0.11
Yb	1.51	0.71	1.35	0.90	1.06	0.64	0.81	0.69
Lu	0.23	0.11	0.21	0.14	0.18	0.10	0.13	0.11
Hf	0.76	0.47	0.92	0.49	0.68	0.43	0.40	0.41
Ta	0.09	0.06	0.07	0.04	0.09	0.05	0.05	0.07
Pb	2.02	0.19	0.90	0.18	0.58	0.69	0.42	0.86
Th	0.13	0.13	0.19	0.11	0.17	0.08	0.11	0.10
U	0.11	0.06	0.15	0.07	0.07	0.07	0.05	0.09

Sample	CC5/051	CC5/052	CC5/053	CC5/054	CC5/055	CC5/056	CC5/057	CC5/059
Lava	UPL	UPL	UPL	UPL	LPL	UPL	BG	UPL
	Akrounda	*Apsiou*	*Gerasa*	*Kapilio*	*Kapilio*	*Ayias Mamas*	*Ayias Mamas*	*Trimklini*
X	7281	2405	369	-2507	-3021	-4141	-4509	-7809
Y	47260	50378	51306	54777	54027	55177	56525	57198
SiO_2								
TiO_2	0.22	0.17	0.47	0.48	0.24	0.19	0.28	0.19
Al_2O_3								
FeO*								
MnO	0.11	0.15	0.16	0.11	0.09	0.12	0.12	0.12
Sc	28	30	42	30	28	32	34	39
Ti	1302	1044	2790	2904	1458	1146	1662	1164
V	140	192	269	163	169	200	197	227
Cr	261	504	38	282	306	623	272	476
Co	32	37	29	32	34	39	25	42
Ni	81	259	30	402	196	257	68	287
Cu	44	7	42	20	62	74	100	102
Zn	52	68	77	49	44	52	47	59
Ga	10	9	14	9	10	6	9	8
Rb	26	1	28	0	0	2	8	10
Sr	39	117	98	110	38	87	61	840
Y	6	6	12	14	8	8	7	8
Zr	10	7	14	24	11	8	12	9
Nb	0.43	2.42	3.54	0.81	0.50	2.39	0.87	0.72
Cs	0.43	0.01	0.46	0.01	0.01	0.04	0.09	0.29
Ba	47	10	57	6	2	49	181	20
La	0.69	0.87	1.37	0.92	0.51	0.92	0.53	0.43
Ce	1.18	1.53	2.50	2.61	1.30	1.60	1.28	0.81
Pr	0.19	0.16	0.29	0.44	0.20	0.17	0.20	0.12
Nd	1.15	0.77	1.47	2.84	1.26	0.83	1.27	0.69
Sm	0.45	0.30	0.66	1.15	0.54	0.33	0.52	0.32
Eu	0.20	0.15	0.31	0.45	0.22	0.15	0.28	0.15
Gd	0.67	0.50	1.14	1.54	0.80	0.59	0.78	0.60
Tb	0.14	0.12	0.25	0.31	0.17	0.13	0.16	0.14
Dy	0.98	0.91	1.81	2.18	1.23	1.07	1.15	1.16
Ho	0.22	0.22	0.41	0.48	0.28	0.26	0.25	0.28
Er	0.66	0.71	1.22	1.42	0.86	0.84	0.76	0.91
Tm	0.11	0.12	0.20	0.22	0.14	0.14	0.12	0.16
Yb	0.71	0.82	1.24	1.40	0.94	0.97	0.79	1.07
Lu	0.12	0.14	0.19	0.22	0.15	0.16	0.12	0.18
Hf	0.37	0.26	0.56	0.80	0.42	0.28	0.45	0.33
Ta	0.03	0.19	0.26	0.05	0.04	0.18	0.06	0.06
Pb	0.58	0.84	0.92	0.25	0.37	0.48	0.36	3.30
Th	0.07	0.26	0.32	0.12	0.07	0.25	0.08	0.12
U	0.06	0.09	0.12	0.07	0.04	0.09	0.05	0.10

Sample	E29	E34	E36	E40	E47	A10	A16	A21	A31	A36
Lava Type	LPL	LPL	LPL	UPL	UPL	LPL	LPL	LPL	LPL	LPL
	Margi	*Margi*	*Margi*	*Margi*	*Margi*	*Analiondas*	*Analiondas*	*Analiondas*	*Analiondas*	*Analiondas*
X	28500	29100	29000	29300	29500	26000	26100	26000	25500	26000
Y	75000	76700	76600	75200	75400	76000	74500	74250	73500	73000
Sc	36	35	37	33	31	37	34	37	35	39
Ti	5297	14057	11535	6478	5874	14026	12242	13944	7798	13898
V	235	317	350	233	216	312	396	470	286	580
Cr	298	4	35	287	358	6	11	15	26	7
Co	29	26	33	31	35	31	32	36	34	33
Ni	88	18	90	60	109	162	28	38	34	22
Cu	16	56	32	92	72	74	47	54	79	40
Zn	59	102	107	54	56	97	135	231	85	96
Ga	13	22	19	13	12	21	16	19	14	19
Rb	12	17	14	1	9	26	28	29	15	16
Sr	80	116	80	90	137	129	74	93	97	137
Y	13	42	37	17	16	37	40	64	21	72
Zr	27	79	62	36	34	87	65	70	37	68
Nb	1.15	1.44	1.10	0.86	0.81	1.45	1.09	1.16	0.77	1.16
Cs	0.37	0.47	0.33	0.02	0.16	0.40	0.48	1.03	0.18	0.25
Ba	20	35	14	23	11	113	123	26	25	239
La	1.08	3.62	2.93	1.49	1.46	3.90	3.01	3.64	1.67	4.49
Ce	2.79	9.07	7.07	4.18	4.14	10.13	9.16	8.98	4.56	7.90
Pr	0.46	1.58	1.33	0.69	0.66	1.64	1.45	2.08	0.74	1.89
Nd	2.86	9.58	8.27	4.14	4.00	9.84	8.80	13.41	4.50	11.81
Sm	1.09	3.41	3.03	1.48	1.43	3.47	3.10	5.04	1.68	4.14
Eu	0.43	1.24	1.11	0.57	0.55	1.28	1.20	1.79	0.64	1.54
Gd	1.48	4.70	4.17	1.99	1.92	4.48	4.29	7.14	2.29	6.27
Tb	0.29	0.89	0.80	0.38	0.36	0.85	0.82	1.30	0.45	1.20
Dy	1.98	6.12	5.48	2.57	2.45	5.71	5.64	8.64	3.11	8.56
Ho	0.43	1.33	1.21	0.56	0.53	1.24	1.26	1.87	0.68	2.03
Er	1.27	3.87	3.57	1.65	1.57	3.71	3.76	5.31	2.02	6.28
Tm	0.21	0.59	0.57	0.26	0.25	0.59	0.59	0.79	0.33	1.02
Yb	1.31	3.56	3.65	1.65	1.56	3.72	3.72	4.77	2.06	6.57
Lu	0.21	0.55	0.58	0.26	0.25	0.60	0.60	0.75	0.33	1.11
Hf	0.92	2.41	1.94	1.13	1.06	2.63	1.99	2.17	1.16	2.14
Ta	0.08	0.10	0.08	0.06	0.06	0.10	0.08	0.08	0.05	0.08
Pb	1.2	1.6	0.7	0.4	0.8	2.1	1.7	1.3	1.2	1.1
Th	0.17	0.30	0.23	0.17	0.16	0.35	0.26	0.28	0.18	0.28
U	0.09	0.19	0.14	0.11	0.08	0.30	0.17	0.25	0.25	0.47

Sample	A8	A4	A26	A30	R10	R16	R18	R2	R6
Lava Type	UPL	UPL	UPL	UPL	LPL	LPL	LPL	UPL	UPL
	Analiondas	*Analiondas*	*Analiondas*	*Analiondas*	*AOP*	*AOP*	*AOP*	*AOP*	*AOP*
X	27000	27100	26500	26000	22700	22540	22440	22200	22500
Y	75000	74400	75500	74250	74060	73560	73300	73250	73250
Sc	40	37	33	31	35	31	32	43	32
Ti	6055	5130	6813	7044	13124	14958	14612	5858	4085
V	202	251	236	233	340	326	316	113	239
Cr	411	539	88	79	9	2	6	353	553
Co	27	34	29	28	36	40	35	28	30
Ni	48	659	50	44	26	17	17	40	114
Cu	71	59	32	17	26	18	27	48	31
Zn	85	86	60	95	111	112	116	75	51
Ga	14	12	12	11	19	25	18	11	8
Rb	20	27	6	5	20	24	13	47	24
Sr	150	161	288	1239	116	135	114	130	95
Y	17	11	16	18	29	59	34	7	11
Zr	33	28	32	37	62	113	68	29	20
Nb	1.02	0.89	0.66	0.65	1.12	1.74	1.08	1.31	0.92
Cs	0.15	0.17	0.22	0.09	0.35	0.50	0.24	0.56	0.53
Ba	23	45	34	85	31	42	19	67	63
La	3.33	1.33	1.43	1.69	2.57	6.55	2.76	1.66	1.12
Ce	3.32	3.15	3.77	4.66	7.03	17.04	8.36	2.10	2.44
Pr	1.04	0.51	0.65	0.78	1.19	2.70	1.35	0.43	0.41
Nd	5.73	2.96	3.96	4.75	7.20	15.86	8.25	2.28	2.51
Sm	1.81	1.07	1.44	1.69	2.62	5.36	2.99	0.77	0.96
Eu	0.66	0.43	0.56	0.65	1.00	1.91	1.13	0.31	0.30
Gd	2.29	1.41	1.93	2.22	3.53	7.01	3.96	0.98	1.33
Tb	0.42	0.27	0.36	0.42	0.67	1.31	0.76	0.20	0.26
Dy	2.78	1.80	2.44	2.82	4.53	8.80	5.09	1.33	1.74
Ho	0.60	0.39	0.53	0.61	0.97	1.94	1.11	0.28	0.38
Er	1.75	1.16	1.54	1.76	2.79	5.78	3.25	0.85	1.11
Tm	0.28	0.18	0.24	0.27	0.43	0.92	0.51	0.14	0.18
Yb	1.75	1.18	1.51	1.74	2.58	5.84	3.20	0.90	1.12
Lu	0.28	0.19	0.24	0.27	0.39	0.95	0.51	0.14	0.18
Hf	1.07	0.92	1.01	1.11	1.95	3.18	2.08	1.02	0.69
Ta	0.07	0.06	0.04	0.04	0.08	0.12	0.08	0.09	0.06
Pb	1.9	2.0	0.5	0.8	1.8	1.4	1.3	2.9	1.6
Th	0.17	0.15	0.16	0.14	0.26	0.42	0.26	0.17	0.11
U	0.17	0.09	0.09	0.16		0.36	0.16	0.09	0.13

Sample	K2	K8	K16	M29	M1	M10	M17	M25	X54	X56	X57
Lava Type	LPL	LPL	UPL	LPL	UPL	UPL	UPL	UPL	Bon	Bon	Bon
	Akaki	*Akaki*	*Akaki*	*Koronia*	*Koronia*	*Koronia*	*Koronia*	*Koronia*	AFB	AFB	AFB
X	14900	15750		-4100	-3550	-3100	-4225	-3900	15000	10500	11000
Y	75800	76730		83400	82880	82350	83460	83300	56000	55500	55500
Sc	29	24	33	26	36	35	34	33	37	33	37
Ti	10465	10363	6313	10068	3042	3093	3320	6842	3042	2662	3224
V	330	88	264	195	224	225	218	235	224	210	227
Cr	5	2	303	9	501	563	520	185	493	427	562
Co	31	24	34	24	48	45	51	34	41	33	43
Ni	15	6	59	14	122	249	181	53	170	108	1277
Cu	19	24	102	40	86	85	83	28	81	69	86
Zn	74	101	74	92	60	61	56	68	54	53	61
Ga	15	16	14	15	11	10	11	16	10	11	10
Rb	7	10	1	8	5	4	5	19	5	1	4
Sr	86	212	82	98	104	68	96	172	307	66	141
Y	25	36	17	30	10	9	10	16	10	8	10
Zr	55	75	22	64	21	17	22	31	11	10	13
Nb	0.91	1.27	1.39	0.78	0.58	0.59	0.60	0.57	0.84	0.74	1.04
Cs	0.06	1.29	0.03	0.49	0.28	0.12	0.11	0.29	0.21	0.01	0.04
Ba	20	78	19	156	16	12	15	18	46	9	48
La	2.08	2.90	1.38	2.09	1.18	0.73	0.94	1.14	0.48	0.54	0.69
Ce	6.09	8.28	3.53	6.50	2.87	1.84	2.44	3.33	1.13	1.18	1.61
Pr	1.03	1.38	0.57	1.12	0.41	0.29	0.37	0.58	0.19	0.18	0.23
Nd	6.28	8.37	3.51	7.08	2.32	1.70	2.14	3.62	1.22	1.16	1.39
Sm	2.27	3.04	1.38	2.63	0.80	0.64	0.79	1.38	0.55	0.50	0.60
Eu	0.82	1.08	0.53	0.96	0.30	0.25	0.31	0.49	0.23	0.20	0.28
Gd	2.96	4.09	1.91	3.54	1.07	0.93	1.07	1.91	0.90	0.80	0.97
Tb	0.57	0.80	0.37	0.68	0.21	0.19	0.21	0.37	0.19	0.17	0.21
Dy	3.88	5.45	2.59	4.67	1.42	1.32	1.47	2.55	1.38	1.22	1.49
Ho	0.85	1.21	0.56	1.02	0.32	0.30	0.33	0.56	0.32	0.28	0.35
Er	2.51	3.59	1.70	3.05	0.99	0.92	1.00	1.67	0.99	0.86	1.07
Tm	0.40	0.58	0.27	0.49	0.16	0.15	0.17	0.27	0.16	0.14	0.18
Yb	2.56	3.72	1.71	3.14	1.08	1.00	1.07	1.71	1.05	0.92	1.16
Lu	0.41	0.60	0.28	0.50	0.18	0.16	0.18	0.28	0.18	0.15	0.19
Hf	1.72	2.36	0.87	2.06	0.70	0.58	0.71	1.04	0.42	0.38	0.50
Ta	0.07	0.09	0.09	0.06	0.04	0.04	0.04	0.04	0.05	0.05	0.07
Pb	0.4	2.0	0.6	1.9	1.8	0.8	0.8	0.6	0.5	0.5	1.1
Th	0.22	0.32	0.19	0.25	0.14	0.10	0.13	0.13	0.08	0.07	0.10
U	0.13	0.16	0.14	0.10	0.11	0.07	0.08	0.18	0.05	0.04	0.06

Sample	X59	X61	G32	S34	X39	X66	X67	X40	X72	X73	X80
Lava Type	Bon AFB	Bon AFB	LPL Kataliondas	LPL Pedeous	LPL Lithrodonda	LPL Diarizos	LPL Diarizos	UPL Ayios Yeorios	UPL Kato Pyrgos	UPL Ayia Marina	UPL Parekklisha
X	11250	-4005	26500	21500	27500	-23000	-22500	25050	-28000	5000	15000
Y	57500	57500	72000	73320	68500	61250	61300	62050	93000	78500	44000
Sc	41	38	36	25	17	35	38	31	28	34	38
Ti	1893	5935	7800	11684	1833	8546	12144	4345	3399	5030	5278
V	232	238	283	243	102	419	136	205	133	235	172
Cr	675	379	55	23	2037	14	1	350	382	203	145
Co	47	39	33	25	108	39	24	36	36	33	36
Ni	1333	620	36	13	887	136	127	170	142	46	45
Cu	90	115	38	26	33	48	54	85	76	112	24
Zn	54	63	72	89	55	80	135	54	51	66	68
Ga	7	13	15	17	5	16	23	11	9	13	13
Rb	1	5	13	6	1	14	21	0	5	5	28
Sr	83	107	95	113	23	73	135	55	62	61	57
Y	6	14	16	40	4	22	86	12	8	14	12
Zr	8	26	39	91	6	34	77	20	21	25	21
Nb	2.22	0.68	0.80	1.39	0.31	0.81	1.60	0.58	0.44	0.86	0.32
Cs	0.05	0.08	0.35	0.21	0.10	0.27	0.33	0.01	0.11	0.18	0.15
Ba	22	8	24	30	21	17	35	5	5	18	137
La	0.88	0.77	1.58	3.48	0.31	1.44	6.02	0.71	0.81	0.94	0.91
Ce	1.71	2.49	4.39	10.00	0.99	3.92	12.31	2.10	2.46	2.63	2.22
Pr	0.18	0.43	0.70	1.65	0.15	0.66	2.03	0.35	0.35	0.44	0.45
Nd	0.81	2.74	4.23	9.91	0.91	4.18	12.53	2.24	2.02	2.80	2.93
Sm	0.28	1.13	1.52	3.51	0.34	1.65	4.59	0.89	0.72	1.11	1.18
Eu	0.11	0.45	0.63	1.23	0.16	0.64	1.62	0.34	0.27	0.43	0.46
Gd	0.49	1.59	2.00	4.66	0.49	2.39	7.04	1.28	0.94	1.57	1.64
Tb	0.11	0.31	0.38	0.90	0.09	0.47	1.38	0.25	0.18	0.32	0.32
Dy	0.89	2.16	2.53	6.12	0.66	3.33	9.99	1.76	1.23	2.21	2.11
Ho	0.21	0.47	0.54	1.34	0.15	0.75	2.38	0.40	0.27	0.49	0.44
Er	0.70	1.39	1.55	3.99	0.44	2.29	7.63	1.20	0.82	1.49	1.22
Tm	0.12	0.22	0.24	0.65	0.07	0.37	1.30	0.19	0.13	0.24	0.19
Yb	0.83	1.40	1.42	4.16	0.46	2.41	8.82	1.23	0.87	1.54	1.11
Lu	0.14	0.23	0.22	0.67	0.07	0.39	1.56	0.20	0.14	0.25	0.17
Hf	0.25	0.85	1.20	2.70	0.21	1.17	2.62	0.68	0.69	0.88	0.73
Ta	0.15	0.04	0.05	0.10	0.01	0.06	0.11	0.03	0.03	0.06	0.02
Pb	0.7	0.5	1.1	1.7	0.3	1.1	2.6	0.5	0.6	1.4	0.6
Th	0.19	0.11	0.19	0.35	0.03	0.15	0.33	0.08	0.12	0.12	0.08
U	0.09	0.08	0.09	0.34	0.02	0.08	0.34	0.04	0.05	0.07	0.08

Sample	91CC45	91CC46	91CC50	91CC55	91CC52	97CC3	91CC2g	91CC2L	91CC3	91CC56	91CC15	91CC24
Lava	UPL	UPL	UPL	UPL	LPL	LPL	LPL	LPL	LPL	UPL	UPL	LPL
	Troulli	*Troulli*	*Avdhellera*	*Avdhellera*	*Avdhellera*	*Troulli*	*Kambia*	*Kambia*	*Kambia*	*Akamas*	*Limni*	*Mandria*
X	56000	56000	52500	52700	52600	56000	21900	21900	21900	-64000	-47000	-15000
Y	74000	74000	74500	74700	74500	77000	71500	71500	71500	83500	77100	58500
SiO_2	43.40	46.17	39.93	41.36	43.95	48.23	52.94	50.69	52.62	40.65	53.82	54.58
TiO_2	0.69	0.63	0.53	0.49	0.43	0.91	1.24	1.32	1.23	0.66	0.30	0.94
Al_2O_3	13.42	16.54	13.87	13.63	14.55	14.91	13.35	14.66	13.84	13.01	13.29	13.76
FeO*	10.17	10.04	8.37	9.52	7.05	10.57	11.32	11.56	12.82	9.63	7.97	11.17
MnO	0.09	0.12	0.12	0.13	0.09	0.18	0.17	0.18	0.18	0.15	0.13	0.18
MgO	6.28	5.14	8.36	6.82	5.49	6.42	3.78	4.91	4.43	6.41	9.09	3.14
CaO	6.87	8.93	8.05	10.66	7.74	8.61	6.77	7.23	7.72	9.70	9.66	7.37
Na_2O	0.57	1.14	0.36	2.13	3.31	2.04	-0.05	0.02	0.02	0.75	0.14	2.25
K_2O	1.18	1.35	1.70	0.84	1.49	0.33	0.00	0.09	0.08	1.20	0.01	0.41
P_2O_5	0.06	0.08	0.06	0.08	0.06	0.08	0.11	0.26	0.13	0.08	0.06	0.09
LOI	17.84	8.77	16.83	13.39	13.76	8.82	8.42	9.88	5.55	18.58	5.38	5.47
Tot	100.57	98.91	98.18	99.05	97.92	101.1	98.05	100.8	98.62	100.82	99.85	99.36
Sc	43	40	39	40	31	35	27	29	32	39	33	32
Ti	4114	3793	3164	2946	2558	5472	7433	7938	7374	3944	1824	5642
V	240	242	248	278	159	351	182	199	397	267	215	288
Cr	50	131	203	155	126	80	8	40	22	112	363	6
Co	31	28	36	37	25	39	23	22	37	32	40	30
Ni	45	257	67	57	46	63	29	185	70	45	210	20
Cu	143	41	63	33	40	276	20	23	53	79	85	98
Zn	63	52	56	52	34	67	78	75	71	63	42	81
Ga	11	13	14	14	10	19	18	19	16	13	12	15
Rb	15	13	16	9	8	2	6	3	5	12	6	7
Sr	941	690	88	80	382	67	117	118	93	713	83	106
Y	12	20	14	19	12	23	37	90	29	24	12	26
Zr	26	23	21	20	15	41	78	84	57	24	18	46
Nb	0.87	0.74	0.76	0.80	0.67	1.37	1.38	1.45	0.99	0.93	0.54	1.03
Cs	0.16	0.19	0.18	0.40	0.19	0.08	0.34	0.12	0.28	0.23	0.36	0.35
Ba	28	11	34	63	15	9	29	14	27	54	17	35
La	0.79	1.35	0.93	1.15	0.84	1.12	2.78	7.77	2.12	1.51	0.80	1.57
Ce	2.17	2.46	2.57	2.63	1.92	4.40	8.82	24.22	6.44	3.21	1.81	4.74
Pr	0.46	0.69	0.46	0.52	0.42	0.74	1.63	4.21	1.20	0.70	0.30	0.88
Nd	2.65	3.96	2.60	2.92	2.36	4.38	9.08	22.98	6.65	4.05	1.62	5.02
Sm	1.12	1.57	1.05	1.16	0.95	1.84	3.40	7.91	2.55	1.61	0.68	2.05
Eu	0.39	0.55	0.41	0.47	0.38	0.72	1.26	2.70	0.96	0.64	0.27	0.79
Gd	1.53	2.23	1.49	1.74	1.37	2.57	4.39	10.69	3.34	2.36	1.05	2.83
Tb	0.32	0.45	0.30	0.35	0.28	0.53	0.87	2.00	0.68	0.49	0.22	0.58
Dy	2.15	3.10	2.11	2.48	1.92	3.61	5.82	13.11	4.59	3.37	1.63	4.03
Ho	0.45	0.66	0.45	0.56	0.41	0.77	1.22	2.76	0.97	0.73	0.37	0.88
Er	1.34	1.95	1.38	1.78	1.23	2.37	3.67	7.92	2.97	2.24	1.23	2.71
Tm	0.21	0.30	0.22	0.28	0.20	0.39	0.58	1.15	0.48	0.35	0.21	0.44
Yb	1.34	1.84	1.43	1.77	1.24	2.55	3.75	6.59	3.10	2.24	1.37	2.86
Lu	0.21	0.28	0.23	0.28	0.20	0.40	0.59	0.99	0.49	0.36	0.23	0.46
Hf	0.93	0.83	0.75	0.69	0.59	1.41	2.40	2.57	1.85	0.86	0.67	1.57
Ta	0.06	0.05	0.05	0.05	0.05	0.10	0.11	0.12	0.08	0.07	0.04	0.08
Pb	1.85	1.01	0.86	1.35	0.97	0.86	1.78	1.33	1.81	1.71	1.74	1.86
Th	0.15	0.11	0.14	0.10	0.10	0.21	0.30	0.31	0.23	0.12	0.12	0.21
U	0.12	0.05	0.07	0.04	0.02	0.03	0.11	0.12	0.08	0.02	0.08	0.10

Sample	85-21	85-117	85-144	YL10	YL13	YL36	YL66	YL15	YL17	YL62	YL68
Lava	UPL	UPL	UPL	LPL	LPL	LPL	LPL	UPL	UPL	BG	BG
	Kalavasos	*Kalavasos*	*Kalavasos*	*Yialias*	*Yialias*	*Yialias*	*Yialias*	*Yialias*	*Yialias*	*Yialias*	*Yialias*
X	25500	26500	25500	30500	30550	28000	25750	30750	31000	24500	25000
Y	50500	50600	51500	71000	71250	70050	70050	71600	72300	70000	70200
SiO_2				46.17	48.54	50.95	46.63			47.18	49.02
TiO_2				1.08	1.49	0.65	0.57			0.54	0.52
Al_2O_3				15.82	15.46	16.51	14.91			14.77	15.26
FeO*				12.53	12.54	10.50	9.23			7.80	8.72
MnO				0.14	0.13	0.19	0.16			0.13	0.31
MgO				8.25	4.77	7.06	8.97			8.48	9.56
CaO				4.08	3.44	11.32	7.85			13.65	6.17
Na_2O				4.07	2.15	1.50	4.11			1.49	4.83
K_2O				1.48	4.23	0.01	1.04			0.67	0.82
P_2O_5				0.08	0.14	0.05	0.07			0.06	0.08
LOI				8.57	5.82	1.23	8.23			5.29	5.36
Tot				102.27	98.71	99.97	101.77			100.06	100.65
Sc	33	41	41	37	37	43	32	34	31	33	38
Ti	2589	2560	2449	6480	8940	3900	3420	9365	5963	3240	3120
V	223	245	243	307	467	333	296	261	233	320	372
Cr	452	511	286	15	6	115	143	11	305	204	168
Co	49	40	38	39	38	40	36	34	40	40	37
Ni	260	112	63	34	16	59	65	16	75	75	65
Cu	88	96	109	38	36	122	38	63	26	83	100
Zn	59	62	59	84	83	66	80	89	58	80	59
Ga	9	10	11	16	20	15	12	17	13	12	11
Rb	5	5	5	33	65	1	7	26	18	7	3
Sr	245	94	109	123	117	82	238	102	108	93	159
Y	8	9	8	25	35	18	19	21	15	14	16
Zr	9	7	7	49	77	26	24	49	33	23	19
Nb	1.26	1.61	1.71	1.02	1.27	0.95	0.74	0.76	0.79	0.57	0.77
Cs	0.17	0.17	0.23	0.35	1.31	0.03	0.31	0.25	0.15	0.04	1.01
Ba	16	15	19	41	155	47	20	75	42	22	222
La	0.48	0.45	0.62	2.96	3.71	1.32	1.47	2.12	1.50	1.02	1.13
Ce	1.02	0.89	1.18	5.93	9.43	3.67	3.24	5.30	4.07	2.86	2.69
Pr	0.14	0.11	0.14	1.23	1.67	0.65	0.65	0.92	0.66	0.52	0.52
Nd	0.87	0.64	0.78	6.43	8.96	3.58	3.58	5.51	3.96	2.87	2.86
Sm	0.42	0.33	0.35	2.21	3.16	1.37	1.33	1.90	1.44	1.15	1.17
Eu	0.17	0.14	0.15	0.83	1.21	0.52	0.52	0.71	0.57	0.48	0.45
Gd	0.73	0.63	0.64	2.84	4.14	1.92	1.99	2.47	1.90	1.64	1.75
Tb	0.16	0.15	0.15	0.55	0.80	0.39	0.40	0.47	0.36	0.34	0.36
Dy	1.21	1.17	1.13	3.70	5.42	2.74	2.79	3.18	2.46	2.23	2.46
Ho	0.28	0.29	0.28	0.77	1.15	0.60	0.60	0.69	0.53	0.47	0.53
Er	0.88	0.94	0.89	2.31	3.50	1.83	1.87	2.03	1.56	1.46	1.58
Tm	0.15	0.16	0.15	0.37	0.56	0.30	0.30	0.32	0.25	0.23	0.25
Yb	0.98	1.10	1.05	2.34	3.51	1.92	1.92	2.03	1.58	1.50	1.59
Lu	0.16	0.19	0.18	0.36	0.56	0.31	0.31	0.32	0.25	0.24	0.25
Hf	0.35	0.27	0.28	1.54	2.38	0.92	0.83	1.46	1.04	0.78	0.68
Ta	0.09	0.11	0.12	0.06	0.10	0.06	0.04	0.05	0.05	0.03	0.05
Pb	0.48	0.49	0.81	2.54	1.75	1.74	0.97	0.67	0.72	0.61	0.55
Th	0.09	0.12	0.15	0.17	0.30	0.17	0.11	0.16	0.15	0.11	0.10
U	0.05	0.05	0.07	0.10	0.31	0.08	0.05	0.12	0.13	0.07	0.05

Appendix 2) Bibliography

Allerton S and Vine FJ, 1987 - Spreading structure of the Troodos ophiolite, Cyprus: some paleomagnetic constraints. Geology Vol. 17, pp 593-597

Allerton S and Vine FJ, 1991 - Spreading evolution of the Troodos ophiolite, Cyprus Geology Vol. 19, pp 637-640

Anonymous, 1972 - Penrose field conference on Ophiolites. Geotimes Vol. 17, pp 24-25

Arndt NT, 1977 - Thick, layered peridotite-gabbro lava flows in Munro Township, Ontario. Canadian Journal of Earth Science Vol. 14, pp 2620–2637

Bagnall PS, 1960 - The geology and mineral resources of the Pano Lefkara - Larnaca area. Geological Survey Department of Cyprus Memorandum #5

Baragar WRA, Lambert MB, Baglow N, Gibson IL, 1990 - The sheeted dyke zone in the Troodos Ophiolite: Ophiolites, Oceanic crustal analogues. Proceedings of the symposium "Troodos 1987", Geological Survey Department, Cyprus, pp 37-51

Bear LM, 1960 - The geology and mineral resources of the Akaki-Lithrodonda area. Geological Survey Department of Cyprus Memorandum #3

Bednarz U and Schmincke HU, 1994 – Petrological and chemical evolution of the north eastern Troodos extrusive series, Cyprus. Journal of Petrologt Vol. 35, pp 489-523

Benn K and Laurent R, 1987 - Intrusive suite documented in the Troodos ophiolite plutonic complex, Cyprus. Geology Vol. 15, pp 821-824

Blome CD and Irwin WP, 1985 - Equivalent radiolarian ages from ophiolitic terranes of Cyprus and Oman. Geology Vol. 13, pp 401-404

Bonatti E, 1976 - Serpentinite protrusions in oceanic crust. Earth and Planetary Science Letters Vol. 32, pp 107-113

Boynton WV, 1984 - Geochemistry of the rare-earth elements: meteorite studies: Rare Earth Element Geochemistry (Ed.) Henderson P, pp 63-114

Cameron WE, Nisbet EG, Dietrich VJ, 1979 - Boninites, komatiites and ophiolitic basalts. Nature Vol. 280, pp 550-553

Cameron WE, 1985 - Petrology of ultramafic lavas and associated rocks of the Troodos massif, Cyprus. Contributions to Mineralogy and Petrology Vol. 89, pp 239-255

Desmet AP, 1976 - Evidence of co-genesis of the Troodos lavas, Cyprus. Geological Magazine Vol.113, pp 165-168

Dilek Y, Thy P, Moores EM, 1990 - Tectonic evolution of the Troodos Ophiolite within the Tethyan Framework. Tectonics Vol. 9 (4), pp 811-823

Erzinger, J, Emmermann R, Mandler M, 1992 - Geochemistry of Altered Lavas of the Troodos Ophiolite, Cyprus Crustal Study Project, Hole CY-2a, in Gibson, I. L., Malpas, J., Robinson, P. T. & Xenophontos, C. (Eds.) Cyprus Crustal Study Project: Initial Report, Holes CY -1 and 1a. Ottawa, Ontario, Canada, Geological Survey of Canada, 81-94.

Flower MFJ and Levine HM, 1987 - Petrogenesis of a tholeiite-boninite sequence from Ayios Mamas, Troodos ophiolite: evidence for splitting of a volcanic arc? Contributions to Mineralogy and Petrology Vol. 97, pp 509-524

Fox PJ and Gallo DG, 1984 - A Tectonic model for ridge-transform-ridge plate boundaries: implications for the structure of oceanic lithosphere. Tectonophysics Vol. 104, pp 205-242

Fretzdorff S, Livermore RA, Devey CW, Leat PT, Stoffers P, 2002 - Petrogenesis of the back-arc East Scotia Ridge, South Atlantic Ocean. Journal of Petrology Vol. 43 (8), pp 1435-1467

Gass IG, 1960 - Ultrabasic Pillow Lavas from Cyprus. Geological Magazine Vol.65 (3) pp 241-251

Gass IG and Masson-Smith D, 1963 - The Geology and gravity anomalies of the Troodos Massif, Cyprus. Philosophical Transactions of the Royal Society of London Vol. 255

Gass IG, 1968 - Is the Troodos Massif of Cyprus a fragment of Mesozoic ocean crust? Nature Vol. 220 p39

Gass IG and Smewing JD, 1973 - Intrusion, extrusion and metamorphism at constructive margins: evidence from the Troodos Massif, Cyprus. Nature Vol. 242, pp 26-29

Gass IG, 1979 - The Margi area: ultramafic pillow lavas and other rock types at the top of the ophiolite sequence: Ophiolites: International Ophiolite Symposium, Cyprus

Gass IG, 1980 – The Troodos Massif: its role in the unravelling of the ophiolite problem and its significance in the understanding of constructive plate margin processes. In Panatayou A (ed) Ophiolites: Proceedings of the International Ophiolite Symposium, Cyprus (1979) pp 23-35

Hebert R and Laurent R, 1990 - Mineral chemistry of the plutonic section of the Troodos ophiolite: New constraints for genesis of arc-related ophiolites. In: Malpas G.J. and Moores E.M. (eds.), Troodos 1987 ophiolites and oceanic lithosphere, pp 149-163.

Hekinian R, Bideau RD, Hebert Y, Niu Y, 1995 - Magmatism in the Garrett Transform Fault (East Pacific Rise near 13° S) Journal of Geophysical Research Vol. 98

Humphries SE, 1984 – The mobility of the rare earth elements in the crust. In, Rare Earth Element Geochemistry (ed. Henderson P, pub Elsevier) pp 315-341

Hurst SD, Moores EM, Varga RJ, 1994 - Structural and geophysical expression of the Solea graben, Troodos Ophiolite, Cyprus. Tectonics Vol. 13-1, pp 139-156

Hynes AJ, Nisbet EG, Smith AG, Welland MJP, Rex DC, 1972 - Spreading and emplacement ages of some ophiolites in the Othris region, eastern central Greece, Z. Dtsch. Geol. Ges. 123.

Hynes A, 1975 - Comments on "The Troodos ophiolitic complex was probably formed in an island arc" by A Myashiro. Earth and Planetary Science Letters Vol. 25, pp 213-216

Jenner GA, Cawood PA, Rautenschlein M, White WM, 1987 - Composition of back-arc basin volcanics, Valu Fa Ridge, Lau Basin: evidence for a slab-derived component in their mantle source. Journal of Volcanology and Geothermal Research Vol. 32, pp 209-222

Juster TC, Grove TL, Perfit MR, 1989 - Experimental constraints on the generation of TiFe basalts, andesites and rhyodacites at the Galapagos Spreading Centre, 85° W and 95° W. Journal of Geophysical Research Vol. 94, pp9251-9274

Kay RW and Senechal RG, 1976 - The Rare Earth Geochemistry of the Troodos ophiolite Complex. Journal of Geophysical Research Vol. 81 (5), pp 964-969

Leat PT, Pearce JA, Barker PF, Lillar IL, Barry TL, Larter RD, 2004 - Magmagenesis and mantle flow at a subducting slab edge: the South Sandwich arc-basin system. Earth and Planetary Science Letters Vol. 27, pp 17-35

MacDonald KC, Kastens K, Speiss FN Miller SP, 1979 - Deep tow studies of the Tamayo Transform Fault. Marine Geophysical Researches Vol. 4, pp 37-70

MacLeod CJ, 1988 – unpublished PhD thesis, Open University

MacLeod CJ, Allerton S, Gass IG, Xenophontos C, 1990 - Structure of a fossil ridge-transform intersection in the Troodos ophiolite. Nature Vol.348, pp 717-720

MacLeod CJ, 1990 - Role of the Southern Troodos Transform Fault in the rotation of the Cyprus microplate: evidence from the Eastern Limassol Forest Complex *In:* Malpas J., Moores, E.M., Panayiotou, A. & Xenophontos, C., (eds.) Ophiolites: Ocean Crustal Analogues. Proceedings of the Symposium 'Troodos 1987", Geological Survey Dept., Nicosia, Cyprus, 75-85.

MacLeod CJ and Murton BJ, 1993 - Structure and tectonic evolution of the Southern Troodos Transform Fault Zone, Cyprus. in Magmatic processes and Plate Tectonics Ed. Prichard HM, Alabaster T, Harris NBW, Neary CR. Geological Society Special Publication 76, pp141-176

Malpas J, 1991 - Crustal accretionary processes in the Troodos Ophiolite, Cyprus : evidence from field mapping and deep crustal drilling. In Ophiolites, Oceanic crustal analogues. Proceedings of the symposium "Troodos 1987", Geological Survey Department, Cyprus, pp 65-74

McCulloch MT and Cameron WE, 1983 - Nd-Sr isotopic study of primitive lavas from the Troodos ophiolite, Cyprus: Evidence for a subduction related setting. Geology Vol. 11, pp 727-731

McDonald GA and Katsura T,1964 - Chemical Composition of Hawaiian Lavas. Journal of Petrology Vol. 5, pp 82-133

Moores EM and Vine FJ, 1971 - The Troodos Massif, Cyprus and other ophiolites as oceanic crust; evaluation and implications. Philosophical Transactions of the Royal

Society of London Vol. A268, pp 433-466

Moores EM, 1975 - Discussion of "Origin of Troodos and other ophiolites: a reply to Hynes". Earth and Planetary Science Letters. Vol. 25, p 223.

Mukasa SB and Ludden JN, 1987 - Uranium lead isotopic ages of plagiogranites from the Troodos ophiolite, Cyprus and their tectonic significance. Geology Vol. 15, pp 825-828

Murton BJ, 1986 - unpublished PhD thesis, Open University

Murton BJ and Gass IG, 1986 - Western Limassol Forest complex Cyprus: Part of an Upper Cretaceous leaky transform fault. Geology Vol. 14, pp 255-258

Murton BJ, 1986 - Anomalous oceanic lithosphere formed in a leaky transform fault: evidence from the Western Limassol Forest Complex, Cyprus. Journal of the Geological Society, London Vol. 143, pp 845-854

Myashiro A, 1973 - The Troodos ophiolitic complex was probably formed in an island arc. Earth and Planetary Science Letters Vol. 19, pp 218-224

Miyashiro, A. 1975a: Origin of the Troodos and other ophiolites: a reply to Hynes. Earth and planetary science letters Vol. 25, pp 217-222.

Miyashiro, A. 1975b: Origin of the Troodos and other ophiolites: a reply to Moores. Earth and planetary science letters Vol. 25, pp 227-235.

Pantazis TM, 1967 - The geology and mineral resources of the Pharmakas-Kalavasos area. Geological Survey Department of Cyprus Memorandum #8

Parkinson, I.J. and Arculus, R.J. 1999. The redox state of subduction zones: insights from arc-peridotites. Chemical Geology, 160, 409-423.

Pearce JA and Cann JR, 1971 - Ophiolite origin investigated by discriminant analysis using Ti, Zr and Y. Earth and Planetary Science Letters Vol. 12, pp 339-349

Pearce JA and Cann JR, 1973 - Tectonic setting of basic volcanic rocks determined using Trace element analyses.Earth and Planetary Science Letters Vol. 19, pp 290-300

Pearce JA, 1975 - Basalt geochemistry used to investigate past tectonic environments on Cyprus. Tectonophysics Vol. 20, pp 47-67

Pearce JA and Norry MJ, 1979 - Petrogenetic implication of Ti Zr Y and Nb variations in volcanic rocks. Contributions to Mineralogy and Petrology Vol. 69, pp 33-47

Pearce JA, 1980 - Geochemical evidence for the genesis and eruptive setting of lavas from Tethyan ophiolites. In Ophiolites : International Ophiolite Symposium, Cyprus (ed. Panatayou A) pp 261-272

Pearce JA, Alabaster T, Shelton AW, Searle MP, 1981 - The Oman ophiolite as a Cretaceous arc-basin complex : evidence and implications. Philosophical Transactions of the Royal Society of London Vol. A300, pp 299-317

Pearce JA, 1982 - Trace element characteristics of lavas from destructive plate margins. In Andesites: Orogenic andesites and related rocks (John Wiley ed. Thorpe RS), pp 522-548

Pearce JA, 1983 - The role of sub-continental lithosphere in magmagenesis at destructive plate margins. In Continental Basalts and Mantle Xenoliths (eds.) Hawksworth CJ and Norry MJ.

Pearce JA, Lippard SJ, Roberts S, 1984 - Characteristics and tectonic significance of supra-subduction zone ophiolites. In Marginal Basin Geology, Geological Society Special Publication Kokelaar and Howells (Eds.), pp 77-94

Pearce JA, Ernewein M, Bloomer SH, Parson LM, Murton BJ, Johnson LH, 1995 - Geochemistry of Lau Basin volcanic rocks: influence of ridge segmentation and arc proximity. In Volcanism associated with extension at consuming plate margins, (ed Smellie JL), Geological Society Special Publication 81, pp 53-75

Pearce JA and Peate DW, 1995 - Tectonic implications of the composition of volcanic arc magmas. Annual review of Earth and Planetary Sciences Vol. 23, pp 251-285

Pearce JA, Stern RJ, Bloomer SH, Fryer P, 2005 - Geochemical Mapping of the Mariana Arc-Basin System: Implications for the Nature and Distribution of Subduction Components (in press)

Peate DW, Kokfelt TF, Hawkesworth CJ, v Calsteren PW, Hergt JM, Pearce JA, 2001 – U-series Isotope data on Lau Basin glasses: the role of subduction-related fluids during melt generation in back-arc basins. Journal of Petrology Vol. 42, No.8, pp 1449-1470.

Portnyagin MV, Danyushevsky LV, Kamenetsky VS, 1997 - Coexistence of two distinct mantle sources during formation of ophiolites: a case study of primitive pillow lavas from the lowest part of the volcanic section of the Troodos ophiolite. Cyprus Contributions to Mineralogy and Petrology Vol.128, pp 287-301

Rautenschlein M, Jenner GA, Hertogen J, Hofmann AW, Kerrich R, Schmincke HU, White WM, 1985 - Isotopic and trace element composition of volcanic glasses from the Akaki canyon, Cyprus: implications for the origin of the Troodos Ophiolite. Earth and Planetary Science Letters Vol. 75, pp 369-383

Richardson CJ, Cann JR, Richards HG, Cowan JG, 1987 - Metal depleted root zones of the Troodos ore-forming hydrothermal systems, Cyprus. Earth and Planetary Science Letters Vol. 84, pp 243-253

Robinson PT, Melson WG, O'Hearn T, Schmincke HU, 1983 - Volcanic glass compositions of the Troodos ophiolite, Cyprus, Geology Vol. 11, pp 400-404

Rogers NW, MacLeod CJ, Murton BJ, 1989 - Petrogenesis of boninitic lavas from the Limassol Forest Complex, Cyprus. in Boninites and related rocks ed. Crawford AJ, pp 288-313

Schilling JD, 1971 - Sea-floor evolution - Rare-earth evidence. Philosophical Transactions of the Royal Society of London Vol. 268, p 633

Schmincke HU, Rautenschlein M, Robinson PT, Mehegan JM, 1983 - Troodos extrusive series of Cyprus: a comparison with oceanic crust. Geology Vol. 11, pp 405-409

Schmincke HU and Bednarz U, 1991 - Pillow, Sheet flow and breccia flow volcanoes and volcano-tectonic hydrothermal cycles in the extrusive series of the north eastern Troodos ophiolite, Cyprus. in Ophiolites, Oceanic crustal analogues. Proceedings of the symposium "Troodos 1987", Geological Survey Department, Cyprus, pp 185-206

Schouten H and Kelemen PB, 2002 - Melt viscosity, temperature and transport processes, Troodos Ophiolite, Cyprus. Earth and Planetary Science Letters Vol. 201, pp 337-352

Shervais JW, 1982 Ti-V plots and the petrogenesis of modern and ophiolitic lavas. Earth and Planetary Science Letters Vol. 59, pp 101-118

Simonian KO and Gass IG, 1978 - Arakapas fault belt, Cyprus: a fossil transform fault. Geological Society of America Bulletin 89, pp 1220-1230

Smewing JD, Simonian KO, Gass IG, 1975 - Metabasalts from the Troodos Massif , Cyprus: Genetic implication deduced from petrography and trace element geochemistry. Contributions to Mineralogy and Petrology Vol. 51, pp 49-64

Smewing JD and Potts PJ, 1976 - Rare earth abundances in basalts and metabasalts from the Troodos Massif, Cyprus. Contributions to Mineralogy and Petrology Vol. 57, pp 248-257

Sobolev AV, Portnyagin MV, Dmitriev LV, Tsameryan OP, Danyushevski LV, Kononkova NN, Shimizu N, Robinson PT, 1993 - Petrology of ultramafic lavas and associated rocks of the Troodos massif, Cyprus. Petrology Vol. 1(4), pp 379-412

Sun SS and McDonough WF, 1989 - Chemical and isotopic systematics of oceanic basalts: implications for mantle composition and processes. In Magmatism in the Ocean Basins, (eds.) Saunders AD & Norry MJ, Geological society special publication 42, pp 313-345

Taylor RN, 1987 - The stratigraphy, geochemistry and petrogenesis of the Troodos Extrusive Sequence, Cyprus unpublished PhD thesis, University of Southampton

Taylor RN and Nesbitt RW, 1988 - Light rare-earth enrichment of supra subduction-zone mantle - evidence from the Troodos Ophiolite, Cyprus. Geology Vol.16 (5), pp 448 - 451

Taylor RN, 1990, - Geochemical stratigraphy of the Troodos extrusive sequence: temporal developments of a spreading centre magma chamber. In Ophiolites, Oceanic crustal analogues. Proceedings of the symposium "Troodos 1987", Geological Survey Department, Cyprus, pp 173-183

Thy P, 1990 - Cryptic variation of a cumulate sequence from the plutonic complex of the Troodos Ophiolite Ophiolites, Oceanic crustal analogues. Proceedings of the symposium "Troodos 1987", Geological Survey Department, Cyprus. pp165-172

Thy P and Xenophontos C, 1991 - Crystallisation order and phase chemistry of glassy lavas from the pillow sequences, Troodos Ophiolite, Cyprus. Journal of Petrology Vol. 32, pp 403-428

Varga RJ and Moores EM, 1985 - Spreading structure of the Troodos ophiolite, Cyprus: Geology Vol. 13, pp 846-850

Varga RJ, 1991 - Models of extension as oceanic spreading centres -evidence from the Solea Graben, Troodos Ophiolite, Cyprus. Journal of Structural Geology Vol. 13, pp 517-537

Verosub KL and Moores EM, 1981 - Tectonic rotations in extensional regimes and their paleomagnetic consequences for oceanic basalts. Journal of Geophysical Research Vol. 86, pp 6335-6349

Wilson RAM, 1959 - The geology of the Xeros-Troodos area. Geological Survey Department of Cyprus Memorandum #1

Wood DA, Joron JL, Treuil M, 1979 - A re-appraisal of the use of trace elements to classify and discriminate between magma series erupted in different tectonic settings. Earth and Planetary Science Letters Vol. 45, pp 326-336

Wood DA,1980 - The Application of a Th-Hf-Ta diagram to problems og tectonomagmatic classification and to establish the nature of crustal contamination of basaltic lavas of the British Tertiary volcanic province. Earth and Planetary Science Letters Vol. 50, pp 11-30